New heavy resonances: from the Electroweak to the Planck scale

Florian Lyonnet

UNIVERSITÉ DE GRENOBLE

THÈSE

Pour obtenir le grade de

DOCTEUR DE L'UNIVERSITÉ DE GRENOBLE

Spécialité : **Physique Subatomique et Astroparticules**

Arrêté ministériel : 7 août 2006

Présentée par

Florian Lyonnet

Thèse dirigée par **Ingo Schienbein**

préparée au sein de **Laboratoire de Physique Subatomique et de Cosmologie**
et de **Ecole doctorale de physique de Grenoble**

New heavy resonances: from the Electroweak to the Planck scale

Thèse soutenue publiquement le **23 Septembre 2014**,
devant le jury composé de :

Mr. Aldo, Deandrea
Prof., Université Claude Bernard Lyon 1, Rapporteur
Mr. Jean-Loïc, Kneur
DR, Laboratoire Charles Coulomb Montpellier, Rapporteur
Mr. Roberto Bonciani
Dr., Università degli Studi di Roma "La Sapienza", Examinateur
Mr. Michael Klasen
Prof., Universität Münster, Examinateur
Mr. François Montanet
Prof., Université Joseph Fourier de Grenoble, Examinateur
Mr. Jean Orloff
Prof., Université Blaise Pascal de Clermont-Ferrand, Examinateur
Mr. Ingo Schienbein
MCF., Université Joseph Fourier, Directeur de thèse

ACKNOWLEDMENGTS

My years at the LPSC have been exciting, intense, and I would like to express my sincere gratitude to all the people that contributed to it on the professional as well as personal level.

I would like to thank the members of my jury, François, Michael, Ingo, Jean, Roberto for their useful comments and in particular Aldo and Jean-Loic for referring my manuscript.

My career as a physicist started with Michael and my first project as a Master II student in the theory group, and I am grateful to him for giving me this opportunity.

Part of this work would not have been possible without the expertise of Roberto to whom I am greatly in debt for everything he has taught me on precision calculations and for the unlimited good mood he spread around the offices along those years. Above all, I would like to thank my supervisor, Ingo, for the freedom he gave to me and his support along those years. Thank you Ingo for sharing your wisdom and for trying to pass on me your admirable rigour and love for perfection. I will miss our countless physics discussions.

I would also like to thank all my collaborators and in particular Florian for walking me through the technicalities of calculating RGEs. My sincere gratitude goes to all my colleagues at the LPSC, Christopher, Mariane, Sabine, Ji-Young, Akin, Jeremy, Suchita, Beranger for making this group such a nice place to work at and with a special thought to Josselin and Tomáš with whom it has been a great pleasure to share the office. In addition, I would like to say how lucky I was to meet Tomáš and how much I appreciated to work with him. I am truly in debt for everything you have taught me, and I am thankful for all the time you devoted to answer my questions, thank you for your endless patience, and thank you for the great moments we spent together.

Along my studies, my parents, family and friends have been a great support and I really appreciated that. In particular, I thank my parents for making me love sciences, and for supporting me in all my choices even though this pushes me further and further away from home.

Finally, I will conclude by thanking Camille, for being here since all those years and for bringing so much happiness into my life. I will be the most happy man with you.

RÉSUMÉ

Le principe d'invariance de jauge local est au centre de la physique des particules moderne. Dans le modèle standard (MS), il repose sur le groupe de jauge ad hoc $\mathrm{SU}(3)_c \times \mathrm{SU}(2)_L \times \mathrm{U}(1)_Y$. L'idée d'étendre ce groupe de jauge est particulièrement attrayante dans une perspective de "Grand Unified Theory" (GUT) où le MS est la limite basse énergie d'une théorie plus fondamentale basée sur un groupe de jauge beaucoup plus large tel que SO(10) ou E_6. En effet, lors de la brisure de symétrie du groupe de GUT au MS, des facteurs de groupe non-brisés supplémentaires, tels que U(1) ou SU(2), peuvent apparaitre. Ce manuscrit est consacré à la phénoménologie de modèles avec un groupe de jauge étendu. En particulier, les études présentées sont centrées sur les modèles basés sur le groupe de jauge $\mathrm{SU}(2) \times \mathrm{SU}(2) \times \mathrm{U}(1)$ dénotés $\mathcal{G}_{221}$. De manière générique, ces modèles prédisent de nouveaux bosons de jauges, Z' et W'.

Après une brève présentation des modèles $\mathcal{G}_{221}$, un nouvau code publique, PyR@TE, qui permet de déterminer les équations du groupe de renormalisation à deux boucles pour une théorie de jauge générique est introduit. Ce code est ensuite utilisé pour déterminer les RGEs des modèles de la classe $\mathcal{G}_{221}$. La suite du manuscrit est dédiée à la présentation des résultats obtenus sur le calcul des corrections radiatives QCD de la production électrofaible d'une paire de quarks top dans le cadre des modèles $\mathcal{G}_{221}$, i.e. en présence d'un nouveau boson de jauge Z'. Ces résultats font l'objet d'une implémentation dans le générateur d'événements Monte Carlo `POWHEG BOX` et les premiers résultats numériques obtenus sont présentés. Les derniers développements concernant le calcul des corrections QCD à la production électrofaible de single-top sont également revus. Enfin, la dernière partie de ce manuscrit est consacrée à l'étude de l'impact de nouvelles résonances W', Z', telles que celles présentes dans les modèles $\mathcal{G}_{221}$, sur l'interaction des neutrinos d'ultra-haute énergie dans l'atmosphère. Ces interactions sont recherchées par l'observatoire Pierre Auger dans les douches de particules produites par l'interaction des rayons cosmiques avec les particules de l'atmosphère.

The principle of local gauge invariance is a pillar of modern particle physics theories and in the SM relies on the ad-hoc gauge group structure $\mathrm{SU}(3)_c \times \mathrm{SU}(2)_L \times \mathrm{U}(1)_Y$. Extending this gauge group is very well motivated in a Grand Unified Theory (GUT) perspective in which the SM is the low-energy limit of a more fundamental theory based on a larger gauge group like SO(10) or E_6. Indeed, the symmetry breaking (SB) of the underlying GUT gauge group, down to the SM one, leaves some additional group factors unbroken, such as U(1) or SU(2). In this spirit, we focus in this manuscript on the phenomenology of extended gauge group models and on the new heavy neutral and charged resonances, generically called Z' and W' predicted by these.

In this manuscript we present different aspects of the phenomenology of the $\mathcal{G}_{221}$ models. After reviewing these extensions, we present a public tool, PyR@TE, that

aims at automating the calculation of RGEs at two-loop for arbitrary gauge theories and exemplify its use with the $\mathcal{G}_{221}$ models. In a second part, we present our results for the calculation of the QCD corrections to the electroweak top-pair production as well as their implementation in a general purpose Monte Carlo generator allowing for a consistent matching of next-to-leading order (NLO) matrix elements with parton shower algorithms, the `POWHEG BOX`. We then review the status of our calculation of the QCD corrections to the electroweak single-top production. Finally, we present a different aspect of the phenomenology of new heavy resonances, Z', W', by studying their impact on the interaction of ultra-high energy neutrinos in the atmosphere. For definiteness we consider the Pierre Auger Observatory, which is sensible to showers initiated by neutrinos of extreme energies up to 10^{12} GeV.

Contents

INTRODUCTION

The Standard Model (SM) of particle physics has emerged over the last century, as many experiments around the world were probing the inner structure of matter, bringing new discoveries, e.g. the W- and Z-bosons at the UA1 [1, 2] and UA2 [3, 4] experiments in 1983. As of today, the SM has been extremely successful in explaining a wealth of experimental data coming from highly-energetic collider as well as low-energy precision experiments. Despite this tremendous success and the lack of anomalous measurements, diverse open questions such as the origin of dark matter (DM), the hierarchy/naturalness problem or the unification of interactions, are motivations to study extensions of the standard theory of particle physics.

From a phenomenological point of view, extending the SM leads to the prediction of new particles that we can search for at experiments and in particular at the Large Hadron Collider (LHC), at CERN. So far, however, these searches have not revealed any traces of new physics and this generically pushes the scale at which new phenomena should occur high into the TeV region, challenging the validity of the arguments to have new physics around the electroweak scale as a solution to the hierarchy problem. The newly discovered Higgs boson [5, 6] also perfectly fits within the SM as its couplings agree with the SM expectations (within the limited precision of the measurements) and its mass, $m_H \simeq 126$ GeV, lies in the range anticipated by the SM fits to electroweak precision data. In addition, the specific values for the Higgs boson and top quark masses allow the SM effective potential to be stable up to very high scales [7]. Of course, it is much too early to discard any new physics at the TeV scale and the upcoming run of the LHC at 13 TeV will shed more light on the situation.

The principle of local gauge invariance is a pillar of modern particle physics theories and in the SM relies on the ad-hoc gauge group structure $\mathrm{SU}(3)_c \times \mathrm{SU}(2)_L \times \mathrm{U}(1)_Y$. Extending this gauge group is very well motivated in a Grand Unified Theory (GUT) perspective in which the SM is the low-energy limit of a more fundamental theory based on a larger gauge group like SO(10) or E_6. Indeed, the symmetry breaking (SB) of the underlying GUT gauge group, down to the SM one, leaves some additional group factors unbroken, such as U(1) or SU(2). In addition, as mentioned above, if we have no principle to fix the scale at which the SM stops being predictive, it is sensible to adopt a bottom-up approach and to study minimal modifications of the SM. In this spirit, we focus in this manuscript on the phenomenology of extended gauge group models and on the new heavy neutral and charged resonances, generically called Z' and W' predicted by these.

Even though it is possible to describe the interactions of such generic Z'- and W'-boson, to the SM fermions, in a completely model independent approach, the resulting Lagrangian possesses too many parameters to successfully carry out relevant phenomenological studies.

In practice, it is therefore necessary to restrict this freedom. For instance, in the Sequential Standard Model (SSM) [8] the couplings of the Z'- and W'-bosons are identical to their SM counter parts and the only free parameter is their mass. Another way of proceeding is to group together several popular models which can be described by a minimal set of parameters, see for instance [9–13]. In the following, we consider new heavy resonances as appearing in a general class of models based on the next-to-minimal extension of the SM gauge group, i.e. when the electroweak gauge group is supplemented by an additional SU(2) factor. In this class, models are grouped according to their theoretical origin.

At the LHC, the searches for additional resonances are mainly done in the Drell-Yan (DY) process with dilepton and lepton plus missing transverse energy final states which has the advantage of being very clean despite the intense hadronic activity. Besides the DY channel, final states involving the top-quark are among the most presumably promising final states because of the special role of the top-quark in many extensions of the SM. The ATLAS and CMS collaborations have performed extensive searches of new spin-one resonances at the LHC for a large number of final states. In Tab. 1, we summarize the searches, that exploited data from the pp runs in 2010 and 2011 at $\sqrt{s} = 7$ TeV (LHC7) and from the pp run in 2012 at $\sqrt{s} = 8$ TeV (LHC8), as well as the corresponding constraints on W' and Z' gauge boson masses. As can be seen, the most stringent limits come from searches with purely leptonic final states, $W' \to \ell + \nu$ [14–22] and $Z' \to \ell^+ + \ell^-$ [23–32] (with $\ell = e, \mu$), leading to lower mass limits of $m_{W'} \gtrsim 3.3$ TeV [14, 18] and $m_{Z'} \gtrsim 3$ TeV [23, 29] for gauge bosons in the SSM. In addition, upper limits on the cross section times the branching ratio, $\sigma \times \mathrm{BR}$, are presented, which can be used to constrain models different from the SSM.

In the first chapter of this manuscript, we review the $\mathcal{G}_{221}$ class of extended gauge group models that we use hereafter for various phenomenological studies. The general setup is presented and the couplings of the new resonances to SM fermions are summarized. Finally, we review the constraints on the parameter space of these models as derived in [63, 64].

Studying the self-consistency of extended gauge group models is very attractive since we can hope to obtain constraints on the parameter space by studying the stability condition. However, this requires to compute the renormalization group equations (RGEs) for models with several gauge groups and additional scalars[1] which can be quite involved especially at the two-loop level. In view of this, we present in the second chapter a public tool that aims at automating the calculation of RGEs at two-loop for arbitrary gauge theories and exemplify its use with the extended gauge group models introduced in Chapter 1.

As seen in Tab. 1, many searches at the LHC consider processes involving top-quarks. With the upcoming run of the LHC at 13 TeV many top-quarks will be produced and precise measurements are expected. In addition, if new physics in the form of heavy resonances is discovered, unravelling the underlying theory and extracting the parameters of the underlying theory will require precise theoretical calculations of top-quark related observables. In Chapter 3, we present our results for the calculation of the QCD corrections to the electroweak top-pair production as well as their implementation in a general purpose Monte Carlo generator allowing for a consistent matching of next-to-leading order (NLO)

[1] These scalars are responsible for the symmetry breaking of this larger gauge group down to the SM.

matrix elements with parton shower algorithms, the POWHEG BOX. Finally, we review the status of our calculation of the QCD corrections to the electroweak single-top production.

Finally, we present in Chapter 4 a different aspect of the phenomenology of new heavy resonances, Z', W', by studying their impact on the interaction of ultra-high energy neutrinos in the atmosphere. For definiteness we consider the Pierre Auger Observatory, which is sensible to showers initiated by neutrinos of extreme energies up to 10^{12} GeV.

In the last chapter we draw our conclusions and give an outlook. Note that details on various calculations presented in this manuscript as well as extra material are relegated to the Appendices.

Reference	$\sqrt{S}$ [TeV]	$\mathcal{L}$ [fb^{-1}]	Mode	Limits [TeV]	Comments
ATLAS:					
JHEP01(2013)29 [33]	7	4.8	dijet distributions	$m_{W'} > 1.68$	
PLB701(2011)50 [17]	7	0.036	$W' \to \ell\nu$	$m_{W'} > 1.49$	SSM
PLB705(2011)28 [16]	7	1.04	$W' \to \ell\nu$	$m_{W'} > 2.15$	SSM
EPJC72(2012)2241 [15]	7	4.7	$W' \to \ell\nu$	$m_{W'} > 2.55$	SSM
ATLAS-CONF-2014-017 [14]	8	20.3	$W' \to \ell\nu$	$m_{W'} > \mathbf{3.27}$	SSM
EPJC72(2012)2056 [34]	7	2.1	$W'_R \to \ell N \to \ell\ell jj$		search for W'_R, N
PRD87(2013)112006 [35]	7	4.7	$WW/WZ \to \ell\nu jj$	$m_{W'} > 0.95$	
ATLAS-CONF-2014-015 [36]	8	20.3	$WZ \to \ell\nu$	$m_{W'} > 1.52$	
PRD85(2012)112012 [37]	7	1.02	$W' \to WZ \to \ell\nu\ell'\ell'$		limits on $\sigma \times BR$
ATLAS-CONF-2013-015 [38]	8	13	$W' \to WZ \to \ell\nu\ell'\ell'$		limits on $\sigma \times BR$
PRL109(2012)081801 [39]	7	1.04	$W' \to t\bar{b}$	$m_{W'_R} > 1.13$	
ATLAS-CONF-2013-050 [40]	8	14	$W' \to t\bar{b} \to \ell\nu b\bar{b}$	$m_{W'_L} > 1.74$, $m_{W'_R} > 1.84$	
PLB719(2013)242 [41]	7	4.6	$Z' \to \tau^+\tau^-$	$m_{Z'} > 1.4$	SSM
ATLAS-CONF-2013-066 [42]	8	19.5	$Z' \to \tau^+\tau^-$	$m_{Z'} > 1.9$	SSM
PRD88(2013)012004 [43]	7	4.7	$Z' \to t\bar{t}$	$\sigma \times BR$ vs $m_{Z'}$	narrow Z'
ATLAS-CONF-2013-052 [44]	8	14	$Z' \to t\bar{t}$	$\sigma \times BR$ vs $m_{Z'}$	narrow Z'
EPJC72(2012)2083 [45]	7	2.05	$Z' \to t\bar{t}$	$\sigma \times BR$ vs $m_{Z'}$	narrow and wide Z'
JHEP01(2013)116 [46]	7		$Z' \to t\bar{t} \to 4j + bb$	$\sigma \times BR$ vs $m_{Z'}$	
PLB700(2011)163 [28]	7	0.04	$Z' \to \ell^+\ell^-$	$m_{Z'} > 1.048$	SSM
PRL107(2011)272002 [27]	7	1.08 (1.21)	$Z' \to \ell^+\ell^-$	$m_{Z'} > 1.83$	SSM
JHEP11(2012)138 [26]	7	4.9	$Z' \to \ell^+\ell^-$	$m_{Z'} > 2.22$	SSM
ATLAS-CONF-2012-129 [25]	8	6	$Z' \to \ell^+\ell^-$	$m_{Z'} > 2.49$	SSM
ATLAS-CONF-2013-017 [24]	8	20	$Z' \to \ell^+\ell^-$	$m_{Z'} > 2.86$	SSM
CERN-PH-EP-2014-053 [23]	8	20.5	$Z' \to \ell^+\ell^-$	$m_{Z'} > \mathbf{2.90}$	SSM
PRD87(2013)052002 [47]	7	4.6	$\ell\ell\ell$		generic search
CMS:					
PLB698(2011)21 [22]	7	0.036	$W' \to e\nu_e$	$m_{W'} > 1.36$	SSM
PLB701(2011)160 [21]	7	0.036	$W' \to \mu\nu_\mu$	$m_{W'} > 1.4$	SSM
JHEP08(2012)023 [20]	7	5	$W' \to \ell\nu$	$m_{W'_R} > 2.5$, $m_{W'_L} > 2.43 \div 2.63$	W'_L, W interference
PRD87(2013)072005 [19]	7; 8	5; 3.7	$W' \to \ell\nu$	$m_{W'} > 2.9$	SSM
CMS-PAS-EXO-12-060 [18]	8	20	$W' \to \ell\nu$	$m_{W'} > \mathbf{3.35}$	SSM; W'_L, W interf.
PRL109(2012)261802 [48]	7	5	$W'_R \to \ell N_\ell$	$(M_{W'_R}, M_{N_\ell})$ exclusions	LR model
CMS-PAS-EXO-12-017 [49]	8	3.6	$W'_R \to \ell N_\ell$	$(M_{W'_R}, M_{N_\ell})$ exclusions	LR model
JHEP05(2011)093 [32]	7	0.04	$Z' \to \ell^+\ell^-$	$m_{Z'} > 1.14$	SSM
PLB714(2012)158 [31]	7	5	$Z' \to \ell^+\ell^-$	$m_{Z'} > 2.33$	SSM
PLB720(2013)63 [30]	7; 8	5.3; 4.1	$Z' \to \ell^+\ell^-$	$m_{Z'} > 2.59$	SSM
CMS-PAS-EXO-12-061 [29]	8	19.6 (20.6)	$Z' \to \ell^+\ell^-$	$m_{Z'} > \mathbf{2.96}$	SSM
PLB716(2012)82 [50]	7	4.9	$Z' \to \tau^+\tau^-$	$m_{Z'} > 1.4$	SSM
PLB704(2011)123 [51]	7	1	$Z', W' \to jj$	$m_{W'} \notin [1.0, 1.51]$	
PRD87(2013)114015 [52]	8	4	$Z', W' \to jj$	$m_{W'} \notin [1.0, 1.73]$, $m_{Z'} \notin [1.0, 1.62]$	
CMS-PAS-EXO-12-059 [53]	8	19.6	$Z', W' \to jj$	$m_{W'} \notin [1.2, 2.29]$, $m_{Z'} \notin [1.2, 1.68]$	
PRL109(2012)141801 [54]	7	5	$W' \to WZ \to 3\ell\nu$	$m_{W'} > 1.143$	SSM
JHEP02(2013)036 [55]	7	5	$W' \to WZ \to jj\ell^+\ell^-, jj\nu\nu$	$m_{W'} \notin [0.7, 0.94]$	SSM
PLB723(2013)280 [56]	7	5	$W' \to WZ \to 4j$	$\sigma \times BR$ vs $m_{W'}$	SSM
CMS-PAS-EXO-12-025 [57]	8	19.6	$W' \to WZ$	$m_{W'} \notin [0.17, 1.45]$	SSM
JHEP01(2013)013 [58]	7	5	$Z', W' \to jjX$, $Z' \to b\bar{b}$	$m_{W'} > 1.92$, $m_{Z'} > 1.47$	SSM
CMS-PAS-EXO-12-023 [59]	8	19.6	$Z' \to b\bar{b}$	$m_{Z'} \notin [1.2, 1.68]$	SSM
JHEP09(2012)029 [60]	7	5	$Z' \to t\bar{t}$	$\sigma \times BR$ vs $m_{t\bar{t}}$	boosted tops
PLB718(2013)1229 [61]	7	5	$W' \to t\bar{b} \to \ell\nu b\bar{b}$	$M_{W'_R} > 1.85$, $M_{W'_L} > 1.51$	W', W interference
PLB717(2012)351 [62]	7	5	$W' \to t\bar{d}$	$M_{W'} > 0.84$	A^t_{FB}, specific model

Table 1: ATLAS and CMS searches for new spin-one gauge bosons (W' and Z') at the LHC using data from the pp runs in 2010 and 2011 at $\sqrt{s} = 7$ TeV and from the pp run in 2012 at $\sqrt{s} = 8$ TeV.

CHAPTER 1
EXTENDED GAUGE GROUP MODELS: $\mathcal{G}_{221}$ CLASS

New heavy resonances are a generic feature of extended gauge group models. While it is possible to have neutral resonances alone in this context, charged resonances are always accompanied by neutral ones. These extensions are attractive because additional group factors are expected from the breaking of larger gauge groups, e.g. SO(10), E_6, in scenarios where the SM is the low-energy limit of some more fundamental theory. However, they do not address the shortcomings of the SM directly. In a bottom-up approach, extending the SM can only be done in a limited number of ways that one can study and characterize i.e. (i) extend the Pointcaré symmetry, (ii) add new particles to the SM spectrum, (iii) increase the space time dimensions, (iv) enlarge the gauge symmetries. Supersymmetry would be an example of (i) while adding a right-handed neutrino to generate neutrino masses via a see-saw mechanism is representative of (ii). Following the idea of (iii) we find Kaluza-Klein theories that attempt to solve the hierarchy/naturalness problem by postulating the existence of extra-dimensions. Finally, the $\mathcal{G}_{221}$ models are illustrative of (iv) and will be the main topic of this chapter.

The simplest extension of the SM gauge group is to add a U(1) group factor. Since U(1) is an abelian group with only one generator, this extension predicts one additional neutral gauge boson denoted Z' in the literature. These extensions were considered soon after the proposal of the $\mathrm{SU}(2)_L \times \mathrm{U}(1)_Y$ electroweak model [65–67] and have been studied at length in the literature. We refer the reader to [68–70] and references therein for reviews on the subject.

Following the same idea, enlarging the SM gauge group with an additional SU(2) group factor is the next-to-simplest extension of the SM gauge structure with the left-right model [71–73] being the most well known and widely studied realization of this setup. On the other hand, despite sharing the same gauge group, various particle content, charge assignment and pattern of symmetry breaking can lead to significantly different phenomenologies at the LHC [74].

There are also other popular extended gauge group models[1] such as the $\mathcal{G}_{331}$, which in some versions have been shown to be consistent with all the SM constraints including the $H \to \gamma\gamma$ rate [75–78]. In addition, these models have a rich DM phenomenology which was investigated in [79–81] as well as [82] and references therein. These models will not be considered in this manuscript.

Since we will present various aspects of the phenomenology of the $\mathcal{G}_{221}$ models in the following chapters, we start by reviewing these extensions. We will follow the classification of [63] according to the pattern of symmetry breaking and discuss the indirect as well as

[1] In $\mathcal{G}_{331}$ models the SM gauge group is replaced by $\mathrm{SU}(3)_c \times \mathrm{SU}(3)_L \times \mathrm{U}(1)_X$.

direct constraints derived in [63, 64]. The parametrisation of the various couplings of the Z'- and W'-bosons to SM fermions are also presented.

1.1 $\mathcal{G}_{221}$ models general features

The $\mathcal{G}_{221}$ models share a common gauge group structure being $\mathrm{SU}(2)_1 \times \mathrm{SU}(2)_2 \times \mathrm{U}(1)_X$. This class groups the Left-Right (LR) [71–73], Un-Unified (UU) [83, 84], Non-Universal (NU) [85, 86], Lepto-Phobic (LP), Hadro-Phobic (HP) and Fermio-Phobic (FP) [87, 88] models which can be characterized in terms of their charge assignments and breaking pattern (**BP**). These models do not contain any new fermionic fields with respect to the SM except for a potential right-handed neutrino, here to complete the right-handed doublet in the extensions where it transforms as a doublet, **2**, under $\mathrm{SU}(2)_2$. The charge assignments for the various models are listed in Tab. 1.1. Note that some of the models might not be free of gauge anomalies, however, we do not consider UV completion of the models and they should be seen as an intermediate step toward a more fundamental theory.

Table 1.1: Charge assignment for the various models of the $\mathcal{G}_{221}$ class. Fields that do not appear in a given column are transforming as singlets.

BP	Model	$SU(2)_1$	$SU(2)_2$	$U(1)_X$
BP-I	Left-right (LR)	$\begin{pmatrix} u_L \\ d_L \end{pmatrix}, \begin{pmatrix} \nu_L \\ e_L \end{pmatrix}$	$\begin{pmatrix} u_R \\ d_R \end{pmatrix}, \begin{pmatrix} \nu_R \\ e_R \end{pmatrix}$	$\frac{1}{6}$ for quarks, $-\frac{1}{2}$ for leptons.
BP-I	Lepto-phobic (LP)	$\begin{pmatrix} u_L \\ d_L \end{pmatrix}, \begin{pmatrix} \nu_L \\ e_L \end{pmatrix}$	$\begin{pmatrix} u_R \\ d_R \end{pmatrix}$	$\frac{1}{6}$ for quarks, Y_{SM} for leptons.
BP-I	Hadro-phobic (HP)	$\begin{pmatrix} u_L \\ d_L \end{pmatrix}, \begin{pmatrix} \nu_L \\ e_L \end{pmatrix}$	$\begin{pmatrix} \nu_R \\ e_R \end{pmatrix}$	Y_{SM} for quarks, $-\frac{1}{2}$ for leptons.
BP-I	Fermio-phobic (FP)	$\begin{pmatrix} u_L \\ d_L \end{pmatrix}, \begin{pmatrix} \nu_L \\ e_L \end{pmatrix}$		$Y_{\mathrm{SM}}$for quarks, Y_{SM} for leptons.
BP-II	Un-unified (UU)	$\begin{pmatrix} u_L \\ d_L \end{pmatrix}$	$\begin{pmatrix} \nu_L \\ e_L \end{pmatrix}$	Y_{SM} for quarks. Y_{SM} for leptons.
BP-II	Non-universal (NU)	$\begin{pmatrix} u_L \\ d_L \end{pmatrix}_{1^{\mathrm{st}},2^{\mathrm{nd}}}, \begin{pmatrix} \nu_L \\ e_L \end{pmatrix}_{1^{\mathrm{st}},2^{\mathrm{nd}}}$	$\begin{pmatrix} u_L \\ d_L \end{pmatrix}_{3^{\mathrm{rd}}}, \begin{pmatrix} \nu_L \\ e_L \end{pmatrix}_{3^{\mathrm{rd}}}$	Y_{SM} for quarks. Y_{SM} for leptons.

We will consider two types of **BP**, **BP-I** and **BP-II**. In **BP-I**, the first SU(2) is identified to $\mathrm{SU}(2)_L$ of the SM and the first stage symmetry breaking (SB) consist in breaking $\mathrm{SU}(2)_2 \times \mathrm{U}(1)_X$ to $\mathrm{U}(1)_Y$ at high scale. The second stage symmetry breaking is the same as in the SM, i.e. $\mathrm{SU}(2)_L \times \mathrm{U}(1)_Y \to \mathrm{U}(1)_{\mathrm{e.m.}}$. **BP-II** starts by the identification of $\mathrm{U}(1)_X$ with $\mathrm{U}(1)_Y$ and the breaking of $\mathrm{SU}(2)_1 \times \mathrm{SU}(2)_2$ to $\mathrm{SU}(2)_L$ at high scale. Again, it is followed by the subsequent breaking of the SM gauge group down to $\mathrm{U}(1)_{\mathrm{e.m.}}$. LR, LP, FP and HP models follow **BP-I** while UU and NU follow **BP-II**.

To achieve the complete chain of SB two scalar fields are required. While in **BP-II** the first stage SB is realized via a bidoublet i.e. $\phi \sim (\mathbf{2}, \bar{\mathbf{2}}, \mathbf{0})$, in **BP-I** we consider two possibilities for the first stage SB: (i) breaking via a doublet $\phi \sim (\mathbf{1}, \mathbf{2}, \frac{\mathbf{1}}{\mathbf{2}})$ (LR-D, LP-D, FP-D, HP-D), (ii) or a triplet scalar $\phi \sim (\mathbf{1}, \mathbf{3}, \mathbf{1})$ (LR-T, LP-T, FP-T, HP-T). Consequently, there are two different scales for the SB at which in turn the two scalars get a vacuum expectation value (*vev*) dynamically breaking the $\mathcal{G}_{221}$ symmetry down to $\mathrm{U}(1)_{\mathrm{e.m.}}$. The *vev* of the various scalars and their quantum numbers are shown in Fig. 1.1.

With two SU(2) and one U(1) gauge factors we have a total of seven generators out of which 3 will be broken by the *vevs* of the Higgses giving longitudinal polarizations to the $W'^{\pm}$ and Z'^0 gauge bosons, leaving 4 degrees of freedom, 3 associated with the masses of the $W^{\pm}$ and Z^0-bosons and one preserved, the generator of $\mathrm{U}(1)_{\mathrm{e.m.}}$.

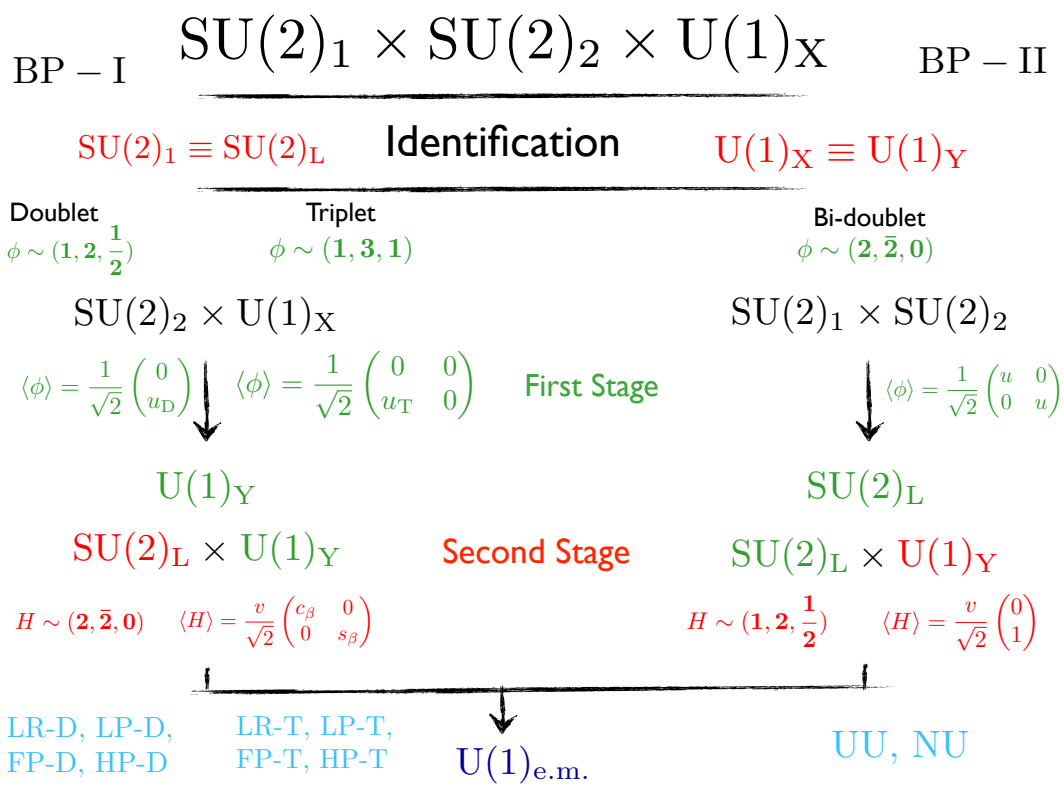

Figure 1.1: **BP** of the $\mathcal{G}_{221}$ group down to $\mathrm{U}(1)_{\mathrm{e.m.}}$. The *vev* of the required scalars are also given.

In what follows we first give some details about the way we treat the scalar triplet fields and then perform the SB in two steps showing how the various gauge bosons acquire

their mass. Finally, we give some details regarding the charged and neutral fermionic currents in the $\mathcal{G}_{221}$ models.

1.1.1 Adjoint fields and covariant derivative

The covariant derivative for a scalar field ϕ charged under a product of n semi-simple gauge groups $\mathcal{G}_1 \times \mathcal{G}_2 \cdots \times \mathcal{G}_n$ is given by :

$$D_\mu \phi_a = \left(\partial_\mu \delta_{ab} + i g_j A_\mu^{\alpha,j} T_{ab}^{\alpha,j}\right) \phi_b \,, \tag{1.1}$$

in which $T^{\alpha,j}$ are the representation matrices for the representation of the group $\mathcal{G}_j$ under which ϕ transforms and $A_\mu^{\alpha,j}$ the corresponding potential vectors. E.g. for a scalar field in the fundamental representation of SU(2), $T^\alpha \equiv \frac{\sigma^\alpha}{2}$, the Pauli matrices while for the triplet scalar field one would use their extension namely:

$$\Sigma_1, \Sigma_2, \Sigma_3 = \frac{1}{\sqrt{2}} \begin{pmatrix} 0 & 1 & 0 \\ 1 & 0 & 1 \\ 0 & 1 & 0 \end{pmatrix} , \frac{1}{\sqrt{2}} \begin{pmatrix} 0 & -i & 0 \\ i & 0 & -i \\ 0 & i & 0 \end{pmatrix} , \frac{1}{\sqrt{2}} \begin{pmatrix} 1 & 0 & 0 \\ 0 & 0 & 0 \\ 0 & 0 & -1 \end{pmatrix} . \tag{1.2}$$

However, as can be seen in Fig 1.1, there exist a very convenient matrix form to represent the fields transforming under the adjoint of SU(n) [89]. Indeed, if $\phi = (\phi_1, \phi_2, \ldots, \phi_n)$ is such a field one can construct a matrix $\Phi \equiv \phi_i T^i$ for an arbitrary non-trivial irreducible representation (irrep). Now, under a gauge transformation we have

$$\phi' = e^{i\theta_a T^a_{\text{adj}}} \phi \,, \tag{1.3}$$

leading to the transformation for Φ'

$$\begin{aligned} \Phi' &\equiv \phi'_i T^i \\ &= \left(e^{i\theta_a T^a_{\text{adj}}}\right)_{ij} \phi_j T^i \\ &\simeq \left(\mathbb{1}\delta_{ij} + i\left(\theta_a T^a_{\text{adj}}\right)_{ij}\right) T^i \phi_j \qquad (1.4) \\ &\simeq \left(T^j + i\left(\theta_a i c_{aji} T^i\right)\right) \phi_j \qquad (1.5) \\ &\simeq \left(T^j + i\theta_a([T^a, T^j])\right) \phi_j \\ &\simeq e^{i\theta_a T^a} \Phi e^{-i\theta_a T^a} \,, \end{aligned}$$

where c_{aij} are the structure constants[2] of the SU(n). Consequently, Φ transforms as a proper unitary operator[3]. Hence, for instance, the triplet scalar field can be represented as

$$\Phi = \frac{\sigma_i}{2}\phi^i = \frac{1}{2}\begin{pmatrix} \phi^3 & \phi_1 - i\phi_2 \\ \phi_1 + i\phi_2 & -\phi^3 \end{pmatrix} .$$

Deducing the covariant derivative for Φ comes directly from Eq. (1.1) and the same kind of manipulations

$$\begin{aligned} D_\mu \Phi &= \partial_\mu \Phi + i g_j A_\mu^{\alpha,j} T_{ab}^{\alpha,j} \phi_b T^a \\ &= \partial_\mu \Phi + i g_j A_\mu^{\alpha,j} \left[T^{\alpha,j}, T^b \phi_b\right] \\ &= \partial_\mu \Phi + i g_j \left[\left(\vec{A}_\mu \cdot \vec{T}\right)^j, \Phi\right] . \end{aligned}$$

[2] By definition structure constants, c_{aij}, satisfy the relation $[T^a, T^i] = i c_{aij} T^j = -L^a_{ij} T^j$

[3] Note that this result is valid for any value of the parameter θ.

1.2 Two-step symmetry breaking and gauge boson masses

One key step in studying particle physics models is to derive the expressions of the masses of the various physical gauge bosons in terms of the fundamental parameters of the theory. This involves going from the gauge eigenstates basis, in which we write the Lagrangian, to the physical basis in which all the mass terms are diagonal. In the following, the various gauge bosons will be denoted by:

$$\mathrm{SU}(2)_1(g_1):\ W^{\mu}_{1;1,2,3},\ \mathrm{SU}(2)_2(g_2):\ W^{\mu}_{2;1,2,3},\ \mathrm{U}(1)_X(g_X):\ X^{\mu}. \tag{1.6}$$

We now calculate the masses for the W-, W'-, Z- and Z'- bosons in the $\mathcal{G}_{221}$ models in two steps to emphasize the dynamics of symmetry breaking and we exemplify this procedure by the models following **BP-I** with a doublet scalar field for the first stage SB (**BP-I**-D), see Fig 1.1.

The kinetic terms for the scalars in the model reads

$$\begin{aligned}
\mathcal{L} \ &\supset\ (D_\mu\phi)^\dagger(D^\mu\phi) + (D_\mu H)^\dagger\,(D^\mu H)\ , \\
&\textbf{BP-I-D:} \\
D_\mu\phi \ &=\ \partial_\mu\phi + i\left(g_2\frac{1}{2}\vec{\sigma}\cdot\vec{W_{2\mu}} + \frac{1}{2}g_X X_\mu\right)\phi\,, \\
D_\mu H \ &=\ \partial_\mu H + i\left(g_1\frac{1}{2}\vec{\sigma}\cdot\vec{W_{1\mu}}H + g_2\frac{1}{2}\vec{\sigma}_{\mathbf{2}^*}\cdot\vec{W_{2\mu}}H\right)\ , \\
&\text{using}\qquad \sigma^a_{\mathbf{2}^*} = -(\sigma^a_{\mathbf{2}})^* = -(\sigma^a_{\mathbf{2}})^T \equiv -(\sigma^a)^T \text{ one obtains} \\
D_\mu H \ &=\ \partial_\mu H + i\left(g_1\frac{1}{2}\vec{\sigma}\cdot\vec{W_{1\mu}}H - g_2 H\frac{1}{2}\vec{\sigma}\cdot\vec{W_{2\mu}}\right)\ .
\end{aligned} \tag{1.7}$$

As in the SM we define charged gauge bosons $W^{\mu,\pm}_{1(2)} = \frac{1}{2}\left(W^{\mu}_{1(2);1} \pm iW^{\mu}_{1(2);2}\right)$ and once ϕ has acquired its *vev* one obtains the charged gauge bosons matrix

$$\left(W^+_{1\mu}\ W^+_{2\mu}\right)\underbrace{\begin{pmatrix} M^2_{W,1\mathrm{st}} & \delta M^2_{W,1\mathrm{st}} \\ \delta M^2_{W,1\mathrm{st}} & M^2_{W',1\mathrm{st}}\end{pmatrix}}_{\mathcal{M}_{\pm,1\mathrm{st}}}\begin{pmatrix} W^{-\mu}_1 \\ W^{-\mu}_2\end{pmatrix}\ ,$$

BP-I-D:

$$\mathcal{M}_{\pm,1\mathrm{st}} = \begin{pmatrix} 0 & 0 \\ 0 & \frac{1}{4}g_2^2u_D^2\end{pmatrix}\ . \tag{1.8}$$

The first thing to note is that in **BP-I**-D only $W_2^{\pm}$ becomes massive after the first stage SB which of course is a consequence of the identification $\mathrm{SU}(2)_1 \equiv \mathrm{SU}(2)_L$.

In the neutral sector spanned by $W_{2;3}, X$ gauge bosons the mass matrix is read off the Lagrangian

$$\frac{1}{2}\left(W_{2;3\mu}\ X_\mu\right)\underbrace{\begin{pmatrix} M^2_{Z,1\mathrm{st}} & \delta M^2_{Z,1\mathrm{st}} \\ \delta M^2_{Z,1\mathrm{st}} & M^2_{Z',1\mathrm{st}}\end{pmatrix}}_{\mathcal{M}_{0,1\mathrm{st}}}\begin{pmatrix} W^{\mu}_{2;3} \\ X^\mu\end{pmatrix}\ ,$$

BP-I-D:

$$\mathcal{M}_{0,1\mathrm{st}} = \frac{1}{4}u_D^2\begin{pmatrix} g_2^2 & -g_2g_X \\ -g_2g_X & g_X^2\end{pmatrix}\ . \tag{1.9}$$

Diagonalizing the neutral mass matrix leads to two states, B, Z' of which the former is massless and named in analogy with the SM, while the mass of the second reads

$$M^2_{Z',\mathrm{1st}} = \frac{1}{4}\left(g_2^2 + g_X^2\right) u_D^2 \,.$$

The mixing angle is easily obtained from the general formula for symmetric two-by-two matrices

$$\begin{pmatrix} a & b \\ b & c \end{pmatrix} \Rightarrow \tan 2\alpha = \frac{2b}{a-c} = \frac{2\tan\alpha}{1-\tan^2\alpha}\,, \tag{1.10}$$

and reads for **BP-I**-D[4]

$$t_\phi \equiv \tan\phi = \frac{g_X}{g_2}\,. \tag{1.11}$$

Hence, after rotating the fields according to t_ϕ we obtain after the first stage SB a massive W', a massive Z' and two massless gauge bosons B and $W^\pm$ related to W_1^μ, W_2^μ and X in our specific case by

$$Z'^\mu = c_\phi W^\mu_{2;3} - s_\phi X^\mu,\ B^\mu = s_\phi W^\mu_{2;3} + c_\phi X^\mu, W'^{\mu\pm} = W_2^{\mu\pm},\ W^{\mu\pm} = W_1^{\mu\pm}.$$

Below the electroweak scale the second scalar field H acquires its *vev* and the second stage SB occurs. The gauge bosons $W'^\pm$ and $W^\pm$ further mix to give the physical states

$$\left(W_\mu^+\ W_\mu'^+\right) \underbrace{\begin{pmatrix} M^2_{W,\mathrm{2nd}} & \delta M^2_{W,\mathrm{2nd}} \\ \delta M^2_{W,\mathrm{2nd}} & 4M^2_{W',\mathrm{1st}} + \delta M_{W',\mathrm{2nd}} \end{pmatrix}}_{\mathcal{M}_{\pm,\mathrm{2nd}}} \begin{pmatrix} W^{-\mu} \\ W'^{-\mu} \end{pmatrix}\,, \tag{1.12}$$

BP-I-D:

$$\mathcal{M}_{\pm,\mathrm{2nd}} = \frac{1}{4}\begin{pmatrix} g_1^2 v^2 & -g_1 g_2 v^2 s_{2\beta} \\ -g_1 g_2 v^2 s_{2\beta} & 4M^2_{W',\mathrm{1st}} + g_2^2 v^2 \end{pmatrix}\,. \tag{1.13}$$

In the neutral sector, we expect to have a massless gauge boson playing the role of the photon as in the SM. It is indeed the case as can be seen by verifying that the determinant of the mass matrix of the states $W_{1;3}$ and B is zero ($\mathcal{M}_{A,Z}$). We then obtain the angle θ and rotate the two fields in order to re-express the neutral sector in terms of the new fields A, Z' and Z'. The explicit form of $\mathcal{M}_{A,Z}$ for **BP-I**-D models is

$$\mathcal{M}_{A,Z} = \frac{g_1^2 v^2}{4}\begin{pmatrix} 1 & -t_\theta \\ -t_\theta & t_\theta^2 \end{pmatrix}\,,\ t_\theta = \frac{g_2 g_X}{g_1\sqrt{g_2^2+g_X^2}}\,, \tag{1.14}$$

$$A^\mu = s_\theta W^\mu_{1;3} + c_\theta B^\mu,\ Z^\mu = c_\theta W^\mu_{1;3} - s_\theta B^\mu\,. \tag{1.15}$$

[4]Note that in the following the cos and sin trigonometric functions are also shortened, e.g. $s_\theta \equiv \sin\theta$, $c_\theta \equiv \cos\theta$ respectively.

This leads us to the second stage SB neutral mass matrix, $\mathcal{M}_{0,2\text{nd}}$

$$\frac{1}{2}\left(Z_\mu \; Z'_\mu\right) \underbrace{\begin{pmatrix} M^2_{Z,2\text{nd}} & \delta M^2_{Z,2\text{nd}} \\ \delta M^2_{Z,2\text{nd}} & 4M^2_{Z',1\text{st}} + \delta M^2_{Z',2\text{nd}} \end{pmatrix}}_{\mathcal{M}_{0,2\text{nd}}} \begin{pmatrix} Z^\mu \\ Z'^\mu \end{pmatrix}, \tag{1.16}$$

BP-I-D:

$$\mathcal{M}_{0,2\text{nd}} = \frac{1}{4}\begin{pmatrix} \dfrac{g_1^2}{c_\theta^2}v^2 & -\dfrac{c_\phi^2 g_1 g_2 g_X v^2}{4} \\ -\dfrac{c_\phi^2 g_1 g_2 g_X v^2}{4} & 4M^2_{Z',1\text{st}} + \dfrac{1}{4}c_\phi^2 g_2^2 v^2 \end{pmatrix}. \tag{1.17}$$

It is interesting to note that both $M^2_{W,2\text{nd}}$ and $M^2_{Z,2\text{nd}}$ can be rewritten into the same form as in the SM by defining $g_L \equiv g_1$ and $g_Y \equiv \left(\frac{1}{g_1^2} + \frac{1}{g_X^2}\right)^{-1/2}$. Finally, one has to diagonalize the matrices in Eqs. (1.13, 1.17), which is done in the limit that the first stage SB occurs at a much higher scale than the electroweak scale, e.g. $u_D \gg v \Rightarrow \delta M^2_{W(Z),2\text{nd}} \ll M^2_{W'(Z'),2\text{nd}}$ leading to

$$\begin{aligned} M^2_{W(Z)} &= M^2_{W(Z),2\text{nd}} - \frac{(\delta M^2_{W(Z),2\text{nd}})^2}{M^2_{W'(Z'),1\text{st}} - M^2_{W(Z),2\text{nd}} + \delta M^2_{W'(Z'),2\text{nd}}}, \\ M^2_{W'(Z')} &= M^2_{W'(Z'),2\text{nd}} + \delta M^2_{W'(Z'),2\text{nd}} + \frac{(\delta M^2_{W(Z),2\text{nd}})^2}{M^2_{W'(Z'),1\text{st}} - M^2_{W(Z),2\text{nd}} + \delta M^2_{W'(Z'),2\text{nd}}}. \end{aligned} \tag{1.18}$$

In the various models this allows us to write down the squared masses for the gauge bosons in expansion of powers of v over u, u_D and u_T.

BP-I-D, $x = \dfrac{v}{u_D} \ll 1$:

$$M^2_{W'} = \frac{1}{4}g_2^2 u_D^2 + \frac{1}{4}g_2^2 u_D^2 x^2 + g_1^2 c_\beta^2 s_\beta^2 u_D^2 x^4 + \mathcal{O}(x^5), \tag{1.19}$$

$$M^2_{Z'} = \frac{1}{4}g_2^2 u_D^2 \left(1 + t_\phi^2\right) + \frac{g_2^2 u_D^2}{4(1+t_\phi^2)}x^2 + \frac{g_2^2 t_\phi^2 + g_1^2(1+t_\phi^2)u_D^2}{4\left(1+t_\phi^2\right)^3}x^4 + \mathcal{O}(x^5), \tag{1.20}$$

BP-I-T, $x = \dfrac{v}{u_T} \ll 1$:

$$M^2_{W'} = \frac{1}{2}g_2^2 u_T^2 + \frac{1}{4}g_2^2 u_T^2 x^2 + \frac{g_1^2}{2}c_\beta^2 s_\beta^2 u_T^2 x^4 + \mathcal{O}(x^5), \tag{1.21}$$

$$M^2_{Z'} = g_2^2 u_T^2 \left(1 + t_\phi^2\right) + \frac{g_2^2 u_T^2}{4(1+t_\phi^2)}x^2 + \frac{g_2^2 t_\phi^2 + g_1^2(1+t_\phi^2)u_T^2}{16\left(1+t_\phi^2\right)^3}x^4 + \mathcal{O}(x^5), \tag{1.22}$$

BP-II, $x = \dfrac{v}{u} \ll 1$:

$$M^2_{W'} = \frac{1}{2}\left(g_1^2 + g_2^2\right)u^2 + \frac{g_2^2 s_\phi^2 u^2}{4}x^2 + \frac{s_\phi^3 g_1^2 u^2}{8}x^4 + \mathcal{O}(x^5), \tag{1.23}$$

$$M^2_{Z'} = \frac{1}{2}\left(g_1^2 + g_2^2\right)u^2 + \frac{g_2^2 s_\phi^2 u^2}{4}x^2 + \frac{s_\phi^3 g_1^2 g_X^2 u^2}{8e^2}x^4 + \mathcal{O}(x^5), \tag{1.24}$$

where we have introduced $e = \dfrac{g_1 g_2 g_X}{\sqrt{g_1^2 g_2^2 + g_1^2 g_X^2 + g_2^2 g_X^2}}$ which will be identified with the electromagnetic charge ($\mathrm{U}(1)_{\mathrm{e.m}}$) later on. We can see from Eqs. (1.19, 1.20, 1.21, 1.22) that in **BP-I**, $M_{W'}$ and $M_{Z'}$ are not degenerated contrary to **BP-II** where the new gauge boson masses are equal up to order x^2 included, Eqs. (1.23, 1.24). Furthermore, we see that the dependence of the masses on β is extremely small in **BP-I** models since the first term involving c_β and s_β is proportional to x^4. This will have two important consequences: (i) gauge boson masses can and will be considered identical in **BP-II**, (ii) the impact of β will be neglected in **BP-I**. Finally, for the expressions of the various mass matrices we refer the reader to Table VI of [63], which we have independently verified.

1.3 Neutral and charged fermionic currents

As the W- and Z- bosons of the SM, the new heavy resonances predicted in the $\mathcal{G}_{221}$ models will couple to the SM fermions. In the same spirit as above, we give the general features of the charged and neutral currents in the $\mathcal{G}_{221}$ models and exemplify the various expressions by the models following **BP-I**-D breaking pattern. Finally, we give the couplings of the Z'- and W'-bosons within all the models.

The starting point is the kinetic term for the fermions

$$\mathcal{L}_{\mathrm{ferm}} = \bar{f}_i \not{D} f_i \,, \tag{1.25}$$

in which the sum runs over all the fermions in the model. The expression for $\not{D}$ depends on the nature of f_i and is therefore different for each model. In order to obtain the couplings of the various gauge bosons to the fermions we begin by performing the rotation corresponding to the first stage SB. Let's write the $\mathcal{L}_{\mathrm{ferm}}$ in terms of the gauge bosons, W, W', A, Z and Z'. In terms of these fields the Lagrangian reads

$$\begin{aligned}\mathcal{L}_{\mathrm{ferm}} = & W^{+\mu} J^+_\mu + W^{-\mu} J^-_\mu + Z^\mu J^0_\mu + A^\mu J_\mu \\ & + W'^{+\mu} K^+_\mu + W'^{-\mu} K^-_\mu + Z'^\mu K^0_\mu \,,\end{aligned} \tag{1.26}$$

where the first line takes the same expression as in the SM and the second line is the new physics contribution

$$\begin{aligned} J_\mu &= e \sum_f Q^f \bar{f} \gamma_\mu f \,, \\ J^0_\mu &= \sqrt{g_L^2 + g_Y^2} \sum_f \left(T^f_{3L} - s_\theta^2 Q^f \right) \bar{f}_L \gamma_\mu f_L - s_\theta^2 Q^f \bar{f}_R \gamma_\mu f_R \,, \\ J^+_\mu &= \frac{g_L}{\sqrt{2}} \left(\bar{d}_L \gamma_\mu P_L u_L + \bar{e}_L \gamma_\mu P_L \nu_L \right) \,, \end{aligned} \tag{1.27}$$

in which the expressions for g_Y and g_L depend on the model (the expressions for models breaking according to **BP-I**-D have been given above see Eq. (1.17)), Q^f is the charge of the fermion f, T^f_{3L} is the third component of the isospin of the unbroken SU(2) gauge group after the first SB[5] for the fermion f, and e plays the role of the electromagnetic

[5] This is given by the sum of T^1_3 and T^2_3 the third isospin component of $\mathrm{SU}(2)_1$ and $\mathrm{SU}(2)_2$ respectively.

charge. Note also that f_L, f_R carry a generation index that we omitted. The expressions for the new currents K^0, $K^\pm$ are model dependent and can be read off Tables IV and V of [63] respectively.

As we have already seen, after the second stage SB the gauge bosons further mix and within the same limit as above, i.e. $u_D, u_T, u \gg v$ we can approximate the charged and neutral physical states by (below, physical states are denoted by a caret, $\wedge$)

$$\begin{aligned}
\hat{Z'}_\mu(\hat{W}'^{\pm}_\mu) &\simeq Z'_\mu(W'^{\pm}_\mu) + \frac{\delta M^2_{Z(W),2\text{nd}}}{M^2_{Z'(W'),1\text{st}} - M^2_{Z(W),2\text{nd}}} Z_\mu(W^\pm_\mu)\,, \\
\hat{Z}_\mu(\hat{W}^\pm_\mu) &\simeq Z_\mu(W^\pm_\mu) - \frac{\delta M^2_{Z(W),2\text{nd}}}{M^2_{Z'(W'),1\text{st}} - M^2_{Z(W),2\text{nd}}} Z'_\mu(W'^{\pm}_\mu)\,.
\end{aligned} \tag{1.28}$$

Inverting Eq. (1.28) and inserting the result in Eq. (1.26) we obtain the new currents after the second SB stage displaying how the SM interactions are modified by the presence of the new resonances

$$\begin{aligned}
\mathcal{L}_{\text{ferm}} = {} & \hat{W}^{+\mu}\left(J^+_\mu - \frac{\delta M^2_{W,2\text{nd}}}{M^2_{W',1\text{st}} - M^2_{W,2\text{nd}}} K^+_\mu\right) + (+ \longleftrightarrow -) \\
& + \hat{W}'^{+\mu}\left(K^+_\mu + \frac{\delta M^2_{W,2\text{nd}}}{M^2_{W',1\text{st}} - M^2_{W,2\text{nd}}} J^+_\mu\right) + (+ \longleftrightarrow -) \\
& + \hat{Z}^\mu\left(J^0_\mu - \frac{\delta M^2_{Z,2\text{nd}}}{M^2_{Z',1\text{st}} - M^2_{Z,2\text{nd}}} K^0_\mu\right) \\
& + \hat{Z}'^{\mu}\left(K^0_\mu + \frac{\delta M^2_{Z,2\text{nd}}}{M^2_{Z',1\text{st}} - M^2_{Z,2\text{nd}}} J^0_\mu\right) \\
& + A^\mu J_\mu\,.
\end{aligned} \tag{1.29}$$

We now define the conventions we are using for the couplings of the new gauge bosons and for that we start from the general Lorentz invariant Lagrangian describing the interaction of generic physical bosons Z' and W' (these will be identified with the mass eigenstates of Eq. (1.28)) with the fermions of the SM[6] [90]:

$$\begin{aligned}
\mathcal{L}^{W'}_{\text{CC}} = \frac{g_W}{\sqrt{2}}\Bigg[& \bar{u}_i\gamma^\mu\left(\left(C^{W'}_{q,L}\right)_{ij} P_L + \left(C^{W'}_{q,R}\right)_{ij} P_R\right) d_j \\
& + \bar{\nu}_i\gamma^\mu\left(\left(C^{W'}_{\ell,L}\right)_{ij} P_L + \left(C^{W'}_{\ell,R}\right)_{ij} P_R\right) e_j\Bigg] W'_\mu + h.c.
\end{aligned} \tag{1.30}$$

$$\begin{aligned}
\mathcal{L}^{Z'}_{\text{NC}} = \frac{g_W}{c_{\theta_W}}\Bigg[& \sum_q \bar{q}_i\gamma^\mu\left(\left(C^{Z'}_{q,L}\right)_{ij} P_L + \left(C^{Z'}_{q,R}\right)_{ij} P_R\right) q_j \\
& + \sum_\ell \bar{\ell}_i\gamma^\mu\left(\left(C^{Z'}_{\ell,L}\right)_{ij} P_L + \left(C^{Z'}_{\ell,R}\right)_{ij} P_R\right) \ell_j\Bigg] Z'_\mu + h.c.
\end{aligned} \tag{1.31}$$

[6] With the addition of a right handed neutrino.

where $q \in \{u_i, d_j\}$, $\ell \in \{\nu_i, e_j\}$ $(i,j = 1,2,3)$. In addition, g_W is the $\mathrm{SU}(2)_L$ gauge couplings and θ_W the Weinberg angle. Finally, the $C_{q,L(R)}$, $C_{\ell,L(R)}$ are the general couplings, a priori complex, parametrizing the interaction of the new resonances. This Lagrangian is a generalization of the SM one which can be recovered by setting $C^{W'}_{q,L} = V_{\mathrm{CKM}}$, $C^{W'}_{\ell,L} = V_{\mathrm{PMNS}}$, $C^{W'}_{q(\ell),R} = 0$, $\left(C^{Z'}_{q(\ell),L}\right)_{ij} = \left(T_{3,q(\ell)} - Q_{q(\ell)} s^2_{\theta_W}\right)\delta_{ij}$ and $\left(C^{Z'}_{q(\ell),R}\right)_{ij} = -Q_{q(\ell)} s^2_{\theta_W}\delta_{ij}$ in which $T_{3,q(\ell)}$ is the third isospin component. Obtaining the couplings of the $\hat{Z}'$ and $\hat{W}'$ gauge bosons of the $\mathcal{G}_{221}$ models can be done by recasting Eq. (1.29) in the form of Eq. (1.31) and Eq. (1.30) respectively.

After some manipulations, these couplings can be expressed in terms of two or three parameters in models following **BP-II** or **BP-I** respectively. For models breaking according to **BP-II** we will denote M the mass of the new particle independently of the nature of the gauge boson since their masses are degenerate, see Eqs. (1.23, 1.24), and t_ϕ, the first SB tangent angle as in Eq. (1.11). For **BP-I** models, we will use either $M_{W'}$ or $M_{Z'}$ and neglect the dependence on β reducing the freedom to only two parameters. The couplings then read [91]

BP-I:

$$\begin{aligned}
C^{W'}_{q,L} &= -\varepsilon^{W'}(t_\phi, M_{W'}, \beta) V_{\mathrm{CKM}} \\
(C^{W'}_{\ell,L})_{ij} &= -\varepsilon^{W'}(t_\phi, M_{W'}, \beta)\delta_{ij} \\
(C^{Z'}_{q(\ell),L})_{ij} &= \left(-s_\theta X_{q(\ell)} t_\phi + \left(T_{3,q(\ell)} + Q_{q(\ell)} s^2_\theta\right)\varepsilon^{Z'}(t_\phi, M_{Z'})\right)\delta_{ij} \\
(C^{Z'}_{q(\ell),R})_{ij} &= \left(s_\theta\left(-X_{q(\ell)} t_\phi + T_{3,q(\ell)}\frac{1}{t_\phi}\right) + Q_{q(\ell)} s^2_\theta \varepsilon^{Z'}(t_\phi, M_{Z'})\right)\delta_{ij}
\end{aligned} \tag{1.32}$$

LR		LP	
$C^{W'}_{q,R}$	$= -t_\theta\left(1 + \frac{1}{t^2_\phi}\right)^{1/2} V_R$	$C^{W'}_{q,R}$	$= -t_\theta\left(1 + \frac{1}{t^2_\phi}\right)^{1/2} V_R$
$(C^{W'}_{\ell,R})_{ij}$	$= -t_\theta\left(1 + \frac{1}{t^2_\phi}\right)^{1/2}\delta_{ij}$	$C^{W'}_{\ell,R}$	$= 0$

(1.33)

HP		FP	
$C^{W'}_{q,R}$	$= 0$	$C^{W'}_{q,R}$	$= 0$
$(C^{W'}_{\ell,R})_{ij}$	$= -t_\theta\left(1 + \frac{1}{t^2_\phi}\right)^{1/2}\delta_{ij}$	$C^{W'}_{\ell,R}$	$= 0$

(1.34)

BP-II:

UU

$$
\begin{array}{ll|ll}
C^{W'}_{q,L} & = \left(\dfrac{1}{t_\phi} - c_\theta \varepsilon(t_\phi, M)\right) V_{\rm CKM} & C^{W'}_{q,R} & = 0 \\
(C^{W'}_{\ell,L})_{ij} & = (-t_\phi - c_\theta \varepsilon(t_\phi, M))\delta_{ij} & C^{W'}_{\ell,R} & = 0 \\
(C^{Z'}_{q,L})_{ij} & = \left(T_{3,q} c_\theta \dfrac{1}{t_\phi} + (T_{3,q} + Q_q s^2_\theta)\varepsilon(t_\phi, M)\right)\delta_{ij} & (C^{Z'}_{q,R})_{ij} & = Q_q s^2_\theta \varepsilon(t_\phi, M)\delta_{ij} \\
(C^{Z'}_{\ell,L})_{ij} & = (-T_{3,\ell} c_\theta t_\phi + (T_{3,\ell} + Q_\ell s^2_\theta)\varepsilon(t_\phi, M))\delta_{ij} & (C^{Z'}_{\ell,R})_{ij} & = Q_\ell s^2_\theta \varepsilon(t_\phi, M)\delta_{ij}
\end{array}
\tag{1.35}
$$

NU

$$
\begin{array}{ll|ll}
\multicolumn{4}{l}{\text{1st and 2nd generations, } (i,j) \in [\![1,2]\!]^2} \\
(C^{W'}_{q(\ell),L})_{ij} & = \left(\dfrac{1}{t_\phi} - c_\theta \varepsilon(t_\phi, M)\right)\delta_{ij} & C^{W'}_{q(\ell),R} & = 0 \\
(C^{Z'}_{q(\ell),L})_{ij} & = \left(T_{3,q(\ell)} c_\theta \dfrac{1}{t_\phi} + (T_{3,q(\ell)} + Q_{q(\ell)} s^2_\theta)\varepsilon(t_\phi, M)\right)\delta_{ij} & (C^{Z'}_{q(\ell),R})_{ij} & = Q_{q(\ell)} s^2_\theta \varepsilon(t_\phi, M)\delta_{ij} \\
\multicolumn{4}{l}{\text{3rd generation}} \\
C^{W'}_{q(\ell),L} & = -t_\phi - c_\theta \varepsilon(t_\phi, M) & C^{W'}_{q(\ell),R} & = 0 \\
C^{Z'}_{q(\ell),L} & = (-T_{3,q(\ell)} c_\theta t_\phi + (T_{3,q(\ell)} + Q_{q(\ell)} s^2_\theta)\varepsilon(t_\phi, M))\delta_{ij} & C^{Z'}_{q(\ell),R} & = Q_{q(\ell)} s^2_\theta \varepsilon(t_\phi, M)
\end{array}
\tag{1.36}
$$

where $T_{3,q(\ell)} \equiv T^1_{3,q(\ell)} + T^2_{3,q(\ell)}$ is, as in Eq. (1.26), the sum of the third components isospin of $\mathrm{SU}(2)_1$ and $\mathrm{SU}(2)_2$, $X_{q(\ell)}$ is the charge of the $q(\ell)$ under $\mathrm{U}(1)_X$, as given in Tab. 1.1, and $V_{\rm CKM}$ has been omitted in the NU model[7]. The functions $\varepsilon^{W'}(t_\phi, M_{W'}, \beta)$, $\varepsilon^{Z'}(t_\phi, M_{Z'})$ and $\varepsilon(t_\phi, M)$ are collecting terms proportional to $s^2_{2\beta}\sqrt{1+t^2_\phi}/(M^2_{W'} t_\phi)$, $1/(t_\phi M^2_{Z'})$ and t_ϕ/M^2 respectively which are negligible in the region of the parameter space unconstrained by low-energy and precision data. In the following, these functions will be neglected and we refer the interested reader to [91] for more details. Within these assumptions, we see that the couplings in **BP-I** do not depend on whether the symmetry is broken via a doublet or a triplet.

The **BP-I** models are sometimes referred to as *right-handed* because of the properties of the W'-boson which does not couple to left-handed fermions. Analogously, models following **BP-II** are named *left-handed* for the similar reasons. It can also be noted that in the LP model the couplings of the W' to leptons are vanishing, i.e. the behaviour of the additional charged resonance is indeed *lepto-phobic*. Inspecting the other couplings of **BP-I** models reveals that the behaviour of the W' in FP and HP models are *fermio-phobic* and *hadro-phobic* respectively.

In the last subsection we discuss the constraints on the $\mathcal{G}_{221}$ models derived from low-energy and precision data as well as direct constraints from colliders.

[7] To restore the CKM matrix it suffices to multiply the W' couplings to quarks by $V_{\rm CKM}$.

1.4 Direct and indirect constraints on the $\mathcal{G}_{221}$ parameter space

Among the various constraints that new physics models have to satisfy, measurements of low-energy observables as well as precision data (from LEP-1 and SLD) are some of the most stringent ones. The authors of [63] have performed a global-fit of the $\mathcal{G}_{221}$ models to 37 observables including LEP-I Z-pole observables, properties of the W-boson, the tau lifetime and many others. The anomalous magnetic moment of the muon as well as observables depending strongly on the extended flavor structure of the $\mathcal{G}_{221}$ models like $\mathrm{Br}(b \to s\gamma)$ are excluded from the fit and an example of their impact can be found in [92].

From this global analysis they have obtained limits on the parameter space from which a lower bound on the masses of the heavy gauge bosons can be extracted. We list below the lower bounds on the masses obtained with this procedure. Note that these bounds always depend on at least one another parameter and that the numbers quoted are only the minima of the lower bounds.

In **BP-I** the bound on W' mass has a stronger model dependence with a constraint that varies between 0.27 to 0.7 TeV.

Table 1.2: Exclusion bounds on W' and Z' $\mathcal{G}_{221}$ gauge boson masses as obtained in [63].

	Model	W' limit [TeV]	Z' limit [TeV]
BP-I	LR-D (T)	0.27 (0.20)	1.6 (1.6)
	LP-D (T)	0.70 (0.50)	1.8 (1.8)
	HP-D (T)	0.40 (0.29)	1.7 (1.7)
	FP-D (T)	0.67 (0.48)	1.7 (1.7)
BP-II	UU	2.5	2.5
	NU	3.6	3.6

New heavy resonances have been actively searched for at the Tevatron and now at the LHC producing more and more stringent constraints on possible new processes. The results of these searches have to be interpreted in a benchmark model often chosen to be the SSM which even though practical is far from capturing all the phenomenological richness of the various $\mathcal{G}_{221}$ models. Therefore, it is necessary to recast the analysis of the various experimental collaborations into the framework of the $\mathcal{G}_{221}$ models in order to extract specific bounds. This work was done in [64] and even though the LHC searches considered are early ones and at 'low' energy (2011, 7 TeV) the bounds obtained are more stringent than the one extracted from Tevatron data for almost all the models[8].

Interestingly, the constraints on the W'-boson mass extracted from LHC7 data are more stringent than the one obtained from low-energy and precision data experiments only for LR-D(T) models. Conversely, the bounds derived on the Z'-boson mass are tighter or at least comparable for all the **BP-I** models in spite of the low-energy and limited luminosity. Furthermore, it was also shown in the same study that the reach of the LHC14 will be very much extended with respect to this analysis. Indeed, large portions of the Z' parameter space up to masses of 5 TeV are expected to be probed while

[8]The data used in the analysis are the following: (i) ATLAS: $pp \to W'^{\pm} \to \ell\nu$, $\int \mathcal{L}dt = 1.04\mathrm{fb}^{-1}$ [16], $pp \to Z' \to \ell^+\ell^-$, $\int \mathcal{L}dt = 1.1\mathrm{fb}^{-1}$ [27]. (ii) CMS: $pp \to Z' \to t\bar{t}$, $\int \mathcal{L}dt = 4.33\mathrm{fb}^{-1}$ [93].

Table 1.3: Constraints obtained from direct searches at the LHC7. The constraints coming from Tevatron were also considered in [64] but were found to be less stringent than the one extracted from LHC data, for almost all the models.

	Model	W' limit [TeV]	Z' limit [TeV]
BP-I	LR-D (T)	1.72 (1.76)	2.25 (3.2)
	LP-D (T)	0.55 (0.55)	1.8 (1.8)
	HP-D (T)	0.46 (0.35)	1.7 (1.7)
	FP-D (T)	0.5 (0.40)	1.75 (1.75)
BP-II	UU	1.7	1.7
	NU	3.1	3.1

improvements in the W'-boson exclusion limits will only be possible for **BP-II** models[9]. Moreover, the latest analyses coming from the LHC [15, 18, 24, 29], see Tab. 1, exclude at the 95 % C.L. SSM Z'- and W'-bosons of masses smaller than 2.86 TeV (ATLAS), 2.96 TeV (CMS) and 3.35 TeV (CMS), 2.55 TeV (ATLAS) respectively. Finally, should such resonances be observed, it will be possible to disentangle the nature of the underlying $\mathcal{G}_{221}$ model in large portions of the parameter space by looking at correlations of observables as was demonstrated in [74].

Models from the $\mathcal{G}_{221}$ class are very well motivated and simple to study since they can be described by two or three free parameters. In this chapter, we have reviewed the specificities of each models and how they can be described in a single class. We derived the expressions of the masses of the Z'- and W'-bosons that appear in these extensions in terms of the fundamental parameters of the models. Furthermore, we summarized the expressions of the new heavy resonances couplings to SM fermions highlighting the characteristic behaviour of the gauge bosons in each extensions. Finally, we detailed the constraints on the parameter space of $\mathcal{G}_{221}$ models, coming both from global fits to precision observables and from collider searches at the Tevatron and LHC.

[9] The exclusion limits should also reach 5 TeV for these models for a wide range of values of the parameters.

CHAPTER 2
AUTOMATIC GENERATION OF RENORMALIZATION GROUP EQUATIONS AT TWO-LOOP WITH PyR@TE

The Standard Model (SM) is an impressively successful theory. It has been tested in a very large number of precision measurements in low-energy experiments and at high-energy colliders, and, despite all efforts, no solid evidence for physics beyond the Standard Model (BSM) has emerged. The recent discovery of a Higgs boson at the Large Hadron Collider at CERN [5, 6] is consistent with this picture. Indeed, the couplings of this particle are in very good agreement with the predictions from the SM, and its mass $m_H \simeq 126$ GeV also lies in the right ballpark anticipated by SM fits to electroweak precision data.

This particular value of the Higgs mass is quite intriguing when analyzing the stability of the electroweak symmetry breaking vacuum and the perturbativity of the underlying dynamics which involves running the couplings from the electroweak scale to higher energies using the renormalization group equations (RGEs) [94]. As a general rule, the β-function of the quartic Higgs coupling λ receives positive (negative) contributions from scalars (fermions), leading to an increasing (decreasing) contribution to the running of λ with increasing energy. Clearly, we need $\lambda > 0$ to have a stable minimum in the Higgs potential. However, slightly negative values of λ are also admissible, if they lead to a metastable vacuum with a lifetime which exceeds the age of the universe. In the SM, given m_H and the mass of the top-quark (which gives the dominant fermionic contribution due to the large Higgs-top Yukawa coupling), one can ask at what scale λ turns negative, thus implying an internal inconsistency and the breakdown of the (perturbative) SM. A detailed analysis of this question depends on (i) the boundary conditions for the RGEs at the weak scale, (ii) the running of the RGEs of the SM (at a given loop order), possibly modified by the presence of extra particles, and (iii) the perturbative validity of the RGEs. The parameters that have the largest effect on the boundary conditions are the Higgs and top-quark mass, as well as the strong coupling constant. Most interestingly, it turns out that with present data the values are just right so that the SM with a (meta-)stable vacuum can be a consistent theory up to very high energies, potentially up to the Planck scale [7, 95].

Of course, the internal consistency of a theory is just a necessary condition for its validity, and there are several reasons of different quality to go beyond the SM. Supersymmetry (SUSY) is one of the best-motivated extensions of the SM. At a technical level, it addresses the hierarchy problem by canceling the large corrections to the Higgs

mass, and the seeming unification of gauge couplings may be indicative of a grand unified theory at a higher scale. However, the conspicuous absence so far of (low-energy) supersymmetry at the LHC[1] has rekindled the interest in non-supersymmetric extensions of the SM[2]. In this chapter we present a tool useful to explore non-supersymmetric BSM scenarios.

In the context of SUSY several public codes exist which numerically evolve the RGEs not only for the minimal supersymmetric standard model, but also for the next-to-minimal supersymmetric standard model [99], for high-scale seesaw scenarios [100, 101] or for R-parity violating models [102, 103]. In addition, the `Mathematica` packages `Susyno` [104] and `SARAH` [105–108] allow since a few years an automated calculation of all β-functions for SUSY models. In contrast, there has not been much effort so far to push also non-SUSY models to that level of automation.

Here, we present a `Python` program [109] that automatically generates the full two-loop renormalization group equations for all (dimensionless and dimensionful) parameters of a general gauge theory. The gauge group, the particle content and many other input parameters can be specified by the user by editing text files in an easy-to-understand format. Once the RGEs for the theory at hand have been calculated by PyR@TE, the results can optionally be exported to LaTeX and `Mathematica`, or stored in a `Python` data structure for further processing by other programs. Also, for the convenience of the user, we have implemented an interactive mode in form of an `IPython Notebook`.

The general RGEs for non-supersymmetric gauge theories have been known at two-loop accuracy for about 30 years [110–115]. In developing PyR@TE, all known typos in the series of papers by Machacek and Vaughn have been taken into account[3], and the code has been validated against several known results in the literature (see Section 2.4.11). Also, independently of the `Python` program, `Mathematica` routines [118] have been developed and cross-checked against PyR@TE, so that we feel confident to have eliminated most sources of possible errors that might affect the correctness of the RGEs.

The scope of PyR@TE is not limited to exploring the stability of the SM electroweak vacuum, as we discussed in some detail above. First, extensions of the SM by weak scale dark matter have been studied in the literature [119]. Second, in cases where the scale Λ is well below a possible unification scale or the Planck scale the knowledge of the RGEs is necessary whenever the boundary conditions are defined at the unification scale. In such a case it is also interesting to study the stability (and perturbativity) of the theory in a similar way as it is done in the SM. Third, in split SUSY scenarios [120] the low-energy spectrum is effectively non-supersymmetric, and therefore requires the most general RGEs.

This chapter is organized as follows. We start by reviewing the various definitions of group theory that are used throughout this part of the manuscript, then we introduce several ideas regarding the renormalization group equations (RGEs) via the example of the massive scalar field theory in Section 2.2 and continue with the RGEs of general gauge theories, Section 2.3. The last two sections, Section 2.4 and 2.5, are devoted to the tool we have developed and its use, PyR@TE, and to an example of its application: the derivation

[1] Clearly, it is much too early to discard the idea of TeV-scale supersymmetry, and the increase in center of mass energy from 8 TeV to 13 TeV will open up the possibility to discover some of the SUSY particles, if they are heavier than originally expected.

[2] For the by now standard motivation for SUSY, we refer the reader to the standard literature [96–98].

[3] See Ref. [116] and the appendix of Ref. [117].

of the two-loop RGEs for the various $\mathcal{G}_{221}$ models presented in Chapter 1.

2.1 Glossary of Group Theory

Since the advent of quantum mechanics, group theory and linear algebra have been at the heart of the mathematical description of nature provided by physics. Concepts such as **Lie groups, Lie algebras** and **representations** are omnipresent in particle physics and we review these concepts in this section. The main goal of this section is to remind the reader of various definitions and to introduce quantities that will be used throughout the chapter, the reader is referred to the literature for more detailed discussions. Note that some of these concepts have already been briefly encountered in the previous chapter. Lie groups and algebras are introduced first. Then, we discuss the concept of representation and terminate with the definitions of **quadratic Casimir operator** and **Dynkin index**.

2.1.1 Lie Groups and Algebras

A key concept we will refer to in the following is that of a Lie algebra, however, the term Lie group is used more often in practice and refers to the underlying group of the algebra. Confusion can arise and we therefore, clarify in turn these two concepts.

A group $\mathcal{G}$ is a set of elements with a multiplicative operation, **group law**, denoted $\cdot$ such that to each ordered pair a, b of elements of $\mathcal{G}$ it associates an element $a \cdot b \in \mathcal{G}$. For $\mathcal{G}$ to be a group, the group law must satisfy the following three axioms [121]

- **Associativity**: $\forall (a, b, c) \in \mathcal{G}^3,\ a \cdot (b \cdot c) = (a \cdot b) \cdot c$.
- **Identity element**: $\exists\, e \in \mathcal{G}$ such that $\forall a \in \mathcal{G}$ we have the relation $a \cdot e = e \cdot a = a$.
- **Inverse element**: $\forall a \in \mathcal{G},\ \exists\, x \in \mathcal{G}$ such that $a \cdot x = x \cdot a = e$. x is called the inverse of element a and is denoted a^{-1}.

Note that in general $a \cdot b \neq b \cdot a$. For this reason a group for which $a \cdot b = b \cdot a$ is called **Abelian**. It is clear from the definition that the number of elements of $\mathcal{G}$ can be finite or not. In the case where they are not in a finite number but can be labelled continuously by a given parameter the group is said to be **continuous**. If in addition, both operations of multiplication and inversion are **analytic** functions of the parameters labelling the elements, and that $\mathcal{G}$ is a **differentiable manifold**, $\mathcal{G}$ is a **Lie group**.

Let $\mathfrak{g}$ be a vector space over some field $\mathbb{K}$ and equipped with an additional internal law $(x, y) \mapsto x \star y$. If $\star$ is bilinear then $\mathfrak{g}$ is an algebra. If in addition $\star$ has the following two properties

- $\forall\, x \in \mathfrak{g}\ x \star x = 0$
- $\forall (x, y, z) \in \mathfrak{g}^3,\ x \star (y \star z) + y \star (z \star x) + z \star (x \star y) = 0$,

then $\mathfrak{g}$ is a **Lie algebra**. The second property is called the Jacobi identity and the product $x \star y$ is called the **Lie bracket** and will be denoted $[x, y]$ as it is often in the literature. Note that the first property along with bilinearity imply that $\star$ is anticommutative, i.e. $x \star y = -y \star x$.

The link between the Lie group and Lie algebra is made via the following map

$$\rho : \mathfrak{g} \longrightarrow T_e\mathcal{G} \tag{2.1}$$
$$x \mapsto x_e \tag{2.2}$$

where $T_e\mathcal{G}$ is the tangent space of the manifold $\mathcal{G}$ at e (and a vector space). ρ is an isomorphism and as such transports the algebra structure of $\mathfrak{g}$ onto the vector space $T_e\mathcal{G}$. Therefore, the algebra is said to describe the local structure of the underlying Lie group near the identity (e). Further details can be found in e.g. [89].

Let $\mathfrak{g}$ be a Lie algebra, since it is a vector space there exist $T_a,\ a = 1, \ldots, N$ elements of $\mathfrak{g}$ that forms a basis. Such elements are called the **generators** of the algebra and N its **dimension**. Each element of $\mathfrak{g}$ can therefore be written as a linear combination of the T_a in which the coefficients can be either real or complex depending on the nature of $\mathfrak{g}$[4].

We now define in turn the concepts of **abelian**, **simple** and **semi-simple** Lie algebras as well as **subalgebra** and **ideals**.

- A Lie algebra $\mathfrak{g}$, is said to be **abelian** if and only if $[\mathfrak{g}, \mathfrak{g}] = 0$ ($\Leftrightarrow \forall (x, y) \in \mathfrak{g}^2,\ [x, y] = 0$). Consequently, $\mathfrak{g}$ can be broken down to several $\mathfrak{u}(1)$ algebras[5].
- Let $\mathfrak{h}$ be a subset of $\mathfrak{g}$, $\mathfrak{h} \subset \mathfrak{g}$. $\mathfrak{h}$ is a **subalgebra** of $\mathfrak{g}$ if it closes under the Lie bracket, i.e. if $[\mathfrak{h}, \mathfrak{h}] \subset \mathfrak{h}$.
- An **ideal** is a subalgebra for which the condition $[\mathfrak{h}, \mathfrak{g}] \subset \mathfrak{h}$ holds. The non trivial ideals of $\mathfrak{g}$ are called **proper ideals**[6].
- A **simple** algebra is an algebra which does not have any proper ideals.
- If $\mathfrak{g}$ has no abelian proper ideals, then it is **semi-simple**.

There is an important result linked to these definitions and another notion: (i) a semi-simple Lie algebra is a direct sum of simple Lie algebras, (ii) the direct sum of simple and abelian Lie algebras is called a **reductive algebra**. This concept is important because gauge symmetries must be given by reductive Lie algebras[7]. Consequently, since abelian Lie algebras are the direct sum of $\mathfrak{u}(1)$'s, the complexity of reductive algebras is comprised in simple algebras.

2.1.2 Representation of Lie algebra

We now move to the concept of **representation** of Lie algebras. Giving a representation of $\mathfrak{g}$ is to associate to each element g of $\mathfrak{g}$ an endomorphism ρ_g

$$\rho_g : V(\mathbb{K}) \longrightarrow V(\mathbb{K})$$
$$x \mapsto \rho_g(x)\,, \tag{2.3}$$

[4] In particle physics, the gauge symmetry are given by real Lie algebra as can be induced from the expression of a gauge transformation [122].

[5] A $\mathfrak{u}(1)$ algebra has an underlying U(1) group.

[6] The trivial ideals are $\mathfrak{g}$ itself and the 0 algebra.

[7] This can be inferred from the gauge transformations of the gauge bosons under the adjoint representation [122].

where V is an arbitrary vector space over a field $\mathbb{K}$. From the endomorphism nature of ρ_g we have that $\forall(\alpha,\beta)\in\mathbb{K}^2,\ \forall(x,y)\in V^2,\ \rho_g(\alpha x+\beta y)=\alpha\rho_g(x)+\beta\rho_g(y)$. To be a representation the map ρ that associates to each g of $\mathfrak{g}$ the endomorphism ρ_g must be a homomorphism (between the two algebras: $\mathfrak{g}$ and the algebra of the endomorphisms of V) i.e. it must preserve the structure of the algebra and hence that $\rho([g_1,g_2])=[\rho(g_1),\rho(g_2)]$. Only finite vector spaces are considered here, so that what we call the **dimension of the representation** is the dimension of V.

In particle physics, the Lie algebras considered are themselves sets of matrices so that there is possible identification between the algebra itself and its trivial representation $\rho=Id$. Subsequently, the set of matrices of $\mathfrak{g}$ is often referred to as the **fundamental** or **defining representation**.

Additional possible confusion arises when V is chosen to be $\mathfrak{g}$ itself. In this case, one can define $\rho: x\mapsto\rho_x\equiv ad_x$ such that $\forall y\in\mathfrak{g},\ ad_x(y)=[x,y]$. By virtue of the Jacobi identity, $\rho\equiv ad$ is linear and preserves the Lie bracket, it is therefore a homomorphism. This representation is called the **adjoint representation** of $\mathfrak{g}$. Considering again the set of generators of $\mathfrak{g}$, $T_a,\ a=1,\dots,N$ since $[T_a,T_b]\in\mathfrak{g},\ \exists f_{abc}$ such that $[T_a,T_b]=f_{abc}T_c$. From $ad_{T_a}(T_b)=[T_a,T_b]=f_{abc}T_c$, ad_{T_a} can be seen as a matrix with entries f_{abc}. The coefficients f_{abc} are called the **structure constants** of the algebra, and are basis dependent.

Another way of defining a n-dimensional representation is to consider a set of N, $n\times n$ dimensional matrices L^a. If these matrices satisfy the same relation as the generators of $\mathfrak{g}$, namely $[L^a,L^b]=f_{abc}L^c$, then they are said to form a representation of $\mathfrak{g}$.

The last point we want to discuss is the definition of **irreducible representations**. Let ρ be a representation of $\mathfrak{g}$ on a vector space V and $W\subset V$ a linear subspace of V. If W is a proper subspace[8] of V which is mapped onto itself by the various generators of $\mathfrak{g}$ then the restriction of ρ to W is a subrepresentation of $\mathfrak{g}$ and ρ is said to be reducible. Equivalently, if the only subrepresentations of ρ are trivial then ρ is irreducible [123].

2.1.3 Casimir operator and Dynkin index

There are three additional definitions that we would like to introduce before concluding this section on group theory.

- The **rank** of an algebra $\mathfrak{g}$ is the number of generators that can be diagonalized simultaneously. For $\mathfrak{su}(\mathfrak{n})$ algebras it is given by $n-1$.
- We will call the dimension of an algebra, the dimension of the adjoint representation. The $\mathfrak{su}(\mathfrak{n})$ algebras have dimension n^2-1.
- Let $T_a,\ a=1,\dots,N$ be a matrix representation, R, of an algebra $\mathfrak{g}$, the **quadratic Casimir** operator C_2 is defined as

$$C_2(R)_{ij}=(T^aT^a)_{ij}\ , \tag{2.4}$$

where the sum over a is implied. We also introduce the Dynkin index of the representation R by

[8] I.e. it is not V itself nor the null space.

$$S_2(R)^{ab} = S_2(R)\delta^{ab} = \mathrm{Tr}\left(T^a T^b\right) . \tag{2.5}$$

For $\mathfrak{su}(\mathfrak{n})$, the Dynkin index of the fundamental representation is $\frac{1}{2}$ while the eigenvalue of the quadratic Casimir is $\dfrac{n^2-1}{2n}$. Note that the quadratic Casimir of the adjoint representation of $\mathfrak{su}(\mathfrak{n})$ is simply n.

For the computation of various Casimir and Dynkin index for different representation we refer the reader to [122, 124].

This concludes this brief section on group theory terminology and we now move on to the renormalization group equations.

2.2 Renormalization Group Equations: ϕ^4 theory

The goal of this section is to introduce various concepts regarding the renormalization group equations and to exemplify them on the ϕ^4 theory. We will introduce the Callan-Symanzik equation along with the definitions of anomalous dimension and beta function.

2.2.1 Renormalization of ϕ^4 theory

We consider the massive scalar theory described by the following Lagrangian

$$\mathcal{L} = \frac{1}{2}\partial_\mu\phi\partial^\mu\phi - \frac{1}{2}m^2\phi^2 - \frac{\lambda}{4!}\phi^4 , \tag{2.6}$$

which describes a self-interacting scalar field with mass parameter m. The Feynman-rules are[9]:

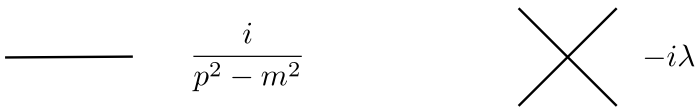

The divergences appearing beyond tree-level in perturbation theory can be absorbed into a redefinition of the mass parameter and coupling, and by renormalizing the wave function in the following way

$$\tilde{\phi} = Z_\phi^{-1/2}\phi,\ \ \tilde{\lambda} = Z_\lambda^{-1}\lambda,\ \ \tilde{m}^2 = Z_m^{-1}m^2 , \tag{2.7}$$

in which we have introduced $\tilde{\phi}$, $\tilde{\lambda}$, $\tilde{m}$ the renormalized wave function, coupling and mass respectively. Z_ϕ, Z_λ, Z_m are the renormalization constants of the theory. They are divergent and cancel the divergences appearing in the theory to yield finite results. Inserting Eq. (2.7) into Eq. (2.6) we can rewrite the Lagrangian in terms of the renormalized quantities

$$\mathcal{L} = \mathcal{L}_0 + \mathcal{L}_{\mathrm{ct}} = \mathcal{L}_0 + (Z_\phi - 1)\frac{1}{2}\partial_\mu\tilde{\phi}\partial^\mu\tilde{\phi} - (Z_m Z_\phi - 1)\frac{1}{2}\tilde{m}^2\tilde{\phi}^2 - (Z_\lambda Z_\phi^2 - 1)\frac{\tilde{\lambda}}{4!}\tilde{\phi}^4 , \tag{2.8}$$

[9] We have omitted the $i\varepsilon$ term in the propagator of the scalar field for simplicity but implicitly assume a $+i\varepsilon$ convention.

where $\mathcal{L}_0$ has the same form as in Eq. (2.6) in which the field and parameters have been replaced by the renormalized quantities. Therefore, we see that the renormalized Lagrangian gives rise to two new interaction terms, see Fig. 2.1.

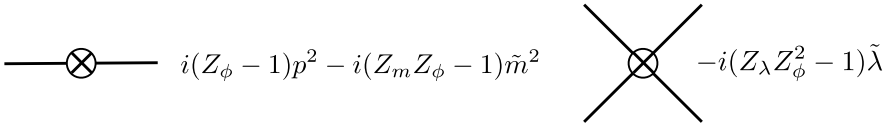

Figure 2.1: Feynman-rules for the counter terms in ϕ^4 theory.

It is our goal now to show how to calculate the renormalization constants from the divergent diagrams of the theory.

At the one-loop level, there are two divergent diagrams, see Fig. 2.2, that we must calculate and we first concentrate on the contributions coming from $\mathcal{L}_0$, ignoring the counter terms.

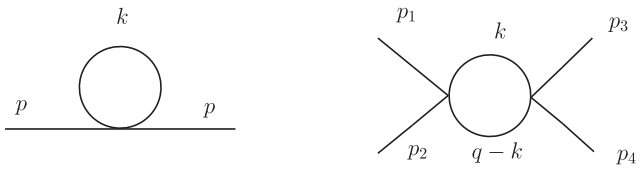

Figure 2.2: Corrections to the propagator and quartic vertex at one-loop in ϕ^4 theory.

Correction to the propagator

The integral corresponding to the diagram[10] is

$$I_2(p^2) = -i\lambda \frac{i}{2} \int \frac{d^4k}{(2\pi)^4} \frac{1}{k^2 - m^2} \,. \tag{2.9}$$

From naive dimensional analysis we can see that the above integral has four powers of k in the numerator and two in the denominator so it diverges quadratically at large k (eventual problems in the infrared regions are not relevant for this discussion). We use dimensional regularization and re-write the integral in $d = 4 - 2\varepsilon$ dimension

$$I_2(p^2) = \frac{\lambda}{2} \int \frac{(\mu)^{4-d} d^dk}{(2\pi)^d} \frac{1}{k^2 - m^2} = \frac{\lambda}{2} (\mu^2)^\varepsilon i \int \frac{d^dk_E}{(2\pi)^d} \frac{1}{-k_E^2 - m^2} \tag{2.10}$$

where as usual, we introduce the renormalization scale μ, with mass dimension to keep the integration measure in four-dimension. Note that we also re-wrote the integral in

[10] Note that the factor $\frac{1}{2}$ comes from the symmetry of the diagram.

Euclidian space on the right-hand side, i.e. $k_0 \to ik_0$, $d^dk \to id^dk_E$. This can now be directly integrated using the general formula [125]

$$\int \frac{dk_E^d}{(2\pi)^d} \frac{1}{(k_E^2 + L^2)^a} = \frac{\Gamma(a - d/2)}{(4\pi)^{d/2}\Gamma(a)} L^{d/2-a} \tag{2.11}$$

leading to

$$I_2(p^2) = -\frac{\lambda}{2}(\mu^2)^\varepsilon i \frac{\Gamma(1 - d/2)}{(4\pi)^{d/2}\Gamma(1)} (m^2)^{d/2-1} = -im^2 \frac{\lambda}{32\pi^2} (4\pi)^\varepsilon \left(\frac{\mu^2}{m^2}\right)^\varepsilon \Gamma(-1 + \varepsilon)\,. \tag{2.12}$$

The fact that the integral diverges quadratically manifests itself in the structure of $\Gamma(-1+\varepsilon)$ which has a pole at $\varepsilon = 0$ and $\varepsilon = 1$. However, since we are interested in the result in the limit $\varepsilon \to 0$ we expand Eq. (2.12) in Laurent series around $\varepsilon = 0$

$$\Gamma(-1 + \varepsilon) \;=\; -\frac{1}{\varepsilon} + (-1 + \gamma_E) + \mathcal{O}(\varepsilon),\; I_2(p^2) = \frac{i\lambda}{32\pi^2} m^2 \left[1 + \Delta + \log(\frac{\mu^2}{m^2})\right], \tag{2.13}$$

in which we introduced $\Delta = \frac{1}{\varepsilon} - \gamma_E + \log(4\pi)$, the $\overline{\text{MS}}$ expansion parameter[11].

The vertex

Applying the Feynman-rules we obtain the integral corresponding to the second diagram of Fig. 2.2.

$$\begin{aligned} I_4(s,t,u) &= \tilde{I}_4(s) + \tilde{I}_4(t) + \tilde{I}_4(u)\,, \\ \tilde{I}_4(q^2) &= \frac{(-i\lambda)^2}{48}(\mu^2)^\varepsilon i^2 \int \frac{d^dk}{(2\pi)^d} \frac{1}{(k^2 - m^2)((q-k)^2 - m^2)}\,, \\ &= \frac{\lambda^2}{48}(\mu^2)^\varepsilon \int \frac{id^dk_E}{(2\pi)^d} \frac{1}{(k_E^2 + m^2)((q-k)_E^2 + m^2)}\,. \end{aligned} \tag{2.14}$$

Note that the factor $1/48$ is a symmetry factor[12] and s, t and u are the usual Mandelstam variables. In order to calculate these integrals we use a method commonly referred to as Feynman parameters in which

$$\begin{aligned} \frac{1}{A_1^{\alpha_1} A_2^{\alpha_2} \dots A_n^{\alpha_n}} =& \frac{\Gamma(\alpha_1 + \alpha_2 + \dots + \alpha_n)}{\Gamma(\alpha_1)\Gamma(\alpha_2)\dots\Gamma(\alpha_n)} \int_0^1 dx_1 dx_2 \dots dx_n \\ & \frac{\delta(1 - x_1 - x_2 - \dots - x_n) x_1^{\alpha_1 - 1} x_2^{\alpha_2 - 1} \dots x_n^{\alpha_n - 1}}{(A_1 x_1 + A_2 x_2 + \dots + A_n x_n)^{\alpha_1 + \alpha_2 + \dots + \alpha_n}} \end{aligned} \tag{2.15}$$

[11] $\overline{\text{MS}}$ denotes a renormalization scheme which will be discussed in a following section.

[12] Symmetry factors come from the contraction of the S-matrix within the Wick theorem. In this case it reads $1/S = 2 \times 2 \times 2 \times 3$ because without distinguishing the momenta diagram 2.2 (right) has the following symmetries: the incoming two lines can be exchanged as well as the two vertices, the branches and the two outgoing lines. Plus, there are three different channels, s, t and u.

which leads to

$$\begin{aligned}
\tilde{I}_4(q_E^2) &= \frac{i\lambda^2}{48}(\mu^2)^\varepsilon \int \frac{d^dk_E}{(2\pi)^d}\frac{\Gamma(2)}{\Gamma(1)\Gamma(1)}\int_0^1 dx_1dx_2\delta(1-x_1-x_2) \\
&\quad \frac{1}{((k_E^2+m^2)x_1+(q_E^2+k_E^2-2q_E\cdot k_E+m^2)x_2)^2} \\
&= \frac{i\lambda^2}{24}(\mu^2)^\varepsilon \int \frac{d^dk_E}{(2\pi)^d}\int_0^1 dx_2 \frac{1}{((k_E^2+m^2+(q_E^2-2q_E\cdot k_E)x_2)^2} \\
&= \frac{i\lambda^2}{24}(\mu^2)^\varepsilon \int \frac{d^dk_E}{(2\pi)^d}\int_0^1 dx_2 \frac{1}{(((k_E-q_Ex_2)^2+m^2+q_E^2x_2(1-x_2))^2} \\
&= \frac{i\lambda^2}{24}(\mu^2)^\varepsilon \int \frac{d^dk_E}{(2\pi)^d}\int_0^1 dx_2 \frac{1}{(((k_E-q_Ex_2)^2+m^2+q_E^2x_2(1-x_2))^2}\,. \qquad (2.16)
\end{aligned}$$

Using Eq. (2.11) again one obtains

$$\begin{aligned}
\tilde{I}_4(q^2) &= \frac{i\lambda^2}{24}(\mu^2)^\varepsilon \int_0^1 dx_2 \frac{\Gamma(2-d/2)}{(4\pi)^{d/2}\Gamma(2)}(m^2-q^2x_2(1-x_2))^{d/2-2} \\
&= \frac{i\lambda^2}{48}(\mu^2)^\varepsilon \frac{1}{16\pi^2}(4\pi)^\varepsilon \int_0^1 dx_2\Gamma(\varepsilon)(m^2-q^2x_2(1-x_2))^{-\varepsilon}\,. \qquad (2.17)
\end{aligned}$$

Expanding the result in Laurent series and using $\Gamma(\varepsilon) = 1/\varepsilon - \gamma_E + \mathcal{O}(\varepsilon)$, we obtain

$$\tilde{I}_4(q^2) = \frac{i\lambda^2}{48}\frac{1}{16\pi^2}\left(\Delta - F(q^2,m,\mu)\right) + \mathcal{O}(\varepsilon)\,, \qquad (2.18)$$

where we have introduced the function $F(q^2,m,\mu) = \int_0^1 dx \log\left[\frac{m^2-q^2x(1-x)}{\mu^2}\right]$. With these corrections at hand we can write down the corresponding (1PI) vertex functions $\Gamma^2(p)$, $\Gamma^4(s,t,u)$

$$\Gamma^2(p) = p^2 - m^2\left(1 - \frac{\lambda}{32\pi^2}\left[\Delta + \log(\frac{\mu^2}{m^2})\right]\right)\,, \qquad (2.19)$$

$$\Gamma^4(s,t,u) = -i\lambda\left(1 - \frac{\lambda}{32\pi^2}\left(3\Delta - F(s,m,\mu) - F(t,m,\mu) - F(u,m,\mu)\right)\right)\,. \qquad (2.20)$$

Renormalization constants in the $\overline{\text{MS}}$ scheme

Obviously, the above (1PI) vertex functions are divergent in the limit $\varepsilon \to 0$ and in order to obtain finite results we need to renormalize them. We already renormalized the ϕ^4 Lagrangian in Eq. (2.8), and showed that it gives rise to two additional interaction terms that we have not considered so far, see Fig. 2.1. Taking them into account, it is immediate

to see how Eqs. (2.19, 2.20) are modified

$$\begin{aligned}\Gamma^2(p) &= p^2(1+(Z_\phi-1)) - m^2\Big((1+(Z_m Z_\phi-1) \\ &\quad -\frac{\lambda}{32\pi^2}\left[\Delta+\log(\frac{\mu^2}{m^2})\right]\Big), \qquad (2.21)\\ \Gamma^4(s,t,u) &= -i\lambda\Big(1+(Z_\lambda Z_\phi^2-1)-\frac{\lambda}{32\pi^2}(3\Delta \\ &\quad -F(s,m,\mu)+F(t,m,\mu)+F(u,m,\mu))\Big), \qquad (2.22)\end{aligned}$$

in which the $\sim$ on m and λ in the counter terms have been dropped since the renormalized and bare parameters are equal up to order λ. Then, the following choice for the renormalization constants renders the vertex functions finite at this order of perturbation theory

$$Z_m^{\overline{\rm MS}} = 1+\frac{\lambda}{32\pi^2}\Delta,\ Z_\lambda^{\overline{\rm MS}} = 1+\frac{\lambda}{32\pi^2}3\Delta,\ Z_\phi^{\overline{\rm MS}} = 1. \qquad (2.23)$$

We subtracted terms proportional to Δ and not only $1/\varepsilon$ in the above expressions as prescribed in the $\overline{\rm MS}$ scheme. Also, we see that the wave function does not get renormalized at one-loop[13]. Finally, according to Eq. (2.7) the bare parameters read

$$\tilde{m} = \left(1-\frac{\lambda}{32\pi^2}\Delta\right)m,\ \tilde{\lambda} = \left(1-\frac{\lambda}{32\pi^2}3\Delta\right)\lambda\,. \qquad (2.24)$$

2.2.2 Invariance of Green functions

In the previous paragraph we have shown that the divergences appearing in the vertex functions could be absorbed into a redefinition of the parameters m^2, λ as well as in the wave function renormalization. The corresponding renormalized connected Green's functions are generated from a renormalized functional $\tilde{W}[\tilde{J}, \tilde{m}^2, \tilde{\lambda}]$ which is obtained from the generating functional $W[J, m^2, \lambda]$ by exchanging the functions and parameters, J, m^2, λ for their renormalized counterparts [125]. By definition, $\tilde{W}$ does not contain any divergences and from the general relation $\delta W[J]/\delta J(x) = \phi(x)$ one can observe that $\tilde{J} = Z_\phi^{1/2} J$, while as a reminder we had defined $\tilde{\phi} = Z_\phi^{-1/2}\phi$, see Eq. (2.7). From the expression for the connected Green's function

$$\tilde{G}_c^{(n)}(x_1,\ldots,x_n) = \frac{1}{i^{n-1}}\frac{\delta^n \tilde{W}[\tilde{J}]}{\delta\tilde{J}(x_1)\ldots\delta\tilde{J}(x_n)}\bigg|_{\tilde{J}=0}, \qquad (2.25)$$

we deduce

$$\tilde{G}_c^{(n)}(x_1,\ldots,x_n) = Z_\phi^{-n/2} G_c^{(n)}(x_1,\ldots,x_n) \Rightarrow \tilde{G}_c^{(n)}(p_1,\ldots,p_n) = Z_\phi^{-n/2} G_c^{(n)}(p_1,\ldots,p_n)\,. \qquad (2.26)$$

Finally, translating the above relation for the vertex function one has

$$\tilde{\Gamma}^{(n)}(p_1,\ldots,p_n) = Z_\phi^{n/2}\Gamma^{(n)}(p_1,\ldots,p_n)\,. \qquad (2.27)$$

[13] It does at the two-loop level though [126].

Thus, we see that the renormalized vertex function is obtained from the vertex function by carrying out the replacements $m \to \tilde{m},\ \lambda \to \tilde{\lambda}$ and multiplying by the wave function renormalization constant for each external leg. Consequently, the renormalized vertex function, $\tilde{\Gamma}^{(n)}$ depends on the renormalization scale μ, through its dependence on $Z_\phi,\ \tilde{m}$ and $\tilde{\lambda}$.

On the other hand, $\Gamma^{(n)}$ is independent of μ and is therefore invariant under the transformation

$$\mu \to \mu',\ \mu\frac{\partial}{\partial\mu}\Gamma^{(n)} = 0\,. \tag{2.28}$$

These transformations form the *renormalization group* [127]. Inserting Eq. (2.27) into Eq. (2.28) we obtain

$$\mu\frac{d}{d\mu}\left[Z_\phi^{-n/2}(\mu)\tilde{\Gamma}^n(p_i,\tilde{m}(\mu),\tilde{\lambda}(\mu),\mu)\right] = 0\,, \tag{2.29}$$

where we have written explicitly the dependences of $\tilde{\Gamma}^{(n)}$ on μ. Performing the derivation in Eq. (2.29) and multiplying through by $Z_\phi^{n/2}$gives

$$\left(-\frac{n}{2}\frac{1}{Z_\phi}\mu\partial_\mu Z_\phi + \mu\partial_\mu\lambda\frac{\partial}{\partial\lambda} + \mu\partial_\mu m\frac{\partial}{\partial m} + \mu\partial_\mu\right)\Gamma^{(n)}(p_i,m(\mu),\lambda(\mu),\mu) = 0\,, \tag{2.30}$$

in which we have dropped the "$\sim$" even though we deal only with renormalized quantities in the following. Introducing the quantities

$$\begin{aligned}\gamma &= \mu\frac{1}{2Z_\phi}\frac{d}{d\mu}Z_\phi\,,\\ \beta(\lambda) &= \mu\frac{\partial}{\partial\mu}\lambda\,,\\ \gamma_m &= \frac{\mu}{m}\frac{\partial}{\partial\mu}m\,,\end{aligned} \tag{2.31}$$

Eq. (2.30) becomes

$$\left(\mu\partial_\mu + \beta(\lambda)\frac{\partial}{\partial\lambda} + m\gamma_m\frac{\partial}{\partial m} - n\gamma\right)\Gamma^{(n)}(p_i,m(\mu),\lambda(\mu),\mu) = 0\,, \tag{2.32}$$

known as the Callan-Symanzik equation [128–130]. It expresses the variation of the renormalized vertex function $\Gamma^{(n)}$ under a change of μ. Note that in a theory with several couplings and fields there are a *beta function* for each coupling similar to $\beta(\lambda)$ and an *anomalous dimension* (γ) for each field (and mass). These quantities encode the response of the couplings and parameters to a change of the renormalization scale μ and they strongly depend on the theory. It is important to note that this equation is independent of perturbation theory even though our previous discussion on renormalization were based on a perturbative treatment. Because of this property, it is possible to use the renormalization group equation to study the proper asymptotic behaviour of Green's functions for large external momenta. Solving the Callan-Symanzik equation one can see that the asymptotic behaviour of the vertex function is governed by the evolution of the mass, coupling as well as anomalous dimension with the scale μ, that is to say, γ_m, $\beta(\lambda)$ and γ.

Beta function

Let us finish this section by looking at the beta function of λ in our ϕ^4 example. From Eq. (2.24) we have

$$\lambda = \tilde{\lambda}\left(1 + \frac{\tilde{\lambda}}{32\pi^2}3\Delta\right) . \tag{2.33}$$

When continuing the theory in d-dimensions, the parameters $\lambda, \tilde{\lambda}$ acquire a mass dimension μ_0^{4-d}, μ^{4-d} of which μ_0 is fixed while μ is identified with the renormalization scale of dimensional regularization. To make this dependence explicit in Eq. (2.33), we introduce two temporary dimensionless parameters $\lambda_0, \tilde{\lambda}_0$ such that $\lambda = \mu_0^{2\varepsilon}\lambda_0$, $\tilde{\lambda} = \mu^{2\varepsilon}\tilde{\lambda}_0$. Expressing Eq. (2.7) in terms of λ_0 and $\tilde{\lambda_0}$ and differentiating with respect to μ we obtain

$$\begin{aligned}
\mu\frac{d}{d\mu}(\lambda_0) &= 0 \\
&= \mu d_\mu\left(Z_\lambda\tilde{\lambda}_0\left(\frac{\mu^2}{\mu_0^2}\right)^\varepsilon\right) \\
&= \mu d_\mu Z_\lambda\tilde{\lambda}_0\left(\frac{\mu^2}{\mu_0^2}\right)^\varepsilon + Z_\lambda\beta(\tilde{\lambda}_0)\left(\frac{\mu^2}{\mu_0^2}\right)^\varepsilon + Z_\lambda\tilde{\lambda}_0 2\varepsilon\left(\frac{\mu^2}{\mu_0^2}\right)^\varepsilon
\end{aligned} \tag{2.34}$$

leading to

$$\beta(\tilde{\lambda}_0) = -2\varepsilon\tilde{\lambda}_0 - \tilde{\lambda}_0\frac{\mu}{Z_\lambda}d_\mu Z_\lambda . \tag{2.35}$$

Applying Eq. (2.35) to our present case we find

$$\begin{aligned}
\beta(\tilde{\lambda}_0) &= -2\varepsilon\tilde{\lambda}_0 - \frac{1}{Z_\lambda}\tilde{\lambda}_0\frac{3\Delta}{32\pi^2}\beta(\tilde{\lambda}_0) \\
&= -2\varepsilon\tilde{\lambda}_0\left(1 - \frac{1}{Z_\lambda}\tilde{\lambda}_0\frac{3\Delta}{32\pi^2}\right) \\
&\overset{\varepsilon\rightrightarrows 0}{} \frac{3\tilde{\lambda}_0^2}{16\pi^2} .
\end{aligned} \tag{2.36}$$

As a consequence the beta function for the coupling parameter λ in ϕ^4 theory is positive. Believing in our simple 1-loop perturbative calculation we observe that conversely to what happens in QCD, the strength of the interaction is always increasing with the renormalization scale.

We have shown in the previous paragraphs that the beta functions (along with the anomalous dimensions) are very important objects of a field theory since they tell us how the parameters will be affected by quantum corrections. With their knowledge, one can study the asymptotic behaviour of the theory by solving the Callan-Symanzik equation.

2.3 Renormalization group equations for a general gauge theory

We have seen in the previous sections the importance of the renormalization group equations for studying the evolution of the parameters of the theory via the example of the

massive scalar theory. We now review how the concepts that we have just introduced are applied to the case of a general gauge field theory to derive the set of evolution equations that dictates the behaviour of the parameters under a change of the renormalization scale μ. These equations form the main object of the implementation in a computer code that will be described in the next section.

The equations presented here are the results of various calculations mainly carried out in the 70's and 80's. Along the years, the computation of coefficients in the renormalization group equations in perturbation theory has been done for several renormalizable quantum field theories. For instance, the QCD beta functions have been calculated at the one- [131–133], two- [134–136], three- [137,138] and finally four-loop [139,140] level. In a scalar theory with self interaction a series of calculation [141,142] have lead to the four-loop beta function for the scalar quartic coupling. For a general renormalizable gauge theory involving scalars, spin-1/2 fermions and vector gauge fields the results for the beta functions were given in [143] at the one-loop level. The various contributions to the evolution equations for the coupling constants at two-loop were finalized in [110–112,114,115].

We start this section by giving some details on how the calculation is performed. Then, we briefly introduce the background field method which is used to calculate the beta functions of the gauge couplings. The RGEs for the Yukawa couplings as well as the quartic terms are discussed. The evolution equations for mass terms and trilinear couplings are also reviewed. Finally, the extension to semi-simple gauge groups is also discussed before concluding with some remarks regarding the SUSY renormalization group equations.

2.3.1 Definitions

We first review the set up of Machacek and Vaughn [110] and the way they extracted the beta functions since the RGEs implemented in our code follow their results[14].

Notations and definitions

The Lagrangian for a general renormalizable gauge field theory with gauge fields A_μ^α associated to a compact simple group $\mathcal{G}$, scalar fields ϕ_a and two component fermion fields ψ_j can be written in the form

$$\mathcal{L} = \mathcal{L}_0 + \mathcal{L}_1 + \mathcal{L}_{\rm GF} + \mathcal{L}_{FP}\,, \tag{2.37}$$

where $\mathcal{L}_{\rm GF}$ and $\mathcal{L}_{FP}$ are the parts corresponding to the gauge fixing and to the ghosts for a general R_ξ gauge[15] [144,145]. $\mathcal{L}_0$ contains all the dimensionless parameters while $\mathcal{L}_1$ contains the remaining dimensionful parameters. They take the form

$$\begin{aligned}\mathcal{L}_0 &= -\frac{1}{4}F^\alpha_{\mu\nu}F^{\mu\nu}_\alpha + \frac{1}{2}D^\mu\phi_a D_\mu\phi_a + i\psi_j^\dagger\sigma^\mu D_\mu\psi_j \\ &- \frac{1}{2}\left(Y^a_{jk}\psi_j\zeta\psi_k\phi_a + \text{h.c.}\right) - \frac{1}{4!}\lambda_{abcd}\phi_a\phi_b\phi_c\phi_d\,, \qquad (2.38)\\ \mathcal{L}_1 &= -\frac{1}{2}\left[(m_f)_{jk}\,\psi_j\zeta\psi_k + \text{h.c.}\right] - \frac{m^2_{ab}}{2}\phi_a\phi_b - \frac{h_{abc}}{3!}\phi_a\phi_b\phi_c\,, \qquad (2.39)\end{aligned}$$

[14] Once proper corrections pointed out along the years have been taken into account.
[15] We will not need the explicit expression for these terms.

in which $\zeta = \pm i\sigma_2$ is the spinor metric. The definition of the gauge field strengths is as follows

$$F^{\alpha}_{\mu\nu} = \partial_\mu A^{\alpha}_{\nu} - \partial_\nu A^{\alpha}_{\mu} + g f^{\alpha\beta\gamma} A^{\beta}_{\mu} A^{\gamma}_{\nu} \,, \tag{2.40}$$

with g the gauge coupling and $f^{\alpha\beta\gamma}$ the structure constants of $\mathcal{G}$. In the R_ξ gauge the gauge field propagator reads

$$D^{\alpha\beta}_{\mu\nu}(k) = \delta^{\alpha\beta} \frac{i}{k^2} \left(-g_{\mu\nu} + (1-\xi) \frac{k_\mu k_\nu}{k^2} \right) . \tag{2.41}$$

Finally, the covariant derivatives for the matter fields are given by

$$D_\mu \phi_a = \left(\partial_\mu \delta_{ab} - i g \theta^{\alpha}_{ab} A^{\alpha}_{\mu} \right) \phi_b \tag{2.42}$$

$$D_\mu \psi_j = \left(\partial_\mu \delta_{jk} - i g t^{\alpha}_{jk} A^{\alpha}_{\mu} \right) \psi_k \,. \tag{2.43}$$

The matrices t^α, θ^α are the hermitian matrix representations for the group generators acting on the fermions and scalars respectively. The scalars are assumed to be real, hence, from the gauge transformation on the scalar fields

$$\begin{aligned} \phi'_a &= e^{i\gamma^\alpha \theta^{\alpha}_{ab}} \phi_b \,, \\ (\phi'_a)^* = \phi'_a &= e^{-i\gamma^\alpha \left(\theta^{\alpha}_{ab}\right)^*} \phi_b \,, \end{aligned} \tag{2.44}$$

which leads to the relation

$$e^{i\gamma^\alpha \left(\theta^{\alpha}_{ab} + (\theta^{\alpha}_{ab})^*\right)} = \delta_{ab} \,, \tag{2.45}$$

we conclude that the matrices θ^α are purely imaginary and since they are hermitian they must be anti-symmetric. This is an important point since, as we will see, these matrices are present in the expressions of the evolution equations for the parameters. This implies that such matrices must be constructed for each scalar field in the theory. Note, that the Pauli matrices do not satisfy this criterion. We will come back to this issue later on.

Beta functions and anomalous dimensions in dimensional regularization

In [110] the calculation of the various beta functions and anomalous dimensions was performed in dimensional regularization using the $\overline{\text{MS}}$ scheme. In order to derive the beta functions one needs to calculate the relevant renormalization constants that can be obtained from the divergent part of the relevant Feynman diagrams. We will start with $\{x_i\}$ the set of dimensionless parameters and show a relation analogous to Eq. (2.31) between the anomalous dimension/beta function and the corresponding renormalization constant within dimensional regularization. The RGEs for the parameters in $\mathcal{L}_1$ can then be inferred from those of the dimensionless parameters and we will investigate these later.

As we have already seen, in dimensional regularization, in order to keep the action dimensionless, the dimension of the parameters are no longer equal to their value in 4 space-time dimensions. By examining the various kinetic terms we can easily find the

dimensionality of the fields and parameters in d-dimension.

$$\begin{aligned}
[\psi_j] &= \frac{d-1}{2}, & [\phi_a] &= \frac{d-2}{2}, & \left[A^\alpha_\mu\right] &= \frac{d-2}{2}, \\
\left[Y^a_{ij}\right] &= d - 2\left(\frac{d-1}{2}\right) - \frac{d-2}{2} & [g] &= \frac{4-d}{2} & [\lambda_{abcd}] &= d - 4\left(\frac{d-2}{2}\right) \\
&= \frac{4-d}{2} = \varepsilon, & &= \varepsilon, & &= 4 - d = 2\varepsilon\,.
\end{aligned} \tag{2.46}$$

In view of Eq. (2.46), any renormalized parameter, $\tilde{x}_k$, is related to the bare one, x_k, through the relation

$$x_k \left(\frac{\mu}{\mu_0}\right)^{-\rho_k \varepsilon} = \tilde{x}_k Z_k = \tilde{x}_k + \sum_{n=1}^{\infty} a_k^{(n)}(x) \frac{1}{\varepsilon^n}\,. \tag{2.47}$$

According to Eq. (2.46) we see that $\rho_k = 1$ for the gauge and Yukawa coupling constants while $\rho_k = 2$ for the quartic coupling constants. The coefficients $a_k^{(n)}(x) \equiv a_k^{(n)}(\{x_i\})$ depend on the other parameters of the Lagrangian and are to be computed in perturbation theory. As in Eq. (2.31) we define the beta functions for the parameter $\tilde{x}_k$ by

$$\beta_k(x) = \mu \frac{d}{d\mu} \tilde{x}_k \Big|_{\varepsilon=0}\,. \tag{2.48}$$

Inserting Eq. (2.47) in Eq. (2.48) it is easy to derive the following relation

$$\begin{aligned}
\mu \frac{d}{d\mu} \tilde{x}_k &= \mu \frac{d}{d\mu} Z_k^{-1} x_k \left(\frac{\mu}{\mu_0}\right)^{-\rho_k \varepsilon} \\
&= -\tilde{x}_k \mu \frac{1}{Z_k} \frac{d}{d\mu} Z_k - \rho_k \varepsilon \tilde{x}_k\,,
\end{aligned} \tag{2.49}$$

which in the limit $\varepsilon \to 0$ gives

$$\beta_k(x) = -\tilde{x}_k \mu \frac{1}{Z_k} \frac{d}{d\mu} Z_k \Rightarrow \mu \frac{d}{d\mu} \tilde{x}_k = \beta_k(x) - \rho_k \varepsilon \tilde{x}_k\,. \tag{2.50}$$

We now differentiate Eq. (2.47) with respect to μ

$$-\rho_k \varepsilon \left(\tilde{x}_k + \sum_{n=1}^{\infty} a_k^{(n)} \frac{1}{\varepsilon^n}\right) = \mu \frac{d}{d\mu} \tilde{x}_k + \sum_{n=1}^{\infty} \sum_l \mu \frac{d\tilde{x}_l}{d\mu} \frac{\partial a_k^{(n)}}{\partial \tilde{x}_l} \frac{1}{\varepsilon^n}\,, \tag{2.51}$$

and collect the finite terms to obtain

$$\beta_k(x) = \sum_l \rho_l \tilde{x}_l \frac{\partial a_k^{(1)}}{\partial \tilde{x}_l} - \rho_k a_k^{(1)}\,, \tag{2.52}$$

where we used Eq. (2.50) to express $\mu \dfrac{d\tilde{x}_k}{d\mu}$ in terms of $\beta_k(x)$ and ρ_k. Therefore, the beta functions are determined by the single order pole in the expansion Eq. (2.47). Furthermore, it is easy to see that the following relation also holds

$$\left(\sum_l \rho_l \tilde{x}_l \frac{\partial}{\partial \tilde{x}_l} + 1\right) a_k^{(n+1)} = \sum_l \beta_l(x) \frac{\partial a_k^{(n)}}{\partial \tilde{x}_l} \quad n \geq 1\,, \tag{2.53}$$

indicating that the higher order poles are all determined by the lowest order pole. This provides a useful cross-check on the calculation.

Applying Eq. (2.52) to Eq. (2.23) we find

$$\beta(\tilde{\lambda}) \;=\; 2\tilde{\lambda}\frac{\partial}{\partial\tilde{\lambda}}\frac{3\Delta\tilde{\lambda}^2}{32\pi^2} - 2\frac{\tilde{\lambda}^2\Delta}{32\pi^2} = \frac{3\tilde{\lambda}^2}{16\pi^2}\,, \tag{2.54}$$

in agreement with our previous result Eq. (2.36). Finally, we will write perturbatively at the two-loop level the various beta functions in the form

$$\beta_{\tilde{x}_k}(x) = \frac{1}{(4\pi)^2}\beta^{(1)}_{\tilde{x}_k} + \frac{1}{(4\pi)^4}\beta^{(2)}_{\tilde{x}_k}\,. \tag{2.55}$$

In order to extract the anomalous dimensions of the various fields we proceed in a similar way and start by writing the wave function renormalization constant of the i-th field, Z_i as an expansion in powers of $1/\varepsilon$

$$Z_i = 1 + \sum_{n=1}^{\infty} C_i^{(n)}\frac{1}{\varepsilon^n}\,. \tag{2.56}$$

Following the convention set in Eq. (2.31) we define the corresponding anomalous dimension by

$$\gamma_i = \frac{1}{2}\mu\frac{d}{d\mu}\ln Z_i\,. \tag{2.57}$$

Performing the derivation and inserting the definition of Z_i, Eq. (2.56), and using Eq. (2.50) we find by equating the finite terms

$$\gamma_i = -\frac{1}{2}\sum_l \rho_l\tilde{x}_l\frac{\partial C_i^{(1)}}{\partial\tilde{x}_l}\,, \tag{2.58}$$

which shows, as for the coupling constants, that the anomalous dimension is entirely determined, order by order, by the lowest pole[16].

We conclude by giving a very useful relation that allows us to avoid performing explicitly the derivation in Eq. (2.58). Indeed, it is easy to see that for the N-loop contribution to $C_i^{(n)}$ one has

$$\sum_l \rho_l\tilde{x}_l\left.\frac{\partial C_i^{(n)}}{\partial\tilde{x}_l}\right|_{N-\text{loop}} = 2NC_i^{(n)}\,. \tag{2.59}$$

It is clear that the strategy to obtain the evolution equations for the couplings as well as the anomalous dimensions of the fields to two-loop order is to evaluate the relevant dimensionally regularized Feynman diagrams to this order, extract the coefficient of the single pole of the corresponding renormalization constants and use Eq. (2.58) and Eq. (2.52). For the beta functions of the gauge coupling it was shown that the *background field* method is much more suited for this kind of computation and we now review its main advantages and characteristics.

[16] A relation similar to Eq. (2.53) can be derived for the anomalous dimensions.

2.3.2 Background field method

Before concluding this section we review the formalism of the *Background field method* (BFM) which greatly simplifies the derivation of the gauge couplings beta functions.

The BFM [146–153] is an approach in which the explicit gauge invariance is preserved even after the introduction of gauge-fixing and ghost terms. This contrasts with the classical approach where the gauge invariance of the classical Lagrangian is no longer manifest once quantum corrections are included. Thus in the background field approach, even unphysical quantities such as the divergent counter-terms are gauge invariant. Calculation in the BFM are thus easier both technically and conceptually. In order to keep the discussion simpler we assume a pure Yang-Mills theory. There is no obstacles to then, add fermions and scalars [115, 154, 155].

The basic idea of the BFM is to split the gauge field into an arbitrary background field $\hat{A}^a_\mu$ and a quantum field A^a_μ which is the variable of integration in the functional integral. After a gauge has been fixed, gauge invariance is preserved only in terms of $\hat{A}^a_\mu$. Therefore, in the background field approach it is desirable to work with background field Green's functions only since they are the one which retain explicit gauge invariance. Moreover, it can be shown that the renormalization even beyond one-loop can be carried out only in terms of the background fields, the quantum fields do not need to be renormalized [156]. In this setup, only the gauge coupling constant and background field need to be renormalized[17] which can be done by simply calculating the two-point function of the $\hat{A}^a_\mu$ field.

Due to the explicit gauge invariance retained in this approach, one can relate the beta function of the gauge coupling constant to the anomalous dimension of the background field. Consequently, the gauge couplings beta functions can be calculated from two-point functions, without the need to calculate vertex corrections as in the conventional approach. Indeed, for example in QCD, denoting Z_3, $\tilde{Z}_3$, Z_2, Z_m and Z_g the renormalization constants of the gluon, ghost, quark fields, and the mass and coupling parameters respectively, the two-point functions of the gauge, ghost and quark fields allow to determine Z_3, $\tilde{Z}_3$, Z_2 and Z_m. However, to obtain information on Z_g one has to at least calculate one of the three-point functions and then extract Z_g in the following way [125]

$$\begin{aligned} \text{Triple gluon vertex} &\Rightarrow Z_1 \equiv Z_g Z_3^{3/2}\,, \\ \text{Gluon-quark vertex} &\Rightarrow Z_{1\text{F}} \equiv Z_g Z_2 Z_3^{1/2}\,, \\ \text{Gluon-ghost vertex} &\Rightarrow \tilde{Z}_1 \equiv Z_g \tilde{Z}_3 Z_3^{1/2}\,, \end{aligned} \tag{2.60}$$

(2.61)

where $\Rightarrow$ means that the three-point function gives access to the corresponding combination of renormalization constants. As a side remark, note that assuming that the Z_gs are all the same we then obtain the *Slavnov-Taylor identity* [157, 158]

$$\frac{Z_1}{Z_3} = \frac{\tilde{Z}_1}{\tilde{Z}_3} = \frac{Z_{1\text{F}}}{Z_2}\,, \tag{2.62}$$

which guarantees the universality of the renormalized coupling constant. Hence, the background field approach is much more efficient to calculate the beta function of the

[17] In principle, the gauge fixing parameter also needs to be renormalized but this can be avoided by going to the Landau-type background field gauge [156].

gauge coupling. Below we review the important results of the BFM and apply it to the calculation of the one-loop gauge coupling beta function in pure Yang-Mills theory.

Calculations in the BFM

The functional integral for the gauge field in the conventional approach is given by

$$Z[J] = \int [dA] \det M_G \exp\left\{ i \int d^4x \left(\mathcal{L} - \frac{1}{2\xi}(G^a)^2 + A^a_\mu J^{a\mu} \right) \right\} , \tag{2.63}$$

in which the integration is over the measure $[dA] \equiv \Pi_{\mu,a}[dA^a_\mu]$, $(M_G)_{ab} = \dfrac{\delta G^a_\mu}{\delta \theta^b}$ is the derivative of the gauge-fixing term under an infinitesimal gauge transformation defined by

$$\delta A^a_\mu = f^{abc}\theta^b A^c_\mu - \frac{1}{g}\partial_\mu \theta^a \, . \tag{2.64}$$

The Lagrangian is simply $-\frac{1}{4}F^{a\mu\nu}F^a_{\mu\nu}$ with $F^a_{\mu\nu} = \partial_\mu A^a_\nu - \partial_\nu A^a_\mu + g f^{abc} A^b_\mu A^c_\nu$. We have already used in the previous section the effective action which is obtained by the Legendre transformation

$$\Gamma[v] = W[J] - \int d^4x J^{a\mu} v^a_\mu, \;\; W[J] = -i \ln Z[J], \;\; v^a_\mu = \frac{\delta W[J]}{\delta J^a_\mu} \, , \tag{2.65}$$

which derivatives with respect to v are the vertex functions. One can define analogous quantities in the BFM where $A^a_\mu \to \hat{A}^a_\mu + A^a_\mu$. However, in this approach the background field is not coupled to the source J, we thus introduce

$$\hat{Z}[J, \hat{A}] = \int [dA] \det M_G \exp\left\{ \int d^4x \left(\mathcal{L}(\hat{A}^a_\mu + A^a_\mu) - \frac{1}{2\xi}(G^a)^2 + A^a_\mu J^{a\mu}) \right) \right\} , \tag{2.66}$$

where the gauge transformation parameter θ^a is defined by

$$\delta A^a_\mu = f^{abc}\theta^b(\hat{A}^c_\mu + A^c_\mu) - \frac{1}{g}\partial_\mu \theta^a \, . \tag{2.67}$$

In addition, similar to $W[J]$ and $\Gamma[v]$ we define $\hat{W}[J, \hat{A}]$ and $\hat{\Gamma}[\hat{v}, \hat{A}]$

$$\hat{W}[J, \hat{A}] = -i \ln \hat{Z}[J, \hat{A}], \;\; \hat{\Gamma}[\hat{v}, \hat{A}] = \hat{W}[J, \hat{A}] - \int d^4x J^{a\mu} \hat{v}^a_\mu, \;\; \hat{v}^a_\mu = \frac{\delta \hat{W}[J, A]}{\delta J^a_\mu} \, . \tag{2.68}$$

Fixing the background gauge condition to

$$G^a = \left(\partial_\mu \delta^{ac} + g f^{abc} A^b_\mu \right) \hat{A}^{c\mu} \, , \tag{2.69}$$

one can show [156] that the BFM effective action $\hat{\Gamma}[\hat{v}, \hat{A}]$ is invariant under the following set of infinitesimal transformations

$$\delta \hat{A}^a_\mu = f^{abc}\theta^b \hat{A}^c_\mu - \frac{1}{g}\partial_\mu \theta^a \, , \tag{2.70}$$

$$\delta \hat{v}^a_\mu = f^{abc}\theta^b \hat{v}^c_\mu \, . \tag{2.71}$$

Consequently, $\hat{\Gamma}[0,\hat{A}]$ is explicitly gauge invariant since the gauge transformation in Eq. (2.70) is just an ordinary gauge transformation for the background field. $\hat{\Gamma}[0,\hat{A}]$ is what is computed in the BFM. It can be related to the conventional effective action $\Gamma[v]$ by

$$\hat{\Gamma}[0,\hat{A}] = \Gamma[v]|_{v=\hat{A}}\,, \tag{2.72}$$

where the effective action in the BFM $\hat{\Gamma}[0,\hat{A}]$ is computed in the gauge Eq. (2.69) while the conventional effective action, $\Gamma[v]$, has to be evaluated with the following gauge fixing term

$$G^a = \partial_\mu A^{a\mu} - \partial_\mu \hat{A}^{a\mu} + g f^{abc} \hat{A}^b_\mu A^{c\mu}\,. \tag{2.73}$$

In general, the vertex functions calculated from the effective action in the gauge of Eq. (2.73) will look very different from the one in the conventional approach and normal gauges, however, Eq. (2.72) assures us that every gauge independent physical quantity will be exactly the same, making it possible to use the BFM to simplify the calculation.

Finally, because explicit gauge invariance is preserved in the BFM, the renormalization constants $Z_{\hat{A}}$, Z_g of the background field and coupling constant respectively are related. Indeed, the divergences appearing in the effective action $\hat{\Gamma}[0,\hat{A}]$ must take an explicit gauge invariant form and are therefore proportional to $F^a_{\mu\nu}F^{a\mu\nu}$ times a divergent constant. Since the renormalized field strengths $\tilde{F}^a_{\mu\nu}$ reads

$$\tilde{F}^a_{\mu\nu} = Z_{\hat{A}}^{-1/2}\left(\partial_\mu \hat{A}^a_\nu - \partial_\nu \hat{A}^a_\mu + g Z_g^{-1} Z_{\hat{A}}^{-1/2} f^{abcd} \hat{A}^b_\mu \hat{A}^c_\nu\right)\,, \tag{2.74}$$

it will only take the form of a constant times $F^a_{\mu\nu}$ if $Z_g = Z_{\hat{A}}^{-1/2}$. Consequently, from Eq. (2.58) we deduce the relation between the anomalous dimension of the background gauge field and the beta function of the gauge coupling in Yang-Mills theory

$$\beta_g = g\gamma_{\hat{A}} = -\frac{1}{2} g^2 \frac{\partial C^{(1)}_{\hat{A}}}{\partial g}\,, \tag{2.75}$$

in which in analogy to Eq. (2.56) we have written

$$Z_{\hat{A}} = 1 + \sum_{n=1}^{\infty} C^{(n)}_{\hat{A}} \frac{1}{\varepsilon^n}\,. \tag{2.76}$$

Example of a calculation in BFM: gauge coupling beta function in Yang-Mills theory

As an illustrative example we now show how the beta function for the gauge coupling parameter in pure Yang-Mills theory can be obtained in the background field method. For that we first need the Feynman rules that can be obtained in the usual way from the Lagrangian. Since we put $A = 0$ in Eq. (2.72) there is no gauge field on the external lines. Because, the integration in the functional integral is only over the quantum field, A, the background fields do not appear in the loops. In Fig 2.3, we show only the modified and new vertices in the BFM, taking all momenta as incoming and indicating background fields by a hat over the group indices.

It is then easy to see that there are only two diagrams that contribute to the two-point function of the background field, see Fig. 2.4: (i) the ghost loop, diagram (a), (ii) and the

gauge field loop, diagram (b). Using the Feynman rules given above one can write down the expression for diagram (a)

$$\begin{aligned} i\hat{\Gamma}^{\rm FP}_{\mu\nu} &= (-1)g^2\mu^{4-d}f^{dbc}f^{cad}\int\frac{d^dk}{(2\pi)^d}\frac{(2k_\mu+q_\mu)(2k_\nu+q_\nu)}{k^2(k+q)^2} \\ &= -g^2\mu^{2\varepsilon}\delta^{ab}C_2(\mathcal{G})\int\frac{d^dk}{(2\pi)^d}\frac{4k_\mu k_\nu+2q_\mu k_\nu+2q_\nu k_\mu+q_\mu q_\nu}{k^2(k+q)^2}\,, \end{aligned} \tag{2.77}$$

in which

$$\begin{aligned} \int\frac{\mu^{2\varepsilon}d^dk}{(2\pi)^d}\frac{k_\mu k_\nu}{k^2(k+q)^2} &= \frac{i\pi^2}{(2\pi)^4}B_{\mu\nu}(q;m_1=0,m_2=0) \\ &= -\frac{i\pi^2}{(2\pi)^4}\frac{\Gamma(1-\varepsilon)^2\Gamma(\varepsilon)}{4\Gamma(2-2\varepsilon)}\left(\frac{4\pi\mu^2}{-q^2}\right)^\varepsilon\left(\frac{1}{d-1}(q^2g_{\mu\nu}-q_\mu q_\nu)-q_\mu q_\nu\right)\,, \end{aligned} \tag{2.78}$$

$$\begin{aligned} \int\frac{\mu^{2\varepsilon}d^dk}{(2\pi)^d}\frac{q_\mu k_\nu}{k^2(k+q)^2} &= \frac{i\pi^2}{(2\pi)^4}q_\mu B_\nu(q;m_1=0,m_2=0) \\ &= -\frac{i\pi^2}{(2\pi)^4}\frac{1}{2}\left(\frac{4\pi\mu^2}{-q^2}\right)^\varepsilon\frac{\Gamma(1-\varepsilon)^2\Gamma(\varepsilon)}{\Gamma(2-2\varepsilon)}q_\mu q_\nu\,, \end{aligned} \tag{2.79}$$

$$\begin{aligned} \int\frac{\mu^{2\varepsilon}d^dk}{(2\pi)^d}\frac{1}{k^2(k+q)^2} &= \frac{i\pi^2}{(2\pi)^4}B_0(q;m_1=0,m_2=0) \\ &= \frac{i\pi^2}{(2\pi)^4}\frac{\Gamma(1-\varepsilon)^2\Gamma(\varepsilon)}{\Gamma(2-2\varepsilon)}\left(\frac{4\pi\mu^2}{-q^2}\right)^\varepsilon\,. \end{aligned} \tag{2.80}$$

Our conventions for the definition of the tensor and scalar integrals $B_{\mu\nu}$, B_μ, B_0 are given in the Appendix B. Summing Eqs. (2.78, 2.79, 2.80), longitudinal terms (terms proportional to only $q_\mu q_\nu$) cancel leaving only the transverse terms

$$i\hat{\Gamma}^{\rm FP}_{\mu\nu} = g^2\delta^{ab}C_2(\mathcal{G})\frac{i\pi^2}{(2\pi)^4}\frac{\Gamma(1-\varepsilon)^2\Gamma(\varepsilon)}{\Gamma(2-2\varepsilon)}\left(\frac{4\pi\mu^2}{-q^2}\right)^\varepsilon\frac{1}{3}\left(q^2g_{\mu\nu}-q_\mu q_\nu\right)\,. \tag{2.81}$$

To extract the anomalous dimension of the background field, only the divergent part of the two-point functions is required. Expending the Eq. (2.81) in Laurent series

$$\Gamma(1-\varepsilon)^2 = 1+\mathcal{O}(\varepsilon),\ \Gamma(2-2\varepsilon)^{-1}=1+\mathcal{O}(\varepsilon),\ \Gamma(\varepsilon)=\frac{1}{\varepsilon}-\gamma_E+\mathcal{O}(\varepsilon)\,, \tag{2.82}$$

$$\hat{\Gamma}^{\rm FP}_{\mu\nu} = \left(\frac{1}{3\varepsilon}\right)\delta^{ab}C_2(\mathcal{G})\frac{g^2}{(4\pi)^2}\left(q^2g_{\mu\nu}-q_\mu q_\nu\right)+\mathcal{O}(\varepsilon)\,, \tag{2.83}$$

we obtain the contribution of the ghost loop to the divergent part of the two-point function. Diagram (b) is calculated in the exact same way and yields

$$\hat{\Gamma}^{\rm VV}_{\mu\nu} = \left(\frac{10}{3\varepsilon}\right)C_2(\mathcal{G})\delta^{ab}\frac{g^2}{(4\pi)^2}\left(q^2g_{\mu\nu}-q_\mu q_\nu\right)+\mathcal{O}(\varepsilon)\,. \tag{2.84}$$

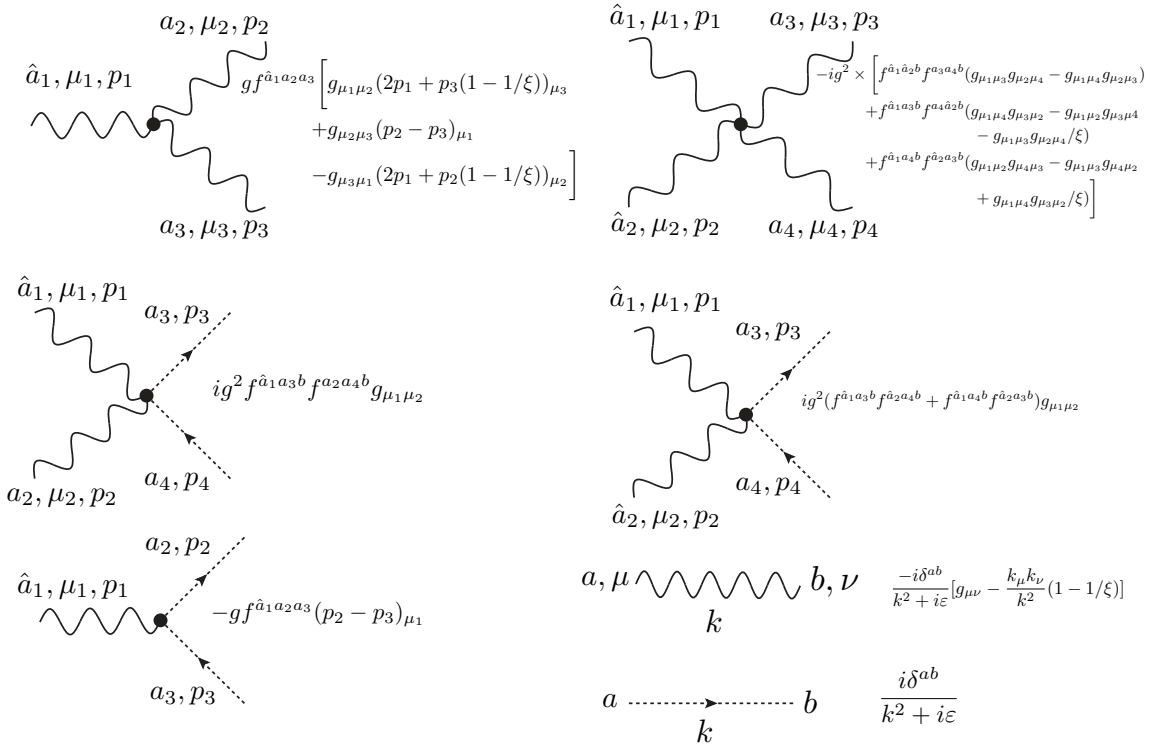

Figure 2.3: Modified vertices with respect to the conventional approach in the BFM. All the momenta have been taken incoming.

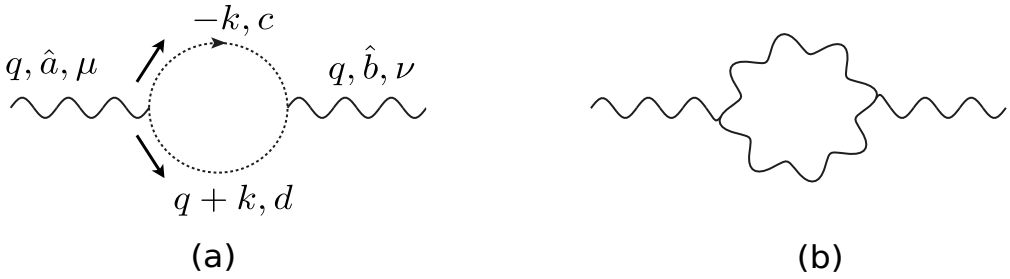

Figure 2.4: Diagrams contributing to the two-point function of the background field in pure Yang-Mills theory. The caret reminds us that the external field is the background field.

In the conventional approach, in contrast to the BFM case, diagram (a) and (b) exhibit longitudinal contributions that cancel against each other. Adding $\hat{\Gamma}^{\rm FP}_{\mu\nu}$ and $\hat{\Gamma}^{\rm VV}_{\mu\nu}$ we determine $Z_{\hat{A}}$ and hence the one-loop beta function of the gauge coupling

$$Z_{\hat{A}} = 1 + \frac{g^2}{(4\pi)^2} C_2(\mathcal{G}) \frac{11}{3\varepsilon}, \;\; \beta_g = -C_2(\mathcal{G}) \frac{g^3}{(4\pi)^2} \frac{11}{3} \,. \tag{2.85}$$

Finally, it can be shown that the Feynman rules involving fermions in the BFM are identical to the ones in the conventional approach, therefore to include the effect of fermions in the above result one only has to add the conventional results for the fermion loop, we refer the interested reader to [154] for details.

2.3.3 Wave function renormalization

Going back to the general gauge field theory introduced in Section 2.3.1, we are now in a position to present the results for the various RGEs that are implemented in PyR@TE (Section 2.4). The results of this section take into account all the typos and mistakes of the original papers that have been reported in the literature, these are nicely summarized in [159].

We denote Z_S^{ab} and Z_F^{ij} the wave function renormalization matrices for the scalar and fermion fields. The contribution of a diagram to the divergent part of Z_S^{ab}, and Z_F^{ij} respectively can be written perturbatively in the form

$$(Z_{i_1 i_2})^{-1} = \frac{1}{(4\pi)^2} S^{(1)}_{i_1 i_2} \left(A^{(1)}\Delta + B^{(1)}\Delta^2 \right) + \frac{1}{(4\pi)^4} S^{(2)}_{i_1 i_2} \left(A^{(2)}\Delta + B^{(2)}\Delta^2 \right) , \tag{2.86}$$

where $Z_{i_1 i_2}$ can be one of the two wave function renormalization quantity, Z_S^{ab}, Z_F^{ij}, and Δ is the usual $\overline{\text{MS}}$ expansion parameter as introduced in Eq. (2.13). $S^{(1),(2)}_{i_1 i_2}$ are group theoretic factors associated with the corresponding diagrams at one- and two-loop order respectively. The anomalous dimensions for the scalar and fermion fields, γ_S^{ab}, γ_F^{ij}, are respectively obtained from Z_S^{ab}, Z_F^{ij}, using Eqs. (2.58, 2.59), and read

$$\gamma_{i_1 i_2} = \sum_{\text{diag}} \left(\frac{1}{(4\pi)^2} A^{(1)} S^{(1)}_{i_1 i_2} + \frac{2}{(4\pi)^4} A^{(2)} S^{(2)}_{i_1 i_2} \right) , \tag{2.87}$$

where the minus sign between Eq. (2.86) and Eq. (2.87) disappears because of the fact that we expand $Z^{-1}_{i_1 i_2}$ rather than Z_{i_1, i_2}. We now give in turn the results for the two anomalous dimensions as well as with some example diagrams[18] for the two-loop order. Note that some details will be given on how to interpret the various group factors in Section 2.4.1.

Scalar anomalous dimension

Example diagrams contributing to the scalar anomalous dimension are shown in Fig. 2.5 and their respective values, $A^{(2)}$, $S^{(2)}_{ab}$ in Tab. 2.1. The diagram (a) groups three contributions depending on the nature of the inside loop: bosonic (GB), fermionic (Ferm.), scalar (Sca.).

In a general gauge theory the anomalous dimension depends not only on g but on many different couplings, e.g. λ, Y. The first line of Fig. 2.5 shows some contributions proportional to g^4 (diagrams (a) and (b)) while line 2 and 3 (diagrams (c), (d), (e)) contains contributions proportional to λ^2, $Y^2 g^2$ and Y^4. The various expressions for $A^{(2)}$ of Tab. 2.1 are not gauge invariant. However, properly combined with the anomalous dimension for the fermions (also gauge dependent, see below) and the corresponding vertex corrections, the Yukawa and quartic coupling constant will be gauge invariant, see Sections 2.3.4 and 2.3.5 below.

[18] Solid lines are fermions, dashed lines represent scalars and wavy lines gauge bosons.

Finally, we reproduce the full result for the anomalous dimension of the scalar field [159]

$$
\begin{aligned}
(\gamma_{ab}^{S})^{(1)} \equiv A^{(1)} S_{ab}^{(1)} &= 2\kappa Y_2^{ab}(S) - g^2(3-\xi) C_2^{ab}(S)\,, && (2.88)\\
(\gamma_{ab}^{S})^{(2)} \equiv 2A^{(2)} S_{ab}^{(2)} &= -g^4 C_2^{ab}(S)\left[\left(\frac{35}{3} - 2\xi - \frac{1}{4}\xi^2\right) C_2(\mathcal{G}) - \frac{10}{3}\kappa S_2(F) - \frac{11}{12} S_2(S)\right] \\
&+ \frac{1}{2}\Lambda_{ab}^2(S) + \frac{3}{2} g^4 C_2^{ac}(S) C_2^{cb}(S) - 3\kappa H_{ab}^2(S) - 2\kappa \bar{H}_{ab}^2(S) \\
&+ 10\kappa g^2 Y_{ab}^{2\mathrm{F}}(S)\,, && (2.89)
\end{aligned}
$$

where $\kappa = 1/2(1)$ for two(four)-component fermions, and

$$
\begin{aligned}
H_{ab}^2(S) &= \frac{1}{2}\mathrm{Tr}\left(Y^a Y^{\dagger b} Y^c Y^{\dagger c} + Y^{\dagger a} Y^b Y^{\dagger c} Y^c\right)\,, \quad Y_{ab}^{2\mathrm{F}}(S) = \frac{1}{2}\mathrm{Tr}\left(C_2(F)(Y^a Y^{\dagger b} + Y^b Y^{\dagger a})\right)\,, \\
\bar{H}_{ab}^2(S) &= \frac{1}{2}\mathrm{Tr}\left(Y^a Y^{\dagger c} Y^b Y^{\dagger c} + Y^{\dagger a} Y^c Y^{\dagger b} Y^c\right)\,, \quad \Lambda_{ab}^2(S) = \frac{1}{6}\lambda_{acde}\lambda_{bcde}\,. \qquad (2.90)
\end{aligned}
$$

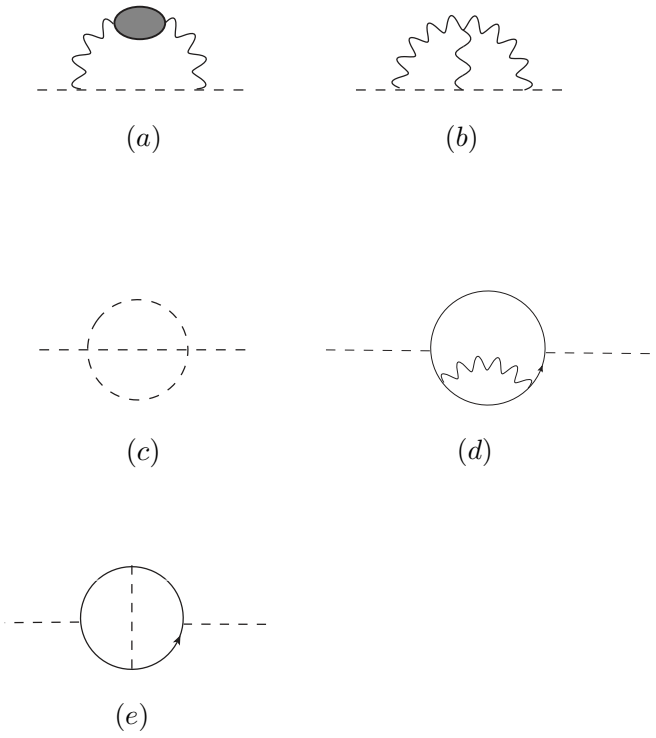

Figure 2.5: Example two-loop diagrams contributing to the anomalous dimension of the scalars.

Fermion anomalous dimension

Again, we show some example diagrams that contribute to the two-loop order anomalous dimension of the fermion fields and their corresponding contributions in Fig. 2.6 and Tab. 2.2. As stated in the previous paragraph the anomalous dimension of the fermion fields depends on the gauge parameter ξ. The full result to one- and two-loop reads

Table 2.1: Contributions $A^{(2)}$, $S^{(2)}_{ab}$ corresponding to the diagrams in Fig. 2.5. For diagram (a) we have split the contribution depending on the nature of the inside loop: bosonic (GB), fermionic (Ferm.), scalar (Sca.).

Diagram	$S^{(2)}_{ab}$	$A^{(2)}$
(a)	$(S^{(2)}_{\text{GB}})_{ab} = -g^4 C_2(S)\delta_{ab} C_2(\mathcal{G})$	$A^{(2)}_{\text{GB}} = \frac{4}{3} + \frac{11}{8}\xi + \frac{3}{8}\xi^2$
	$(S^{(2)}_{\text{Ferm.}})_{ab} = -g^4 C_2(S)\delta_{ab} 40\kappa S_2(F)$	$A^{(2)}_{\text{Ferm.}} = -\frac{5}{3}$
	$(S^{(2)}_{\text{Sca.}})_{ab} = -g^4 C_2(S)\delta_{ab} S_2(S)$	$A^{(2)}_{\text{Sca.}} = -\frac{11}{24}$
(b)	$\delta_{ab}\frac{1}{2} g^4 C_2(S) C_2(\mathcal{G})$	$-\frac{63}{8} + \frac{15}{4}\xi + 2\xi^2$
(c)	$\frac{1}{6}\lambda_{acde}\lambda_{bcde}$	$\frac{1}{4}$
(d)	$\kappa\delta_{ab} g^2 \frac{1}{2}\text{Tr}\left(C_2(F)(Y^a Y^{\dagger b} + Y^b Y^{\dagger a})\right)$	$-\xi$
(e)	$\kappa\delta_{ab}\frac{1}{2}\text{Tr}\left(Y^a Y^{\dagger c} Y^b Y^{\dagger c} + Y^{\dagger a} Y^c Y^{\dagger b} Y^c\right)$	-1

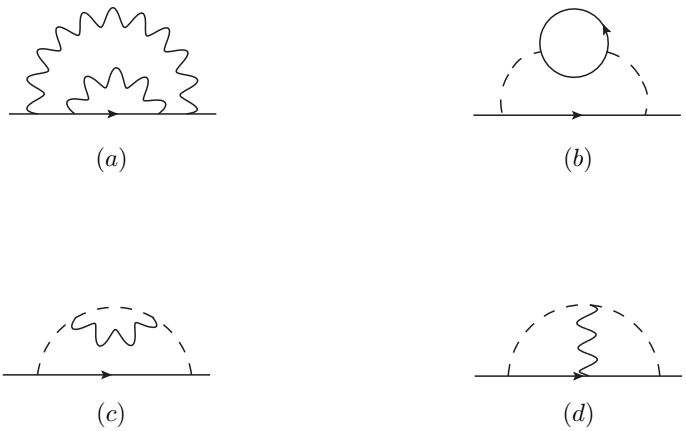

Figure 2.6: Example diagrams contributing to the two-loop anomalous dimension of the fermion fields.

$$
\begin{aligned}
(\gamma^{\text{F}}_{ij})^{(1)} \equiv A^{(1)} S^{(1)}_{ij} &= \frac{1}{2}(Y^a Y^{\dagger a})_{ij} + g^2 C_2(F)_{ij}\xi\,, \\
(\gamma^{\text{F}}_{ij})^{(2)} \equiv 2A^{(2)} S^{(2)}_{ij} &= 18(Y^a Y^{\dagger b} Y^b Y^{\dagger a})_{ij} - \frac{3}{2}\kappa(Y^a Y^{\dagger b})_{ij} Y_2^{ab}(S) \\
&+ g^2\left[\frac{9}{2} C_2^{ab}(S)(Y^a Y^{\dagger b})_{ij} - \frac{7}{4}(C_2(F) Y^a Y^{\dagger a})_{ij} - \frac{1}{4}(Y^a C_2(F) Y^{\dagger a})_{ij}\right] \\
&+ -g^4 C_2(F)_{ij}\left[\left(\frac{25}{4} + 2\xi + \frac{1}{4}\xi^2\right) C_2(\mathcal{G}) - 2\kappa S_2(F) - \frac{1}{4} S_2(S)\right] \\
&- \frac{3}{2} g^4 \left[C_2(F)\right]^2_{ij}\,. \qquad (2.91)
\end{aligned}
$$

The brackets $(\dots)_{ij}$ mean that we take the i, j element of the matrix delimited by the

Table 2.2: Contributions $A^{(2)}$, $S_{ij}^{(2)}$ corresponding to the diagrams in Fig. 2.6.

Diagram	$S_{ij}^{(2)}$	$A^{(2)}$
(a)	$g^4 \left[C_2(F)\right]_{ij}^2$	$-\frac{1}{4}\xi^2$
(b)	$\kappa(Y^a Y^{\dagger b})_{ij} \frac{1}{2}\mathrm{Tr}\left(Y^{\dagger a}Y^b + Y^{\dagger b}Y^a\right)$	$-\frac{3}{4}$
(c)	$g^2(Y^b Y^{\dagger a})_{ij} C_2(S)_{ab}$	$\frac{1}{8}(5+\xi)$
(d)	$g^2(Y^b t^\alpha Y^{\dagger a})_{ij}\theta^\alpha_{ba}$	$-\frac{1}{4}(6-\xi)$

dots. Note that the explicit dependence on θ^α and t^α of diagram (d) disappears in the final result.

Gauge coupling constant beta function

As discussed at length in Section 2.3.2 the beta function of the gauge coupling parameter is more efficiently calculated in the BFM, and we reproduce the two-loop result here for completeness, Eq. (2.92).

$$\begin{aligned}\beta(g) &= -\frac{g^3}{(4\pi)^2}\left\{\frac{11}{3}C_2(\mathcal{G}) - \frac{4}{3}\kappa S_2(F) - \frac{1}{6}S_2(S) + \frac{2\kappa}{(4\pi)^2}Y_4(F)\right\} \\ &- \frac{g^5}{(4\pi)^4}\left\{\frac{34}{3}\left[C_2(\mathcal{G})\right]^2 - \kappa\left[4C_2(F) + \frac{20}{3}C_2(\mathcal{G})\right]S_2(F)\right. \\ &\left. - \left[2C_2(S) + \frac{1}{3}C_2(\mathcal{G})\right]S_2(S)\right\}, \end{aligned} \tag{2.92}$$

where $Y_4(F)$ is defined through

$$Y_4(F) = \frac{1}{d(\mathcal{G})}\mathrm{Tr}\left(C_2(F)Y^a Y^{+a}\right) , \tag{2.93}$$

in which $d(\mathcal{G})$ is the dimension of the gauge group, i.e. the dimension of the adjoint representation.

2.3.4 Yukawa terms

The next result that we review here is the beta function for the Yukawa coupling. Following the definition for the renormalization matrix for the scalar, fermion and background fields, Eq. (2.86) we define

$$(Z_{aij})^{-1} = \frac{1}{(4\pi)^2}S^{(1)}_{aij}\left(A^{(1)}\Delta + B^{(1)}\Delta^2\right) + \frac{1}{(4\pi)^4}S^{(2)}_{aij}\left(A^{(2)}\Delta + B^{(2)}\Delta^2\right) . \tag{2.94}$$

We show some example diagrams of ladder topology that contribute to the renormalization of the Yukawa vertex in Fig. 2.7 along with their contribution to Z_{aij} in Tab. 2.3.

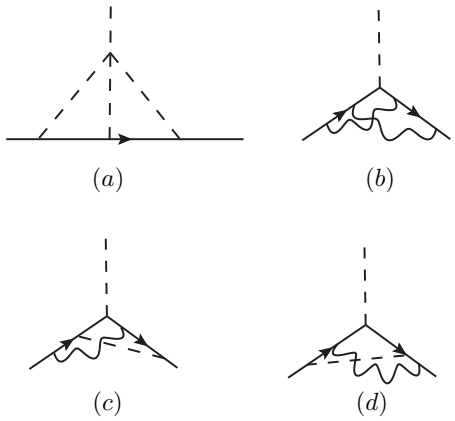

Figure 2.7: Example diagrams contributing to the two-loop anomalous dimension of the Yukawa vertex.

Table 2.3: Contributions $A^{(2)}$, $S^{(2)}_{aij}$ corresponding to the diagrams in Fig. 2.7.

Diagram	$S^{(2)}_{aij}$	$A^{(2)}$
(a)	$\lambda_{abcd}(Y^b Y^{\dagger c} Y^d)_{ij}$	-1
(b)	$(t^\beta t^\alpha Y^a t^\beta t^\alpha)_{ij}$	$(-3+6\xi+\xi^2)$
$(c)+(d)$	$(Y^b t^\alpha Y^{\dagger a} Y^b t^\alpha + t^\alpha Y^b Y^{\dagger a} t^\alpha Y^b)_{ij}$	$3-\xi$

The beta function for the Yukawa coupling constant is obtained as a combination of the anomalous dimension of the proper vertex correction, $\gamma^{Y^a}_{ij}$ obtained from Z_{aij}, the anomalous dimension of the scalar and fermion fields in the following way

$$\beta^a_{ij} \equiv \mu \frac{dY^a_{ij}}{d\mu} = \gamma^{Y^a}_{ij} + (\gamma^{\mathrm{F}\dagger} Y^a)_{ij} + (Y^a \gamma^{\mathrm{F}})_{ij} + \gamma^S_{ab} Y^b_{ij} \tag{2.95}$$

As already mentioned, all the gauge dependent parts on the right-hand side of Eq. (2.95)

cancel against each other to leave β^a_{ij} gauge invariant. Putting all these together leads to

$$
\begin{aligned}
(\beta^a_{ij})^{(1)} &= \frac{1}{2}\left[Y_2(F)^\dagger Y^a + Y^a Y_2(F)\right]_{ij} + 2(Y^b Y^{\dagger a} Y^b)_{ij} + 2\kappa Y^b_{ij} Y_2^{ab}(S) \\
&\quad -3g^2\{C_2(F), Y^a\}_{ij}\,, \qquad (2.96)\\
(\beta^a_{ij})^{(2)} &= 2(Y^c Y^{\dagger b} Y^a (Y^{\dagger c} Y^b - Y^{\dagger b} Y^c))_{ij} - \left(Y^b\left[Y_2(F)Y^{\dagger a} + Y^{\dagger a} Y_2^\dagger(F)\right]Y^b\right)_{ij} \\
&- \frac{1}{8}\left[Y^b Y_2(F) Y^{\dagger b} Y^a + Y^a Y^{\dagger b} Y_2^\dagger(F) Y^b\right]_{ij} - 4\kappa Y_2^{ac}(S)(Y^b Y^{\dagger c} Y^b)_{ij} - 2\kappa Y^b_{ij}\bar{H}^2_{ab}(S) \\
&- \frac{3}{2}\kappa Y_2^{bc}(S)(Y^b Y^{\dagger c} Y^a + Y^a Y^{\dagger c} Y^b)_{ij} - 3\kappa Y^b_{ij} H^2_{ab}(S) - 2\lambda_{abcd}(Y^b Y^{\dagger c} Y^d)_{ij} \\
&+ \frac{1}{2}\Lambda^2_{ab}(S) Y^b_{ij} + 3g^2\{C_2(F), Y^b Y^{\dagger a} Y^b\}_{ij} + 5g^2(Y^b\{C_2(F), Y^{\dagger a}\}Y^b)_{ij} \\
&- \frac{7}{4}g^2[C_2(F)Y_2^\dagger(F)Y^a + Y^a Y_2(F) C_2(F)]_{ij} + 6g^2(H^a_{2t})_{ij} + 10\kappa g^2 Y^b_{ij} Y^{2\mathrm{F}}_{ab}(S) \\
&- \frac{1}{4}g^2[Y^b C_2(F) Y^{\dagger b} Y^a + Y^a Y^{\dagger b} C_2(F) Y^b]_{ij} \\
&+ 6g^2[C_2^{bc}(S)(Y^b Y^{\dagger a} Y^c)_{ij} - 2C_2^{ac}(S)(Y^b Y^{\dagger c} Y^b)_{ij}] + 6g^4 C_2^{ab}(S)\{C_2(F), Y^b\}_{ij} \\
&+ \frac{9}{2}g^2 C_2^{bc}(S)(Y^b Y^{\dagger c} Y^a + Y^a Y^{\dagger c} Y^b)_{ij} - \frac{3}{2}g^4\{[C_2(F)]^2, Y^a\}_{ij} \\
&+ g^4\left[-\frac{97}{6}C_2(\mathcal{G}) + \frac{10}{3}\kappa S_2(F) + \frac{11}{12}S_2(S)\right]\{C_2(F), Y^a\}_{ij} \\
&- \frac{21}{2}g^4 C_2^{ab}(S) C_2^{bc}(S) Y^c_{ij} \\
&+ g^4 C_2^{ab}(S)\left[\frac{49}{4}C_2(\mathcal{G}) - 2\kappa S_2(F) - \frac{1}{4}S_2(S)\right] Y^b_{ij}\,, \qquad (2.97)
\end{aligned}
$$

where we have defined

$$
\begin{aligned}
Y_2(F) &= Y^{+a} Y^a\,, \qquad (2.98)\\
H^a_{2t} &= t^{\alpha *} Y^a Y^{\dagger b} t^{\alpha *} Y^b + Y^b t^\alpha Y^{\dagger b} Y^a t^\alpha\,. \qquad (2.99)
\end{aligned}
$$

It is a useful check of consistency to see that indeed the terms depending on the gauge parameter ξ cancel in the expression for β^a_{ij}. Also, we see that the matrices of the fermion representations, t^α appear in the final result making it necessary to apply this result to a specific model.

2.3.5 Quartic terms

The calculation of the beta function for the quartic coupling to two-loop order is quite involved with many diagrams contributing. Following the previous definitions of Z_{ab}, Z_{ij} and Z_{aij} we define the scalar quartic vertex renormalization Z_{abcd} by

$$
(Z_{abcd})^{-1} = \frac{1}{(4\pi)^2} S^{(1)}_{abcd}\left(A^{(1)}\Delta + B^{(1)}\Delta^2\right) + \frac{1}{(4\pi)^4} S^{(2)}_{abcd}\left(A^{(2)}\Delta + B^{(2)}\Delta^2\right)\,. \qquad (2.100)
$$

In Fig. 2.8, we show some examples of the vertex corrections ordered by their power of the gauge coupling, from no power (top line) to 6 powers of g. The corresponding

contributions $A^{(2)}S^{(2)}_{abcd}$ can be found in Tab. 2.4. As for the Yukawa coupling constant the corrections to the vertex are gauge dependent. When combined with the anomalous dimension of the scalar fields the cancellation occurs leaving the beta function of the quartic interaction gauge independent as it should. Note also that some diagrams do not have any contribution to $A^{(2)}$ and are therefore not present in the final result, see diagrams (a) and (b)[19]. The invariants appearing in Tab. 2.4 are defined by

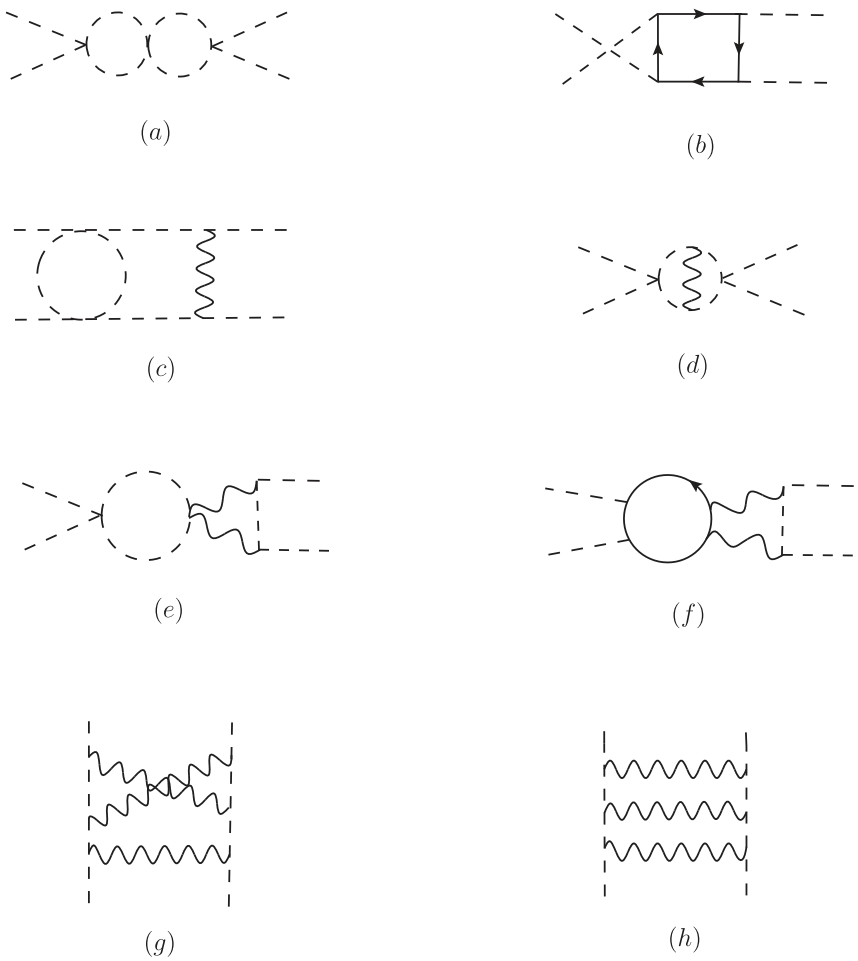

Figure 2.8: Example diagrams contributing to the divergent part of Z_{abcd}. From bottom to top the diagrams are respectively proportional to 6, 4, 2 and no powers of g.

[19]These diagrams are divergent but have only poles of second order and therefore do not contribute.

Table 2.4: Contributions $A^{(2)}$, $S^{(2)}_{abcd}$ corresponding to the diagrams in Fig. 2.8.

Diagram	$S^{(2)}_{aij}$	$A^{(2)}$
(a)	Λ^3_{abcd}	0
(b)	κH^λ_{abcd}	0
(c)	$g^2\left(\bar{\Lambda}^{2S}_{abcd}+\Lambda^{2g}_{abcd}\right)$	ξ
(d)	$g^2\Lambda^{2g}_{abcd}$	$-(3-\xi)$
(e)	$g^4 A^\lambda_{abcd}$	$\frac{5}{4}$
(f)	$g^4\kappa B^Y_{abcd}$	$-2\xi^2$
(g)	$g^6\left(\frac{1}{4}A^g_{abcd}-\frac{1}{8}C_2(\mathcal{G})A_{abcd}\right)$	$2\xi^3$
(h)	$g^6\left(\frac{1}{4}A^g_{abcd}-\frac{3}{8}C_2(\mathcal{G})A_{abcd}\right)$	$-2\xi^2(3-\xi)$

$$
\begin{aligned}
A_{abcd} &= \frac{1}{8}\sum_{\text{perm.}}\{\theta^\alpha,\theta^\beta\}_{ab}\{\theta^\alpha,\theta^\beta\}_{cd}\,, & \Lambda^2_{abcd} &= \frac{1}{8}\sum_{\text{perm.}}\lambda_{abef}\lambda_{efcd}\,,\\
\Lambda^3_{abcd} &= \frac{1}{8}\sum_{\text{perm.}}\lambda_{abef}\lambda_{efgh}\lambda_{ghcd}\,, & H^\lambda_{abcd} &= \frac{1}{2}\sum_{\text{perm.}}\lambda_{abef}\,\mathrm{Tr}\left(Y^cY^{\dagger d}Y^eY^{\dagger f}\right)\right)\,,\\
\bar{\Lambda}^{2S}_{abcd} &= \frac{1}{8}\sum_{\text{perm.}}C_2(S)^{fg}\lambda_{abef}\lambda_{cdeg}\,, & \Lambda^{2g}_{abcd} &= \frac{1}{8}\sum_{\text{perm.}}\lambda_{abef}\lambda_{cdgh}\theta^\alpha_{eg}\theta^\alpha_{fh}\,,\\
A^\lambda_{abcd} &= \frac{1}{4}\sum_{\text{perm.}}\lambda_{abef}\{\theta^\alpha,\theta^\beta\}_{ef}\{\theta^\alpha,\theta^\beta\}_{cd}\,, & A^g_{abcd} &= \frac{1}{8}f^{\alpha\beta\gamma}f^{\rho\sigma\gamma}\sum_{\text{perm.}}\{\theta^\alpha,\theta^\sigma\}_{ab}\{\theta^\beta,\theta^\gamma\}_{cd}\,,
\end{aligned}
$$

$$
B^Y_{abcd} = \frac{1}{4}\sum_{\text{perm.}}\{\theta^\alpha,\theta^\beta\}_{ab}\,\mathrm{Tr}\left(t^{\alpha *}t^{\beta *}Y^cY^{\dagger d}+Y^ct^\alpha t^\beta Y^{\dagger d}\right)\,, \tag{2.101}
$$

where $\sum_{\text{perm.}}$ represents the sum over the 4! permutations of the external indices a, b, c and d. At this stage, it is already apparent that a determination by hand of the two-loop beta function for a given theory is tedious and prone to error due to the numerous combinations and summations that one has to carry out in order to reduce the general formula given above into a specific set of RGEs. This is especially true for theories with many different scalars as illustrated by the group factors entering the quartic coupling beta functions shown above, Eq. (2.101).

Finally, for completeness we give the full result for the two-loop beta function for the scalar quartic coupling obtained by combining the anomalous dimension of the scalar quartic vertex and the anomalous dimension for scalar fields in the following way

$$
\beta_{\lambda_{abcd}} \equiv \mu\frac{d\lambda_{abcd}}{d\mu} = \gamma_{abcd}+\sum_k \gamma^S_{kk}\lambda_{abcd}\,, \tag{2.102}
$$

where $k \in \{a,b,c,d\}$ and γ_{abcd} is the anomalous dimension related to Z_{abcd} by Eq. (2.87).

$$\beta^{(1)}_{\lambda_{abcd}} = \Lambda^2_{abcd} - 8\kappa H_{abcd} + 2\kappa\Lambda^Y_{abcd} - 3g^2\Lambda^S_{abcd} + 3g^4 A_{abcd}\,, \tag{2.103}$$

$$\begin{aligned}
\beta^{(2)}_{\lambda_{abcd}} = {} & \\
& \frac{1}{2}\sum_i \Lambda^2(i)\lambda_{abcd} - \bar{\Lambda}^3_{abcd} - 4\kappa\bar{\Lambda}^{2Y}_{abcd} + \kappa\left\{8\bar{H}^\lambda_{abcd} - \sum_i \left[3H^2(i) + 2\bar{H}^2(i)\right]\lambda_{abcd}\right\} \\
+ \; & 4\kappa(H^Y_{abcd} + 2\bar{H}^Y_{abcd} + 2H^3_{abcd}) + g^2\left\{2\bar{\Lambda}^{2S}_{abcd} - 6\Lambda^{2g}_{abcd} + 4\kappa(H^S_{abcd} - H^F_{abcd})\right. \\
+ \; & \left. 10\kappa\sum_i Y^{2\mathrm{F}}(i)\lambda_{abcd}\right\} - g^4\left\{\left[\frac{35}{3}C_2(\mathcal{G}) - \frac{10}{3}\kappa S_2(F) - \frac{11}{12}S_2(S)\right]\Lambda^S_{abcd} - \frac{3}{2}\Lambda^{SS}_{abcd}\right. \\
- \; & \left. \frac{5}{2}A^\lambda_{abcd} - \frac{1}{2}\bar{A}^\lambda_{abcd} + 4\kappa(B^Y_{abcd} - 10\bar{B}^Y_{abcd})\right\} \\
+ \; & g^6\left\{\left[\frac{161}{6}C_2(\mathcal{G}) - \frac{32}{3}\kappa S_2(F) - \frac{7}{3}S_2(S)\right]A_{abcd} - \frac{15}{2}A^S_{abcd} + 27A^g_{abcd}\right\},
\end{aligned} \tag{2.104}$$

where to the already defined group factors, Eq. (2.101), one has to introduce the following ones

$$H_{abcd} = \frac{1}{4}\sum_{\text{perm.}} \mathrm{Tr}\left(Y^a Y^{\dagger b} Y^c Y^{\dagger d}\right)\,, \qquad \Lambda^Y_{abcd} = \sum_i Y_2(i)\lambda_{abcd}\,,$$

$$\bar{B}^Y_{abcd} = \frac{1}{4}\sum_{\text{perm.}} \{\theta^\alpha,\theta^\beta\}_{ab}\mathrm{Tr}\left(t^{\alpha *} Y^c t^\beta Y^{\dagger d}\right)\,, \qquad \bar{\Lambda}^3_{abcd} = \frac{1}{4}\sum_{\text{perm.}} \lambda_{abef}\lambda_{cegh}\lambda_{dfgh}\,,$$

$$\bar{H}^\lambda_{abcd} = \frac{1}{8}\sum_{\text{perm.}} \lambda_{abef}\mathrm{Tr}\left(Y^c Y^{\dagger e} Y^d Y^{\dagger f} + Y^{\dagger c} Y^e Y^{\dagger d} Y^f\right)\,, \qquad \bar{\Lambda}^{2Y}_{abcd} = \frac{1}{8}\sum_{\text{perm.}} Y_2^{fg}(S)\lambda_{abef}\lambda_{cdeg}\,,$$

$$H^Y_{abcd} = \sum_{\text{perm.}} \mathrm{Tr}\left(Y_2(F) Y^{\dagger a} Y^b Y^{\dagger c} Y^d\right)\,, \qquad \Lambda^S_{abcd} = \sum_i C_2(i)\lambda_{abcd}\,,$$

$$H^3_{abcd} = \frac{1}{2}\sum_{\text{perm.}} \mathrm{Tr}\left(Y^a Y^{\dagger b} Y^e Y^{\dagger c} Y^d Y^{\dagger e}\right)\,, \qquad H^S_{abcd} = \sum_i C_2(i) H_{abcd}\,,$$

$$H^F_{abcd} = \sum_{\text{perm.}} \mathrm{Tr}\left(\{C_2(F), Y^a\} Y^{\dagger b} Y^c Y^{\dagger d}\right)\,, \qquad \Lambda^{SS}_{abcd} = \sum_i \left[C_2(i)\right]^2 \lambda_{abcd}\,,$$

$$\bar{A}^\lambda_{abcd} = \frac{1}{4}\sum_{\text{perm.}} \lambda_{abef}\{\theta^\alpha,\theta^\beta\}_{ce}\{\theta^\alpha,\theta^\beta\}_{df}\,, \qquad A^S_{abcd} = \sum_i C_2(i) A_{abcd}\,,$$

$$\bar{H}^Y_{abcd} = \frac{1}{2}\sum_{\text{perm.}} \mathrm{Tr}\left(Y^e Y^{\dagger a} Y^e Y^{\dagger b} Y^c Y^{\dagger d} + Y^{\dagger e} Y^a Y^{\dagger e} Y^b Y^{\dagger c} Y^d\right)\,, \tag{2.105}$$

with $i \in \{a,b,c,d\}$ and $\Lambda^2(i) \equiv \Lambda^2_{ab}(S)\big|_{a=b=i}$, $H^2(i) \equiv H^2_{ab}(S)\big|_{a=b=i}$, $\bar{H}^2(i) \equiv \bar{H}^2_{ab}(S)\big|_{a=b=i}$ and $Y^{2\mathrm{F}}(i) \equiv Y^{2\mathrm{F}}_{ab}(S)\big|_{a=b=i}$ are the eigenvalues of the invariants of $\Lambda^2_{ab}(S)$, $H^2_{ab}(S)$, $\bar{H}^2_{ab}(S)$, $Y^{2\mathrm{F}}_{ab}(S)$. A more precise definition of the various terms entering Eqs. (2.104, 2.105) will be given in a forthcoming section when we will discuss the implementation of these equations in PyR@TE, Section 2.4.1.

2.3.6 Including mass and trilinear terms

All the evolution equations for the couplings present in $\mathcal{L}_0$ have now been presented and we turn to the parameters of $\mathcal{L}_1$, the dimensional parameters, Eq. (2.39). In principle, one has to repeat the calculation entirely for each term, extract the anomalous dimension of the various operator and combine it with the anomalous dimensions of the scalar and fermion fields to obtain the corresponding beta function. Fortunately, this can be avoided by noting the following three points

(i) the RGEs for the fermion mass terms can be inferred from the beta function of the Yukawa couplings by taking the a index to be a dummy index,

(ii) for the trilinear scalar interaction terms it suffices to take one external index to be dummy in the beta function of the quartic scalar interaction coupling, a, b, c or d,

(iii) scalar mass terms are also obtained from the beta function of the quartic coupling by taking two indices to be dummy.

Dummy, here, means that the corresponding field does not propagate and do not have any gauge interaction. Doing so, we can see that the trilinear couplings enter the RGE of the fermion mass at the two-loop level while the fermion mass contribute to the beta function of the trilinear coupling at one-loop already. Finally, the scalar mass beta function receives contributions from both the fermion mass and trilinear terms at one-loop. The results[20] are quite lengthy and we do not include them here and refer the interested reader to [159] instead.

2.3.7 Extension to semi-simple gauge groups

So far, all the results presented above were for a simple gauge group $\mathcal{G}$. However, theories based on a product of simple gauge groups are very common in particle physics and to accommodate these models the above results need to be modified accordingly. Fortunately, it is possible to obtain the corresponding RGEs by applying substitution rules [111]. To understand the requirements needed if the gauge structure is now a product of simple gauge groups with at most one abelian factor let us say, $\mathcal{G}_1 \times \mathcal{G}_2 \cdots \times \mathcal{G}_n$ with coupling constants $g_1, g_2, \ldots g_n$, one has to associate a gauge coupling factor g for each generator θ^α or t^α and a factor g^2 for each Casimir or Dynkin index. Then a careful inspection of the Feynman diagrams leads to the following replacement rules for the gauge coupling constants RGEs

$$
\begin{aligned}
g^3 C_2(\mathcal{G}) &\to g_k^3 C_2(\mathcal{G}_k)\,, & g^3 S_2(R) &\to g_k^3 S_2^k(R)\,,\\
g^5 [C_2(\mathcal{G})]^2 &\to g_k^5 [C_2(\mathcal{G}_k)]^2\,, & g^5 C_2(\mathcal{G}) S_2(R) &\to g_k^5 C_2(\mathcal{G}_k) S_2^k(R)\,,\\
g^5 C_2(R) S_2(R) &\to \sum_l g_k^3 g_l^2 C_2^l(R) S_2^k(R)\,,
\end{aligned}
\tag{2.106}
$$

[20] As for the results above the expressions are coming from the latest summary [159].

in which k, l are subgroup indices, and R denotes either S or F. Then, for the replacement rules of the other beta functions we have

$$\begin{aligned} g^2 C_2(R) &\to \sum_k g_k^2 C_2^k(R)\,, & g^4 C_2(\mathcal{G}) C_2(R) &\to \sum_k g_k^4 C_2(\mathcal{G}_k) C_2^k(R)\,, \\ g^4 S_2(R) C_2(R') &\to \sum_k g_k^4 S_2^k(R) C_2^k(R')\,, & g^4 C_2(R) C_2(R') &\to \sum_{k,l} g_k^2 g_l^2 C_2^k(R) C_2^l(R')\,. \end{aligned} \tag{2.107}$$

For the group factors H_{2t}^a, B_{abcd}^Y and $\bar{B}_{abcd}^Y$ one has to give a different group index to each representation matrix i.e. $\theta^\alpha \to \theta_k^\alpha$ and $\theta^\beta \to \theta_l^\beta$, same for t^α, t^β. The g^4 factor are also split into $\sum_{k,l} g_k^2 g_l^2$, e.g. $g^4 B_{abcd}^Y$ is replaced by

$$g^4 B_{abcd}^Y = \frac{g^4}{4} \sum_{\text{perm.}} \{\theta^\alpha, \theta^\beta\}_{ab} \text{Tr}\left(t^{\alpha *} t^{\beta *} Y^c Y^{\dagger d} + Y^c t^\alpha t^\beta Y^{\dagger d}\right) \tag{2.108}$$

$$\to \sum_{k,l} g_k^2 g_l^2 \sum_{\text{perm.}} \{\theta_k^\alpha, \theta_l^\beta\} \text{Tr}\left(t_k^{\alpha *} t_l^\beta Y^c Y^{\dagger d} + Y^c t_k^\alpha t_l^\beta Y^{\dagger d}\right)\,. \tag{2.109}$$

The final set of substitution rules are expressed in terms of the following quantity

$$\Lambda_{ab,cd} = \theta_{ac}^\alpha \theta_{bd}^\alpha\,, \tag{2.110}$$

so that A_{abcd} can be written in the form

$$A_{abcd} = \frac{1}{4} \sum_{\text{perm.}} \left(\Lambda_{ac,ef} \Lambda_{ef,bd} + \Lambda_{ae,fd} \Lambda_{eb,cd}\right)\,, \tag{2.111}$$

and the substitution rule simply as

$$g^2 \Lambda_{ab,cd} \to \sum_k g_k^2 \Lambda_{ab,cd}\,. \tag{2.112}$$

Consequently, the last substitution rules read

$$\begin{aligned} g^4 A_{abcd} &\to \frac{1}{4} \sum_{\text{perm.}} \left(\Lambda_{ac,ef} \Lambda_{ef,bd} + \Lambda_{ae,fd} \Lambda_{eb,cf}\right), \\ g^6 S_2(R) A_{abcd} &\to \frac{1}{4} \sum_{k,l} g_k^4 g_l^2 S_2^k(R)\,, \\ g^6 C_2(\mathcal{G}) A_{abcd} &\to \frac{1}{4} \sum_{k,l} g_k^4 g_l^2 C_2(\mathcal{G}_k) \sum_{\text{perm.}} \left(\Lambda_{ac,ef}^k \Lambda_{ef,bd}^l + \Lambda_{ae,fd}^k \Lambda_{eb,cf}^l\right), \\ g^6 A_{abcd}^S &\to \sum_k \sum_i g_k^2 C_2^k(i) \frac{1}{4} \sum_{l,m} g_l^2 g_m^2 \sum_{\text{perm.}} \left(\Lambda_{ac,ef}^l \Lambda_{ef,bd}^m + \Lambda_{ae,fd}^l \Lambda_{eb,cf}^m\right), \\ g^6 A_{abcd}^g &\to \sum_k g_k^6 A_{abcd}^g(k)\,. \end{aligned}$$

This set of substitution rules are in principle straightforward to apply even though they make the calculation by hand yet a bit more challenging. Computational wise they make the computation significantly more demanding since the time for computing terms proportional to g^4 grows quadratically with the number of gauge groups.

2.3.8 What about supersymmetric theories?

In principle, the general beta functions reviewed in the previous sections can be used to calculate evolution equations for supersymmetric theories. However, there is one difficulty to this. As explained in Section 2.3, the general equations have been obtained using dimensional regularization (DREG) and the $\overline{\text{MS}}$ renormalization scheme which is known to violate explicitly supersymmetry because it introduces a mismatch between the gauge boson and gaugino number of degrees of freedom. Therefore, the use of DREG is not appropriate and one should rather rely on dimensional reduction (DRED) which manifestly preserves supersymmetry. It has been shown that in DREG SUSY is violated in the finite parts of one-loop graphs and in the divergent terms of two-loop contributions. Consequently, the beta functions calculated in the two schemes will differ starting at the two-loop order [160]. One way out is to use translation rules to go from $\overline{\text{MS}}$ scheme to DR or $\overline{\text{DR}}$ which have been given in [160]. The results of this approach can be found in [160] and a direct calculation using dimensional reduction [161] or supergraph methods [162] are also available in the literature[21].

When using the first method, the general equations need to be specialized to the SUSY case before doing the translation into the DR scheme. Doing so, the RGEs significantly simplifies and the final expressions are much shorter. In addition, because quartic terms in SUSY come from the D terms and are therefore related to the gauge couplings of the theory, one does not need the RGEs for the quartic terms. Since these beta functions are responsible for most of the complexity (including the need of a specific matrix representation for the scalar) of applying the general equations to specific theories because of the multiple sums they require, deriving evolution equations for SUSY models is much simpler than for general theories.

This concludes our review of the results for the two-loop beta functions of a general gauge theory. We have presented the evolution equations for dimensionless parameters such as gauge, Yukawa and scalar quartic coupling constants in the $\overline{\text{MS}}$ scheme to the second order in perturbation theory. In addition, we discussed how the RGEs for the fermion and scalar mass terms as well as the scalar trilinear terms can be obtained. Note that we did not discuss kinetic mixing because it is not implemented in PyR@TE, comments on this issue are given in Section 2.4.12.

2.4 PyR@TE

It is clear from the previous section that deriving the full set of two-loop RGEs for a specific model from the general equations is tedious and prone to error. In this section we present a python code that we called PyR@TE for "Python RGEs @ Two-loop for Everyone" which implements the equations presented in Section 2.3 for an arbitrary Lagrangian[22]. We first provide details about the meaning of the various group factors appearing in the RGEs and the meaning of the general equations. Then, the structure of the code is briefly introduced before explaining the installation of PyR@TE and its use. We also discuss the validation of the results and give more information about the supported gauge groups, irreducible representations and already implemented models. Finally, we discuss future

[21] Obviously, these results agree with each other.

[22] The technical limitation of PyR@TE will be presented below.

possible directions to extend the code such as considering modifications induced by kinetic mixing, including the running of *vevs* and higher order corrections.

2.4.1 Implementing the equations

In this paragraph, we want to explicit the meaning of the various terms in the RGEs presented in Section 2.3, emphasizing the set in which the various indices must be varied. This is done in the view of being able to write algorithms implementing these results. The first step we take is to give more details on the construction of the matrices forming representations of the real degrees of freedom of complex scalar fields. Then, we re-write the various RGEs equations and show how the SM result is recovered.

Generators for scalars

In the calculation the scalar fields are assumed to be real and the θ^α matrices to be purely imaginary and anti-symmetric. To get the correct form of these generators we can start with a complex scalar φ which transforms similar to the complex fermion as

$$\varphi \to e^{i\epsilon^\alpha t^\alpha}\varphi\,. \tag{2.113}$$

We can now define a real vector Φ which consists of the real and imaginary component of φ

$$\Phi = \begin{pmatrix} \mathrm{Re}(\varphi) \\ \mathrm{Im}(\varphi) \end{pmatrix}\,. \tag{2.114}$$

Φ transforms according to

$$\Phi \to e^{i\epsilon^\alpha \theta^\alpha}\Phi\,, \tag{2.115}$$

from where we can obtain the relation

$$\theta^\alpha = i\begin{pmatrix} \mathrm{Im}(t^\alpha) & \mathrm{Re}(t^\alpha) \\ -\mathrm{Re}(t^\alpha) & \mathrm{Im}(t^\alpha) \end{pmatrix}\,. \tag{2.116}$$

We can demonstrate this construction at the example of the fundamental representation of SU(2). Note, that this is equivalent to embedding SU(2) into SO(4). The complex, Hermitian generators for SU(2) are proportional to the Paul matrices

$$\{\sigma_1,\sigma_2,\sigma_3\} = \left\{\begin{pmatrix} 0 & 1 \\ 1 & 0 \end{pmatrix}, \begin{pmatrix} 0 & -i \\ i & 0 \end{pmatrix}, \begin{pmatrix} 1 & 0 \\ 0 & -1 \end{pmatrix}\right\}\,. \tag{2.117}$$

Now, applying the relation 2.116 to all three matrices, we obtain the following set of generators

$$\{\tilde{\Sigma}_1,\tilde{\Sigma}_2,\tilde{\Sigma}_3\} = i\left\{\begin{pmatrix} 0 & 0 & 0 & 1 \\ 0 & 0 & 1 & 0 \\ 0 & -1 & 0 & 0 \\ -1 & 0 & 0 & 0 \end{pmatrix}, \begin{pmatrix} 0 & -1 & 0 & 0 \\ 1 & 0 & 0 & 0 \\ 0 & 0 & 0 & -1 \\ 0 & 0 & 1 & 0 \end{pmatrix}, \begin{pmatrix} 0 & 0 & 1 & 0 \\ 0 & 0 & 0 & -1 \\ -1 & 0 & 0 & 0 \\ 0 & 1 & 0 & 0 \end{pmatrix}\right\}\,. \tag{2.118}$$

These matrices are indeed antisymmetric and imaginary and we can check that they satisfy the same commutation relations as the σ's:

$$\left[\tilde{\Sigma}_1, \tilde{\Sigma}_2\right] = 2i\tilde{\Sigma}_3, \tag{2.119}$$

$$\left[\tilde{\Sigma}_1, \tilde{\Sigma}_3\right] = -2i\tilde{\Sigma}_2, \tag{2.120}$$

$$\left[\tilde{\Sigma}_2, \tilde{\Sigma}_3\right] = 2i\tilde{\Sigma}_1\,. \tag{2.121}$$

Gauge interactions

We now give some details on the general formula presented in the previous section and as a first step we concentrate on the terms involving only gauge interactions. The basic objects to calculate the one- and two-loop β-functions for the gauge couplings in absence of any matter interaction are the quadratic Casimir operator C_2 and the Dynkin index S_2 of the gauge group. Those indices can be related to the generators t^α for fermions and θ^α for scalars introduced in Section 2.3.1

$$C_2^{ab}(S) = \theta^\alpha_{ac}\theta^\alpha_{cb}\,, \qquad S_2(S)\delta_{AB} = \mathrm{Tr}(\theta^\alpha\theta^\beta)\,, \tag{2.122}$$

$$C_2^{ab}(F) = t^\alpha_{ac}t^\alpha_{cb}\,, \qquad S_2(F)\delta_{\alpha\beta} = \mathrm{Tr}(t^\alpha t^\beta)\,. \tag{2.123}$$

The first step is to make the meaning of the indices more explicit. For this purpose we assume that we have a gauge sector which is a direct product of n non-Abelian gauge groups and at most one Abelian gauge group U(1). The non-Abelian groups are labeled with small letters: $\mathrm{U}(1) \times \mathcal{G}_1 \times \cdots \times \mathcal{G}_k \times \cdots \times \mathcal{G}_n$. In the case of several U(1)$'s$ the situation is more involved due to the impact of kinetic mixing [163]. Rules to derive the entire two-loop RGEs in this context have just recently been given in Ref. [164].

For the charge indices with respect to the non-Abelian gauge groups we are going to use Greek letters in the following. In addition, there are sets of fermion fields $\psi^1 \ldots \psi^{n_f}$ and real scalars $\phi^1 \ldots \phi^{n_s}$ which can be charged under these gauge groups. Moreover, all fields can come in an arbitrary number of generations $\mathcal{N}_F^i$ respectively $\mathcal{N}_S^i$ so that in general each field carries $n+1$ indices. Using these conventions, we can rewrite the group constants for one particular non-Abelian gauge group k as

$$\begin{aligned} C_{2,k}^{\psi^i_{g_i,\alpha_1\ldots\alpha_k\ldots\alpha_n}\psi^j_{g_j,\beta_1\ldots\beta_k\ldots\beta_n}}(F) &= \delta_{ij}\delta_{g_ig_j}\delta_{\alpha_1\beta_1}\ldots\delta_{\alpha_{k-1}\beta_{k-1}}\delta_{\alpha_{k+1}\beta_{k+1}}\ldots\delta_{\alpha_n\beta_n}\mathcal{C}_k(\Lambda(\psi^i))\,, \\ S_{2,k}^{\psi^i_{g_i,\alpha_1\ldots\alpha_k\ldots\alpha_n}\psi^j_{g_j,\beta_1\ldots\beta_k\ldots\beta_n}}(F) &= \delta_{ij}\delta_{g_ig_j}\delta_{\alpha_1\beta_1}\ldots\delta_{\alpha_{k-1}\beta_{k-1}}\delta_{\alpha_{k+1}\beta_{k+1}}\ldots\delta_{\alpha_n\beta_n}\mathcal{S}_k(\Lambda(\psi^i))\,, \end{aligned} \tag{2.124}$$

and similar for scalars. Here, we introduced $\mathcal{C}_k(\Lambda)$ and $\mathcal{S}_k(\Lambda)$ which are the quadratic Casimir and Dynkin index of an irrep with highest weight Λ with respect to the gauge group k. $\mathcal{C}$ can be calculated using the well-known formula

$$\mathcal{C}(\Lambda) = \langle\Lambda, \Lambda + 2\delta\rangle\,, \tag{2.125}$$

with $\delta = (1, 1, \ldots, 1)$ in the Dynkin basis. The Dynkin index is normalized in a way that the value for the fundamental irrep is $\frac{1}{2}$:

$$\mathcal{S}_k(\Lambda) = \frac{N_k(\Lambda)}{N(\mathcal{G}_k)}\mathcal{C}_k(\Lambda)\,. \tag{2.126}$$

Here, $N(\Lambda)$ is the dimension of the irrep and $N(\mathcal{G})$ the dimension of the adjoint representation. For the Abelian gauge group we have

$$\begin{aligned} C_{2,U(1)}^{\psi^i_{g_i,\alpha_1\ldots\alpha_k\ldots\alpha_n}\psi^j_{g_j,\beta_1\ldots\beta_k\ldots\beta_n}}(F) &= S_{2,U(1)}^{\psi^i_{g_i,\alpha_1\ldots\alpha_k\ldots\alpha_n}\psi^j_{g_j,\beta_1\ldots\beta_k\ldots\beta_n}}(F) \\ &= \delta_{ij}\delta_{g_ig_j}\delta_{\alpha_1\beta_1}\ldots\delta_{\alpha_n\beta_n}Q(\psi^i)^2\,. \end{aligned} \tag{2.127}$$

Q is the charge of the field which might include a GUT normalization. We can now define the Dynkin index summed over all states present in the model:

$$\tilde{S}_{2,k}(S) = \sum_{s=1}^{n_s}\prod_{l=1}^{n}\mathcal{N}_S^s\tilde{N}(\Lambda(s))_{lk}\mathcal{S}_k(\Lambda(s))\,, \tag{2.128}$$

$$\tilde{S}_{2,k}(F) = \sum_{f=1}^{n_f}\prod_{l=1}^{n}\mathcal{N}_F^f\tilde{N}(\Lambda(f))_{lk}\mathcal{S}_k(\Lambda(f))\,, \tag{2.129}$$

with

$$\tilde{N}(\Lambda)_{lk} = \begin{cases} N_l(\Lambda) & \text{if } l\neq k, \\ 1 & \text{else if } l=k\,. \end{cases} \tag{2.130}$$

For the Abelian gauge group we get

$$\tilde{S}_{2,U(1)}(S) = \sum_{s=1}^{n_s}\prod_{l=1}^{n}\mathcal{N}_S^s N_l(\Lambda(s))Q(s)^2\,, \tag{2.131}$$

$$\tilde{S}_{2,U(1)}(F) = \sum_{f=1}^{n_f}\prod_{l=1}^{n}\mathcal{N}_F^f N_l(\Lambda(f))Q(f)^2\,. \tag{2.132}$$

With these results, the one-loop β functions of a particular gauge coupling $g_{\mathcal{G}_k}$ is calculated via

$$\beta(g_{\mathcal{G}_k}) = -\frac{g_{\mathcal{G}_k}^3}{16\pi^2}\left(\frac{11}{3}C(\mathcal{G}_k) - \frac{2}{3}\tilde{S}_{2,k}(F) - \frac{1}{6}\tilde{S}_{2,k}(S)\right)\,, \tag{2.133}$$

where $C(\mathcal{G})$ is the quadratic Casimir operator in the adjoint representation.

We want to clarify these expression with the example of the SM, but concentrate for brevity just on the non-Abelian sector. That means, we have the gauge groups $\mathrm{SU}(2)_L\times\mathrm{SU}(3)_C$, the fermionic fields[23] $q(2,3)$, $\bar{u}(1,\bar{3})$, $\bar{d}(1,\bar{3})$, $l(2,1)$, $e(1,1)$ and two real scalars $\phi_h(2,1)$, $\sigma_h(2,1)$ which are stemming from one complex Higgs doublet

$$H = \frac{1}{\sqrt{2}}(\phi_h + i\sigma_h)\,. \tag{2.134}$$

All fermions appear in $\mathcal{N}_G$ generations while we restrict the generation of Higgs fields to one. Hence, we obtain:

$$\tilde{S}_{2,1}(F) = \mathcal{N}_G\left[3\cdot\mathcal{S}_{\mathrm{SU}(2)}(\Lambda(q)) + \mathcal{S}_{\mathrm{SU}(2)}(\Lambda(l))\right] = 2\mathcal{N}_G\,, \tag{2.135}$$

$$\tilde{S}_{2,1}(S) = \mathcal{S}_{\mathrm{SU}(2)}(\Lambda(\phi^h)) + \mathcal{S}_{\mathrm{SU}(2)}(\Lambda(\sigma^h)) = 1\,, \tag{2.136}$$

$$\tilde{S}_{2,2}(F) = \mathcal{N}_G\left[2\cdot\mathcal{S}_{\mathrm{SU}(3)}(\Lambda(q)) + \mathcal{S}_{\mathrm{SU}(3)}(\Lambda(d)) + \mathcal{S}_{\mathrm{SU}(3)}(\Lambda(u))\right] = 2\mathcal{N}_G\,. \tag{2.137}$$

[23] In brackets we show the quantum numbers with respect to $\mathrm{SU}(2)_L\times\mathrm{SU}(3)_C$.

In addition, $\mathcal{C}(\mathrm{SU}(N)) = N$ holds. Hence, we obtain from 2.133

$$\beta(g_2) = -\frac{g_2^3}{16\pi^2}\left(\frac{11}{3}2 - \frac{2}{3}2\mathcal{N}_G - \frac{1}{6}\right) = -\frac{g_2^3}{16\pi^2}\left(\frac{43}{6} - \frac{4}{3}\mathcal{N}_G\right), \tag{2.138}$$

$$\beta(g_3) = -\frac{g_3^3}{16\pi^2}\left(\frac{11}{3}3 - \frac{2}{3}2\mathcal{N}_G\right) = -\frac{g_3^3}{16\pi^2}\left(11 - \frac{4}{3}\mathcal{N}_G\right). \tag{2.139}$$

Here, we have introduced the short form $g_2 = g_{\mathrm{SU}(2)}$ and $g_3 = g_{\mathrm{SU}(3)}$. We continue with the two-loop β-functions. We have to clarify the meaning of

$$|C(\mathcal{G})|^2, \qquad S(R)C(\mathcal{G}), \qquad S(R)C(R), \tag{2.140}$$

with $R = S, F$. The easy part is $|C(\mathcal{G})|^2$ which results for a SU(N) gauge group in N^2. We can use the already introduced $\tilde{S}$ to express $S(R)C(\mathcal{G})$ as

$$S(R)C(\mathcal{G}) \to \tilde{S}_{2,k}C(\mathcal{G}_k). \tag{2.141}$$

Furthermore, the correct multiplicity for the term $S(R)C(R)$ can be obtained by inspecting a representative Feynman diagram. The result is

$$(S(R)C(R))_k \equiv \sum_r \sum_l g_k^2 g_l^2 \mathcal{N}_r \mathcal{S}_k(\Lambda(r))\mathcal{C}_l(\Lambda(r)) \prod_m \tilde{N}(\Lambda(r))_{mk} \tag{2.142}$$

with $r = s$ if $R = S$ or f if $R = F$. Note, there is no (implicit) sum over k. Hence, the two-loop contributions stemming purely from gauge interactions to the β functions are in general given by

$$\begin{aligned}\beta^{(2)}(g_{\mathcal{G}_k}) = -\frac{g_{\mathcal{G}_k}}{(16\pi^2)^2}\Bigg[g_{\mathcal{G}_k}^4\frac{34}{3}|C(\mathcal{G}_k)|^2 - \frac{1}{2}\left(4(S(F)C(F))_k + \frac{20}{3}\tilde{S}_{2,k}(F)C(\mathcal{G}_k)\right) \\ - \left(2(S(S)C(S))_k + \frac{1}{3}\tilde{S}_{2,k}(S)C(\mathcal{G}_k)\right)\Bigg].\end{aligned} \tag{2.143}$$

For a SU(N) gauge group this can be simplified by using $|C(\mathcal{G}_k)| = N$ and $|C(\mathcal{G}_k)|^2 = N^2$. For the same particle content as above we obtain

$$(S(F)C(F))_1 = \mathcal{N}_G\left(\frac{3}{2}g_2^4 + 2g_2^2g_3^2\right), \tag{2.144}$$

$$(S(S)C(S))_1 = \frac{3}{4}g_2^4, \tag{2.145}$$

$$(S(F)C(F))_2 = \mathcal{N}_G\left(\frac{3}{4}g_2^2g_3^2 + \frac{8}{3}g_3^4\right), \tag{2.146}$$

and end up with the β functions

$$\begin{aligned}
\beta^{(2)}(g_2) &= -\frac{g_2}{(16\pi^2)^2}\left[g_2^4\frac{34}{3}2^2-\frac{1}{2}\left(4\mathcal{N}_G\left(\frac{3}{2}g_2^4+2g_2^2g_3^2\right)+\frac{20}{3}\cdot 2\cdot 2\cdot\mathcal{N}_G\cdot g_2^4\right)\right.\\
&\qquad\left.-\left(2\cdot\frac{3}{4}g_2^4+\frac{1}{3}\cdot 2\cdot g_2^4\right)\right]\\
&= -\frac{g_2}{(16\pi^2)^2}\left[\frac{138}{4}g_2^4-\mathcal{N}_G\left(\frac{49}{3}g_2^4+4g_2^2g_3^2\right)-\frac{13}{6}g_2^4\right], \qquad (2.147)\\
\beta^{(2)}(g_3) &= -\frac{g_3}{(16\pi^2)^2}\left[g_3^4\cdot\frac{34}{3}\cdot 3^2-\frac{1}{2}\left(4\mathcal{N}_G\left(\frac{3}{4}g_2^2g_3^2+\frac{8}{3}g_3^4\right)+\frac{20}{3}\cdot 2\cdot 3\mathcal{N}_G\cdot g_3^4\right)\right]\\
&= -\frac{g_3}{(16\pi^2)^2}\left[102g_3^4-\mathcal{N}_G\left(\frac{76}{3}g_3^4+\frac{3}{2}g_2^2g_3^2\right)\right]. \qquad (2.148)
\end{aligned}$$

Matter interactions

From Eqs. (2.38, 2.39) the potential of a general renormalizable quantum field theory consists of the following terms:

$$\begin{aligned}
-\mathcal{V} &= \frac{1}{2}(Y^a_{jk}\psi_j\xi\psi_k\phi_a-(m_f)_{jk}\psi_j\xi\psi_k+h.c.)\\
&\quad+\frac{1}{4!}\lambda_{abcd}\phi_a\phi_b\phi_c\phi_d-\frac{1}{2}m^2_{ab}\phi_a\phi_b-\frac{1}{3!}h_{abc}\phi_a\phi_b\phi_c\,. \qquad (2.149)
\end{aligned}$$

Note that a tadpole term $t\phi$, which is in principle possible for a gauge singlet is not present, since it can always be absorbed into a shift of ϕ. Using the same conventions as introduced in Section 2.4.1, we can re-write 2.149 as

$$\begin{aligned}
-\mathcal{V} &= \frac{1}{2}\sum_{i,j,k}[C_{\alpha_1\beta_1\gamma_1}\cdot\dots\cdot C_{\alpha_n\beta_n\gamma_n}]Y^{\phi^k_{g_1,\alpha_1\dots\alpha_n}}_{\psi^i_{g_2,\beta_1\dots\beta_n}\psi^j_{g_3,\gamma_1\dots\gamma_n}}\phi^k_{g_1,\alpha_1\dots\alpha_n}\psi^i_{g_2,\beta_1\dots\beta_n}\xi\psi^j_{g_3,\gamma_1\dots\gamma_n}+h.c.\\
&\quad-\frac{1}{2}\sum_{i,j}[C_{\alpha_1\beta_1}\cdot\dots\cdot C_{\alpha_n\beta_n}](m_f)_{\psi^i_{g_1,\alpha_1\dots\alpha_n}\psi^j_{g_3,\beta_1\dots\beta_n}}\psi^i_{g_1,\alpha_1\dots\alpha_n}\xi\psi^j_{g_3,\beta_1\dots\beta_n}+h.c.\\
&\quad+\frac{1}{4!}\sum_{i,j,k,l}[C_{\alpha_1\beta_1\gamma_1\delta_1}\cdot\dots\cdot C_{\alpha_n\beta_n\gamma_n\delta_n}]\lambda_{\phi^i_{g_1,\alpha_1\dots\alpha_n}\phi^j_{g_2,\beta_1\dots\beta_n}\phi^k_{g_3,\gamma_1\dots\gamma_n}\phi^l_{g_4,\delta_1\dots\delta_n}}\\
&\qquad\qquad\phi^i_{g_1,\alpha_1\dots\alpha_n}\phi^j_{g_2,\beta_1\dots\beta_n}\phi^k_{g_3,\gamma_1\dots\gamma_n}\phi^l_{g_4,\delta_1\dots\delta_n}\\
&\quad-\frac{1}{3!}\sum_{i,j,k}[C_{\alpha_1\beta_1\gamma_1}\cdot\dots\cdot C_{\alpha_n\beta_n\gamma_n}]h_{\phi^i_{g_1,\alpha_1\dots\alpha_n}\phi^j_{g_2,\beta_1\dots\beta_n}\phi^k_{g_3,\gamma_1\dots\gamma_n}}\phi^i_{g_1,\alpha_1\dots\alpha_n}\phi^j_{g_2,\beta_1\dots\beta_n}\phi^k_{g_3,\gamma_1\dots\gamma_n}\\
&\quad-\frac{1}{2}\sum_{i,j}[C_{\alpha_1\beta_1}\cdot\dots\cdot C_{\alpha_n\beta_n}]m^2_{\phi^i_{g_1,\alpha_1\dots\alpha_n}\phi^j_{g_2,\beta_1\dots\beta_n}}\phi^i_{g_1,\alpha_1\dots\alpha_n}\phi^j_{g_2,\beta_1\dots\beta_n}\,. \qquad (2.150)
\end{aligned}$$

Here, we introduced the Clebsch-Gordan coefficient (CGC), C, which vanish for combinations of fields which are not gauge invariant. In addition, to simplify the notation we kept also a charge ('dummy') index for fields which are not charged under a particular gauge group. In this case relations like $C_{\alpha\beta\gamma}=C_{\alpha\gamma}$ hold for a dummy index β, of course.

Finally, we are going to define the following objects:

$$\mathcal{Y}^{\phi^i_{g_i,\alpha_1\ldots\alpha_n}}_{\psi^j_{g_j,\beta_1\ldots\beta_n}\psi^k_{g_k,\gamma_1\ldots\gamma_n}} = -\frac{\partial^3\mathcal{V}}{(\partial\phi^i_{g_i,\alpha_1\ldots\alpha_n})(\partial\psi^j_{g_j,\beta_1\ldots\beta_n})(\partial\psi^k_{g_k,\gamma_1\ldots\gamma_n})}\,, \tag{2.151}$$

$$\mathcal{M}_{\psi^j_{g_j,\beta_1\ldots\beta_n}\psi^k_{g_k,\gamma_1\ldots\gamma_n}} = -\frac{\partial^2\mathcal{V}}{(\partial\psi^j_{g_j,\beta_1\ldots\beta_n})(\partial\psi^k_{g_k,\gamma_1\ldots\gamma_n})}\,, \tag{2.152}$$

$$\mathcal{L}^{\phi^i_{g_i,\alpha_1\ldots\alpha_n}\phi^j_{g_j,\beta_1\ldots\beta_n}\phi^k_{g_k,\gamma_1\ldots\gamma_n}\phi^l_{g_l,\delta_1\ldots\delta_n}} = -\frac{\partial^4\mathcal{V}}{(\partial\phi^i_{g_i,\alpha_1\ldots\alpha_n})(\partial\phi^j_{g_j,\beta_1\ldots\beta_n})(\partial\phi^k_{g_k,\gamma_1\ldots\gamma_n})(\partial\phi^l_{g_l,\delta_1\ldots\delta_n})}\,, \tag{2.153}$$

$$\mathcal{H}^{\phi^i_{g_i,\alpha_1\ldots\alpha_n}\phi^j_{g_j,\beta_1\ldots\beta_n}\phi^k_{g_k,\gamma_1\ldots\gamma_n}} = -\frac{\partial^3\mathcal{V}}{(\partial\phi^i_{g_i,\alpha_1\ldots\alpha_n})(\partial\phi^j_{g_j,\beta_1\ldots\beta_n})(\partial\phi^k_{g_k,\gamma_1\ldots\gamma_n})}\,, \tag{2.154}$$

$$\mathcal{M}_{\mathcal{S}}{}^{\phi^i_{g_i,\alpha_1\ldots\alpha_n}\phi^j_{g_j,\beta_1\ldots\beta_n}} = -\frac{\partial^2\mathcal{V}}{(\partial\phi^i_{g_i,\alpha_1\ldots\alpha_n})(\partial\phi^j_{g_j,\beta_1\ldots\beta_n})}\,. \tag{2.155}$$

The objects $\mathcal{Y}$, $\mathcal{H}$, $\mathcal{L}$, $\mathcal{M}$ and $\mathcal{M}_{\mathcal{S}}$ are independent of the ordering of their arguments and contain all necessary information about the involved states in the most explicit way and can therefore be used to build up algorithms to calculate the β functions for any given model if the particle content and the potential is provided. For this purpose, it is, of course, necessary to express the general formulae, see Section 2.3, by using these objects. We show this at the example of the one-loop β function of the Yukawa couplings which reads Eq. (2.97)

$$\begin{aligned}(\beta^a_{ij})^{(1)} &= \frac{1}{2}[Y^bY^{\dagger b}Y^a + Y^aY^{\dagger b}Y^b]_{ij} + 2\left(Y^bY^{\dagger a}Y^b\right)_{ij} \\ &\quad + \frac{1}{2}Y^b_{ij}\mathrm{Tr}(Y^{\dagger a}Y^b + Y^{\dagger b}Y^a) - 3g^2\{C_2(F), Y^a\}_{ij}\,.\end{aligned} \tag{2.156}$$

Using our most explicit notation, these terms are written as

$$
\begin{aligned}
&\left(\beta^{(1)}\right)^{\phi^i_{g_i,\alpha_1\ldots\alpha_n}}_{\psi^j_{g_j,\beta_1\ldots\beta_n}\psi^k_{g_k,\gamma_1\ldots\gamma_n}} = \\
&\frac{1}{2}\sum_{s_1,f_1,f_2}\sum_{o,p,q}\sum_{\eta,\rho,\sigma}\Bigg[\mathcal{Y}^{\phi^{s_1}_{g_o,\eta_1\ldots\eta_n}}_{\psi^j_{g_j,\beta_1\ldots\beta_n}\psi^{f_1}_{g_p,\rho_1\ldots\rho_n}}\left(\mathcal{Y}^{\phi^{s_1}_{g_o,\eta_1\ldots\eta_n}}_{\psi^{f_1}_{g_p,\rho_1\ldots\rho_n}\psi^{f_2}_{g_q,\sigma_1\ldots\sigma_n}}\right)^\dagger\mathcal{Y}^{\phi^i_{g_i,\alpha_1\ldots\alpha_n}}_{\psi^{f_2}_{g_q,\sigma_1\ldots\sigma_n}\psi^k_{g_k,\gamma_1\ldots\gamma_n}} + \\
&\qquad+\mathcal{Y}^{\phi^i_{g_i,\alpha_1\ldots\alpha_n}}_{\psi^j_{g_j,\beta_1\ldots\beta_n}\psi^{f_1}_{g_p,\rho_1\ldots\rho_n}}\left(\mathcal{Y}^{\phi^{s_1}_{g_o,\eta_1\ldots\eta_n}}_{\psi^{f_1}_{g_p,\rho_1\ldots\rho_n}\psi^{f_2}_{g_q,\sigma_1\ldots\sigma_n}}\right)^\dagger\mathcal{Y}^{\phi^{s_1}_{g_o,\eta_1\ldots\eta_n}}_{\psi^{f_2}_{g_q,\sigma_1\ldots\sigma_n}\psi^k_{g_k,\gamma_1\ldots\gamma_n}}\Bigg] \\
&+2\sum_{s_1,f_1,f_2}\sum_{o,p,q}\sum_{\eta,\rho,\sigma}\Bigg[\mathcal{Y}^{\phi^{s_1}_{g_o,\eta_1\ldots\eta_n}}_{\psi^j_{g_j,\beta_1\ldots\beta_n}\psi^{f_1}_{g_p,\rho_1\ldots\rho_n}}\left(\mathcal{Y}^{\phi^i_{g_i,\alpha_1\ldots\alpha_n}}_{\psi^{f_1}_{g_p,\rho_1\ldots\rho_n}\psi^{f_2}_{g_q,\sigma_1\ldots\sigma_n}}\right)^\dagger\mathcal{Y}^{\phi^{s_1}_{g_o,\eta_1\ldots\eta_n}}_{\psi^{f_2}_{g_q,\sigma_1\ldots\sigma_n}\psi^k_{g_k,\gamma_1\ldots\gamma_n}} \\
&+\frac{1}{2}\sum_{s_1,f_1,f_2}\sum_{o,p,q}\sum_{\eta,\rho,\sigma}\Bigg[\mathcal{Y}^{\phi^{s_1}_{g_o,\eta_1\ldots\eta_n}}_{\psi^j_{g_j,\beta_1\ldots\beta_n}\psi^k_{g_k,\gamma_1\ldots\gamma_n}}\Bigg(\left(\mathcal{Y}^{\phi^i_{g_i,\alpha_1\ldots\alpha_n}}_{\psi^{f_1}_{g_p,\rho_1\ldots\rho_n}\psi^{f_2}_{g_q,\sigma_1\ldots\sigma_n}}\right)^\dagger\mathcal{Y}^{\phi^{s_1}_{g_o,\eta_1\ldots\eta_n}}_{\psi^{f_2}_{g_q,\sigma_1\ldots\sigma_n}\psi^{f_1}_{g_p,\rho_1\ldots\rho_n}} \\
&\qquad+\left(\mathcal{Y}^{\phi^{s_1}_{g_o,\eta_1\ldots\eta_n}}_{\psi^{f_1}_{g_p,\rho_1\ldots\rho_n}\psi^{f_2}_{g_q,\sigma_1\ldots\sigma_n}}\right)^\dagger\mathcal{Y}^{\phi^i_{g_i,\alpha_1\ldots\alpha_n}}_{\psi^{f_2}_{g_q,\sigma_1\ldots\sigma_n}\psi^{f_1}_{g_p,\rho_1\ldots\rho_n}}\Bigg)\Bigg]+ \\
&-3\sum_n g_n^2\sum_{f_1}\sum_o\sum_\eta\Bigg[C^{\psi^j_{g_j,\beta_1\ldots\beta_n}\psi^{f_1}_{g_o,\eta_1\ldots\eta_n}}_{2,n}\mathcal{Y}^{\phi^i_{g_i,\alpha_1\ldots\alpha_n}}_{\psi^{f_1}_{g_o,\eta_1\ldots\eta_n}\psi^k_{g_k,\gamma_1\ldots\gamma_n}} \\
&\qquad\qquad+\mathcal{Y}^{\phi^i_{g_i,\alpha_1\ldots\alpha_n}}_{\psi^j_{g_j,\beta_1\ldots\beta_n}\psi^{f_1}_{g_o,\eta_1\ldots\eta_n}}C^{\psi^{f_1}_{g_o,\eta_1\ldots\eta_n}\psi^k_{g_k,\gamma_1\ldots\gamma_n}}_{2,n}\Bigg] \\
&-3g^2\sum_{f_1}\sum_o\sum_\eta\Bigg[C^{\psi^j_{g_j,\beta_1\ldots\beta_n}\psi^{f_1}_{g_o,\eta_1\ldots\eta_n}}_{2,U(1)}\mathcal{Y}^{\phi^i_{g_i,\alpha_1\ldots\alpha_n}}_{\psi^{f_1}_{g_o,\eta_1\ldots\eta_n}\psi^k_{g_k,\gamma_1\ldots\gamma_n}} \\
&\qquad\qquad+\mathcal{Y}^{\phi^i_{g_i,\alpha_1\ldots\alpha_n}}_{\psi^j_{g_j,\beta_1\ldots\beta_n}\psi^{f_1}_{g_o,\eta_1\ldots\eta_n}}C^{\psi^{f_1}_{g_o,\eta_1\ldots\eta_n}\psi^k_{g_k,\gamma_1\ldots\gamma_n}}_{2,U(1)}\Bigg]\,. \qquad (2.157)
\end{aligned}
$$

The most general expressions look quite involved. Therefore, we are going to clarify their usage at the example of the SM, but concentrate again on the non-Abelian sector. The Yukawa part of the SM potential is usually written as:

$$-\mathcal{V} = Y_d^{ij}H^\dagger d_i q_j + Y_e^{ij}H^\dagger e_i l_j + Y_u^{ij}H u_i q_j\,. \qquad (2.158)$$

Here, i,j are the generation indices of the SM fermions and all isospin and charge indices are only implicit. We can make the following association:

$$\psi^1_{g_j,\alpha_1\alpha_2} = q_{j,\alpha_1\alpha_2}\,, \qquad \psi^2_{g_j,\alpha_1\alpha_2} = u_{j,\alpha_2}\,, \qquad (2.159)$$

$$\psi^3_{g_j,\alpha_1\alpha_2} = d_{j,\alpha_2}\,, \qquad \psi^4_{g_j,\alpha_1\alpha_2} = l_{j,\alpha_1}\,, \qquad \psi^5_{g_j,\alpha_1\alpha_2} = e_j \qquad (2.160)$$

$$\phi^1_{g_j,\alpha_1\alpha_2} = \phi^h_{\alpha_1}\,, \qquad \phi^2_{g_j,\alpha_1\alpha_2} = \sigma^h_{\alpha_1}\,. \qquad (2.161)$$

Together with Eq. (2.134) and Eq. (2.150), the potential given in Eq. (2.158) becomes

$$\begin{aligned}
-\mathcal{V} \;=\; & \frac{1}{\sqrt{2}} Y^{\phi^h_{\alpha_1}}_{d_{i,\beta_2} q_{j,\gamma_1\gamma_2}} \delta_{\beta_2\gamma_2}\delta_{\alpha_1\gamma_1}\phi^h_{\alpha_1} d_{i,\beta_2} q_{j,\gamma_1\gamma_2} - \frac{i}{\sqrt{2}} Y^{\sigma^h_{\alpha_1}}_{d_{i,\beta_2} q_{j,\gamma_1\gamma_2}} \delta_{\beta_2\gamma_2}\delta_{\alpha_1\gamma_1}\sigma^h_{\alpha_1} d_{i,\beta_2} q_{j,\gamma_1\gamma_2} \\
& + \frac{1}{\sqrt{2}} Y^{\phi^h_{\alpha_1}}_{e_i l_{j,\gamma_1}} \delta_{\alpha_1\gamma_1}\phi^h_{\alpha_1} e_i l_{j,\gamma_1} - \frac{i}{\sqrt{2}} Y^{\sigma^h_{\alpha_1}}_{e_i l_{j,\gamma_1}} \delta_{\alpha_1\gamma_1}\sigma^h_{\alpha_1} e_i l_{j,\gamma_1} \\
& + \frac{1}{\sqrt{2}} Y^{\phi^h_{\alpha_1}}_{u_{i,\beta_2} q_{j,\gamma_1\gamma_2}} \delta_{\beta_2\gamma_2}\epsilon_{\alpha_1\gamma_1}\phi^h_{\alpha_1} u_{i,\beta_2} q_{j,\gamma_1\gamma_2} + \frac{i}{\sqrt{2}} Y^{\sigma^h_{\alpha_1}}_{u_{i,\beta_2} q_{j,\gamma_1\gamma_2}} \delta_{\beta_2\gamma_2}\epsilon_{\alpha_1\gamma_1}\sigma^h_{\alpha_1} u_{i,\beta_2} q_{j,\gamma_1\gamma_2} \,.
\end{aligned} \tag{2.162}$$

Here, we already introduced the CGC

$$C^{2,2}_{\alpha\beta} = \epsilon_{\alpha\beta}\,, \qquad C^{2^*,2}_{\alpha\beta} = C^{2,2^*}_{\alpha\beta} = \delta_{\alpha\beta}\,, \tag{2.163}$$

for SU(2) as well as

$$C^{\bar{3},3}_{\alpha\beta} = C^{3,\bar{3}}_{\alpha\beta} = \delta_{\alpha\beta}\,, \tag{2.164}$$

for SU(3). Using Eq. (2.151) we can calculate the $\mathcal{Y}$'s we need:

$$\mathcal{Y}^{\sigma^h_{\alpha_1}}_{u_{i,\beta_2} q_{j,\gamma_1\gamma_2}} = \tfrac{i}{\sqrt{2}} Y_u^{ij}\delta_{\beta_2\gamma_2}\epsilon_{\alpha_1\gamma_1}\,, \qquad \mathcal{Y}^{\phi^h_{\alpha_1}}_{u_{i,\beta_2} q_{j,\gamma_1\gamma_2}} = \tfrac{1}{\sqrt{2}} Y_u^{ij}\delta_{\beta_2\gamma_2}\epsilon_{\alpha_1\gamma_1} \tag{2.165}$$

$$\mathcal{Y}^{\sigma^h_{\alpha_1}}_{d_{i,\beta_2} q_{j,\gamma_1\gamma_2}} = -\tfrac{i}{\sqrt{2}} Y_d^{ij}\delta_{\beta_2\gamma_2}\delta_{\alpha_1\gamma_1}\,, \qquad \mathcal{Y}^{\phi^h_{\alpha_1}}_{d_{i,\beta_2} q_{j,\gamma_1\gamma_2}} = \tfrac{1}{\sqrt{2}} Y_d^{ij}\delta_{\beta_2\gamma_2}\delta_{\alpha_1\gamma_1} \tag{2.166}$$

$$\mathcal{Y}^{\sigma^h_{\alpha_1}}_{e_i l_{j,\gamma_1}} = -\tfrac{i}{\sqrt{2}} Y_e^{ij}\delta_{\alpha_1\gamma_1}\,, \qquad \mathcal{Y}^{\phi^h_{\alpha_1}}_{e_i l_{j,\gamma_1}} = \tfrac{1}{\sqrt{2}} Y_e^{ij}\delta_{\alpha_1\gamma_1}\,. \tag{2.167}$$

All other combinations of fields vanish. Inserting this into Eq. (2.157) and evaluating all sums we would obtain the one-loop β function for all Yukawa couplings. For instance, the β-function of Y_d can be calculated using the relation

$$\beta^{(1)}_{Y_d^{ij}} = \sqrt{2}(\beta^{(1)})^{\phi^h_{\alpha_1}}_{d_{i,\beta_2} q_{j,\gamma_1\gamma_2}} \delta_{\beta_2\gamma_2}\delta_{\alpha_1\gamma_1} \equiv \sqrt{2}(\beta^{(1)})^{\phi^h_1}_{d_{i,2} q_{j,12}} \tag{2.168}$$

First, we multiplied the β function by $\sqrt{2}$ since $\mathcal{Y}^{\phi^h}_{dq}$ corresponds to $\frac{Y_d}{\sqrt{2}}$, while we want to have the running of Y_d. Furthermore, we restricted ourselves to an explicit combination of external color charges and isospin indices. This has been done to simplify the following calculation. To point out the main steps of the calculation, we concentrate on the fourth and fifth line of Eq. (2.157):

$$\begin{aligned}
\beta^{(1)}_{Y_d^{ij}} \;=\; & \sqrt{2}\Bigg[\dots \\
& \frac{1}{2} \sum_s \sum_{f_1,f_2} \sum_{p,q=1}^{\mathcal{N}_F^f} \sum_{\eta_1=1}^{2} \sum_{\sigma_1=1}^{2} \sum_{\rho_1=1}^{2} \sum_{\rho_2=1}^{3} \sum_{\sigma_2=1}^{3} \Bigg[\mathcal{Y}^{\phi^s_{\eta_1}}_{d_{i,1} q_{j,12}} \Bigg(\\
& \qquad \left(\mathcal{Y}^{\phi^h_1}_{\psi^{f_1}_{p,\rho_1\rho_2}\psi^{f_2}_{q,\sigma_1\sigma_2}} \right)^\dagger \mathcal{Y}^{\phi^s_{\eta_1}}_{\psi^{f_2}_{q,\sigma_1\sigma_2}\psi^{f_1}_{p,\rho_1\rho_2}} \\
& \qquad + \left(\mathcal{Y}^{\phi^s_{\eta_1}}_{\psi^{f_1}_{p,\rho_1\rho_2}\psi^{f_2}_{q,\sigma_1\sigma_2}} \right)^\dagger \mathcal{Y}^{\phi^h_1}_{\psi^{f_2}_{q,\sigma_1\sigma_2}\psi^{f_1}_{p,\rho_1\rho_2}} \Bigg) \Bigg] \\
& + \dots \Bigg] \,.
\end{aligned} \tag{2.169}$$

First, one has to evaluate the sum over s and f_1, f_2. The non-vanishing contributions are

$$\psi^{f_{1,2}} = d, q\,, \qquad \psi^{f_{1,2}} = u, q\,, \qquad \psi^{f_{1,2}} = l, e \tag{2.170}$$

while only

$$\phi^s = \phi^h \tag{2.171}$$

is possible. For $\phi^s = \sigma^h$ the two terms in the sum enter with a different sign and cancel each other. All terms are calculated in the same way, and we pick for further discussion $\psi^{f_1} = d$, $\psi^{f_2} = q$:

$$\begin{aligned}
\beta^{(1)}_{Y_d^{ij}} &= \sqrt{2}\Bigg[\cdots + \frac{1}{2}\sum_{p,q}\sum_{\eta_1,\sigma_1}\sum_{\rho_2,\sigma_2}\Bigg[\mathcal{Y}^{\phi^h_{\eta_1}}_{d_{i,2}q_{j,12}}\Bigg(\left(\mathcal{Y}^{\phi^h_1}_{d_{p,\rho_2}q_{q,\sigma_1\sigma_2}}\right)^\dagger \mathcal{Y}^{\phi^h_{\eta_1}}_{q_{q,\sigma_1\sigma_2}d_{p,\rho_2}} \\
&\qquad + \left(\mathcal{Y}^{\phi^h_{\eta_1}}_{d_{p,\rho_2}q_{q,\sigma_1\sigma_2}}\right)^\dagger \mathcal{Y}^{\phi^h_1}_{q_{q,\sigma_1\sigma_2}d_{p,\rho_2}}\Bigg)\Bigg] + \dots\Bigg] \\
&= \cdots \frac{\sqrt{2}}{2}\sum_{p,q}\sum_{\eta_1,\sigma_1}\sum_{\rho_2,\sigma_2}\Bigg[\left(\frac{1}{\sqrt{2}}Y_d^{ij}\delta_{1\eta_1}\right)\left(\frac{1}{\sqrt{2}}Y_d^{pq,\dagger}\delta_{1\sigma_1}\delta_{\rho_2\sigma_2}\right)\left(\frac{1}{\sqrt{2}}Y_d^{qp}\delta_{\eta_1\sigma_1}\delta_{\rho_2\sigma_2}\right) + \\
&\qquad + \left(\frac{1}{\sqrt{2}}Y_d^{ij}\delta_{1\eta_1}\right)\left(\frac{1}{\sqrt{2}}Y_d^{pq,\dagger}\delta_{\eta_1\sigma_1}\delta_{\rho_2\sigma_2}\right)\left(\frac{1}{\sqrt{2}}Y_d^{qp}\delta_{1\sigma_1}\delta_{\rho_2\sigma_2}\right)\Bigg] + \dots \\
&= \cdots + \frac{1}{4}Y_d^{ij}\sum_{p,q}(3Y_d^{pq,\dagger}Y_d^{qp} + 3Y_d^{pq,\dagger}Y_d^{qp}) + \dots \\
&= \cdots + \frac{3}{2}Y_d^{ij}\mathrm{Tr}(Y_d^\dagger Y_d) + \dots
\end{aligned} \tag{2.172}$$

Here, one can see nicely the appearance of the color factor due to the sum over the charges of the internal particles. The other terms can be obtained similarly: $\psi^{f_1} = q$ and $\psi^{f_2} = d$ results in the same coefficient, i.e. one gains a factor of two. For $\psi^{f_{1,2}} = q, u$ one gets the same result as for q, d with Y_d replaced by Y_u, while for $\psi^{f_{1,2}} = l, e$ one gets this term with $Y_d \to Y_e$ together with a relative factor of $\frac{1}{3}$ because of the missing color factor. In sum, we end up with the well known result

$$\beta^{(1)}_{Y_d} = \frac{1}{16\pi^2}\left[Y_d\left(3\mathrm{Tr}(Y_d^\dagger Y_d) + 3\mathrm{Tr}(Y_u^\dagger Y_u) + \mathrm{Tr}(Y_e^\dagger Y_e)\right) + \dots\right]. \tag{2.173}$$

The same approach holds for all other terms and even at the two-loop level. To cover also the evaluation of the quartic coupling and the Higgs mass terms given by

$$-\mathcal{V} = -\frac{1}{2}\lambda|H^\dagger H|^2 + \mu^2 H^\dagger H\,, \tag{2.174}$$

the following objects are needed in addition:

$$\mathcal{L}^{\phi^h_{\alpha_1}\phi^h_{\beta_1}\phi^h_{\gamma_1}\phi^h_{\delta_1}} = \lambda(\delta_{\alpha_1\beta_1}\delta_{\gamma_1\delta_1} + \delta_{\alpha_1\gamma_1}\delta_{\beta_1\delta_1} + \delta_{\alpha_1\delta_1}\delta_{\beta_1\gamma_1}) \tag{2.175}$$

$$\mathcal{L}^{\sigma^h_{\alpha_1}\sigma^h_{\beta_1}\sigma^h_{\gamma_1}\sigma^h_{\delta_1}} = \lambda(\delta_{\alpha_1\beta_1}\delta_{\gamma_1\delta_1} + \delta_{\alpha_1\gamma_1}\delta_{\beta_1\delta_1} + \delta_{\alpha_1\delta_1}\delta_{\beta_1\gamma_1}) \tag{2.176}$$

$$\mathcal{L}^{\phi^h_{\alpha_1}\phi^h_{\beta_1}\sigma^h_{\gamma_1}\sigma^h_{\delta_1}} = \lambda\delta_{\alpha_1\beta_1}\delta_{\gamma_1\delta_1} \tag{2.177}$$

$$\mathcal{M}_{\mathcal{S}}{}^{\phi^h_{\alpha_1}\phi^h_{\beta_1}} = -\mu^2\delta_{\alpha_1\beta_1} \tag{2.178}$$

$$\mathcal{M}_{\mathcal{S}}{}^{\sigma^h_{\alpha_1}\sigma^h_{\beta_1}} = -\mu^2\delta_{\alpha_1\beta_1} \tag{2.179}$$

As an example to demonstrate this, we pick the term $\propto \mu^2\lambda$ in the one-loop β-function of μ^2. This terms is stemming from

$$\beta^{(1)}_{m^2_{ab}} = m^2_{ef}\lambda_{abef} + \dots \tag{2.180}$$

which results in the most explicit form in

$$\beta^{(1)}_{\mu^2} = -(\beta^{(1)})^{\phi^h_i\phi^h_j} \equiv -(\beta^{(1)})^{\phi^h_1\phi^h_1} = -\sum_{s_1,s_2}\sum_{\eta_1,\rho_1} \mathcal{M}_{\mathcal{S}}{}^{\phi^{s_1}_{\eta_1}\phi^{s_2}_{\rho_1}} \mathcal{L}^{\phi^{s_1}_{\eta_1}\phi^{s_2}_{\rho_1}\phi^h_1\phi^h_1} + \dots \tag{2.181}$$

Here, we used again a particular choice for the isospin indices. The only, non-vanishing combinations are $\phi^{s_1} = \phi^{s_2} = \sigma^h$ and $\phi^{s_1} = \phi^{s_2} = \phi^h$. Hence, we obtain

$$\begin{aligned}
\beta^{(1)}_{\mu^2} &= -\sum_{\eta_1,\rho_1}\left[\mathcal{M}_{\mathcal{S}}{}^{\sigma^h_{\eta_1}\sigma^h_{\rho_1}}\mathcal{L}^{\sigma^h_{\eta_1}\sigma^h_{\rho_1}\phi^h_1\phi^h_1} + \mathcal{M}_{\mathcal{S}}{}^{\phi^h_{\eta_1}\phi^h_{\rho_1}}\mathcal{L}^{\phi^h_{\eta_1}\phi^h_{\rho_1}\phi^h_1\phi^h_1}\right] + \dots \\
&= -\sum_{\eta_1,\rho_1}\left[-\mu^2\delta_{\eta_1\rho_1}\lambda\delta_{\eta_1\rho_1} - \mu^2\delta_{\eta_1\rho_1}\lambda(\delta_{\eta_1\rho_1} + 2\delta_{1\eta_1}\delta_{1\rho_1})\right] + \dots \\
&= 6\mu^2\lambda + \dots
\end{aligned} \tag{2.182}$$

2.4.2 Installation

PyR@TE is free software under the terms of the GNU General Public License and can be downloaded from the following web page:

http://pyrate.hepforge.org

To install PyR@TE, simply open a shell and type:

```
1 cd $HOME
2 wget http://pyrate.hepforge.org/downloads/pyrate-1.1.2.tar.gz
3 tar xfvz pyrate-1.1.2.tar.gz
4 cd pyrate-1.1.2/
```

For definiteness, we will assume here and in the following that you want to install PyR@TE in your home directory (cf. line 1 in the listing above). Otherwise, simply replace " $HOME" by a directory of your choice. At the time of writing, PyR@TE is available in the version 1.1.2, and later you may need to replace this by a more recent version number[24] (cf. line 2). Unpacking the tar ball (line 3) will then create a subdirectory that contains PyR@TE. We will describe how to run the program in Section 2.4.3.

PyR@TE has the following minimal software requirements:

- `Python` $\geq$ 2.7.1[25] [166]
- `NumPy` $\geq$ 1.7.1 [167] and `SciPy` 0.12.0 [168]
- `SymPy` $\geq$ 0.7.2 [169]

[24] All versions of PyR@TE will be available in the "Downloads" section of our web page [165].

[25] PyR@TE was developed with `Python` 2.7.1 but should work with more recent versions with the exception of `Python` 3 for which it has not been tested.

- `IPython` $\geq$ 0.12 [170]
- `PyYAML` $\geq$ 3.10 [171]

Most of these packages ship with any standard Linux distribution and are by default pre-installed on your system, but in case they are not, you can easily install them. All but one are available in the standard repositories and can be installed by the respective package manager of your system, e.g. " yum install SymPy" for a Fedora-based distribution and " apt-get install python-sympy" for a Debian-based one. For PyYAML, you have to visit its web page [171] and follow the installation instructions.

If `SymPy` 0.7.2 is not available for your system in the repositories (or not in the correct version[26]), you can easily install it by downloading the source code from its web page [169]:

```
1 wget https://github.com/sympy/sympy/archive/sympy-0.7.2.tar.gz
2 tar xfvz sympy-0.7.2
3 mv sympy-sympy-0.7.2/sympy $HOME/pyrate-1.1.2/
```

After unpacking the tarball (line 2), move the subdirectory " SymPy" to where PyR@TE is installed (line 3). In the next section, we will explain in detail how to run PyR@TE.

2.4.3 Running PyR@TE: first steps

We will first describe how to run PyR@TE from the command line and later explain in some detail the interactive mode. Throughout this section, we will use the SM to illustrate how to use PyR@TE, since it is the theory people are most familiar with. Also, for the SM the output of PyR@TE can easily be compared to the literature.

To run PyR@TE, open a shell, change to the directory where it is installed and enter:

```
python pyR@TE.py -m models/SM.model
```

The option " -m" (or " --Model") is used to read in a model file, in this case the SM. For now, we defer the discussion of how to create a model file to Section 2.4.5 and proceed directly with the calculation of the RGEs. Because the calculations can be quite time-consuming, PyR@TE does not calculate them by default. Rather, the user has complete freedom over the parts of the calculation he needs. For instance, to calculate the RGEs for the gauge, Yukawa or quartic couplings, one would add the options " --Gauge-Couplings", " --Yukawas", " --Quartic-Couplings", respectively, or alternatively " -gc", " -yu" or " -qc":

```
python pyR@TE.py -m ./models/SM.model -gc -yu -qc
```

After PyR@TE terminates and the shell prompt reappears, the results of the calculation will be available in the newly created subdirectory " $HOME/pyrate-1.1.0/results". Specifically, the LaTeX file " RGEsOutput.tex" contains the RGEs and a summary of the settings and of the model for which the calculation was done. We will discuss other forms of output later in Section 2.4.6. Before we go into those details, we would first like to give an exhaustive list of the options used to control PyR@TE.

[26] If `SymPy` 0.7.3 is available on your system, you can patch it so that it works with PyR@TE. You can find detailed instructions on how to do this on our web page [165].

2.4.4 Settings and options

PyR@TE and the type of output it generates are controlled by various options that we have summarized in Tab. 2.5. Alternatively, one can also obtain the complete list of options by typing

```
python pyR@TE.py --help
```

at the shell prompt. Most options are self-explanatory, and we will therefore not go into any details at this point. In later sections, we will illustrate their use by providing examples.

As the number of options increases, it is more convenient to save all settings in a file which can then be passed to PyR@TE instead of appending a long string of options[27]:

```
python pyR@TE.py -f SMsets.settings
```

The input file " SMsets.settings" is written in YAML [172] which is a human-readable format for storing information that can also be easily accessed by a computer. The lines in this file have the following generic structure:

```
keyword: value
```

Here, " keyword" is a keyword predefined in PyR@TE, and " value" is either a path, a filename or a Boolean, i.e. " True" or " False". For example, a typical " SMsets.settings" file could look like this:

Listing 2.1: SMsets.settings

```
# YAML 1.1
---
Model: ./models/SM.model
Gauge-Couplings: True
Quartic-Couplings: True
Yukawas: True
ScalarMass: False
Two-Loop: False
verbose: True
```

Note that (i) strings need not be delimited by quotes, (ii) you can only use spaces as whitespace, i.e. tabulators are not allowed, and (iii) the space after ":" is mandatory. For the keys that can be used in the settings file, we refer the reader again to Tab. 2.5.

2.4.5 Implementing your own model

The previous sections described how to run PyR@TE to calculate the RGEs for a given model. In this paragraph we will explain how to create your own model file that you can use with PyR@TE. As before, we will use the SM as an epitome to explain the format of the model file. In Appendix D, we give several examples of model files for various extensions of the SM. These examples and many more are also available in the " models" subdirectory that ships with PyR@TE.

[27] Note that we provide no default settings file and that you have to create your own one e.g. by copying the lines given in listing 2.1.

Table 2.5: List of all options that can be used to control PyR@TE. Note that the last two are only available in versions 1.1.x

Option	Keyword | Default	Description
--Settings/-f	- | -	Specify the name of a *.settings* file.
--Model/-m	Model | -	Specify the name of a . *model* file.
--verbose/-v	verbose | False	Set verbose mode.
--VerboseLevel/-vL	VerboseLevel | Critical	Set the verbose level: *Info, Debug, Critical*
--Gauge-Couplings/-gc	Gauge-Couplings | False	Calculate the gauge couplings RGEs.
--Quartic-Couplings/-qc	Quartic-Couplings | False	Calculate the quartic couplings RGEs.
--Yukawas/-yu	Yukawas | False	Calculate the Yukawa RGEs.
--ScalarMass/-sm	ScalarMass | False	Calculate the scalar mass RGEs.
--FermionMass/-fm	FermionMass | False	Calculate the fermion mass RGEs.
--Trilinear/-tr	Trilinear | False	Calculate the trilinear term RGEs.
--All-Contributions/-a	all-Contributions | False	Calculate all the RGEs.
--Two-Loop/-tl	Two-Loop | False	Calculate at two-loop order.
--Weyl/-w	Weyl | True	The particles are Weyl spinors.
--LogFile/-lg	LogFile | True	Produce a log file.
--LogLevel/-lv	LogLevel | Info	Set the log level: *Info, Debug, Critical*
--LatexFile/-tex	LatexFile | RGEsOutput.tex	Set the name of the LaTeX output file.
--LatexOutput/-texOut	LatexOutput | True	Produce a LaTeX output file.
--Results/-res	Results | ./results	Set the directory of the results
--Pickle/-pkl	Pickle | False	Produce a pickle output file.
--PickleFile/-pf	PickleFile | RGEsOutput.pickle	Set the name of the pickle output file.
--TotxtMathematica/-tm	ToM | False	Produce an output to Mathematica.
--TotxtMathFile/-tmf	ToMF | RGEsOutput.txt	Set the name of the Mathematica output file.
--Export/-e	Export | False	Produce the numerical output.
--Export-File/-ef	ExportFile | BetaFunction.py	File in which the beta functions are written.
--Skip/-sk	Skip | ''	Set the various terms that can be neglected during the calculation.
--Only/-onl	Only | {}	Set a dictionary of terms you want to calculate.

The three ingredients needed to define a model file are the gauge group, the particle content and the scalar potential. The general form of the model file is similar to that of the settings file already described in Section 2.4.4. Consider the following model file given in listing 2.2. The first line indicates that this is a YAML file. Lines 3-5 indicate the author of the model, the filename and the date when it was created.

Listing 2.2: models/SM.model

```
1  # YAML 1.1
2  ---
3  Author: Florian Lyonnet
4  Date: 11.04.2013
5  Name: SM
6  Groups: {'U1': U1, 'SU2L': SU2, 'SU3c': SU3}
7
8  ################################
9  #Fermions assumed weyl spinors
10 ################################
11 Fermions: {
12     Qbar: {Gen: 3, Qnb:{ U1: -1/6, SU2L: -2, SU3c: -3}},
13     Lbar: {Gen: 3, Qnb:{ U1: 1/2, SU2L: -2, SU3c: 1}},
14     uR: {Gen: 3, Qnb:{ U1: 4/6, SU2L: 1, SU3c: [1,0]}},
15     dR: {Gen: 3, Qnb:{ U1: -1/3, SU2L: 1, SU3c: 3}},
16     eR: {Gen: 3, Qnb:{ U1: -1, SU2L: 1, SU3c: 1}}
17 }
18
19 ##############################
20 #Real Scalars, none in the SM
21 ##############################
```

```
22
23  RealScalars: {
24  }
25
26  ######################################################
27  #Complex Scalars : give names for the real components
28  ######################################################
29
30  CplxScalars: {
31    H: {RealFields: [Pi,I*Sigma], Norm: 1/Sqrt(2), Qnb : {U1: 1/2, SU2L: 2,
        SU3c: 1}},
32    H*: {RealFields: [Pi,-I*Sigma], Norm: 1/Sqrt(2), Qnb : {U1: -1/2, SU2L:
        -2, SU3c: 1}}
33  }
34
35  Potential: {
36
37  ######################################
38  # All particles must be defined above !
39  ######################################
40
41  Yukawas:{
42    'Y_{u}': {Fields: [Qbar,uR,H*], Norm: 1},
43    'Y_{d}': {Fields: [Qbar,dR,H], Norm: 1},
44    'Y_{e}': {Fields: [Lbar,eR,H], Norm: 1}
45   },
46  QuarticTerms: {
47   \Lambda_1 : {Fields : [H,H*,H,H*], Norm : 1/2}
48   },
49  ScalarMasses: {
50   \mu_1 : {Fields : [H*,H], Norm : 1}
51   }
52  }
```

On line 6 you find the definition of the gauge group labelled by the keyword " Groups". The gauge group is a product of simple Lie algebras and any number of U(1) factors (note, however, that we have not implemented kinetic mixing between the U(1) factors). In turn, each simple Lie algebra or U(1) is associated with a user-defined name (e.g. " SU3c" on line 6), and a predefined PyR@TE keyword that specifies the Lie algebra as a mathematical object (cf. SU(3) on line 6). So far, we have implemented SU(N) for $N = 2, \ldots, 6$ and U(1), and in Appendix A we present a list of irreducible representations (irreps) that are currently recognized by PyR@TE. Note that this list will be extended in future versions of PyR@TE.

Next, we discuss how to add particles to our model (lines 11-33 in listing 2.2). We distinguish between " Fermions", " RealScalars" and " CplxScalars". Each particle is defined by giving it a name and then listing all its quantum numbers, cf. e.g. line 12 in listing 2.2:

```
Qbar: {Gen: 3, Qnb:{ U1: -1/6, SU2L: -2, SU3c: -3}}
```

Here, " Gen" is a predefined keyword denoting the number of generations, but the names for the gauge group factors correspond to those specified by the user on line 6. The number of generations for a given particle can in principle be kept general, but then PyR@TE will not be able to perform some basic simplifications and the result may look more complicated. The gauge quantum numbers (specified via the keyword " Qnb") can either be specified by the dimension of the corresponding irrep[28], or their Dynkin labels

[28]For simple gauge group factors we use a minus sign to distinguish between a representation and its complex conjugate one. For a U(1) factor the quantum number corresponds to the usual U(1) charge in some physics normalization.

(see definition of " uR" on line 14). This is possible for all simple gauge groups, but for SU(2) we have to use a slightly more complicated notation, since we need to distinguish between a given representation and its complex conjugate[29]: "$(n-1,)$" will correspond to the n-dimensional representation, and "$(n-1,\text{True})$" to its complex conjugate. Note that internally all the quantum numbers are translated to Dynkin labels, so if the dimension of a given irrep does not define it uniquely, the user has to use the Dynkin labels. A table with all the irreps that can be used in PyR@TE is given in Appendix A.

Let us now turn to discussing how to add scalars (lines 23-33 in listing 2.2). Real scalars are declared by using the keyword " RealScalars" and then specifying their gauge quantum numbers (see below for examples including real scalars). For complex scalars (keyword " CplxScalars"), one has to name the real degrees of freedom using the keyword " RealFields" because each complex field will be split into real components during the calculation. The user can choose a convenient normalization for the complex scalar using the keyword " Norm". Also note that you have to declare H^* explicitly (see line 32).

We mention in passing that in order to simplify the notation we have introduced a short-hand syntax. The preceding declarations (lines 1-33 in listing 2.2) can also be rewritten in the form given in listing 2.3.

Listing 2.3: Short-hand syntax for the SM model file

```
1  Groups: [U1,SU2,SU3]
2  Fermions: {
3     Qbar: [3, -1/3, -2,-3],
4     Lbar: [3, 1,-2,1],
5     uR: [3,4/3,1, [1,0]],
6     dR: [3,-2/3, 1,3],
7     eR: [3,-2,1,1]
8  }
9  RealScalars: {
10 }
11 CplxScalars: {
12   H: {RealFields: [Pi,I*Sigma], Norm: 1/Sqrt(2), Qnb : [1, 2,  1]},
13   H*: {RealFields: [Pi,-I*Sigma], Norm: 1/Sqrt(2), Qnb : [-1,-2,1]}
14 }
```

We now come to the potential which is introduced by the keyword " Potential" (lines 35-51 in listing 2.2) and has five parts, each preceded by its own keyword: Yukawa interactions (" Yukawas"), quartic terms (" QuarticTerms"), scalar masses (" ScalarMasses"), trilinear interactions (" TrilinearTerms"), and fermion masses (" FermionMasses"). Each term in one of the five parts is represented by a coupling constant (e.g. "mu_1" on line 50), a number of fields (" [H*,H]") and a numerical factor (" Norm : 1"). Note that for the coupling constant we can use LaTeX notation[30]which will then be used for the output.

Addition in versions 1.1.x

The last two options of the table Tab. 2.5 are only available since versions 1.1.x. The fisrt one allows the user to skip some of the terms directly at the calculation level. The different pieces that can be skipped are defined according to [116], e.g. a viable entry would be

[29]In SU(2) any representation is equivalent to its complex conjugate one, but for contracting the SU(2) indices this change of basis matters.

[30]In this case, quotation marks must be used so that the string is recognized as a latex expression.

```
Skip: ['CAabcd','CL2abcd']
```

would skip equations Eqs. (43) and (39) of [116]. Note that the label are identical to the ones defined in the article with a "C" added in front and with the subtitution "Lambda→L". All the existing label as well as their precise definition can be seen in "Source/Core/RGEsDefinition.py". The second option, "Only" allows the user to calculate only some of the constants defined in the Lagrangian while keeping the dependance on the others. E.g. in a model in which three quartic terms are defined, "lambda1, lambda2, lambda3", the user might be interested only in the RGE of "lambda1" while keeping the terms involving "lambda2, lambda3" in the calculation. This is accomplished via the option "Only".

```
Only: {'QuarticTerms': ['\lambda2','\lambda3']}
```

The user must pass the whole argument as a string if using the 'Only' option via the command line, e.g.

```
python pyR@TE -m models/2HDM.model
   --Only ''{'QuarticTerms': ['\lambda3']}''
```

Appart from these two new options we also introduced the possibility to define sums of terms. For instance, declaring the term $\lambda_1(H^\dagger H H^\dagger \phi - \phi^\dagger H H^\dagger H)$ in PyR@TE one would need to enter

```
lambda_1: {Fields: [[H*,H,H*,Phi],[Phi*,H,H*,H]],Norm: [1,-1]}
```

in which the norm could also be a single number, e.g. 1/2 in case where both terms have the same normalization. This allows for a much more efficient disentangling of the various RGEs that mix with each others.

2.4.6 Output

In this section we explain in some more detail the various formats in which PyR@TE can generate output.

LaTeX With the option " --Latex-Output", PyR@TE generates a LaTeX file whose name can be set by " --LatexFile" followed by a filename. This is the most convenient way to obtain the RGEs in a human-readable format. The file will be saved in the directory specified by the option " --Results", or, more conveniently, set in a settings file (cf. 2.1 on page 73).

Pickle As the name suggests, Pickle is used to efficiently store Python data structures (in our case the partial or full results of our calculations) for later use. It is particularly useful when combined with the interactive mode to be described below. We refer the reader to Tab. 2.5 for a short description of the options " --Pickle" and " --PickleFile".

Mathematica To export results to Mathematica, PyR@TE can produce a text file with lines that can be directly copy-pasted into a Mathematica notebook. This option is controlled by the switches " --TotxtMathematica" and " --TotxtMathFile" (see Tab. 2.5 for more details).

2.4.7 Numerical evaluation

The RGEs generated by PyR@TE can be directly solved and visualized in one of two ways: Either from within `Python` or in a Mathematica notebook. We will describe in turn both approaches.

Solving within Mathematica

The option " --TotxtMathematica" also produces a file[31] that ends on " _numerics.m" that contains the equations as well as the information required by `Mathematica` to solve the RGEs. The package " RunPyRate_RGEs.m" which is included in the directory " Source/Output" prepares the equations for `Mathematica` and uses its internal routines to solve the system. For instance, one would enter the following lines in `Mathematica`:

```
1 PATH = "$HOME/pyrate-1.0.0/";
2 Get[PATH <> "results/RGEsOutput.txt_numeric.m"];
3 Get[PATH <> "/Source/Output/RunPyRate_RGEs.m"];
4 IncludeOffDiagonal=True;
5 AllParameters
```

Line 1 tells `Mathematica` where PyR@TE is installed. Line 2 points to the file where the results are stored, and line 3 loads the package to solve the RGEs. The switch " IncludeOffDiagonal=True" instructs `Mathematica` to include the full matrix structure of the parameters in solving the RGEs and not to neglect off-diagonal entries. By contrast, " IncludeOffDiagonal=False" will neglect the off-diagonal terms. Note that the variable " AllParameters" contains all the different RGEs that can be solved i.e. all the ones for which the user can set initial values and explore the results. After the initialization, a routine called " RunRGEs" is available that takes as input the starting and ending points of the interval over which the RGEs are to be integrated as well as the initial values of the parameters. Passing a last argument with values " True/False" will tell `Mathematica` to ignore or not the two loop contributions in the RGEs if they are available[32].

```
running=RunRGEs[3, 16, {g1->0.36, gSU2L->0.65, gSU3c->1.08},False];
```

The first and second inputs are the logarithms of the scales where the running starts and ends, respectively. If Landau poles appear, `Mathematica` will terminate before reaching the end point. The third input is the initialization of the parameters that have non-zero values at the starting scale. For instance, to run the gauge couplings in the SM from 1 TeV to 10^{16} GeV and to plot the result, simply enter:

[31] If the filename is not set by " --TotxtMathFile", the default name " RGEsOutput.txt_numerics.m" will be chosen.

[32] This is only possible since version 1.0.3

```
Plot[{g1[x],gSU2L[x],gSU3c[x]} /.running[[1]],{x,3,16}];
```

This example is also included in the file " Example.nb" inside the PyR@TE directory.

Using `Python`

Now we explain how to run the RGEs from within `Python`. With the options " --Export" and " --Export-File"[33] PyR@TE creates two files: The first one contains the results of the calculation in a form that is amenable to numerical analysis (i.e. `NumPy` objects). The second one, named `SolveRGEs.py`, is a `Python` script that solves[34] the RGEs stored in the first file and contains instructions on how to plot the results with Matplotlib. Note that the user is responsible for setting the interval over which the RGEs will be integrated (start and end points) and also the initial values of the parameters. In a schematic way there are three steps to be done to solve the RGEs within our framework:

(i) Create an instance of the RGEclass, our own class to represent the RGEs of a given model. This is done by calling the constructor of the class which takes three inputs. The name of the function encoding the beta functions (declared inside BetaFunction.py), number of equations contained in the system as well as a list of the labels to identify the different equations.

```
myrges = RGEclass(beta_function_toymodel,3,labels=['g1','g2','g3'])
```

(ii) Set the `Y0` attributes of the instance just created (myrges in this example) to the initial values.

```
myrges.Y0 = [0.36,0.65,1.08]
```

(iii) Call the method `solve_rges` of the RGEclass instance to solve the RGEs. This method takes in input the initial scale, the final scale, the step of iteration[35] as well as an optional dictionary `assumptions` that we will describe below. Note the scale value must be given in $\log_{10}$ as in the `Mathematica` case.

```
myrges.solve_rges(3,16,0.1,assumptions={})
```

Once these three steps have been done, the user can access the results via the `Sol` attributes of the instance which is a dictionary e.g.

```
myrges.Sol['g1']#contains the values calculated for the 'g1' equation
```

Note that the results are stored according to the labels specified when creating the instance. The `assumptions` dictionary allows the user to customize the solving of the RGEs. By default there are two switches implemented which are `'two-loop': True/False` and `'diag': True/False`. The first one will turn-off all the two-loop contributions when

[33] If this option is skipped, the file will be named " BetaFunction.py" by default.

[34] We use python.scipy.integrate [168] to numerically solve ordinary differential equations.

[35] i.e. $(t_f - t_i)/t_s$ fixes the number of points calculated, where t_i is the initial scale, t_f the final scale and t_s the step.

set to `False` and the second one will turn-off the off-diagonal term when set to `False`. However, one can look into the " BetaFunction.py" file and implement one's own switches as desired. The file generated when calling PyR@TE with the option " --Export" is ready to use and carries all the steps described here for your specific model. The only input from the user is the initial values that have to be set. Comments that will guide the eye of the user to perform the necessary modifications are present in this file.

In the next section we will introduce a user interface à la `Mathematica`, called an `IPython Notebook`, in which we can perform all the tasks described so far in an interactive way.

2.4.8 The interactive mode

A very convenient and user friendly way of using PyR@TE is to combine our code with an `IPython Notebook` [170]. The first thing to do is to start it by typing in the PyR@TE directory[36]:

```
cd $HOME/pyrate-1.1.2/
ipython notebook
```

The `IPython Notebook` will then start in your default browser, and you will see all the available notebooks that are located in the PyR@TE directory. You can now start executing one of these notebooks by simply clicking on the link. An easy way to get started is to look at one of the tutorials available online and/or to go through the InteractivePyRaTE.ipynb file located in the PyR@TE directory.

Running PyR@TE from within a notebook

An IPython Notebook, that we will simply call notebook in the following, is a web interface inside which you can execute any `Python` command. Once you open a new notebook you have access to cells (as in `Mathematica`) in which you execute any python command of your will as well as external python scripts. Therefore, to run PyR@TE from within the notebook simply enters in one of the cell :

```
%run pyR@TE.py -m models/SM.model -a -v
```

and then press `shift+Enter` to execute the cell. You will see the same output as when executing this command from the shell appear on the webpage. The main advantage of the notebook is that once the execution is finished, all the variables defined during the run are accessible. Therefore, one has access to the results of the calculation and can study them directly inside the notebook. Note that the equations are stored in the `RGEs` list and can be access like this :

```
#first result depending on the model it can be the gauge couplings
#or something else
RGEs[0]
```

[36] The `IPython Notebook` is included in recent installations of `ipython`. If you are using an older version, you can download it from its web page [170] or use the command " pip install ipython" (recommended) which should also take care of possible dependencies. If not pre-installed, the package manager " pip" can be installed by hand or using " easy_install pip".

All the algebraic equations are rendered in latex directly[37] inside the notebook and a right click on one of the equations gives you the possibility to get the latex code directly. In order to make full use of this framework we developed a Toolbox that implements various functions to do common tasks including the export of results, simplifications of equations and comparison of models. All the functions in the Toolbox are now described in the next section.

2.4.9 The Toolbox

To load the Toolbox from a notebook, make sure that the path `'./Source/Output'` is available (automatic if you have run PyR@TE in the same notebook otherwise you may need to run `import sys sys.path.append('./Source/Output')`). Then import the Toolbox via the regular python command, i.e.

```
from Toolbox import *
```

We now describe all the functions present in the Toolbox and exemplify them when necessary.

```
ExportToLatex(FileName,Expression,AModel)
ExportToMathematica(FileName,Expression,AModel)
ExportToPickle(FileName,Expression,AModel,description='')
ExportBetaFunction(FileName,AModel)
```

(i) `FileName` is the name of the output file

(ii) `Expression` is the list containing the results i.e. RGEs

(iii) `AModel` is the model instance of the ModelClass i.e. model

(iv) `description` is a string which contains some additional description of the results being stored in the pickle file

These can only be called after a run of PyR@TE inside the same notebook since the variables `RGEs` and `model` are defined during the run. Therefore these functions will always be called with the values `model` and `RGEs` for the values `Expression` and `AModel` respectively. They execute the same actions as the corresponding run options : `--LatexOutput`,`--TotxtMathematica`, `--Pickle` and `--Export`.

```
getoneloop(Expression)
gettwoloop(Expression)
```

Where `Expression` in the first two functions can be either a list, a dictionary or an algebraic expression. These functions, get rid of the factor $1/4\pi$,$1/(4\pi)^2$ respectively.

[37] to start the latex printing the user might need to type in the command `init_printing(using_latex=True)`

```
loadmodel(FileName)
```

where `FileName` is a pickle file containing a model i.e. a calculation that has been saved via the function `ExportToPickle` or during a previous run (e.g. a calculation done with the option `--Pickle`). Hence someone can load multiple results in the same notebook and study them.

```
CompareModels(Model1,Model2,subrules=[],display=False):
```

Where `Model1` and `Model2` are either two strings pointing to a pickle file containing a model or two models loaded in the notebook via the `loadmodel` function. This function calculates the differences for each terms present in both models and display them if `display` is set to `True` else it just returns the result of the comparison as a list where each entry correspond to a different beta function. Finally, the `subrules` argument can be a list of tuple where each tuple contains a replacement rule i.e. of the form `(old symbol, new symbol)` that will be apply to each beta function difference.

```
settozero(Expression,ListofSymols)
```

where `Expression` is an algebraic expression and `ListofSymbols` is a list of symbols[38] that must be set to zero. This function set all the symbols in `ListofSymbols` to zero as well as the traces and matrix multiplications consistently.

2.4.10 Pitfalls

There are some subtleties in the implementation of a model to which we would like to draw the user's attention. We start with commenting on the restrictions concerning the input format. To ascertain that `Python` interprets all parts of the model file correctly, the user must make sure that:

(a) only spaces and line breaks can be used as whitespace, i.e. tabulators are not allowed,

(b) there is a space after each colon,

(c) each element in any input file except for the last one should be separated by a comma.

In addition, beware that no operation on the fields is recognized, i.e. for complex conjugated fields one needs to introduce a new symbol. For complex scalars, the real degrees of freedom have to be defined together with the required normalization. The Yukawa matrices are assumed to be symmetric in generation space. Therefore, if e.g. some Yukawa terms are antisymmetric, PyR@TE will return zero.

Finally, all indices are contracted automatically by PyR@TE. For this purpose a database with the most common Clebsch-Gordan coefficients (CGCs) has been created, see Appendix A. This database uses the following conventions:

[38] the symbols must be proper Sympy symbols declared e.g. `Yu=Symbol('Y_u')`

Normalization We assume a set of n fields ϕ_i with dimensions D_i under an SU(N) gauge group. We will denote the CGC that gives the contraction of indices to an invariant combination as $\mathcal{C}$, i.e.

$$\mathcal{C}_{i_1 i_2 \ldots i_n} \phi_{i_1} \phi_{i_2} \ldots \phi_{i_n}. \tag{2.183}$$

does not transform under SU(N). Here, the i_x, $x = 1, \ldots, n$ are the charge indices with respect to the gauge group. In contrast to `Susyno` which has been used to create the database of CGCs we use a different normalization. Our convention is that

$$\sum_{i_1=1}^{D_1} \sum_{i_2=1}^{D_2} \cdots \sum_{i_n=1}^{D_n} |\mathcal{C}_{i_1 i_2 \ldots i_n}|^2 = \max(D_i). \tag{2.184}$$

With this normalization we reproduce for instance the standard CGCs for all bilinear terms, but also those for SU(2)$_L$ triplets with non-zero hypercharge and color sextets. However, we do not distinguish between SU(2)$_L$ triplets with and without hypercharge and use the same CGCs for both of them. Therefore, our convention for triplets without hypercharge is different to the standard one by a factor $1/\sqrt{2}$.

Conjugate irreps In general, conjugate irreps are either defined by the corresponding Dynkin indices or by a negative dimension. However, we would like to stress that

(a) the **2** under SU(2) is related to its conjugate representation **2***. Nevertheless, it is possible to use `" -2"` to represent **2*** which is then treated as a doublet with an additional $i\sigma_2$. For instance, the tensor product $\mathbf{2^*} \otimes \mathbf{2}$ is contracted with the Kronecker δ_{ij} whereas $\mathbf{2} \otimes \mathbf{2}$ by the anti-symmetric tensor ϵ_{ij}. This shows up e.g. in the case of the SM Yukawa couplings Y_d and Y_u.

(b) For self-conjugate representations like the adjoint ones, there are two ways to obtain a gauge singlet. To distinguish these two cases it is possible to use `-A` as dimension of the adjoint of SU(N). The convention is then that bilinear terms of the form $\boldsymbol{A}^* \otimes \boldsymbol{A}$ are always contracted with a Kronecker δ_{ij}, while for $\boldsymbol{A} \otimes \boldsymbol{A}$ the CGCs as calculated by `Susyno` are used. For instance, $\mathbf{3} \otimes \mathbf{3}$ in SU(2) is contracted by a matrix of the form

$$\begin{pmatrix} 0 & 0 & 1 \\ 0 & -1 & 0 \\ 1 & 0 & 0 \end{pmatrix} \tag{2.185}$$

while for $\mathbf{3}^* \otimes \mathbf{3}$ the three-dimensional identity matrix is used.

2.4.11 Validation

In the literature, there are very few models for which the RGEs at two-loop have been calculated for all dimensionless and dimensionful parameters. Therefore, we have also independently developed routines in `Mathematica` to calculate the full two-loop RGEs for all terms. These routines will be merged with the `SARAH` [105–108] in an upcoming version. For all tested models we had full agreement between PyR@TE and the results obtained by the new `SARAH` routines.

In the following, we present the comparisons between the results obtained with PyR@TE and the RGEs for some models presented in the literature. The reason for

choosing this subset of models is twofold. For one thing, they represent a broad variety of interactions so that we could obtain non-trivial tests for PyR@TE. For another, these are the models for which the RGEs have been calculated at two-loop for a large number of parameters.

Standard Model

We find full agreement for all parameters at the two-loop level with the results given in Ref. [116] including the full CP and flavor structure. This also confirms that the differences pointed out in Ref. [116] in comparison to the earlier results of Refs. [111, 112] are correct.

Standard Model with real scalar singlet

For the SM extended by a real scalar singlet field and a Dirac doublet [119] we find complete agreement for all dimensionless parameters, where we have applied the same approximation that only third generation Yukawa couplings contribute.

Standard Model with real scalar triplet

The RGEs for all dimensionless parameters for the SM extended by a real scalar triplet and a Dirac doublet are given in Ref. [119]. Making the same approximation as in Ref. [119], i.e. neglecting the Yukawa interactions for the first two generations of SM fermions, we find disagreement at the one- and two-loop level in the following parameters: $\Delta b^{(2)}_{\lambda_H}$, $b^{(1)}_{\kappa_T}$, $b^{(2)}_{\kappa_T}$, $b^{(1)}_{\lambda_T}$, $b^{(2)}_{\lambda_T}$.

Standard Model with Majorana singlet fermion and Dirac doublet

The RGEs for all dimensionless parameters for the SM extended by a real singlet fermion and a Dirac doublet are given in Ref. [119]. We find complete agreement with these results by taking the same approximation that only third generation Yukawa couplings contribute.

Standard Model with complex scalar doublet

The two Higgs doublet model is one of the most widely studied extensions of the SM. In the literature, the results for the β-functions are mostly available at one-loop level, see e.g. Ref. [173] and references therein. We agree with those results. In addition, Ref. [119] contains also partial two-loop results for which we also find agreement in the limit that only third generation Yukawas are taken into account.

Standard Model with Majorana triplet fermion and Dirac doublet

The one- and two-loop β-functions for all dimensionless parameters for the SM extended by a fermionic Majorana triplet and Dirac doublet are given in Ref. [119]. We find full agreement with their results, if we (i) take the limit of vanishing Yukawa couplings for the first two generations, (ii) include a relative factor of $\sqrt{2}$ in the definition of the Yukawa-like couplings of the triplet. This factor stems from a different normalization of the triplet (see also Section 2.4.10).

$B-L$ extended Standard Model

The one-loop RGEs for an extension of the SM by an additional $\mathrm{U}(1)_{B-L}$, right-handed neutrinos and a SM singlet complex scalar with $B-L$ charge 2 have been calculated in Ref. [174]. These results contain a contribution originating from the kinetic mixing which is not yet calculated by PyR@TE. In the limit of $\tilde{g} \to 0$ we find almost full agreement. Only the coefficient of the contribution proportional to $\mathrm{Tr}(Y_M^4)$ in the RGE for λ_2 should read -16 and not -1. This issue has been confirmed in a private discussion with one of the authors of Ref. [174].

SM extended by a complex triplet and vectorlike doublets

Partial one-loop results for the SM extended by a complex scalar and vectorlike doublets are given in Ref. [175]. However, we find the following disagreements: In the quartic coupling $\lambda_{\Delta H}$ the terms $\mathrm{Tr}(f_L^\dagger f_L f_L^\dagger f_L + f_\psi^\dagger f_\psi f_\psi^\dagger f_\psi)$ cannot be present, since they would need four triplets as external fields. In the β-function for the Yukawa couplings f_L and f_ψ, we do not find the terms $3 f_L f_\psi^\dagger f_\psi$ and $3 f_\psi f_L^\dagger f_L$, respectively. In addition, we also find disagreement in the coefficients for the trilinear coupling. The full details can be obtained by running PyR@TE.

SM with neutrino Yukawa couplings

The RGEs for the SM extended by right handed neutrinos have been given at the two-loop level for all dimensionless parameters in Ref. [176]. However, as it was already pointed out in Ref. [117], the terms at two-loop are missing. In addition, we find many more terms in disagreement with Ref. [176]. Also, we have some disagreement in some terms in the two-loop β-function of λ.

SM with a fourth generation of vectorlike fermions

The SM extended by a vector-like fourth generation has been studied in Ref. [177]. The authors have calculated the RGEs for the Yukawa couplings and the quartic Higgs coupling at one-loop in the limit, where the fourth generation quark masses are of the order the cut-off scale. The results we obtain with PyR@TE are identical for all the couplings they have listed.

2.4.12 Beyond...

In the near future, extensions of PyR@TE will be done in mainly two directions that we discuss here in turn. Also, in the longer term, implementing available partial results for the three-loop RGEs of a general theory, as well as contributing to the evaluation of the missing ones, is possible.

Include Kinetic mixing

In Section 2.3.7, we presented the various substitution rules to be applied in cases where the gauge group of the theory at hand is a product a simple gauge groups, i.e. $\mathcal{G} = \mathcal{G}_1 \times \cdots \times \mathcal{G}_n$

with at most one abelian factor. When there are several abelian factors present, *kinetic mixing* can appear and these equations must be modified to take it into account.

Indeed, the field strength tensors of the various abelian groups can mix together and a general kinetic term, gauge and Lorentz invariant can be written in the form

$$\mathcal{L}_{\text{kin.}} \supset -\frac{1}{4}(F^{\mu\nu})^T \xi F_{\mu\nu}\,, \tag{2.186}$$

where the n abelian field strength tensors have been grouped in a n dimensional vector $F_{\mu\nu}$ and ξ is a $n \times n$ real symmetric matrix. Consequently, in the case of kinetic mixing there are $\frac{1}{2}n(n-1)$ additional dynamical parameters to deal with. The direct way of addressing this issue would be to (i) calculate the evolution equations for these new parameters, (ii) and to calculate the modifications induced by these new terms to the usual beta functions such as gauge couplings, Yukawas, etc.The results of this approach can be found in [178].

Alternatively, it was recently suggested to treat the abelian sector as a whole and to describe it by a general real $n \times n$ gauge coupling matrix G [164]. It can be shown that the off-diagonal entries of G come form the ξ parameter after it has been absorbed into the redefinition of the gauge fields. Subsequently, the method consists in re-writing the general RGEs by replacing all the polynomials including individual gauge couplings by the relevant matrix structures, with no need to deal with the evolution equations for the ξ matrix. The result of this approach is a set of substitution rules that can be easily applied to the general equations to take into account kinetic mixing. For the sake of illustration we give as an example the following replacement rule for the one-loop beta function of the gauge couplings

$$g^3 S_2(S) \to G \sum_a W_a^S (W_a^S)^T\,, \tag{2.187}$$

in which the sum is over the scalars and where the quantity W_a^S is defined by

$$W_a^S \equiv G^T Q_a^S\,. \tag{2.188}$$

Q_a^S is the vector of U(1) charges of the scalar a. This second approach will be implemented in PyR@TE in very near future.

Broken symmetries and the running of vacuum expectation values

In Section 2.3 we presented the full two-loop RGEs for all the dimensionful and dimensionless parameters of a general gauge field theory. However, in the case where we deal with spontaneously broken gauge symmetries, one also has to take care of the renormalization of scalar vacuum expectation values. These are not gauge invariant physical quantities, but because of their central role, one needs to address this issue.

The renormalization of a *vev* v can be generically written in the form

$$v \to v + \delta v = \sqrt{Z}\,(v + \delta\bar{v})\,, \tag{2.189}$$

in which $\sqrt{Z}$ is the field renormalization constant of the corresponding scalar field. $\delta\bar{v}$ characterizes how differently from the scalar field v renormalizes. In [179], the authors

showed that $\delta\bar{v}$ vanishes only in gauges that break local gauge invariance but preserve global gauge invariance, e.g. the Landau gauge. For instance, this is not the case of the R_ξ gauge in which consequently $\delta\bar{v}$ is non vanishing. In addition, $\delta\bar{v}$ can be linked to the field renormalization constant $\sqrt{\hat{Z}}$ of a suitable chosen scalar background field. Hence, the calculation of the beta function of the *vev* can be obtained from a simple two-point function. The results in the R_ξ gauge at one- and two-loop order have been calculated by the same authors and can be found in [180]. As for the kinetic mixing, these results will be implemented in PyR@TE in the future.

Higher order corrections

As mentioned at the beginning of this section, partial three-loop results are available in the literature. Among them, the beta functions of the SM gauge coupling constants have been calculated up to three-loop order, see [181, 182] and references therein for intermediate computations that lead to the full result. The dominant contributions to the beta functions for the top-quark Yukawa have been calculated in [183] and the full result is also now available [184]. Finally, for the scalar sector, the dominant contributions to the three-loop scalar self-interaction of the Higgs bosons were calculated in [183] and the full result in [185]. All these results even though limited to the SM case could be implemented in PyR@TE.

This concludes our section on PyR@TE, where we have presented in details how to write in the most explicit form suitable for implementation the general equations for the beta functions of the various parameters of an arbitrary gauge theory. The use of PyR@TE was also discussed and many examples of model implementations are available in Appendix D. To conclude, we gave an outlook on future developments of the code.

2.5 Renormalization group equations of the $\mathcal{G}_{221}$ models

PyR@TE has been extensively presented in the previous section and as an example of its application, we now turn to the calculation of the full set of two-loop RGEs in the $\mathcal{G}_{221}$ models as introduced in Chapter 1. The idea here is to show on a concrete example how to use our code and to give some general comments about the structure of the RGEs. In order to keep the discussion short, we will focus on models following **BP-I** and show what is the impact on the RGEs of having a first SB mediated via a doublet or a triplet. All the Yukawa couplings are ignored in the following.

We start this section by defining the various parameters we consider, then give the input files and discuss the results at one- and two-loop order.

2.5.1 Implementation of the various $\mathcal{G}_{221}$ realizations

There are two points that we have not discussed in Chapter 1 about $\mathcal{G}_{221}$ models: the Yukawa sector, and the scalar potential. As discussed in the introduction, we will not bother with the Yukawa couplings here since our goal is simply to illustrate how PyR@TE works.

In **BP-I** models we have the following scalar fields

$$H \sim \left(\mathbf{2}, \overline{\mathbf{2}}, \mathbf{0}\right), \ \textbf{BP-I}\text{–D}: \ \phi \sim (\mathbf{1}, \mathbf{2}, \frac{\mathbf{1}}{\mathbf{2}}), \ \textbf{BP-I}\text{–T}: \ \phi \sim (\mathbf{1}, \mathbf{3}, \mathbf{1}). \tag{2.190}$$

The potential depends on the fields ϕ, H, $\phi^\dagger$ and $H^\dagger$ and because of the $\mathrm{U}(1)_X$ charge of ϕ, the terms in the potential cannot have odd numbers of ϕ fields. We are not interested in writing down the potential in matrix form and we will simply give the list of fields in each term as is required for PyR@TE. Hence $(h_1 \otimes h_2)$ means that we contract the fields h_1 and h_2 into a singlet. In this notation, independently of the breaking pattern (**BP-I**-D or **BP-I**-T) we will consider the following potential

$$\begin{aligned}
\mathcal{V} =& \mu_\phi \left(\phi^\dagger \otimes \phi\right) + \mu_{H,1} \left(H \otimes H + H^\dagger \otimes H^\dagger\right) + \mu_{H,2} \left(H^\dagger \otimes H\right) \\
&+ \lambda_\phi \left(\phi^\dagger \otimes \phi\right) \left(\phi^\dagger \otimes \phi\right) \\
&+ \lambda_{H,1} \left(H^\dagger \otimes H^\dagger\right) \left(H \otimes H\right) \\
&+ \lambda_{H,2} \left(\left(H^\dagger \otimes H^\dagger\right) \left(H^\dagger \otimes H\right) + h.c.\right) \\
&+ \lambda_{H,3} \left(\left(H^\dagger \otimes H^\dagger\right) \left(H^\dagger \otimes H^\dagger\right) + h.c\right) \\
&+ \lambda_{H,4} \left(\left(H^\dagger \otimes H\right) \left(H^\dagger \otimes H\right) + h.c.\right) \\
&+ \lambda_{\phi H,1} \left(\left(\phi^\dagger \otimes \phi\right) \left(H \otimes H + h.c.\right)\right) \\
&+ \lambda_{\phi H,2} \left(\left(\phi^\dagger \otimes \phi\right) \left(H^\dagger \otimes H\right)\right) .
\end{aligned} \tag{2.191}$$

The charge assignment of the various fermions depends on the model and we show in listing D.1 of Appendix D only the LR-D model input file. The others are trivial modifications of the `Particle` part of this one and we do not spell them out[39].

2.5.2 Analytic result at 1-loop: Gauge Couplings

The first thing to do to check the consistency of a set of RGEs is to look at the gauge couplings beta functions. Indeed, they depend only on the particle content and charge assignment of the various fields. Therefore, if something is wrong in the model file it is most likely apparent in the beta functions of the gauge coupling constants. The result for the one-loop beta functions of the gauge couplings reads

$$\begin{matrix} \text{LR} \\ \text{HP} \\ \text{LP} \\ \text{FP} \end{matrix} := \left[\begin{array}{cccc} -\frac{17}{6} & -3 & \frac{17}{6} & -7 \\ -\frac{35}{6} & -3 & \frac{35}{6} & -7 \\ -\frac{23}{6} & -3 & \frac{23}{6} & -7 \\ -\frac{41}{6} & -3 & \frac{41}{6} & -7 \end{array}\right]_{\mathrm{D}}, \left[\begin{array}{cccc} -\frac{7}{3} & -3 & \frac{11}{3} & -7 \\ -\frac{16}{3} & -3 & \frac{20}{3} & -7 \\ -\frac{10}{3} & -3 & \frac{14}{3} & -7 \\ -\frac{19}{3} & -3 & \frac{23}{3} & -7 \end{array}\right]_{\mathrm{T}}, \tag{2.192}$$

where for each line (model) we write in the four columns the coefficients of the terms $g^3_{\mathrm{SU}(2)_2} \equiv g^3_2$, $g^3_{\mathrm{SU}(2)_1} \equiv g^3_1$, $g^3_{\mathrm{U}(1)_X} \equiv g^3_X$, $g^3_{\mathrm{SU}(3)_c} \equiv g^3_3$ for the doublet and triplet cases. At one-loop, these are the only contributions. We draw the reader's attention to the following points:

(i) The first thing to note is that across the **BP-I** models, the fields charged under $\mathrm{SU}(3)_c$ and $\mathrm{SU}(2)_1$ are the same. Therefore, we expect the corresponding beta functions g_3, g_1 (second and fourth column) to be identical for all the models.

[39] They are available with the code in the `models` directory.

(ii) Also, for a given model (LR, LP, HP, FP) the difference between the doublet and triplet cases resides in the coefficients of g_2^2 and g_X^3 which is traced back to the quantum numbers of the doublet and triplet fields (the shift is the same for all the models).

(iii) The relative size of one coefficient with respect to the same one in a different model is also easily understood from the charge assignment. For instance, we have $\beta_{g_2} \supset -\frac{17}{6}g_2^3$ for the LR-D model and $\beta_{g_2} \supset -\frac{35}{6}g_2^3$ for the HP-D model. From Eq. (2.92) we have $\beta(g) \sim g^3\left\{-C_2(\mathcal{G}) + S_2(F) + S_2(S)\right\}$, hence if the coefficient of $g_2^3 < 0$ it means that the more particles are charged under this group the smaller the coefficient will be in absolute value. Consequently, LR-D has a smaller coefficient with respect to HP-D because of the additional doublet charged under $\mathrm{SU}(2)_2$.

These kind of arguments are very useful to see how a model is affected by a modification of the particle content or charge assignment.

2.5.3 Analytic result at 1-loop: Quartic Couplings

There are seven quartic coupling constants in $\mathcal{V}$ for which we calculate the RGEs. With so many terms, the one-loop calculation takes about 20 minutes for one model while in comparison, for the SM it takes about 3 minutes on the same computer.

One issue that arises with so many terms in the potential is that of finding a combination of the external indices of the scalar fields which is such that only the beta function of the quartic term we want to calculate gives a non zero contribution.

To illustrate this point, let us consider $\lambda_{H,1}, \lambda_{H,3}$ and $\lambda_{H,4}$ terms in the above potential and write $H_{ij} = (\pi_{ij} + i\sigma_{ij})$ where i, j represent the indices of $\mathrm{SU}(2)_1$, $\mathrm{SU}(2)_2$, respectively. It then follows

$$\begin{aligned}
\mathcal{V} = \sum_{i,j,k,l,m,n,p,q\in[\![1,2]\!]^8} \Big\{ & \lambda_{H,1}\varepsilon_{ik}\varepsilon_{jl}\varepsilon_{mp}\varepsilon_{nq}\left(\pi_{ij}+i\sigma_{ij}\right)\left(\pi_{kl}+i\sigma_{kl}\right)\left(\pi_{mn}-i\sigma_{mn}\right)\left(\pi_{pq}-i\sigma_{pq}\right) \\
& + \lambda_{H,3}\Big(\varepsilon_{ik}\varepsilon_{jl}\varepsilon_{mp}\varepsilon_{nq}\left(\pi_{ij}-i\sigma_{ij}\right)\left(\pi_{kl}-i\sigma_{kl}\right)\left(\pi_{mn}-i\sigma_{mn}\right)\left(\pi_{pq}-i\sigma_{pq}\right) \\
& \quad + \varepsilon_{ik}\varepsilon_{jl}\varepsilon_{mp}\varepsilon_{nq}\left(\pi_{ij}+i\sigma_{ij}\right)\left(\pi_{kl}+i\sigma_{kl}\right)\left(\pi_{mn}+i\sigma_{mn}\right)\left(\pi_{pq}+i\sigma_{pq}\right)\Big) \\
& + \lambda_{H,4}\delta_{ik}\delta_{jl}\delta_{mp}\delta_{nq}\left(\pi_{ij}+i\sigma_{ij}\right)\left(\pi_{kl}-i\sigma_{kl}\right)\left(\pi_{mn}+i\sigma_{mn}\right)\left(\pi_{pq}-i\sigma_{pq}\right)\Big\} + \dots ,
\end{aligned} \tag{2.193}$$

in which we wrote explicitly the Clebsch-Gordan coefficients for the products $\mathbf{2}\otimes\mathbf{2} \longleftrightarrow \varepsilon$ and $\mathbf{2}\otimes\overline{\mathbf{2}} \longleftrightarrow \delta$. We now take the derivative of Eq. (2.193) with respect to the exterior field configuration, $\pi_{ab}\pi_{cd}\pi_{ef}\pi_{gh}$ as explained[40] in Section 2.4.1 and fix the choice of isospin

[40] This choice is arbitrary and in practice we calculate the various derivatives with respect to the possible external field configurations. For instance, we could also take the derivative with respect to $\pi_{ab}\sigma_{cd}\pi_{ef}\sigma_{gh}$.

values $a, b, c, d, e, f, g, h \equiv 1, 2, 2, 1, 1, 2, 2, 1$.

$$\begin{aligned}
\frac{\partial^4 \mathcal{V}}{\partial\pi_{ab}\partial\pi_{cd}\partial\pi_{ef}\partial\pi_{gh}} = & \sum_{i,j,k,l,m,n,p,q\in[\![1,2]\!]^8} \\
& 4\lambda_{H,1}\varepsilon_{ik}\varepsilon_{jl}\varepsilon_{mp}\varepsilon_{nq}\Big(\delta_{1i}\delta_{1k}\delta_{1n}\delta_{1q}\delta_{2j}\delta_{2l}\delta_{2m}\delta_{2p} + \delta_{1i}\delta_{1l}\delta_{1m}\delta_{1q}\delta_{2j}\delta_{2k}\delta_{2n}\delta_{2p} \\
& + \delta_{1i}\delta_{1l}\delta_{1n}\delta_{1p}\delta_{2j}\delta_{2k}\delta_{2m}\delta_{2q} + \delta_{1j}\delta_{1k}\delta_{1m}\delta_{1q}\delta_{2i}\delta_{2l}\delta_{2n}\delta_{2p} \\
& + \delta_{1j}\delta_{1k}\delta_{1n}\delta_{1p}\delta_{2i}\delta_{2l}\delta_{2m}\delta_{2q} + \delta_{1j}\delta_{1l}\delta_{1m}\delta_{1p}\delta_{2i}\delta_{2k}\delta_{2n}\delta_{2q}\Big) \\
& + 8\lambda_{H,3}\varepsilon_{ik}\varepsilon_{jl}\varepsilon_{mp}\varepsilon_{nq}\Big(\delta_{1i}\delta_{1k}\delta_{1n}\delta_{1q}\delta_{2j}\delta_{2l}\delta_{2m}\delta_{2p} + \delta_{1i}\delta_{1l}\delta_{1m}\delta_{1q}\delta_{2j}\delta_{2k}\delta_{2n}\delta_{2p} \\
& + \delta_{1i}\delta_{1l}\delta_{1n}\delta_{1p}\delta_{2j}\delta_{2k}\delta_{2m}\delta_{2q} + \delta_{1j}\delta_{1k}\delta_{1m}\delta_{1q}\delta_{2i}\delta_{2l}\delta_{2n}\delta_{2p} \\
& + \delta_{1j}\delta_{1k}\delta_{1n}\delta_{1p}\delta_{2i}\delta_{2l}\delta_{2m}\delta_{2q} + \delta_{1j}\delta_{1l}\delta_{1m}\delta_{1p}\delta_{2i}\delta_{2k}\delta_{2n}\delta_{2q}\Big) \\
& + 4\lambda_{H,4}\delta_{ik}\delta_{jl}\delta_{mp}\delta_{nq}\Big(\delta_{1i}\delta_{1k}\delta_{1n}\delta_{1q}\delta_{2j}\delta_{2l}\delta_{2m}\delta_{2p} + \delta_{1i}\delta_{1l}\delta_{1m}\delta_{1q}\delta_{2j}\delta_{2k}\delta_{2n}\delta_{2p} \\
& + \delta_{1i}\delta_{1l}\delta_{1n}\delta_{1p}\delta_{2j}\delta_{2k}\delta_{2m}\delta_{2q} + \delta_{1j}\delta_{1k}\delta_{1m}\delta_{1q}\delta_{2i}\delta_{2l}\delta_{2n}\delta_{2p} \\
& + \delta_{1j}\delta_{1k}\delta_{1n}\delta_{1p}\delta_{2i}\delta_{2l}\delta_{2m}\delta_{2q} + \delta_{1j}\delta_{1l}\delta_{1m}\delta_{1p}\delta_{2i}\delta_{2k}\delta_{2n}\delta_{2q}\Big)\,. \qquad (2.194)
\end{aligned}$$

Finally, carrying out the sums one obtains

$$\frac{\partial^4 \mathcal{V}}{\partial\pi_{12}\partial\pi_{21}\partial\pi_{12}\partial\pi_{21}} = 16\lambda_{H,1} + 32\lambda_{H,3} + 8\lambda_{H,4}\,, \qquad (2.195)$$

where the three quartic couplings, $\lambda_{H,1}, \lambda_{H,3}, \lambda_{H,4}$ are still present. Any other combination of a, b, c, d, e, f, g, h leads either to the same result or 0 or $24\lambda_{H,4}$, hence it is not possible to disentangle the three quartic coupling constants with this external field combination. Actually, any other combination would lead to similar results (but different coefficients) and in the end one has to write a linear system and invert it to access all the constants. This is done in PyR@TE automatically[41] and the result reads for the various quartic couplings

[41] Actually, PyR@TE is not able to solve the system of linear equations, it rather calculates the beta function of the full linear relation for the couplings that cannot be disentangled.

BP-I-D:

$$\begin{aligned}
\beta_{\lambda_{H,1}} &= 16\lambda_{H,1}^2 + 24\lambda_{H,1}\lambda_{H,4} - 9\lambda_{H,1}g_1^2 - 9\lambda_{H,1}g_2^2 + 24\lambda_{H,2}^2 + 128\lambda_{H,3}^2 \\
&\quad + 4\lambda_{H\phi,1}^2 - \frac{1}{2}\lambda_{H\phi,2}^2 + \frac{3}{2}g_1^2 g_2^2 \,, \qquad (2.196) \\
\beta_{\lambda_{H,2}} &= 48\lambda_{H,1}\lambda_{H,2} + 96\lambda_{H,2}\lambda_{H,3} + 48\lambda_{H,2}\lambda_{H,4} - 9\lambda_{H,2}g_1^2 - 9\lambda_{H,2}g_2^2 \\
&\quad + 4\lambda_{H\phi,1}\lambda_{H\phi,2} \,, \qquad (2.197) \\
\beta_{\lambda_{H,3}} &= 48\lambda_{H,1}\lambda_{H,3} + 12\lambda_{H,2}^2 + 24\lambda_{H,3}\lambda_{H,4} - 9\lambda_{H,3}g_1^2 - 9\lambda_{H,3}g_2^2 + 2\lambda_{H\phi,1}^2 \,, \\
&\qquad (2.198) \\
\beta_{\lambda_{H,4}} &= 16\lambda_{H,1}^2 + 16\lambda_{H,1}\lambda_{H,4} + 48\lambda_{H,2}^2 + 64\lambda_{H,3}^2 + 32\lambda_{H,4}^2 - 9\lambda_{H,4}g_1^2 \\
&\quad - 9\lambda_{H,4}g_2^2 + 2\lambda_{H\phi,2}^2 + \frac{9}{8}g_1^4 + \frac{3}{4}g_1^2 g_2^2 + \frac{9}{8}g_2^4 \,, \qquad (2.199) \\
\beta_{\lambda_\phi} &= 16\lambda_{H\phi,1}^2 + 4\lambda_{H\phi,2}^2 + 24\lambda_\phi^2 - 3\lambda_\phi g_X^2 - 9\lambda_\phi g_2^2 + \frac{3}{8}g_X^4 + \frac{3}{4}g_X^2 g_2^2 \\
&\quad + \frac{9}{8}g_2^4 \,, \qquad (2.200) \\
\beta_{\lambda_{H\phi,1}} &= 16\lambda_{H,1}\lambda_{H\phi,1} + 12\lambda_{H,2}\lambda_{H\phi,2} + 48\lambda_{H,3}\lambda_{H\phi,1} + 4\lambda_{H,4}\lambda_{H\phi,1} \\
&\quad + 8\lambda_{H\phi,1}\lambda_{H\phi,2} + 12\lambda_{H\phi,1}\lambda_\phi - \frac{3}{2}\lambda_{H\phi,1}g_X^2 - \frac{9}{2}\lambda_{H\phi,1}g_1^2 \\
&\quad - 9\lambda_{H\phi,1}g_2^2 \,, \qquad (2.201) \\
\beta_{\lambda_{H\phi,2}} &= 8\lambda_{H,1}\lambda_{H\phi,2} + 48\lambda_{H,2}\lambda_{H\phi,1} + 20\lambda_{H,4}\lambda_{H\phi,2} + 16\lambda_{H\phi,1}^2 + 4\lambda_{H\phi,2}^2 \\
&\quad + 12\lambda_{H\phi,2}\lambda_\phi - \frac{3}{2}\lambda_{H\phi,2}g_X^2 - \frac{9}{2}\lambda_{H\phi,2}g_1^2 - 9\lambda_{H\phi,2}g_2^2 + \frac{9}{4}g_2^4 \,, \qquad (2.202)
\end{aligned}$$

BP-I-T:

$$\begin{aligned}
\beta_{\lambda_{H,1}} &= 16\lambda_{H,1}^2 + 24\lambda_{H,1}\lambda_{H,4} - 9\lambda_{H,1}g_1^2 - 9\lambda_{H,1}g_2^2 + 24\lambda_{H,2}^2 + 128\lambda_{H,3}^2 \\
&\quad + 6\lambda_{H\phi,1}^2 + \frac{3}{2}g_1^2 g_2^2 \,, \qquad (2.203) \\
\beta_{\lambda_{H,2}} &= 48\lambda_{H,1}\lambda_{H,2} + 96\lambda_{H,2}\lambda_{H,3} + 48\lambda_{H,2}\lambda_{H,4} - 9\lambda_{H,2}g_1^2 - 9\lambda_{H,2}g_2^2 \\
&\quad + 6\lambda_{H\phi,1}\lambda_{H\phi,2} \,, \qquad (2.204) \\
\beta_{\lambda_{H,3}} &= 48\lambda_{H,1}\lambda_{H,3} + 12\lambda_{H,2}^2 + 24\lambda_{H,3}\lambda_{H,4} - 9\lambda_{H,3}g_1^2 - 9\lambda_{H,3}g_2^2 \\
&\quad + 3\lambda_{H\phi,1}^2 \,, \qquad (2.205) \\
\beta_{\lambda_{H,4}} &= 16\lambda_{H,1}^2 + 16\lambda_{H,1}\lambda_{H,4} + 48\lambda_{H,2}^2 + 64\lambda_{H,3}^2 + 32\lambda_{H,4}^2 - 9\lambda_{H,4}g_1^2 \\
&\quad - 9\lambda_{H,4}g_2^2 + 3\lambda_{H\phi,2}^2 + \frac{9}{8}g_1^4 + \frac{3}{4}g_1^2 g_2^2 + \frac{9}{8}g_2^4 \,, \qquad (2.206) \\
\beta_{\lambda_\phi} &= 16\lambda_{H\phi,1}^2 + 4\lambda_{H\phi,2}^2 + 20\lambda_\phi^2 - 12\lambda_\phi g_X^2 - 24\lambda_\phi g_2^2 + \frac{3}{2}g_2^4 \,, \qquad (2.207) \\
\beta_{\lambda_{H\phi,1}} &= 16\lambda_{H,1}\lambda_{H\phi,1} + 12\lambda_{H,2}\lambda_{H\phi,2} + 48\lambda_{H,3}\lambda_{H\phi,1} + 4\lambda_{H,4}\lambda_{H\phi,1} \\
&\quad + 16\lambda_{H\phi,1}\lambda_\phi - 6\lambda_{H\phi,1}g_X^2 - \frac{9}{2}\lambda_{H\phi,1}g_1^2 - \frac{33}{2}\lambda_{H\phi,1}g_2^2 \,, \qquad (2.208) \\
\beta_{\lambda_{H\phi,2}} &= 8\lambda_{H,1}\lambda_{H\phi,2} + 48\lambda_{H,2}\lambda_{H\phi,1} + 20\lambda_{H,4}\lambda_{H\phi,2} + 16\lambda_{H\phi,2}\lambda_\phi \\
&\quad - 6\lambda_{H\phi,2}g_X^2 - \frac{9}{2}\lambda_{H\phi,2}g_1^2 - \frac{33}{2}\lambda_{H\phi,2}g_2^2 \,. \qquad (2.209)
\end{aligned}$$

Of course, these RGEs are valid only above the electroweak scale when both scalars run in the loops. Furthermore, these RGEs do not depend on a specific realization of the $\mathcal{G}_{221}$ model since at one-loop, all the particle propagators in the loops are connected to scalars at both ends and can therefore only be scalars or gauge bosons (we ignore the Yukawa couplings). Consequently, only the type of first stage SB matters, doublet or triplet. The following comments are in order:

(i) The difference between the doublet and triplet case RGEs is mild and for terms that are present in both equations it comes only from the Clebsh-Gordan coefficients. For instance, the term $\lambda_{H\phi,1}\lambda_{H\phi,2}$ in $\beta_{\lambda_{H,2}}$. Furthermore, only terms involving the triplet field can be different (this also includes the gauge boson corrections like A_{abcd}).

(ii) A good cross check that we properly disentangled the various beta functions of the quartic coupling constants is that there are no terms of the form $\beta_{\lambda_i} \supset g^2\lambda_j,\ i \neq j$ in the result. These terms come from $-3g^2\Lambda^S_{abcd} \sim \lambda_{abcd}$, see Eq. (2.105), and must be proportional to the quartic coupling constant corresponding to the beta function being considered.

(iii) The beta functions of $\lambda_{H,1,2,3,4}$ do not have terms proportional to g_X since H is not charged under $\mathrm{U}(1)_X$ and analogously the beta function of λ_ϕ do not have terms proportional to g_1.

(iv) Finally, contrary to what would naively be expected, in some of the beta functions, the term proportional to λ^2 of the corresponding beta function does not appear. It is indeed the case for $\beta_{\lambda_{H,2}}$ where only mixed contributions are present in the result e.g. $\lambda_{H,1}\lambda_{H,2}$. This behaviour also appears in the RGEs of the 2HDM model.

The last result we present is the beta functions for the mass terms $\mu_\phi, \mu_{H,1}$ and $\mu_{H,2}$.

2.5.4 Analytic result at 1-loop: Scalar mass terms

Finally, we give the results for the three mass terms in the potential Eq. (2.191):

$$\begin{aligned}
\beta_{\mu_\phi} &= 32\lambda_{H\phi,1}\mu_{H,1} + 8\lambda_{H\phi,2}\mu_{H,2} + 12\lambda_\phi\mu_\phi - \frac{3}{2}g_X^2\mu_\phi - \frac{9}{2}g_2^2\mu_\phi\,, \\
\beta_{\mu_{H,1}} &= 16\lambda_{H,1}\mu_{H,1} + 12\lambda_{H,2}\mu_{H,2} + 48\lambda_{H,3}\mu_{H,1} + 4\lambda_{H,4}\mu_{H,1} + 4\lambda_{H\phi,1}\mu_\phi \\
&\quad -\frac{9}{2}g_1^2\mu_{H,1} - \frac{9}{2}g_2^2\mu_{H,1}\,, \\
\beta_{\mu_{H,2}} &= 8\lambda_{H,1}\mu_{H,2} + 48\lambda_{H,2}\mu_{H,1} + 20\lambda_{H,4}\mu_{H,2} + 4\lambda_{H\phi,2}\mu_\phi \\
&\quad -\frac{9}{2}g_1^2\mu_{H,2} - \frac{9}{2}g_2^2\mu_{H,2}\,.
\end{aligned} \tag{2.210}$$

Similar remarks to the ones done for the quartic coupling constants apply here and we do not repeat them. In the next part we investigate numerically the size of the differences between SB occurring via a doublet or a triplet at one-loop.

2.5.5 Numerical study of the $\mathcal{G}_{221}$ RGEs

Using the interactive mode of PyR@TE, Section 2.4.8, we can easily solve the system of coupled differential equations formed by the RGEs above. We fix the initial parameters arbitrarily to some values and compare the evolution of **BP-I**-D and **BP-I**-T models[42]. The initial values for the gauge couplings are fixed as follows

$$\begin{aligned} g_1(M_Z) &\equiv g^{\rm SM}_{{\rm SU}(2)_L}(M_Z) = 0.65,\ g_{{\rm SU}(3)_c}(M_Z) \equiv g^{\rm SM}_{{\rm SU}(3)_c}(M_Z), \\ g_X(M_Z) &= 0.4,\ g_2(M_Z) = \sqrt{\frac{g_X^2 g_Y^2}{g_X^2 - g_Y^2}} = 0.78\,, \end{aligned} \tag{2.211}$$

where we have enforced the relation between g_X, g_2 and g_Y as well as the one between g_1 and $g_{{\rm SU}(2)_L}$ coming from SB. Finally, we set all the other parameters at M_Z to 0.01.

In Fig. 2.9 we show the result at one-loop for the various gauge couplings of the model. We remind the reader of the fact that β_{g_1} and β_{g_3} are independent of the model. For the other two gauge coupling constants we see that the difference between **BP-I**-D and **BP-I**-T for a given model is small and of about 5% at most.

Below, in Fig. 2.10, we present the evolution of all the dimensionless and dimensionful parameters of the potential. To avoid too many curves on the same plot, and because the effects are similar from one model to the other, we show only one or two triplet results for each parameter. In all the cases, the pattern of modifications is similar for the other models.

With these initial conditions, the variation between the two SB ranges from 1-2% for $\mu_{H,1}, \lambda_{H,1}, \lambda_{H,3}, \lambda_{H,4}$ to about 8% for $\mu_{H,2}$ and $\lambda_{H,2}, \mu_{H,2}$. Very different behaviours between the doublet and triplet case are observed in the evolution of $\lambda_\phi, \lambda_{H\phi,1}, \lambda_{H\phi,2}$ and μ_ϕ as expected since they involve directly the field ϕ. The change of sign in the beta function of λ_ϕ (i.e. the sign of the slope of λ_ϕ) in the LR-T and HP-T models comes from the fact that the positive contributions to the beta function proportional to g_X^4 and $g_X^2 g_2^2$ are absent in the triplet version of the model. In addition, the negative contributions $-3\lambda_\phi g_X^2, -9\lambda_\phi g_2^2$ are enhanced to $-12\lambda_\phi g_X^2, -24\lambda_\phi g_2^2$, respectively, as can be seen in Eqs. (2.200, 2.207). Similar arguments can be used to explain the striking difference in the behaviour of $\beta_{\lambda_{H\phi,2}}$.

2.5.6 Comparison one vs two loop

Finally, we turn to the two-loop results. The differences in the beta functions of the gauge coupling and mass terms beta functions can be explained by arguments similar to the ones already made above, we therefore will not repeat them and concentrate instead on the quartic couplings. The results can be found in Appendix C.

We have seen at one-loop that the beta functions for the various quartic couplings depend only on the representation of the scalar field mediating the first stage SB. At the two-loop level, once the scalar field content is fixed, there are only two terms that can give rise to differences across the models. Closely inspecting Eq. (2.104), we see that these

[42] Our principal goal here is to see whether the difference between **BP-I**-D and **BP-I**-T models can be sizeable.

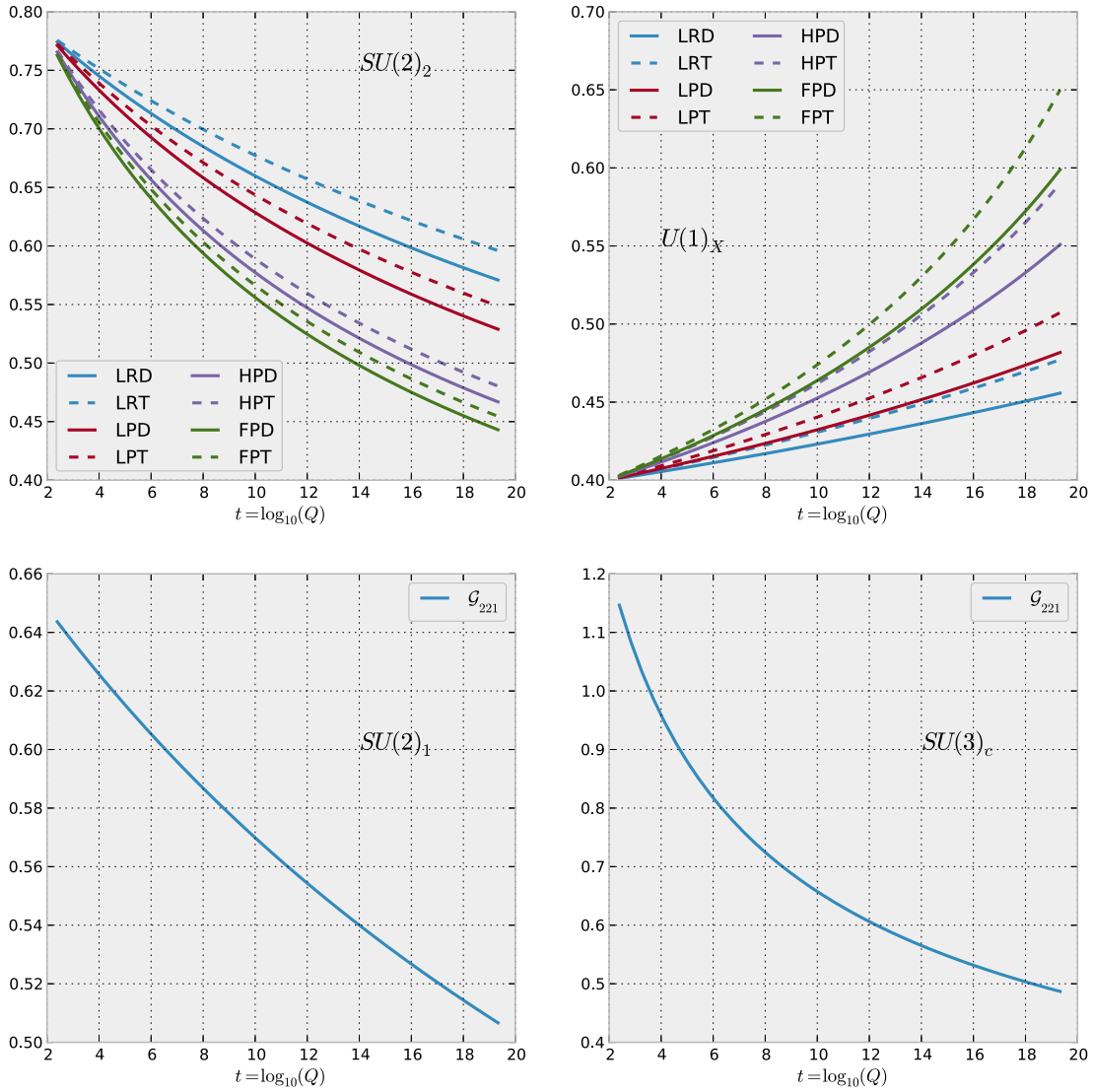

Figure 2.9: Evolution of the gauge coupling constants in the **BP-I**-D and **BP-I**-T realizations @1-Loop. The scale Q is given in units of GeV.

two terms are

$$g^4 \tfrac{10}{3} \kappa S_2(F) \Lambda^S_{abcd} \,, \;\; -g^6 \tfrac{32}{3} \kappa S_2(F) A_{abcd} \,. \tag{2.212}$$

Therefore, the two-loop beta functions for the quartic couplings can be written in the form

$$\beta^{(2)}_{\lambda_i}(M) = \tilde{\beta}^{(2)}_{\lambda_i}(M) + \Delta_{\lambda_i} \,, \tag{2.213}$$

where M denotes any of the realizations (LR, LP, FP, HP) and in which $\tilde{\beta}^{(2)}_{\lambda_i}(M)$ is the model dependent part and Δ_{λ_i} the model independent contribution. The results for Δ_{λ_i} are quite lengthly. Therefore,we only give here the result for λ_ϕ for a SB mediated by a

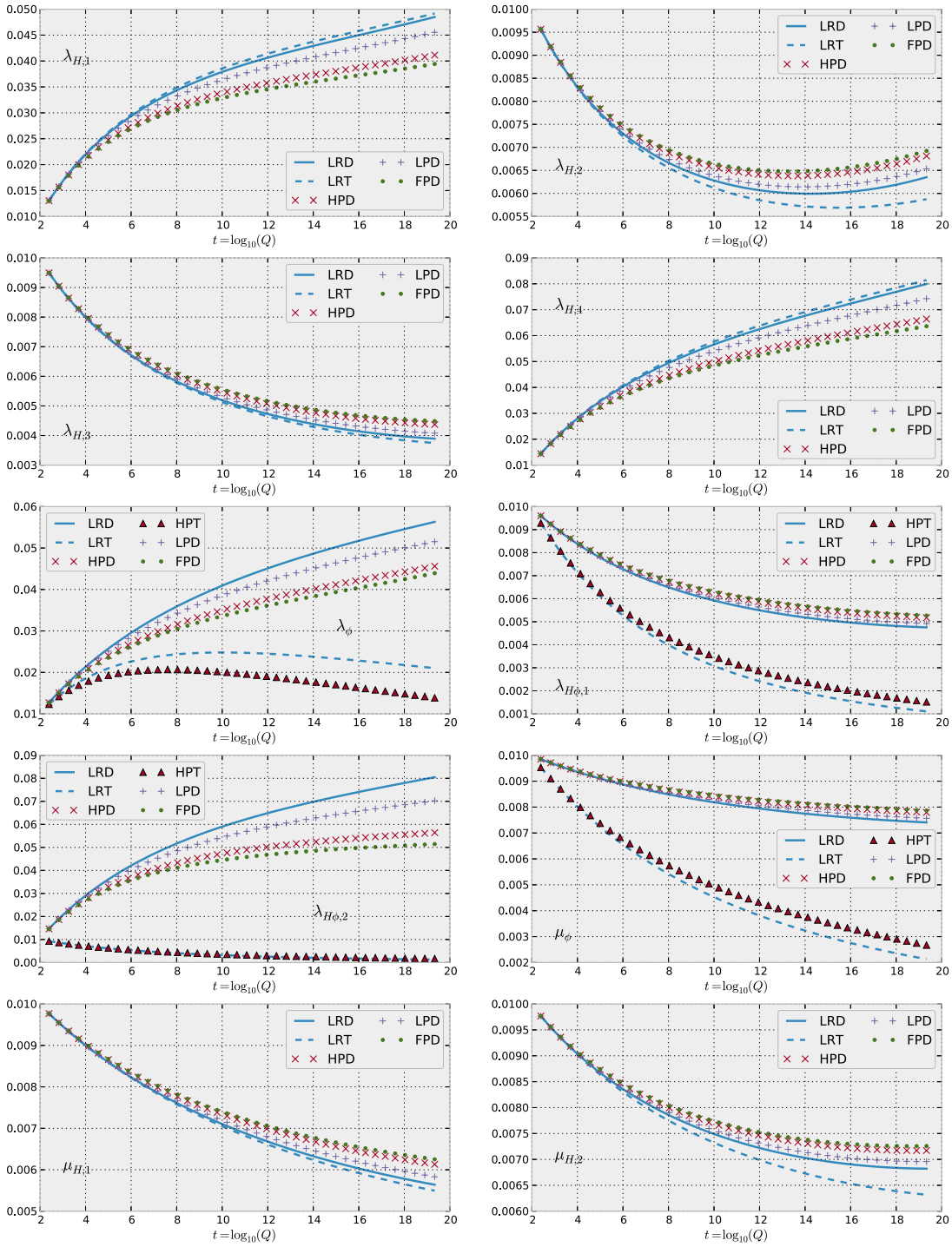

Figure 2.10: Evolution of the quartic coupling constants and scalar mass parameters in the **BP-I**-D and **BP-I**-T realizations @1-Loop.

doublet for illustration and refer the reader to Appendix C for the complete set of RGEs.

The model independent part reads

$$\begin{aligned}\Delta^{\rm D}_{\lambda_\phi} &= -192\lambda^2_{H\phi,1}\lambda_{H\phi,2} - 160\lambda^2_{H\phi,1}\lambda_\phi + 96\lambda^2_{H\phi,1}g_1^2 + 96\lambda^2_{H\phi,1}g_2^2 - 16\lambda^3_{H\phi,2} \\ &- 40\lambda^2_{H\phi,2}\lambda_\phi + 24\lambda^2_{H\phi,2}g_1^2 + 24\lambda^2_{H\phi,2}g_2^2 + 15\lambda_{H\phi,2}g_2^4 - 312\lambda^3_\phi \\ &+ 36\lambda^2_\phi g_1^2 + 108\lambda^2_\phi g_2^2\,, \end{aligned} \tag{2.214}$$

while the model dependent parts are given by

LR-D:

$$\tilde\beta_{\lambda_\phi} = +\frac{389}{24}\lambda_\phi g_X^4 + \frac{39}{4}\lambda_\phi g_X^2 g_2^2 - \frac{29}{8}\lambda_\phi g_2^4 - \frac{187}{48}g_X^6 - \frac{367}{48}g_X^4 g_2^2 - \frac{317}{48}g_X^2 g_2^4 + \frac{277}{16}g_2^6\,, \tag{2.215}$$

LP-D:

$$\tilde\beta_{\lambda_\phi} = +\frac{449}{24}\lambda_\phi g_X^4 + \frac{39}{4}\lambda_\phi g_X^2 g_2^2 - \frac{89}{8}\lambda_\phi g_2^4 - \frac{235}{48}g_X^6 - \frac{415}{48}g_X^4 g_2^2 - \frac{269}{48}g_X^2 g_2^4 + \frac{325}{16}g_2^6\,, \tag{2.216}$$

HP-D:

$$\tilde\beta_{\lambda_\phi} = +\frac{569}{24}\lambda_\phi g_X^4 + \frac{39}{4}\lambda_\phi g_X^2 g_2^2 - \frac{209}{8}\lambda_\phi g_2^4 - \frac{331}{48}g_X^6 - \frac{511}{48}g_X^4 g_2^2 - \frac{173}{48}g_X^2 g_2^4 + \frac{421}{16}g_2^6\,, \tag{2.217}$$

FP-D:

$$\tilde\beta_{\lambda_\phi} = +\frac{629}{24}\lambda_\phi g_X^4 + \frac{39}{4}\lambda_\phi g_X^2 g_2^2 - \frac{269}{8}\lambda_\phi g_2^4 - \frac{379}{48}g_X^6 - \frac{559}{48}g_X^4 g_2^2 - \frac{125}{48}g_X^2 g_2^4 + \frac{469}{16}g_2^6\,, \tag{2.218}$$

which indeed are all of the form specified in Eq. (2.212).

To conclude this section, we illustrate the impact of the two-loop corrections by performing a simple numerical analysis. We follow the same procedure as for the one-loop case and use identical initial conditions, cf. Eq. (2.211).

In Fig. 2.11, we show for the various gauge couplings the ratio of the one-loop over the two-loop prediction. We see that the impact of the two-loop corrections varies between a few per mille for the $\mathrm{SU}(2)_1$ and $\mathrm{SU}(3)_c$ groups, and to a few percents for $\mathrm{U}(1)_X$ and $\mathrm{SU}(2)_2$.

Finally, in Fig. 2.12, we show the ratio of one-loop over two-loop predictions for all the quartic couplings and mass terms involved in the potential and for various models. As before, we see that the impact is of a few percents. Note however, that a few percent modification in the value of the quartic couplings can have drastic impact on the stability bound of the effective potential as it is the case in the SM [7].

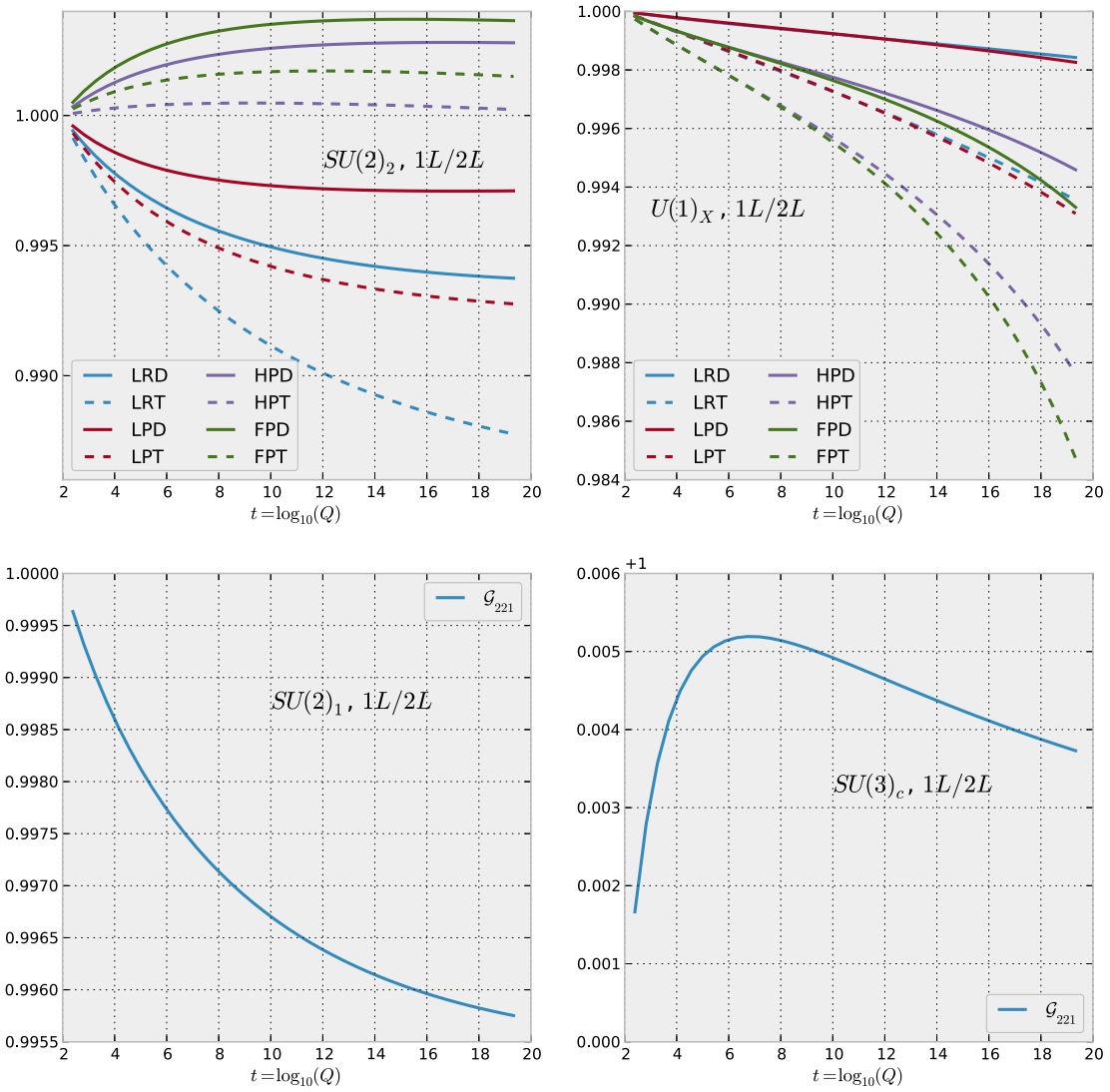

Figure 2.11: Ratio of one-loop over two-loop predictions for various models and the four gauge groups factors of the $\mathcal{G}_{221}$ models.

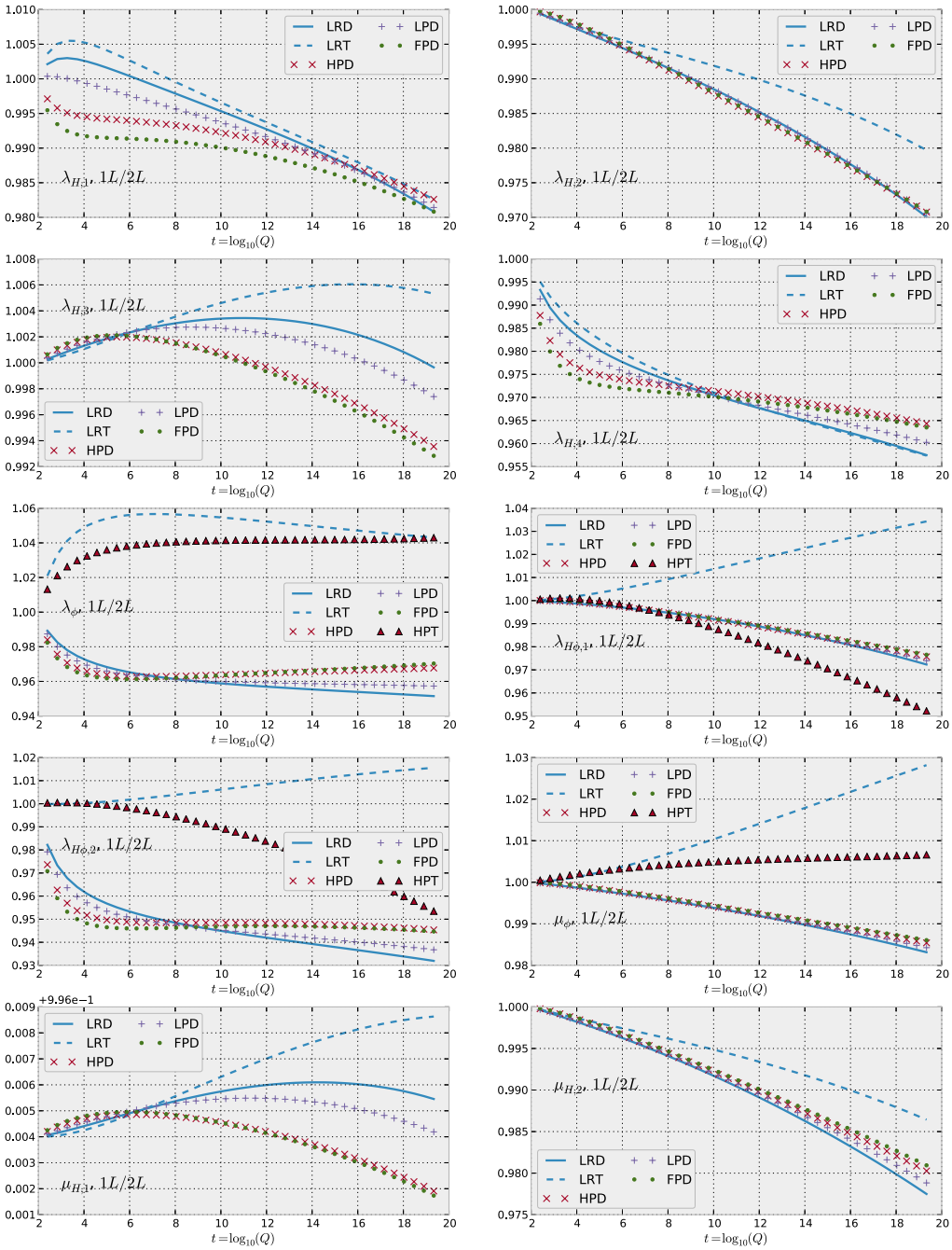

Figure 2.12: Ratio of one-loop over two-loop predictions for all the quartic couplings and scalar mass terms of the $\mathcal{G}_{221}$ potential. We show the ratio for various models and first stage symmetry breaking.

This concludes this chapter on the automation of the generation of two-loop RGEs for general gauge field theories. After having introduced the issue we presented a tool that we dubbed PyR@TE for Python Renormalization group equations @ Two-loop for Everyone that aims at calculating the algebraic system of coupled first order differential equations that governs the scale evolution of the parameters of the theory. PyR@TE is easy to use: Once the user specifies in an intuitive format the gauge group and the particle content of a given model, the RGEs are generated, and, for ease of inspection, directly exported to LaTeX. Also, the results can be exported to `Mathematica` where the RGEs can be numerically solved and plotted. Furthermore, we have developed an interactive mode in form of an `IPython Notebook` that mimics much of the functionality of `Mathematica`.

Since the calculations that lead to the RGEs are if not difficult so at least involved, we paid special attention to validating our results. To that end, we not only compared the RGEs generated by PyR@TE with complete or partial results that are available in the literature, but also developed `Mathematica` routines that are now part of version 4 of `SARAH`. With `SARAH` 4 we find complete agreement, whereas we have some disagreement with some results in literature (even at the one-loop level).

Finally, we used PyR@TE to derive the two-loop RGEs of the $\mathcal{G}_{221}$ models exemplifying the capabilities of the code, especially for models with many quartic terms for which a calculation by hand would be very challenging.

We believe that PyR@TE can make an important contribution to exploring physics beyond the Standard Model. We have developed the code in the spirit that calculational or technical details should not stop us exploring new scenarios and that one should make sensible use of computer-aided calculations.

CHAPTER 3
W', Z' AT THE LHC: QCD CORRECTIONS TO TOP-PAIR AND SINGLE-TOP PRODUCTIONS

New heavy resonances that appear in some extensions of the SM have broad consequences. Indeed, because they mix[1] with the SM W- and Z-bosons, all the SM processes involving the electroweak gauge bosons are sensitive to the new particles. In the previous chapter, we have investigated the RGEs at the two-loop level of the $\mathcal{G}_{221}$ models which predict such new resonances. Complementary to this study, we now focus on the LHC phenomenology of these new resonances.

Discovered in 1995 at the $p\bar{p}$ collider, Tevatron [186, 187] the top-quark is significantly different from the other quarks. Its heavy mass[2] of $173.34 \pm 0.27(stat) \pm 0.71(syst)$ GeV [188] or equivalently its short life-time, confers the top-quark the ability to decay before it hadronizes, a major difference with respect to all the other quarks. This property offers a unique opportunity to study a bare quark and effects due to its spin via the angular correlations of its decay products. At the LHC the top-quark is mainly produced via the following processes:(i) top-pair production, $pp \to t\bar{t}$, (ii) single-top, $pp \to t\bar{q}$ or, single-top associated with W production, $pp \to Wt$. When the LHC reaches its nominal energy of $\sqrt{s} = 14$ TeV and luminosity of 10 fb^{-1}/yr, 10^6 top-pairs and almost as many single-tops are expected to be produced each year. Therefore, it will be feasible to perform precision measurements of the top-quark mass, production cross sections as well as various kinematic distributions and the mixing angle of the CKM matrix, $V_{tb}^{\rm CKM}$. Any deviation from the SM predictions will be a hint towards new physics.

Due to its mass close to the electroweak scale, new physics contributions to top-quark observables are expected to be particularly sizeable[3]. Leading order (LO) predictions in theories beyond the standard model usually suffice to design search strategies or to derive exclusion bounds in the parameter space of new physics scenarios. After the first run of the LHC, it seems that new physics is not so much around the corner we expected and the scale of new physics might be higher than previously envisaged. Consequently, it is probable that future measured deviations will be smaller than first hoped and disentangling various new physics scenarios will only be feasible if we have precise theoretical predictions for various observables. Furthermore, accurate determination of the parameters of the underlying theory clearly requires precision that is beyond LO.

[1] Note that this is not necessary but indeed the case for $\mathcal{G}_{221}$ models on which we focus here.

[2] From the latest combination of ATLAS, CDF, CMS and D0.

[3] This assumes that new physics responsible for the electroweak symmetry breaking couples to the top-quark and is not too far from the electroweak scale.

In practice, precise predictions must also account for the busy environment of hadronic colliders, including multi-parton effects and underlying events. In addition, parton shower effects have been shown to be important and must be taken into account for realistic simulations at the hadron level. In order to achieve this, multi-purpose Monte Carlo event generators such as Pythia [189] and HERWIG [190] are used. However, these tools provide only LO accuracy for the hard process.

In order to merge the NLO accuracy of hard scattering processes with the parton shower (PS) techniques, two methods have been proposed: (i) the MC@NLO [191–193] method is based on a careful modification of the NLO result to match the parton shower with the advantage that it does not require any modification of the shower Monte Carlo (SMC) program. On the other hand, the modifications are specific to a given SMC and showering variable. Moreover, as a result of the whole procedure, negative event weights may appear. (ii) As an alternative, the POWHEG method [194] allows for the matching of NLO hard process matrix elements with PS. It does not need to generate negative weighted events but historically required the implementation of p_T ordered showers[4]. Around this method, a framework has been developed, the `POWHEG BOX` [195] which greatly simplifies the implementation of NLO hard process matrix elements in SMC.

In this chapter, we present our calculation of the QCD corrections to the electroweak top-pair production and report on the ongoing calculation of the QCD corrections to the electroweak single-top production in presence of additional generic neutral and charged gauge bosons, Z' and W'. Before the completion of this work a similar calculation of the top-pair production has appeared [196]. However, contrary to the calculation by Melnikov et al. we also provide an implementation of our result in the `POWHEG BOX` framework, hence allowing for realistic collider phenomenology. Note that part of our results for the top-pair production have already been presented in [91]. However, for completeness, we review all the steps of the calculation and focus on the last technicalities of the calculation including the treatment of QED divergences and their implementation in the `POWHEG BOX` as well as on the numerical results.

We start this chapter by describing the various theoretical tools that we use to perform the calculation in Section 3.1. Section 3.2 and Section 3.3 present in turn the specificities of both calculations of the top-pair and single-top production at NLO QCD while in Section 3.4 we provide the reader with some details about the `POWHEG BOX` implementation. Finally, the last section is dedicated to the numerical results, Section 3.5.

3.1 Next-to-Leading order techniques

Loop calculations are a complicated enterprise which was made possible along the years only by the advent of various techniques and methods. At the same time, tools implementing some of these ideas have been designed which renders the calculation of QCD corrections more *accessible*. In spite of all these efforts, the amount of input from the user as well as the tasks left to him are still considerable depending on the calculation. In order to reduce the input from the user and in the view of reusing our computations for later purposes, our group has developed a set of python script, that we dubbed bsmLoops. bsmLoops links several tools already existing to perform different steps of the computation

[4] Truncated showers were also needed [194].

considerably reducing user input. We use a Feynman diagram approach where we generate the diagrams/amplitude squared using QGRAF/DIANA interfaced to FORM to perform the algebraic manipulations (Lorentz contractions, traces). Once this task is performed, we automatically extract the integrals which we reduce to a basis of scalar integrals, called master integrals, using Integration-By-Parts identities (IBPs) via the REDUZE program. Note that up to this point the computation is fully automatic. We then evaluate the master integrals in terms of (Generalized) Harmonic Polylogarithm, (G)HPLs which is done using the differential equation method, see Section 3.1.3. The real contributions to the corresponding process are also calculated using our code.

In this first section, we review the various theoretical techniques that we use for the calculation of virtual QCD corrections to the electroweak top-pair and single-top productions, and comment on the steps that are automatized and what is left to the user. More details on our code can be found in [91].

3.1.1 Dimensional Regularization

The first issue one has to face when calculating observables at NLO is the appearance of divergent integrals. Indeed, the virtual amplitude of a given process involves the integral over the internal momentum of the virtual particle in the loop. This integral will in general be improper in four dimension and one has to find a way of regularizing it. Note that since we calculate modulus of amplitudes squared, we only deal with scalar integrals, i.e. that do not have any free Lorentz indices.

An elegant solution to this problem has been found in the form of what we nowadays call *dimensional regularization* [197]. This techniques consist in extending the usual four dimensional Minkowski space time to an arbitrary dimension that we will denote d. Subsequently, integrals that were previously divergent in $d = 4$ are now properly defined in arbitrary dimension $d \neq 4$. The divergences will appear in the final results as poles in $d = 4$ but the integration can be carried out.

As a defining example, let us consider the following integral

$$\int \frac{d^4k}{(2\pi)^4} \frac{1}{(k^2 - m^2)^n} , \tag{3.1}$$

where k is the momentum of the internal particle over which we integrate, m its mass and n an arbitrary integer. It is clear from naive dimensional arguments that the above integral is UV divergent (large momentum) for $n \leq 2$. In the limit $m \to 0$, it is also IR (small momentum) divergent for $n \geq 2$. In dimensional regularization, this integral in d-dimension reads

$$\mu^{4-d} \int \frac{d^dk}{(2\pi)^d} \frac{1}{(k^2 - m^2)^n} , \tag{3.2}$$

in which we introduced an arbitrary parameter μ with mass dimension to conserve the dimension of the integral[5]. This is now a proper integral that can be integrated (details on how to perform such integrations were given in Chapter 2) leading to

$$\mu^{4-d} \int \frac{d^dk}{(2\pi)^d} \frac{1}{(k^2 - m^2)^n} \sim \mu^{4-d} \frac{\Gamma(n - d/2)}{(4\pi)^{d/2}\Gamma(n)} (m^2)^{d/2-n} , \tag{3.3}$$

[5]Note that the momentum k is now a d-dimensional vector $k^\mu = (k^0, k^1, \ldots, k^{d-1})$. Consistently, the metric tensor is such that $g^\mu_\mu = d$.

in which the poles are contained in the poles of the Euler gamma function $\Gamma(n-d/2)$. As expected, we still have that the result of this integral is divergent for $n \leq 2$ as can be inferred from the expansion, $\Gamma(n-d/2) = \Gamma(n-2) + \mathcal{O}((d-4))$ and the properties of the gamma function.

Dimensional regularization, gives us a way of isolating the poles in the integrals and perform the calculation while keeping track of them. This is extremely powerful and handy. In the following, we will explain how the poles disappear in a complete calculation when we discuss *renormalization* as well as *spontaneous emissions of soft particles*.

One implication of promoting the integrals in d-dimension, is that we also have to extend the Dirac algebra to d dimensions. Consequently, instead of 4 gamma matrices, γ^μ, we now have d of them with $\mu \in [\![0, d-1]\!]$. Since we are only interested in the limit $d = 4$, we can set the normalization of the gamma matrices to $\mathrm{Tr}\,(\gamma^\mu\gamma^\nu) = 4g^{\mu\nu}$. This is simpler than using the definition $\mathrm{Tr}\,(\gamma^\mu\gamma^\nu) = 2^{d/2}g^{\mu\nu}$, that one would expect from the definition of a Clifford algebra and leads to the same results in the limit $d = 4$ [125].

One final complication comes from the treatment of γ_5 in d-dimension. The reason is that $\gamma_5 = \frac{i}{4!}\varepsilon_{\mu\nu\rho\sigma}\gamma^\mu\gamma^\nu\gamma^\rho\gamma^\sigma$ is a purely 4-dimensional object and cannot be consistently extended to d-dimensions. Several prescriptions have been put forward to get around this problem and in our calculation we will rely on Larin prescription [198] which amounts to do the substitution $\gamma_\mu\gamma_5 = i\frac{1}{3!}\varepsilon_{\mu\nu\rho\sigma}\gamma^\nu\gamma^\rho\gamma^\sigma$ and then carry out the calculation in d-dimension. However, by doing so, the Ward identities are violated starting at one-loop and one has to perform an extra finite renormalization for γ_5 in order to restore the Ward identities and hence preserve gauge invariance. It is important to note that this renormalization is to be done on a vertex per vertex basis since purely vector currents should not get affected by this renormalization. In Section 3.1.4 we will give the expression for this extra renormalization constant needed for our calculation.

3.1.2 Integration By Parts identities and Master integrals

The dimensionally regularized scalar integrals satisfy Integration-By-Parts identities (IBPs) [199, 200]. These identities link scalar integrals within the same *auxiliary topology* and allow one to reduce the number of loop integrals present in the problem, to a smaller set of *master integrals*. Consequently, there is no need to calculate all the scalar integrals appearing in the problem but only a handful of them, the master integrals.

In the following we will refer to the propagator denominators by $\mathcal{D}$. They take the form $\mathcal{D} = (q^2 - a)$ where q is a linear combination of loop momenta k_i and external momenta p_i, a is a constant.

An auxiliary topology [201] is defined by a set of n propagator denominators $\mathcal{A} \equiv \{\mathcal{D}_1, \dots, \mathcal{D}_n\}$ which satisfies the following properties: (i) each scalar product of a loop momentum k_i with another loop momentum k_j or an external momentum p_j can be expressed as a linear combination of the $\mathcal{D}_i$ and kinematic invariants, (ii) this decomposition must be unique. Subsequently, all the scalar loop integrals can be written in the form

$$I(i_1, i_2, \dots) = \mu^{4-d} \int \frac{d^d k}{(2\pi)^d} \frac{1}{\mathcal{D}^{i_1}\mathcal{D}^{i_2}\dots}\,, \tag{3.4}$$

in which $i_1, i_2, \dots$ are the powers of the propagator denominators and can in general take positive, negative integer values or can be null. Note that property (i) is essential to the

reduction algorithms to guarantee that within two consecutive steps we stay within the same ensemble of propagator denominators appearing in the loop integrals, the auxiliary topology.

In dimensional regularization, the integral over a total derivative is zero. As a consequence the following equality holds

$$\int d^d k_i \frac{\partial}{\partial k_i^\mu} \left[q^u I(i_1, i_2, \dots) \right] = 0 \,, \tag{3.5}$$

where q is an arbitrary loop or external momentum and μ is summed over contrary to i which is fixed. Carrying out the derivation leads to the IPBs. If the auxiliary topology is constructed form n loop momenta and $m+1$ external lines, one can build $n(m+n)$ such relations for each integral.

Let's now see how this works on the simplest example, and consider the tadpole integral

$$I_T(i_1 = 1) = \mu^{4-d} \int \frac{d^d k}{(2\pi)^d} \frac{1}{\mathcal{D}_1^{i_1}} \,, \; \mathcal{D}_1 = k^2 + m^2 \,. \tag{3.6}$$

In the associated diagram, there is no external momentum and therefore there is only one IBP associated to I_T

$$\int d^d k \frac{\partial}{\partial k^\mu} \left(\frac{k^\mu}{\mathcal{D}_1} \right) = \int d^d k \frac{d}{\mathcal{D}_1} + \int d^d k k^\mu \frac{-2k^\mu}{\mathcal{D}_1^2} = 0$$

$$I_T(2) = \frac{-(d-2)}{2m^2} I_T(1) \,, \tag{3.7}$$

where we have used the relation $k^2 = \mathcal{D}_1 - m^2$ between the two lines. This relation can be easily generalized to arbitrary i_1

$$I_T(i_1 + 1) = \frac{-(d-2i_1)}{2i_1 m^2} I_T(i_1) \,. \tag{3.8}$$

This example is extremely simple and in general one obtains a linear combination of the $I(i_1, i_2, \dots)$ (for various $i_1, i_2, \dots$) with coefficients composed out of the external momenta invariants, dimension d and the denominator powers i_i.

A slightly more involved example is that of the equal masses two-point function

$$I_{\mathcal{A}}(1,1) = \mu^{4-d} \int \frac{d^d k}{(2\pi)^d} \frac{1}{\mathcal{D}_1 \mathcal{D}_2} \,, \mathcal{D}_1 = k^2 + m^2 \,, \mathcal{D}_2 = (p+k)^2 + m^2 \,, \tag{3.9}$$

with two independent momenta k^μ and p^μ. Since $k^2 = \mathcal{D}_1 - m^2$ and $p \cdot k = \frac{1}{2} \left(\mathcal{D}_2 - \mathcal{D}_1 - p^2 \right)$, $\mathcal{A} = \{\mathcal{D}_1, \mathcal{D}_2\}$ is a proper auxiliary topology. The following system of IBPs can then be written

$$\begin{aligned} \int d^d k \frac{\partial}{\partial k^\mu} \left(\frac{k^\mu}{\mathcal{D}_1 \mathcal{D}_2} \right) &= 0 \\ \int d^d k \frac{\partial}{\partial k^\mu} \left(\frac{p^\mu}{\mathcal{D}_1 \mathcal{D}_2} \right) &= 0 \,, \end{aligned} \tag{3.10}$$

and leads to

$$\begin{aligned}\int d^dk \frac{d}{\mathcal{D}_1\mathcal{D}_2} + \int d^dk \left(-\frac{2k^2}{\mathcal{D}_1^2\mathcal{D}_2} - \frac{2(p+k)\cdot k}{\mathcal{D}_1\mathcal{D}_2^2}\right) &= 0 \\ \int d^dk \left(-\frac{2k\cdot p}{\mathcal{D}_1^2\mathcal{D}_2} - \frac{2(p+k)\cdot p}{\mathcal{D}_1\mathcal{D}_2^2}\right) &= 0\,. \end{aligned} \tag{3.11}$$

Expressing the scalar products in terms of the inverse denominators one obtains

$$\begin{aligned} &I_{\mathcal{A}}(1,2) - I_{\mathcal{A}}(2,1) = 0 \\ &(d-3)I_{\mathcal{A}}(1,1) + (4m^2+p^2)I_{\mathcal{A}}(1,2) - I_{\mathcal{A}}(0,2) = 0\,, \end{aligned} \tag{3.12}$$

and finally using Eq. (3.8) and $I_{\mathcal{A}}(0,i) = I_T(i)$

$$I_{\mathcal{A}}(1,2) = -\frac{(d-3)}{4m^2+p^2} I_{\mathcal{A}}(1,1) - \frac{(d-2)}{2m^2(p^2+4m^2)} I_{\mathcal{A}}(1,0)\,. \tag{3.13}$$

Hence, we see that the two-point function with a squared propagator can be reduced in terms of the simple equal masses two-point function and the tadpole.

As shown in the second example, the IBPs for a given auxiliary topology form a homogeneous system of linear equations with the integrals as unknowns. However, this system is under-determined and it is therefore impossible to solve for all the loop integrals. The left-over integrals in terms of which the others are expressed are called the master integrals, e.g. $I_{\mathcal{A}}(1,1)$, $I_{\mathcal{A}}(1,0)$ in the previous example. We will present the master integrals for the problem at hand in a coming section.

Generating all the IBPs for a given problem is straightforward and the difficulty of this method resides in solving the system of IBPs, the *reduction*. There exist several methods to solve a system of IBPs and in our work we use the Laporta [202] algorithm as implemented in the public tool REDUZE 2[6] [201, 204].

3.1.3 Solving the master integrals

Even though the number of scalar integrals that have to be calculated is greatly reduced during the reduction, one usually ends-up with a handful of master integrals for which a solution must be sought. For one loop calculations, many of the master integrals that are commonly encountered are well known in the literature and this step can actually be skipped. However, since in principle the master integrals must be calculated we review an interesting method to find such solutions, the *differential equation method* [205]. Note that other methods can be employed such that for instance the application of Mellin-Barnes transformation to all propagators [206, 207] or the negative dimension approach [208] which are both based on a direct evaluation of the integral.

The differential equation method is a technique that avoids the explicit integration over the loop momenta but relies on solving a differential equation satisfied by the scalar integral itself. To illustrate this method we derive the differential equation satisfied by the already encountered equal masses two-point function, see Eq. (3.9)

$$I_{\mathcal{A}}(1,1) = \mu^{4-d} \int \frac{d^dk}{(2\pi)^d} \frac{1}{\mathcal{D}_1\mathcal{D}_2}\,, \mathcal{D}_1 = k^2+m^2\,, \mathcal{D}_2 = (p+k)^2+m^2\,. \tag{3.14}$$

[6] Note that the Laporta algorithm is also implemented in older tools e.g. AIR [203].

Using the relation

$$p^\mu \frac{d}{dp^\mu} = p^\mu \frac{d}{dp^2}\frac{dp^2}{dp^\mu} = p^\mu \frac{d}{dp^2} 2p_\mu = 2p^2 \frac{d}{dp^2}\,, \tag{3.15}$$

we calculate the derivative of $I_{\mathcal{A}}(1,1)$

$$\begin{aligned}
\frac{d}{dp^2} I_{\mathcal{A}}(1,1) &= \frac{1}{2p^2} p^\mu \frac{d}{dp^\mu} \mu^{4-d} \int \frac{d^dk}{(2\pi)^d} \frac{1}{\mathcal{D}_1 \mathcal{D}_2} \\
&= \frac{1}{2p^2} p^\mu \mu^{4-d} \int \frac{d^dk}{(2\pi)^d} \frac{-2(p+k)_\mu}{\mathcal{D}_1 \mathcal{D}_2^2} \\
&= -\frac{1}{2} I_{\mathcal{A}}(1,2) - \frac{1}{2p^2} I_{\mathcal{A}}(1,1) - \frac{(d-2)}{4m^2p^2} I_{\mathcal{A}}(1,0)\,,
\end{aligned} \tag{3.16}$$

which involves $I_{\mathcal{A}}(1,1)$ but also $I_{\mathcal{A}}(1,2)$ and $I_{\mathcal{A}}(1,0)$. Now, the central point of this method is to inject the IBPs inside this equation to obtain a differential equation. Using the IBPs derived in the previous section, Eq. (3.13), we obtain a non-homogeneous first order differential equation for the integral $I_{\mathcal{A}}(1,1)$

$$\frac{dI_{\mathcal{A}}(1,1)}{dp^2} = -\frac{1}{2}\left[\frac{1}{p^2} - \frac{(d-3)}{p^2+4m^2}\right] I_{\mathcal{A}}(1,1) - \frac{(d-2)}{4m^2}\left[\frac{1}{p^2} - \frac{1}{p^2+4m^2}\right] I_{\mathcal{A}}(1,0)\,. \tag{3.17}$$

This case is actually quite simple and can be solved analytically for a generic value of the parameter d. First, the initial condition has to be determined. This is done by using the regular property of $I_{\mathcal{A}}(1,1)$ in $p^2 \to 0$ and the subsequent relation $\lim_{p^2\to 0} p^2 \frac{d}{dp^2} I_{\mathcal{A}}(1,1) = 0$ [209]. Multiplying Eq. (3.17) by p^2 and taking the limit $p^2 \to 0$ we have

$$0 = -\frac{1}{2} \lim_{p^2\to 0} I_{\mathcal{A}}(1,1) - \frac{(d-2)}{4m^2} I_{\mathcal{A}}(1,0)\,, \tag{3.18}$$

from which we obtain the initial condition

$$\lim_{p^2\to 0} I_{\mathcal{A}}(1,1) = -\frac{(d-2)}{2m^2} I_{\mathcal{A}}(1,0)\,. \tag{3.19}$$

The solution to the homogeneous part is immediate and reads

$$\tilde{I}_{\mathcal{A}} = k z^{-1/2} (1+z)^{(d-3)/2}\,, \tag{3.20}$$

where we have introduced the dimensionless parameter $z = p^2/4m^2$. The variation of the constant method is well suited to determine the solution of the inhomogeneous part. Indeed, considering $k(z)$ as a function of z and calculating the derivative of Eq. (3.20)

$$\begin{aligned}
k' z^{-1/2} (1+z)^{(d-3)/2} &= -\frac{(d-2)}{4a}\left(\frac{1}{z} - \frac{1}{1+z}\right) I_{\mathcal{A}}(1,0) \\
k &= \frac{(d-2)}{4a} I_{\mathcal{A}}(1,0) \int_0^z dt\, t^{1/2}(1+t)^{(1-d)/2} - t^{-1/2}(1+t)^{(3-d)/2}\,,
\end{aligned} \tag{3.21}$$

we find

$$\hat{I}_{\mathcal{A}}(1,0) = z^{-1/2}(1+z)^{d-3/2} \frac{(d-2)}{4a} I_{\mathcal{A}}(1,0) \int_0^z t^{1/2}(1+t)^{(1-d)/2} - t^{-1/2}(1+t)^{(3-d)/2} dt\,. \tag{3.22}$$

Note that the two integrals in the last equation are representations of the hypergeometric function [209]. Finally, the full result is given by the sum of the two solutions $I_{\mathcal{A}}(1,1) = \tilde{I}_{\mathcal{A}}(1,1) + \hat{I}_{\mathcal{A}}(1,1)$. The differential equation method, is a powerful method that has been applied to many cases in the literature with great success, see for instance [210].

3.1.4 Renormalization

Divergent loop integrals are inherent to any calculation that goes beyond the leading order. Here, we concentrate on divergences that appear for large values of the integration momenta (UV) keeping in mind that in a theory with massless particles divergences in the limit of small momenta can also be present. For a virtual amplitude of a given process, after the integrals have been calculated in d-dimension the UV as well as IR divergences are extracted as poles[7] of $1/\varepsilon = 2/(4-d)$. The renormalization procedure consists in treating the UV divergences by redefining the parameters and fields of the theory. We have already shown in Chapter 2 how the divergences in ϕ^4 theory could be absorbed into a re-definition of the scalar field wave function, gauge parameter and quartic coupling to give finite predictions. In this part, we give some details on the renormalization procedure that we use in our calculation.

The Lehmann-Symanzik-Zimmermann (LSZ) reduction formula [211–213] allows one to link the renormalized squared amplitude to the bare one via the following relation

$$\tilde{\mathcal{M}} = \prod_n Z_{\mathrm{WF},n}^{1/2} \mathcal{M}(\{\tilde{x}_i\}) \,, \tag{3.23}$$

in which $Z_{\mathrm{WF,n}}^{1/2}$ are the wave function renormalization constants for each one of the n external legs and $\{\tilde{x}_i\}$ denotes the set of renormalized coupling parameters of the theory. They are obtained from the corresponding bare parameters by multiplicative renormalization

$$\tilde{x}_i = Z_i x_i \,, \tag{3.24}$$

where we introduced the renormalization constants Z_i. These constants are obtained in perturbation theory by calculating the divergent parts of the diagrams and are scheme dependent.

We now expand the relation of Eq. (3.23) in the case at hand, i.e. the QCD corrections to electroweak processes. Both, the electroweak top-pair and the single-top production amplitudes are of the order $\mathcal{O}(\alpha_{EW}^2)$ at tree level and therefore the QCD corrections at the order $\mathcal{O}(\alpha_S \alpha_{EW}^2)$. They can be written in the form

$$\mathcal{M} = \left(\frac{\alpha_{EW}}{\pi}\right)^2 \mathcal{M}_{0;2} + \frac{\alpha_S}{\pi}\left(\frac{\alpha_{EW}}{\pi}\right)^2 \mathcal{M}_{1;2} + \dots \,, \tag{3.25}$$

where $\dots$ represents higher order corrections and indices $m;n$ represents the power of α_S, α_{EW} respectively. Since the corrections that we consider are of first order in α_S and have the same order in α_{EW} as the tree level contributions there is no correction to either α_S or α_{EW} and we have

$$\delta Z_{\alpha_{EW}} = 1 + \mathcal{O}(\alpha_{EW}), \;\; \delta Z_{\alpha_S} = 1 + \mathcal{O}(\alpha_S) \,. \tag{3.26}$$

In addition, the only quark considered massive is the top-quark and its mass does not need to be renormalized either as will be shown in Section 3.2. Therefore, we only need to carry out the wave function renormalization

$$Z_{\mathrm{WF},n} = 1 + \frac{\alpha_S}{\pi}\delta Z_{\mathrm{WF,n}} + \mathcal{O}\left(\left(\frac{\alpha_s}{\pi}\right)^2\right) \,. \tag{3.27}$$

[7] UV singularities will appear as single pole while IR divergences can lead to single or double poles.

Expanding Eq. (3.23) and inserting Eqs. (3.25, 3.27) one obtains

$$\begin{aligned}\tilde{\mathcal{M}} &= \prod_n \left(1+\frac{\alpha_S}{\pi}\delta Z_{\mathrm{WF},n}\right)^{1/2}\left(\left(\frac{\alpha_{EW}}{\pi}\right)^2\mathcal{M}_{0;2}+\frac{\alpha_S}{\pi}\left(\frac{\alpha_{EW}}{\pi}\right)^2\mathcal{M}_{1;2}+\dots\right)\\ &= \left(\frac{\alpha_{EW}}{\pi}\right)^2\mathcal{M}_{0;2}+\frac{\alpha_S}{\pi}\left(\frac{\alpha_{EW}}{\pi}\right)^2\underbrace{\left(\mathcal{M}_{1;2}+\sum_n\frac{1}{2}\delta Z_{\mathrm{WF},n}\mathcal{M}_{0;2}\right)}_{\tilde{\mathcal{M}}^{(1)}}+\mathcal{O}(\alpha_S^2\alpha_{EW}^2)\,.\end{aligned} \tag{3.28}$$

Hence, the procedure to obtain the renormalized amplitude is straightforward: (i) Calculate the virtual corrections of order $\mathcal{O}(\alpha_S\alpha_{EW}^2)$, $\mathcal{M}_{1;2}$, (ii) multiply the Born evaluated in d-dimension[8], $\mathcal{M}_{0;2}$, by the sum of adequate wave function renormalization, (iii) and sum the two contributions $\tilde{\mathcal{M}}^{(1)}$ and $\mathcal{M}_{0;2}$. The renormalized amplitude thus obtained, $\tilde{\mathcal{M}}$, does not contain any UV divergence anymore. Note however, that single and double poles in ε are still present in the virtual amplitude since we have not dealt with the IR divergences yet.

We list below the various renormalization wave function constants that we use in Eq. (3.28). The top-quark wave function is renormalized on-shell (OS) while the massless quark fields are renormalized in the $\overline{\mathrm{MS}}$ scheme in which the renormalization constant vanish for on-shell partons. Therefore, we are left with only the top-quark field renormalization constant which reads in $d=4-2\varepsilon$ dimension [214]

$$\delta Z^{\mathrm{OS}}_{\mathrm{WF},t} = (4\pi)^{\varepsilon}\Gamma(1+\varepsilon)\left(\frac{\mu^2}{m_t^2}\right)C_F\left(-\frac{3}{4\varepsilon}-\frac{1}{1-2\varepsilon}\right)\,. \tag{3.29}$$

As explained in Section 3.1.1 if one uses the Larin prescription for treating the γ^5 matrices in dimensional regularization, an extra finite renormalization has to be performed in order to restore the Ward identities. This renormalization constant has been calculated up to three-loops in the $\overline{\mathrm{MS}}$ scheme in [198] and reads at one-loop

$$Z_5 = 1-\frac{\alpha_S}{\pi}C_F+\mathcal{O}(\alpha_S^2)\,. \tag{3.30}$$

However, it must be noted that only the terms involving γ^5 and products of γ^5 should be multiplied by corresponding powers of Z_5. Consequently, it is often more practical to calculate a dedicated expression for the Born in which the axial couplings of the gauge bosons have been multiplied by Z_5 in such a way that this modified Born can be directly added to the other counter terms to complete the renormalization procedure.

Note that in bsmLoops, the renormalization is not yet done automatically and one has to carry it directly in FORM. Note however, that some template files are provided so that only the expressions of the various wave function renormalization constants and their combination multiplying the Born must be provided. Automating this procedure is one of the important steps towards which the efforts will be directed in the future.

[8]This is necessary in order to obtain all the finite pieces from the multiplication with the divergent renormalization constants and understood in the definition of the $\overline{\mathrm{MS}}$ scheme.

3.1.5 Infrared structure of the virtual corrections

Even though renormalization tames the UV divergences, it does not address the issue of soft (low-momentum) and collinear (small-angle) singularities that are present both in the real and virtual contributions (referred to as infrared divergences (IR)). According to the Kinoshita-Lee-Nauenberg theorem [215, 216] in a theory with massless fields, transition rates are free of the infrared (soft and collinear) divergences if the summation over the initial and final degenerate states is carried out. That is to say, the IR divergences in the real and virtual contributions cancel. However, in hadron collisions, the left-over collinear singularities coming from initial state radiations due to the violation of the KLN theorem must be absorbed in the re-definition of the PDFs.

Schematically, at LO we can write a given cross section of a 2 to n process as the integration of the partonic Born cross section over the phase space of the n outgoing partons

$$\sigma^{LO} = \int d\mathbf{\Phi}_n \mathcal{L}\mathcal{B} \equiv \int_n d\hat{\sigma}^{\mathcal{B}}\,, \tag{3.31}$$

$d\mathbf{\Phi}_n$ is a set of variables characterizing the n-particle phase space, $\mathcal{L} = f(x_1)f(x_2)$ is the product of parton density functions with x_i being the momentum fraction of the incoming partons and $\mathcal{B}$ is the Born matrix element. $d\hat{\sigma}^B$ is the Born cross section and can be calculated in 4-dimension. Following the same notation, the NLO contribution to the total cross section takes the form

$$\sigma^{NLO} = \int_{n+1} d\hat{\sigma}^{\mathcal{R}} + \int_n d\hat{\sigma}^{\mathcal{V}^{\text{ren.}}} + \int_n d\hat{\sigma}^{\mathcal{C}}\,, \tag{3.32}$$

in which we indicate by a subscript n, $n+1$ the dimension of the phase space similar to the definition in Eq. (3.31). All the terms on the right-hand side of Eq. (3.32) are separately divergent while the sum, σ^{NLO}, must be finite for well defined observables. The singularities in the virtual contribution are expressed in dimensional regularization as powers of $1/\varepsilon$ while the IR divergences in the real contribution are phase space singularities. Therefore, it is clear that the cancellation of the divergences in exclusive observables cannot be achieved numerically and the various pieces must be regularized separately before any numerical integration. The last term on the right-hand side of Eq. (3.32), the collinear counter term arises from the redefinition of the PDFs. Indeed, within the factorization theorem, additional radiation from the initial state with low momentum with respect to $\sim \mu_f$ are described by the PDFs. Since the splittings leading to collinear singularities are universal we are free to absorbed these divergences in the definition of the PDFs. In order to obtain a finite partonic cross section the collinear divergences absorbed in the PDFs must be subtracted which is referred to as collinear counter terms and are contained in $d\hat{\sigma}^{\mathcal{C}}$.

We now review the idea of the subtraction method in combination with the dipole formalism which aims at providing a technique to perform the above mentioned regularization. Here we only briefly review the presentation of [217, 218] to which we refer the reader for additional information. Note that several other methods for the treatment of infrared divergencies exist including phase-space slicing methods, e.g. [219], or the Frixione-Kunszt-Signer (FKS) dipole subtraction [220].

The basic idea of the subtraction method is to add and subtract an *auxiliary cross section*, $d\sigma^{\mathcal{A}}$ to the NLO cross section which acts as a local counter term for $d\hat{\sigma}^{\mathcal{R}}$. It

must be an approximation of $d\hat{\sigma}^{\mathcal{R}}$ such as to have the same pointwise singular behaviour in d-dimension as $d\hat{\sigma}^{\mathcal{R}}$ itself. In addition, it must be simple enough so that it can be integrated in d-dimension analytically over the single-parton subspaces that lead to the soft and collinear divergences to yield $1/\varepsilon$ poles. These poles can then be combined with the ones in $d\hat{\sigma}^{\mathcal{V}^{\text{ren.}}}$ to cancel the remaining infrared singularities. The key point of this method relies in being able to construct such an object independently of the process[9] and with the required properties. This can be achieved within the dipole formalism as explained now.

The main result of [218] is a prescription to construct $d\sigma^{\mathcal{A}}$ as a sum of various contributions called *dipoles*. A given dipole contribution describes the soft and collinear radiation from a pair of ordered partons, the *emitter* and the *spectator*. Only the kinematics of the emitter leads to singularities while the spectator carries information on the color and spin correlations of the real cross section $d\hat{\sigma}^{\mathcal{R}}$. The auxiliary cross section can then be written

$$d\sigma^{\mathcal{A}} = \sum_{\text{dipoles}} d\hat{\sigma}^{\mathcal{B}} \otimes dV_{\text{dipole}}\,, \tag{3.33}$$

where dV_{dipole}, the dipole factors, encode the two-parton decay of the emitters. These factors are universal and can be obtained from the QCD factorization formulae in the soft and collinear limits. Note that the symbol $\otimes$ means that the spin and color correlations are included. dV_{dipole} can be made fully integrable analytically [218] and in a process independent way leading to

$$\int_{n+1} d\sigma^{\mathcal{A}} = \sum_{\text{dipoles}} \int_{n} d\hat{\sigma}^{\mathcal{B}} \otimes \int_{1} dV_{\text{dipole}} = \int_{n} d\hat{\sigma}^{\mathcal{B}} \otimes \mathbf{I}\,. \tag{3.34}$$

with the *universal factor* $\mathbf{I}$ defined as

$$\mathbf{I} = \sum_{\text{dipoles}} \int_{1} dV_{\text{dipole}}\,. \tag{3.35}$$

$\mathbf{I}$ contains the $1/\varepsilon$ poles that will cancel the infrared divergences in the virtual contribution $d\hat{\sigma}^{\mathcal{V}^{\text{ren.}}}$. Consequently, the cross section for the NLO contribution reads symbolically

$$\begin{aligned}
\sigma^{NLO} &= \sigma^{NLO}_{n+1}(p) + \sigma^{NLO}_{n}(p) + \int_0^1 dx \hat{\sigma}^{NLO}_{n}(x; xp) \\
&= \int_{n+1} d\hat{\sigma}^{\mathcal{R}}(p) - \sum_{\text{dipoles}} d\hat{\sigma}^{\mathcal{B}}(p) \otimes dV_{\text{dipole}} \\
&\quad + \int_n \left[d\hat{\sigma}^{\mathcal{V}^{\text{ren.}}}(p) + d\hat{\sigma}^{\mathcal{B}}(p) \otimes \mathbf{I} \right] \\
&\quad + \int_0^1 dx \int_n \left[d\hat{\sigma}^{\mathcal{B}}(xp) \otimes (\mathbf{P} + \mathbf{K})(x) \right]\,.
\end{aligned} \tag{3.36}$$

The contributions $\sigma^{NLO}_{n+1}(p)$ and $\sigma^{NLO}_{n}(p)$ with $n+1$- and n- partons kinematics respectively, are separately finite. The third term on the first line is a left-over from the cancellation

[9] Each term is constructed from universal pieces that only depend on the masses of the external particles.

of the divergences in the collinear counter terms. It involves a NLO cross section with n parton kinematics and an additional one-dimensional integration with respect to the longitudinal momentum fraction x. As explicitly written on the last line of Eq. (3.36), it comes from the convolution of the Born cross section $d\hat{\sigma}^{\mathcal{B}}(xp)$ with x-dependent functions $\mathbf{P}$ and $\mathbf{K}$ that are universal and finite for $\varepsilon \to 0$. The various expressions for the universal factors, $\mathbf{I}$, dV_{dipole}, $\mathbf{P}$ and $\mathbf{K}$ can be found in [217, 218]. Note that dV_{dipole} includes contributions from the collinear counter terms as required to make $d\hat{\sigma}^{\mathcal{R}}$ finite.

In practice, once the finite part of the virtual amplitude, the real and the Born cross sections (as well as Born correlated amplitudes) are known, σ^{NLO} can be constructed following Eq. (3.36) in an automated manner. We will come back to this when we discuss the `POWHEG BOX` implementation of our results, see Section 3.4. However, in order to check the consistency of our virtual amplitudes with the corresponding Born, one can verify analytically that $d\hat{\sigma}^{\mathcal{V}^{\text{ren.}}}(p) + d\hat{\sigma}^{\mathcal{B}}(p) \otimes \mathbf{I}$ yields a finite result. Details for the processes at hand will be given later on in the manuscript, see Section (3.2).

3.2 Top-pair production

In the first section of this chapter we have presented various theoretical tools and explained the general method we use to carry out the calculation of the NLO QCD corrections to the electroweak top-pair and single-top productions. We now give some details on the order $\mathcal{O}(\alpha_S \alpha_{EW}^2)$ contributions to the top-pair production in the framework of the $\mathcal{G}_{221}$ models, i.e. in addition to the SM γ and Z-boson an extra Z'-boson is considered. For the sake of generality, we consider the axial and vector part of the Z'-boson couplings arbitrary flavour diagonal so that we can accommodate the various $\mathcal{G}_{221}$ models, see Eqs. (1.30, 1.31). In addition, the top-quarks in the final state will be considered on-shell and stable since their subsequent decay can be handled automatically at leading order accuracy by a general purpose Monte Carlo event generator. Finally, all the calculations presented in this chapter are performed in the Feynman gauge.

The partonic top-pair production up to NLO has the following perturbative expansion

$$\hat{\sigma}^{NLO} = \hat{\sigma}_{2;0}(\alpha_S^2) + \hat{\sigma}_{0;2}(\alpha_{EW}^2) + \hat{\sigma}_{3;0}(\alpha_S^3) + \hat{\sigma}_{2;1}(\alpha_S^2 \alpha_{EW}) + \hat{\sigma}_{1;2}(\alpha_S \alpha_{EW}^2) + \hat{\sigma}_{0;3}(\alpha_{EW}^3)\,, \quad (3.37)$$

where as previously mentioned the indices $m;n$ represent the powers of α_S and α_{EW} respectively. Out of the six terms in the expansion we concentrate on the two that are highlighted in red i.e. $\hat{\sigma}_{0;2}$ the LO electroweak cross section and its QCD corrections in $\hat{\sigma}_{1;2}$. Even though the inequality $\alpha_S^2 \alpha_{EW} > \alpha_S \alpha_{EW}^2$ let us foresee that $\hat{\sigma}_{1;2}$ will likely yield a smaller correction than $\hat{\sigma}_{2;1}$ it will likely be more relevant for new physics searches at the LHC due to the role of the resonant Z'-boson. In addition, while the calculation of $\hat{\sigma}_{1;2}$ can be carried out in a model independent way as long as the Z' couplings are kept general, $\hat{\sigma}_{2;1}$ will be highly model dependent due to the rich structure of the scalar sector in $\mathcal{G}_{221}$ models.

In the SM, all the above contributions have been calculated: (i) cross sections and distributions including QCD effects of $\mathcal{O}(\alpha_S)^3$ were computed in [221–224], (ii) part of the electroweak corrections of order $\mathcal{O}(\alpha_S^2 \alpha_{EW})$ were investigated in [225], neglecting the interferences between QCD and electroweak interactions, (iii) finally, the rest of the corrections were calculated in a series of papers including the effects of the Z-gluon interferences [219, 226–228].

3.2.1 Leading-order contribution

In Fig. 3.1 we show the order $\mathcal{O}(\alpha_{EW})$, tree level diagrams. The squared matrix element is obtained by interfering all possible diagrams together. Summing over the spin of final state particles and averaging over the initial ones we obtain the Born matrix element, $\mathcal{B}$. We perform this calculation in 4 and d-dimension as the latter is required for the calculation of the counter terms used for the renormalization as explained in Section 3.1.4.

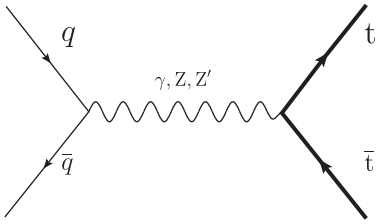

Figure 3.1: Tree level Feynman diagrams to the electroweak top-pair production. The three gauge bosons exchange, γ, Z, Z', are considered.

The diagrams are generated automatically using bsmLoops which uses QGRAF and DIANA to translate it into amplitudes. The traces for each interference term are then calculated using FORM and summed together. The result is already quite lengthy due to the general structure of the Z' couplings and reads for a general interference term[10] $\mathcal{B}_q(B, B')$ [91]

$$\begin{aligned}\mathcal{B}_q(B,B') = \frac{2\alpha_{EW}^2}{\hat{s}^2 D_B D_{B'} s_W^4} \Big\{ &\hat{s}(\hat{t}-\hat{u}) \left(A_B^q B_{B'}^q + A_{B'}^q B_B^q\right) \left(A_B^{\mathrm{t}} B_{B'}^{\mathrm{t}} + A_{B'}^{\mathrm{t}} B_B^{\mathrm{t}}\right) + \\ &\left(A_B^q A_{B'}^q + B_B^q B_{B'}^q\right) \left[\left(\hat{t}^2+\hat{u}^2+4\hat{s}m_{\mathrm{t}}^2 - 2m_{\mathrm{t}}^4\right) A_B^{\mathrm{t}} A_{B'}^{\mathrm{t}} + \left(\hat{t}^2+\hat{u}^2-2m_{\mathrm{t}}^4\right) B_B^{\mathrm{t}} B_{B'}^{\mathrm{t}}\right] \Big\} \\ &\Big\{ \left[(\hat{s}-M_B^2)(\hat{s}-M_{B'}^2) + m_B m_{B'} \Gamma_B \Gamma_{B'}\right] + i\left[(\hat{s}-M_B^2) m_{B'} \Gamma_{B'} - (\hat{s}-M_{B'}^2) m_B \Gamma_B\right] \Big\} \ ,\end{aligned} \tag{3.38}$$

where $B, B' \in \{\gamma, Z, \mathrm{Z}'\}$, the subscript q denotes the flavor of the incoming massless parton and $\hat{s}$, $\hat{t}$, $\hat{u}$ are the usual partonic Mandelstam variables[11]. $D_B, D_{B'}$ come from the product of denominators of the propagators and take the usual form

$$D_\gamma = \frac{1}{\hat{s}^2}, \ D_Z = \frac{1}{(\hat{s}-M_Z^2)^2 + m_Z^2\Gamma_Z^2}, \ D_{Z'} = \frac{1}{(\hat{s}-M_{Z'}^2)^2 + m_{Z'}^2\Gamma_{Z'}^2} \, . \tag{3.39}$$

The coefficients $A^q_{B(B')}, B^q_{B(B')}, A^{\mathrm{t}}_{B(B')}, B^{\mathrm{t}}_{B(B')}$, are proportional to the axial (A) and vector (B) couplings of the various gauge bosons to massless (q) and top (t) quark. Their expressions have been collected in Appendix E. To take into account the finite width of the Z- and Z'-bosons we introduced the complex masses, $m_{Z(Z')} \to m_{Z(Z')} - i\Gamma_{Z(Z')}/2$ such that our propagator for a massive gauge boson B, reads

$$\frac{1}{q^2 - m_B^2 + i\Gamma_B m_B + \Gamma_B^2/4} \, . \tag{3.40}$$

[10] Note that the flux factor $1/2\hat{s}$ is included.

[11] Note that we use the Pauli-Dirac metric in which the dot product has an overall minus sign with respect to the Bjorken-Drell metric. Details on this metric as well as recipes on how to convert between the two formulae can be found in [229].

Consequently, the following relation between m_B^2 and M_B^2 holds: $M_{Z(Z')}^2 = m_{Z(Z')}^2 - \Gamma_{Z(Z')}^2/4$.

Subsequently, the expression for the total Born matrix element can be written in terms of general interference terms as

$$\mathcal{B} = \sum_q \left(\mathcal{B}_q(\gamma,\gamma) + \mathcal{B}_q(Z,Z) + \mathcal{B}_q(\mathrm{Z}',\mathrm{Z}') + \sum_{B\neq B'} \mathcal{B}_q(B,B') \right) , \tag{3.41}$$

where we sum over all the possible light quarks in the initial state $q \in \{\mathrm{d},\mathrm{u},\mathrm{s},\mathrm{c},\mathrm{b}\}$. Note that, the general interference term contains an imaginary part, Eq. (3.38). However, as expected, it drops out in the final amplitude due to the relation $\mathcal{B}_q(B',B) = \mathcal{B}_q(B,B')^*$.

3.2.2 Virtual contribution

We now summarise the result for the virtual corrections to the electroweak top-pair production. From the LO diagrams, Fig. 3.1, it is clear that there are only two types of virtual corrections to calculate: vertex corrections to either the initial or final state particles. Indeed, since the electroweak gauge bosons are color singlets the interference of the Born amplitude with the box diagrams shown in Fig. 3.2 are proportional to $\mathrm{Tr}(T^a)$ and therefore vanish. Summing the interferences of any of the diagrams in Fig. 3.3 with the LO ones, Fig. 3.1 lead to the virtual amplitude.

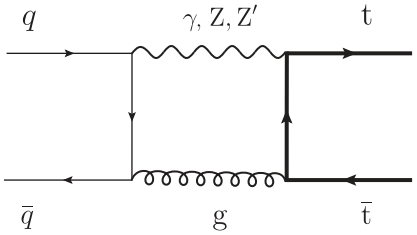

Figure 3.2: Example of box diagram of order $\mathcal{O}(\alpha_S\alpha_{EW})$ leading to vanishing contribution. Note that this diagram would contribute to observables at order $\mathcal{O}(\alpha_S^2\alpha_{EW})$.

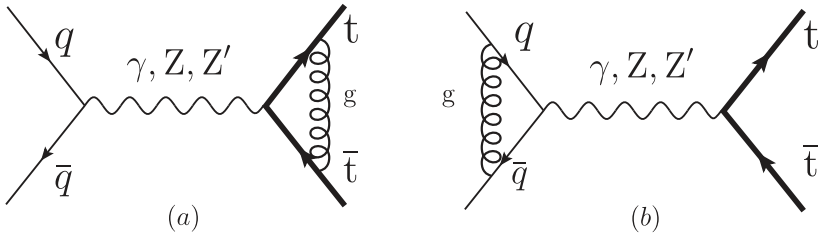

Figure 3.3: Virtual corrections to the electroweak top-pair production of order $\mathcal{O}(\alpha_S\alpha_{EW})$.

Master integrals and renormalization

As explained in Section 3.1 the virtual amplitude is regularized using dimensional regularization and the various scalar integrals are reduced to a basis of master integrals. For

the calculation of the corrections of order $\mathcal{O}(\alpha_S\alpha_{EW}^2)$ we have reduced 30 distinct loop integrals to a set of 3 master integrals: (i) the massive one-point function referred to as the **massive tadpole**, (ii) the equal masses two-point function known as the **massive bubble** (iii) and the massless two-point function, the **massless bubble**. The solution of these master integrals can be obtained via the differential equation method and are well known, see e.g. [230]. All the other integrals encountered during the calculation can be expressed in terms of these three integrals by solving the system of IBPs. The full solution is too lengthly and we do not show it here.

After this step, the IR as well as UV singularities in the virtual amplitude are expressed as poles of $1/\varepsilon$ and $1/\varepsilon^2$. The UV divergences are tamed by the renormalization procedure as outlined in Section 3.1.4. There we showed that the counter term that must be added to the virtual amplitude in order to cancel the UV poles is of the form

$$\sum_{n\in\{q,\bar{q},\mathrm{t},\bar{\mathrm{t}}\}} \frac{1}{2}\delta Z_{\mathrm{WF},n}\mathcal{M}_{0;2}\,. \tag{3.42}$$

where $\mathcal{M}_{0;2}$ refer to the Born amplitude. Since the initial partons are massless we only have the two top-quarks in the final states that need to be renormalized. Therefore the counter term for the top-pair production is simply given by $\delta Z_{\mathrm{WF,t}}\mathcal{M}_{0;2}$. In addition, because there is no diagram containing corrections to the top-quark propagator the top-quark mass does not need to be renormalized and we are left with only one contribution to the counter term.

Dipole subtraction

As explained above, a good cross check of the consistency of the calculation and in particular of the Born and the virtual is to construct the dipoles by hand, add them to the virtual amplitude and confirm that the cancellation of $1/\varepsilon$ poles occurs. In other words, the sum $d\hat{\sigma}^{\mathcal{V}^{\mathrm{ren.}}} + d\hat{\sigma}^{\mathcal{B}} \otimes \mathbf{I}$ must be finite.

The case of the electroweak top-pair production is simplified by the fact that there is no colour correlation between the initial and final state[12]. Therefore, the integrated dipole $\mathbf{I}$ take the following form [218]

$$\mathbf{I} = \mathbf{I}_{\mathrm{init.}} + \mathbf{I}_{\mathrm{final}}\,, \tag{3.43}$$

with only an initial and final part. $\mathbf{I}_{\mathrm{init.}}$ and $\mathbf{I}_{\mathrm{final}}$ can be both obtained from the general formula

$$\begin{aligned}\mathbf{I}(\varepsilon,\mu^2,p_i,m_i) \;=\; -\frac{\alpha_S}{2\pi}\frac{(4\pi)^\varepsilon}{\Gamma(1-\varepsilon)}\frac{1}{\mathbf{T}_i^2}\mathbf{T}_i\cdot\mathbf{T}_j \times \left[\mathbf{T}_i^2\left(\frac{\mu^2}{s_{ij}}\right)^\varepsilon V_j(m_i,m_j,\varepsilon)+\Gamma_j(m_j,\varepsilon)\right] \\ +i\leftrightarrow j + \text{finite terms}\,,\end{aligned} \tag{3.44}$$

in which we wrote only the divergent pieces since we are interested in the singular structure of $d\hat{\sigma}^{\mathcal{V}^{\mathrm{ren.}}}$. $\mathbf{T}_j$ is the colour matrix associated to the parton j. Introducing the structure constants and matrix representation of the fundamental representation of $\mathrm{SU}(3)_c$, f_{abc}, t^l_{ab}

[12] For now, we do not define what colour correlation means, we will come back to this when we calculate the Born colour correlated amplitudes.

we have for gluons $\mathbf{T}^l_{cb} = if_{clb}$ while for quarks and anti-quarks we have $\mathbf{T}^l_{ab} = t^l_{ab}$ and $\mathbf{T}^l_{ab} = -t^l_{ab}$ respectively. These definitions are such that the colour factors reduces in our case to $T_i^2 = C_F$ and $T_i \cdot T_j = -C_F$, where $C_F = 4/3$ is the value of the Casimir operator acting on the fundamental representation. Also, $s_{ij} = 2p_i \cdot p_j$.

The expression for V_j and Γ_j for the massless initial partons and top-quarks are given by

$$V_j(0,0,\varepsilon) = \frac{1}{\varepsilon^2}\,, \qquad V_j(m_t,m_t,\varepsilon) = \frac{1}{\varepsilon}\frac{1}{v_{ji}}\ln\rho\,,$$
$$\Gamma_j(0,\varepsilon) = \frac{\gamma_q}{\varepsilon}\,, \qquad \Gamma_j(m_j,\varepsilon) = \frac{C_F}{\varepsilon}\,, \tag{3.45}$$

in which $v_{ji} = \sqrt{1-\frac{p_j^2 p_i^2}{(p_i\cdot p_j)^2}}$, $\rho = \sqrt{\frac{1-v_{ji}}{1+v_{ji}}}$ and $\gamma_{j=q} = 3/2C_F$. Collecting, Eqs. (3.44, 3.45) and the various definitions we obtain the final expression for $\mathbf{I}_{\text{init.}}$ and $\mathbf{I}_{\text{final}}$

$$\begin{aligned}
\mathbf{I}_{\text{init.}} &= \frac{2\alpha_S}{2\pi}\frac{(4\pi)^\varepsilon}{\Gamma(1-\varepsilon)}\left(\left(\frac{\mu^2}{\hat{s}}\right)^\varepsilon\frac{C_F}{\varepsilon^2}+\frac{\gamma_q}{\varepsilon}\right) + \text{finite terms} \\
\mathbf{I}_{\text{final}} &= \frac{2\alpha_S}{2\pi}\frac{(4\pi)^\varepsilon}{\Gamma(1-\varepsilon)}\left(\frac{C_F}{\varepsilon}\left(\frac{\mu^2}{\hat{s}-2m_t^2}\right)^\varepsilon\frac{1+x^2}{1-x^2}\ln x+\frac{C_F}{\varepsilon}\right) + \text{finite terms}\,,
\end{aligned} \tag{3.46}$$

where we introduced a convenient variable x defined by $\hat{s} = -m_t^2\frac{(1-x)^2}{x}$. Note that we see again that the double poles come only from the initial state partons.

3.2.3 Real emissions

The last set of corrections to the process of our interest involves the emission of one extra parton. We divide these corrections in two groups depending on the nature of the incoming partons: $q\bar{q}$ and $gq(\bar{q})$. Indeed, while at LO the top-pair production is necessarily initiated by a quark/anti-quark pair, there is a new channel opening up at order $\mathcal{O}(\alpha_S\alpha_{EW}^2)$ and the real emission can be also be initiated by a gluon/quark. In Fig. 3.4 and Fig. 3.5 we show the Feynman diagrams of the $2 \to 3$ processes that contribute to the real emission. Contrary to the virtual corrections that have to be interfered with LO diagrams the real emission diagrams are interfered with themselves to yield the appropriate $\mathcal{O}(\alpha_S\alpha_{EW}^2)$ order.

In the $q\bar{q}$ channel, diagrams (a) and (b) have only singularities associated to the emitted gluon in the final states when it becomes soft. On the other hand, diagrams (c) and (d) exhibit a divergent behaviour both when the radiated gluon becomes soft, collinear or soft and collinear to the emitting parton. The gq and $g\bar{q}$ channels do not have any soft singularities but have some collinear ones (except for diagram (a)). Indeed, inspecting diagram (b) we see that the internal quark propagating can be collinear to the initial gluon while in diagrams (c) and (d) it is the internal gauge boson, in case it is a photon, that can be collinear to the initial parton, leading to other collinear singularities.

In summary, the soft and soft and collinear divergences cancel the ones in the virtual amplitude while the collinear singularities, also called mass singularities must be absorbed into the PDFs by means of the mass factorization. The fact that the collinear divergences appearing in diagrams (c) and (d) involve a photon has two consequences: (i) we have to

introduce a PDF for the photon inside the proton, (ii) the corresponding underlying Born process shown in Fig. 3.6, $\gamma g \to t\bar{t}$, must be added to the calculation. This cancellation can in principle be done analytically by regularizing in d-dimension the integral of the real amplitude over the additional radiated parton phase space making apparent the singularities as poles of $1/\varepsilon_{\text{soft}}$ (soft), $1/\varepsilon_{\text{coll.}}$ (collinear[13]) or $1/\varepsilon^2$ (for the regions where the soft and collinear divergences overlap). The squared pole and soft one are equal and opposite in sign to the ones in the virtual amplitude. Within the dipole formalism, this is much easier since the singularities are treated directly in the $n+1$-parton phase space. Finally, the collinear counter terms in Eq. (3.32) are taking care of the left-over collinear singularities (giving rise to $1/\varepsilon_{\text{coll.}}$) which have been absorbed into the PDFs.

Even though the photon induced top-pair production at LO is of order $\mathcal{O}(\alpha_S\alpha_{EW})$ and is therefore a contribution of $\sigma_{1;1}$, it must be included for a consistent treatment of the divergences. As we will see in Section (3.5) this channel is numerically important with respect to the corrections. The calculation of this process follows from simple application of the Feynman rules and we do not detail it here. We will discuss it in Section 3.4 when introducing the *spin-correlated Born* amplitude. The expression for the real corrections can be found in [91].

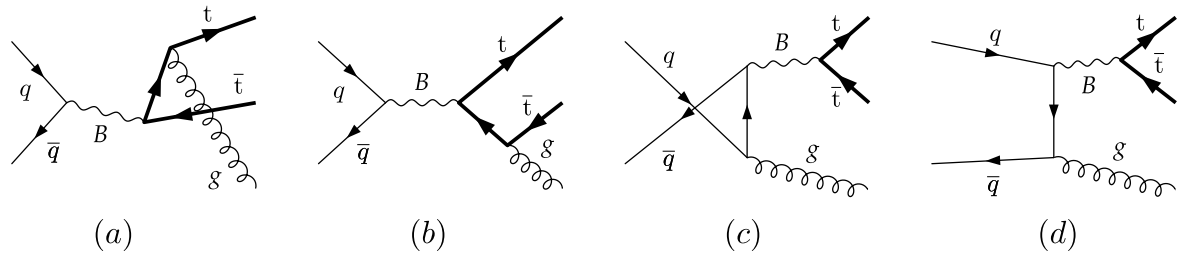

Figure 3.4: Real diagrams for the contributions of order $\mathcal{O}(\alpha_S\alpha_{EW}^2)$ with $q\bar{q}$ as initial state. Note that $B \in \{\gamma, Z, Z'\}$.

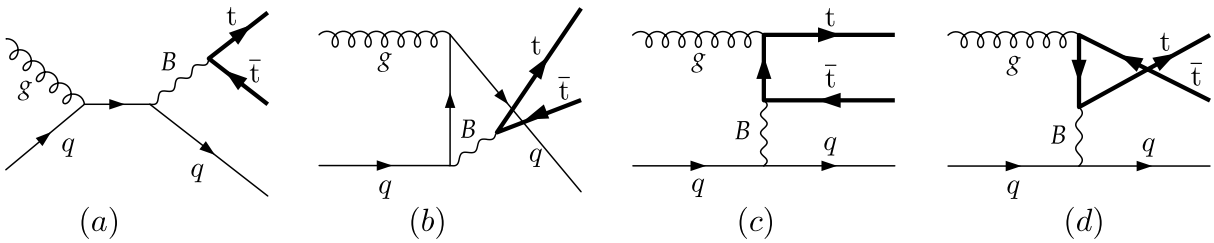

Figure 3.5: Real diagrams for the contributions of order $\mathcal{O}(\alpha_S\alpha_{EW}^2)$ with gq initial state. Similar diagrams contribute to the $g\bar{q}$ channel. Note that $B \in \{\gamma, Z, Z'\}$.

This concludes our presentation of the electroweak top-pair production calculation at order $\mathcal{O}(\alpha_s\alpha_{EW}^2)$. We have made great use of the techniques presented in the first section of this chapter to obtain the Born cross section, the renormalized virtual amplitude as well as the real corrections. We are one step away of being able to describe the implementation of the calculation in a general purpose Monte Carlo generator but we first present the second calculation at hand namely the single-top production in presence of a heavy W'-boson.

[13]Note that the coefficient in front of the poles of the collinear and soft regions are the same.

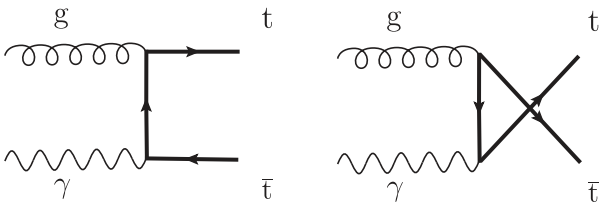

Figure 3.6: Photon induced top-pair production of order $\mathcal{O}(\alpha_S\alpha_{EW})$. Note that these diagrams must be added for a consistent subtraction of the singularities, see text.

3.3 Single-top: a status report

Analogously to what we did for the top-pair production, we now give some details on the second calculation we are interested in namely the single-top production.

As we have seen in Chapter 1, a common feature of the $\mathcal{G}_{221}$ models is the prediction of new neutral as well as charged gauge bosons, Z', W'. With the LHC soon running at 13 TeV, many top-quarks will be produced in the coming years and precision measurements of top-quark related processes will be possible. In this view, having precision calculations of as many observables as possible is essential to make full use of the future experimental measurements. In addition, with the combination of the previously presented calculation of the electroweak top-pair production we will be able to study correlations of these observables which has been shown to be a very good way of disentangling the underlying theory, hence extending the study in [74] to NLO.

In order to be as general as possible, the axial and vector part of the W' couplings to fermions are kept general and we calculate the processes

$$q\bar{q}' \to W, W' \to \mathrm{t\bar{b}}\,, \;\; \mathrm{b}q \to W, W' \to \mathrm{t}q' \tag{3.47}$$

in which q and q' are arbitrary up-type and down-type light quarks respectively. Even though the b-quark luminosity is largely suppressed the b quark initiated t-channel contribution is significant and we include it in addition to the resonant s-channel.

3.3.1 Leading-order cross section

The leading order cross section of the electroweak single-top production proceeds in the SM via the exchange of a W-boson and is of order $\mathcal{O}\left(\alpha_{EW}^2\right)$. As for the top-pair production the QCD corrections are therefore of order $\mathcal{O}(\alpha_S\alpha_{EW}^2)$, and we show the LO diagrams in Fig. 3.7. This process proceed either via s- or t-channel (diagram (a), (b) respectively) and since the b-quark is either in the initial or final state the two classes of diagrams do not interfere with each other. For renormalization purposes we calculate the Born in 4 and d-dimensions and show here the expression in the limit $d = 4$ including the sum and average over the spin of final and initial state particles as well as the relevant flux factor. The Born cross section can be decomposed as

$$\mathcal{B} = \sum_{q\in\{\mathrm{u,c}\}} \sum_{i\in\{s,t\}} \sum_{B,B'\in\{W,W'\}} \mathcal{B}_q^i(B, B'),\,, \tag{3.48}$$

with

$$\begin{aligned}\mathcal{B}_q^i(B,B) &= \frac{1}{256\hat{s}}\frac{\alpha_{EM}^2}{s_W^4} D_B^i D_B^i r_B^i \left(c_{1,B}^q \chi_1^i + c_{2,B}^q \chi_2^i\right) \\ \mathcal{B}_q^i(B,B') &= \frac{1}{256\hat{s}}\frac{\alpha_{EM}^2}{s_W^4} D_B^i D_{B'}^i \tilde{r}^i \left(d_1^q \chi_1^i + d_2^q \chi_2^i\right) \,,\end{aligned}$$

and where the various coefficients read

$$\begin{aligned}
r_B^s &= (\Gamma_B^4 + 16(m_B^2-\hat{s})^2 + 8\Gamma_B^2(m_B^2+\hat{s}))\,, & r_B^t &= (\Gamma_B^4 + 16(m_B^2-\hat{t})^2 + 8\Gamma_B^2(m_B^2+\hat{t}))\,,\\
\chi_1^s &= \hat{s}(\hat{s}+2\hat{t}-m_t^2)\,, & \chi_2^s &= (\hat{s}^2+2\hat{s}\hat{t}+2\hat{t}^2-m_t^2(\hat{s}+2\hat{t}))\,,\\
\chi_1^t &= -\hat{t}(2\hat{s}+\hat{t}-m_t^2)\,, & \chi_2^t &= (2\hat{s}^2+2\hat{s}\hat{t}+\hat{t}^2-m_t^2(2\hat{s}+\hat{t}))\,,\\
c_{1,B}^q &= 4a_B^q a_B^t b_B^q b_B^t & c_{2,B}^q &= ((a_B^q)^2+(b_B^q)^2)((a_B^t)^2+(b_B^t)^2)\,,\\
D_B^s &= \frac{1}{(\hat{s}-M_B^2)^2+m_B^2\Gamma_B^2}\,, & D_B^t &= \frac{1}{(\hat{t}-M_B^2)^2+m_B^2\Gamma_B^2}\,,
\end{aligned}$$

$$\begin{aligned}
\tilde{r}^s &= 16\Gamma_W\Gamma_{W'}m_W m_{W'} + \Gamma_W^2(\Gamma_{W'}^2 - 4m_{W'}^2 + 4\hat{s}) - 4(m_W^2-\hat{s})(\Gamma_{W'}^2 - 4m_{W'}^2+4\hat{s}))\,,\\
\tilde{r}^t &= 6\Gamma_W\Gamma_{W'}m_W m_{W'} + \Gamma_W^2(\Gamma_{W'}^2 - 4m_{W'}^2 + 4\hat{t}) - 4(m_W^2-\hat{t})(\Gamma_{W'}^2 - 4m_{W'}^2+4\hat{t}))\,,\\
d_1^q &= (b_{W'}^q a_W^q + a_{W'}^q b_W^q)(a_W^t b_{W'}^t + a_{W'}^t b_W^t)\,,\\
d_2^q &= (b_{W'}^q b_W^q + a_{W'}^q a_W^q)(a_{W'}^t a_W^t + b_{W'}^t b_W^t)\,.
\end{aligned} \tag{3.49}$$

In the above expressions we have introduced the axial, a_B^q, a_B^t, and vector, b_B^q, b_B^t, couplings of a gauge boson B, (W or W') to a light-quark doublet ($\begin{pmatrix}\mathrm{u}\\ \mathrm{d}\end{pmatrix}$ or $\begin{pmatrix}\mathrm{c}\\ \mathrm{s}\end{pmatrix}$) and top/bottom-quark doublet respectively. Note that for the SM the CKM matrix is included in the definition of the couplings such that e.g. $a_W^u = b_W^u = (V_{\mathrm{CKM}})_{ud}$, $a_W^t = b_W^t = (V_{\mathrm{CKM}})_{tb}$. Finally, s_W is the sine of the Weinberg angle.

3.3.2 Virtual corrections

Single-top production is mediated by uncolored gauge bosons which leads to a small set of virtual corrections: (i) For the s-channel, only initial and final state vertex corrections lead to non vanishing contributions, while box diagrams as the one shown in Fig. 3.8 are irrelevant, (ii) in the t-channel, however, it is the corrections between two initial particles that need not be calculated instead.

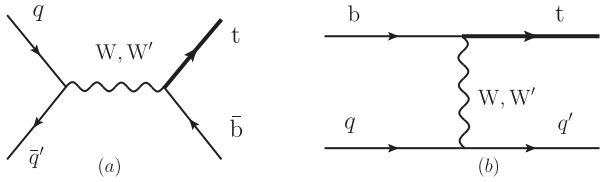

Figure 3.7: Leading-order diagrams contributing to the Born cross section of the single-top production at order $\mathcal{O}(\alpha_S\alpha_{EW})$.

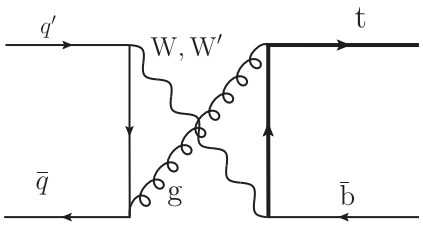

Figure 3.8: Example of s-channel virtual correction, box diagram, that do not contribute to the virtual amplitude.

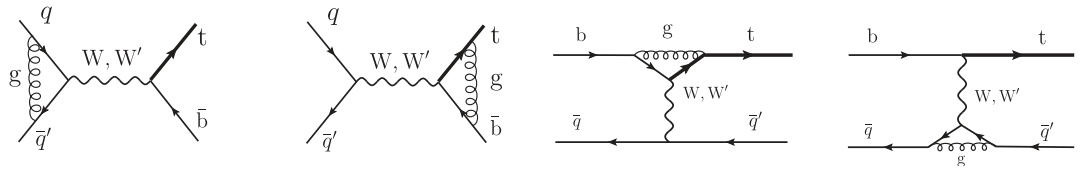

Figure 3.9: Diagrams contributing to the order $\mathcal{O}(\alpha_S \alpha_{EW}^2)$ virtual corrections to the s- and t-channel.

Reduction and master integrals

The corrections presented above lead to 30 different scalar integrals divided into two auxiliary topologies for the s-channel and identically for the t-channel. In both cases, these integrals can be reduced to three master integrals using the REDUZE 2 program as explained in Section 3.1. Among these master integrals the massive one-point function, referred to as massive tadpole, and the massless bubble, have already been encountered in the top-pair production calculation. In addition to these two, there is one additional master that is required for the single-top which is the **half-massive two-point function**. The expression for this master is also known and can be found in [231].

Renormalization

The renormalization of the single-top production is very similar to the top-pair production. Indeed, there are no corrections to either α_S or m_t for the very same reasons, see Section 3.2.2, and we renormalize the top-quark wave function on-shell while the massless quarks (including the b-quark) are renormalized in the $\overline{\text{MS}}$ scheme in which the renormalization constant is one. Therefore the overall renormalization constant reads

$$\sum_{n \in \text{out.part.}} \frac{1}{2} \delta Z_{\text{WF},n} \mathcal{M}_{0;2} = \frac{1}{2} Z_{\text{WF,t}} \mathcal{M}_{0;2} \,, \tag{3.50}$$

in which $\mathcal{M}_{0;2}$ is the Born amplitude.

Dipole subtraction

After renormalization, the virtual amplitude still suffers from IR divergences and we check using the dipole subtraction of Catani-Seymour that the infrared structure of our virtual amplitude is consistent with the Born i.e. that

$$d\hat{\sigma}^{\mathcal{B}} \otimes \mathbf{I} + d\hat{\sigma}^{\mathcal{V}^{\text{ren.}}} \,, \tag{3.51}$$

is finite. For this process the integrated dipoles can be decomposed in two parts

$$\mathbf{I} = \mathbf{I}_{\text{init.}} + \mathbf{I}_{\text{final}}\,, \tag{3.52}$$

in which the initial state integrated dipole is identical as in the case of top-pair production while the final state one must be modified to take into account the fact that only one of the final state particle is massive.

$$\begin{aligned}
\mathbf{I}_{\text{init.}} &= \frac{2\alpha_S}{2\pi}\frac{(4\pi)^\varepsilon}{\Gamma(1-\varepsilon)}\left(\left(\frac{\mu^2}{\hat{s}}\right)^\varepsilon\frac{C_F}{\varepsilon^2}+\frac{\gamma_q}{\varepsilon}\right)+\text{finite terms}\\
\mathbf{I}_{\text{final}} &= \frac{\alpha_S}{2\pi}\frac{(4\pi)^\varepsilon}{\Gamma(1-\varepsilon)}\left(2C_F\left(\frac{\mu^2}{\hat{s}-m_t^2}\right)^\varepsilon\left(\frac{1}{2\varepsilon^2}+\frac{1}{2\varepsilon}\ln\frac{m_t^2}{\hat{s}-mt^2}\right)\right.\\
&\quad\left.+\frac{C_F}{\varepsilon}+\frac{\gamma_q}{\varepsilon}\right)+\text{finite terms}\,.
\end{aligned} \tag{3.53}$$

3.3.3 Final remarks

As a conclusion, we have calculated the virtual corrections at order $\mathcal{O}(\alpha_S\alpha_{EW}^2)$ to single-top production. The real contributions have not been considered yet and once this is finalized, the `POWHEG BOX` implementation as described in the next section will be feasible for the single-top as well. For the top-pair production, all the various pieces have been calculated and we now present the implementation in `POWHEG BOX`.

3.4 `POWHEG BOX` implementation

Shower Monte Carlo (SMC) programs play a central role in comparing data and theory predictions at colliders. Indeed, it is the only way to describe the complexity of hadron collisions and all the LHC phenomenology is based on their use. However, SMCs only provide leading-log accuracy for the shower via the collinear approximation of spontaneous emissions while the partonic hard process is described by LO matrix elements. Increasing the accuracy of the shower algorithms is very difficult and most of the effort over the last years has been directed towards improving the description of the hard process scattering by making use of the available partonic calculations at NLO. Since, shower algorithms already approximate NLO corrections the problem of including NLO matrix element in SMC is that of avoiding double-counting between the hard process description and the shower. The ultimate goal is that inclusive observables are described at NLO accuracy while the leading-logarithmic accuracy of the shower in the collinear regions is preserved.

In order to avoid overlapping descriptions, two methods have been put forward: (i) first, the MC@NLO method was suggested [191], (ii) and later, the POWHEG method was introduced in [194, 232].

The MC@NLO method solves the double-counting problem by subtracting from the exact NLO result its approximation as implemented in the SMC. Therefore, it depends on the exact implementation of the SMC and must be calculated analytically for each SMC. On the other hand, these subtraction terms are process-independent and can therefore be calculated once and for all. Since there is no reason for the subtraction term to be smaller than the NLO cross section, the MC@NLO method yields some events with negative

weights (at the end, physical distributions must turn out to be positive). To summarize, infrared-safe observables have NLO accuracy, the shower is summing collinear emissions at leading-log accuracy and the soft and collinear regions are left to the SMC (i.e. they are treated properly if the SMC has this capability). The MC@NLO method has been used for many processes [192, 233] including heavy quark pair and single-top production.

The main motivation for the Positive Weight Hardest Emission Generator (POWHEG), as suggested by its name, is to match NLO matrix element with existing SMC program in such a way that only positive weighted events are generated. In addition, this was shown to be achievable independently of the SMC program provided it implements p_T-ordered showers or allows for the implementation of a p_T veto. To solve the double-counting problem, POWHEG generates the first emission with a modified Sudakov form factor using the full NLO accuracy while the subsequent emissions are controlled by the usual p_T-ordered SMC algorithms[14]. If the SMC used with the POWHEG method is transverse momentum-ordered and double-log accurate, then the POWHEG method retains the double-log accuracy.

Matching NLO calculation with SMC following the POWHEG method has been partly automated via a computer framework called the `POWHEG BOX`. This framework is a collection of algorithms in Fortran 77 which deal with many aspects of the subtraction procedure:

(i) The `POWHEG BOX` finds all the singular regions.

(ii) It constructs the soft and collinear counter terms.

(iii) It builds the collinear remnants which are the left-over of the PDFs redefinition.

(iv) It generates the event with Born kinematics including virtual corrections.

(v) Finally, it adds the hardest emission according to the POWHEG Sudakov form factor.

Hence, the user input in the form of numerical routines is limited and comprises the list of all flavour structures of the Born and real processes, the Born phase space, the Born squared, color- and spin-correlated amplitudes, the finite part of the virtual amplitude and the real squared amplitudes. Once these have been specified the `POWHEG BOX` does the rest and the output of the `POWHEG BOX` can then be interfaced to any SMC to obtained various physical distributions. Several processes are already available in the `POWHEG BOX` including single-top and single-top W associated production, Higgs boson production in gluon fusion and many others [234–236].

A description of the POWHEG method is beyond the scope of this manuscript and we refer the reader to [91, 195, 232] for more details. In the following, we review the various pieces that must be provided by the user.

3.4.1 Colour-correlated Born amplitudes

To calculate the subtraction terms in the dipole formalism, the `POWHEG BOX` needs the information on the colour correlations between each pair of two external legs. The

[14] Or angle-ordered with p_T veto.

colour-correlated Born, $\mathcal{B}_{ij}$, contains this information and is formally defined by

$$\mathcal{B}_{ij} = -N \sum_{\substack{\text{spins}\\\text{colours}}} \mathcal{M}_{\{c_k\}} \left(\mathcal{M}^{\dagger}_{\{c_k\}}\right)_{\substack{c_i \to c'_i\\ c_j \to c'_j}} T^a_{c_i,c'_i} T^a_{c_j,c'_j}\,, \tag{3.54}$$

where $\mathcal{M}_{\{c_k\}}$ is the Born amplitude and $\{c_k\}$ the colour indices of all the external coloured particles. The suffix in $\mathcal{M}^{\dagger}_{\{c_k\}}$ indicates that the colour indices of partons i, j are substituted with primed indices. N is the appropriate normalization factor including the flux factor. For incoming quarks (as well as outgoing anti-quarks), $T^a_{\alpha,\beta} = t^a_{\alpha\beta}$, for incoming anti-quarks (as well as outgoing quarks) $T^a_{\alpha,\beta} = -t^a_{\beta\alpha}$ while $T^a_{\alpha,\beta} = if_{cab}$ for gluons.

From colour conservation we have the relation

$$\sum_{i,i\neq j} \mathcal{B}_{ij} = C_{f_j}\mathcal{B}\,, \tag{3.55}$$

where C_{f_j} is the quadratic Casimir of the colour representation of particle j. $\mathcal{B}_{ij}$ is a symmetric matrix and only off diagonal terms need to be calculated.

For the $q\bar{q}$ initiated electroweak top-pair production, this trivially leads to

$$\frac{1}{2s_b}\mathcal{B}_{ij} = C_F\mathcal{B}\,, \tag{3.56}$$

for two incoming or outgoing particles and zero otherwise, $C_F = 4/3$.

As we have seen in Section 3.2.3, we also have to include the photon-gluon induced pair production process in order to treat the QED divergence occurring in the qg real channel for which we also need to calculate the colour-correlated Born. The colour structure of this diagram, see Fig. 3.6, factorizes in the amplitude and we can therefore calculate directly the colour-correlated Born in terms of the Born. The colour factor of this process reads

$$\mathcal{C} = t^a_{\alpha\beta}t^b_{\beta\alpha}\delta^{ab} = \frac{N_c^2-1}{2} = 4\,. \tag{3.57}$$

Applying Eq. (3.54) to each pair of external legs of this process we obtain the following values for the various coefficients

$$\begin{aligned}
\mathcal{B}_{13} &= -\frac{1}{\mathcal{C}}t^a_{\alpha\beta}t^{a'}_{\beta\alpha'}T^e_{a,a'}T^e_{\alpha\alpha'}\mathcal{B} = -t^a_{\alpha\beta}t^{a'}_{\beta\alpha'}if_{aea'}(-t^e_{\alpha'\alpha})\frac{\mathcal{B}}{\mathcal{C}}\\
&= -if_{a'ea}\mathrm{Tr}(t^{a'}t^e t^a)\frac{\mathcal{B}}{\mathcal{C}} = \frac{1}{2}N_c\mathrm{Tr}(t^a t^a)\frac{\mathcal{B}}{\mathcal{C}}\\
&= \frac{1}{2}N_c\mathcal{B}
\end{aligned} \tag{3.58}$$

$$\begin{aligned}
\mathcal{B}_{14} &= \mathcal{B}_{13} = \frac{1}{2}N_c\mathcal{B}\\
\mathcal{B}_{34} &= -\frac{1}{\mathcal{C}}\mathcal{B}t^a_{\alpha\beta}t^b_{\beta'\alpha'}T^e_{\beta\beta'}T^e_{\alpha\alpha'}\delta^{ab} = \mathrm{Tr}(t^a t^e t^a t^e)\frac{1}{\mathcal{C}}\mathcal{B} = \frac{-1}{2N_c}\mathcal{B}\,.
\end{aligned} \tag{3.59}$$

Of course, the relation Eq. (3.55), holds as can be explicitly verified.

$$\begin{aligned}\mathcal{B}_{1,3}+\mathcal{B}_{1,4} &= \left(\frac{1}{2}N_c+\frac{1}{2}N_c\right)\mathcal{B}=C_A\mathcal{B}\\ \mathcal{B}_{3,4}+\mathcal{B}_{3,1} &= \left(\frac{-1}{2N_c}+\frac{1}{2}N_c\right)\mathcal{B}=\frac{N_c^2-1}{2N_c}\mathcal{B}=C_F\mathcal{B}\,.\end{aligned} \tag{3.60}$$

Note that this cross check is implemented in `POWHEG BOX`.

3.4.2 Spin-correlated Born amplitude

In the `POWHEG BOX`, the spin-correlated Born squared, $B_j^{\mu\nu}$ is defined to be non zero if leg j is a gluon. It is obtained by leaving un-contracted the indices of the j^{th} leg following the definition

$$B_j^{\mu\nu}=\sum_{\{i\},s_j,s_j'}\mathcal{M}(\{i\},s_j)\mathcal{M}^\dagger(\{i\},s_j')(\varepsilon_{s_j}^\mu)^*\varepsilon_{s_j'}^\nu\,, \tag{3.61}$$

in which $\mathcal{M}(\{i\},s_j)$ is the Born amplitude, $\{i\}$ represents collectively all the remaining spins and colours of the incoming and outgoing particles and s_j is the spin of the j^{th} particle. In addition, the $\varepsilon_{s_j}^\mu$ are polarization vectors normalized as

$$\sum_{\mu,\nu}g_{\mu\nu}(\varepsilon_{s_j}^\mu)^*\varepsilon_{s_j'}^\nu=-\delta_{s_js_j'}\,. \tag{3.62}$$

As for the colour-correlated Born we have a closure relation, namely

$$\sum_{\mu,\nu}g_{\mu\nu}\mathcal{B}_j^{\mu\nu}=-\mathcal{B}\,. \tag{3.63}$$

Since processes without external gluons lead to vanishing contributions, we only have to consider the photon-gluon induced top-pair production. At this point one has to be careful and also calculate the contribution from the external photon. Indeed, the QED divergence present in the qg channel cannot be detected by the `POWHEG BOX` in its present implementation and we will have to modify the code so that it actually treats the QED singularity along with the other divergences. However, this will only be possible if the corresponding dipoles can be constructed by `POWHEG BOX`, and we consequently have to provide the adequate spin-correlated Born amplitude.

To illustrate the form of the result we show the expression for $\mathcal{B}_2^{\mu\nu}$ where the subscript 2 designates the photon leg consistently with the diagram shown in Fig. 3.6. Applying the above procedure leads to the following expression

$$\mathcal{B}_2^{\mu\nu} = \frac{16\pi^2\alpha_{EW}\alpha_S Q_t^2}{\hat{s}m_t^2z_1^2y_1^2}\left(\begin{pmatrix}p_1^\mu & p_2^\mu & p_3^\mu\end{pmatrix}\mathcal{A}_1\begin{pmatrix}p_1^\nu\\ p_2^\nu\\ p_3^\nu\end{pmatrix}-\mathcal{A}_2g^{\mu\nu}\right)\,, \tag{3.64}$$

in which Q_t is the top-quark electric charge, $\mathcal{A}_{1,2}$ are a three-by-three matrix and a scalar, composed of combinations of the kinematics variables, and where y_1 and z_1 have the following definition

$$y_1=\left(1-\frac{\hat{t}}{m_t^2}\right)\quad z_1=\left(1-\frac{\hat{u}}{m_t^2}\right)\,. \tag{3.65}$$

Finally, $\mathcal{A}_1$ and $\mathcal{A}_2$ read

$$\begin{aligned}
\mathcal{A}_1 &= \begin{pmatrix} 8z_1^2 & 2\mathcal{P}_2 z_1 & -8\mathcal{P}_1 z_1 \\ 2\mathcal{P}_2 z_1 & 4(\mathcal{P}_1 - z_1)^2 z_1 & 6\mathcal{P}_1 z_1^2 - 4z_1^3 - 2\mathcal{P}_1^2(2+z_1) \\ -8\mathcal{P}_1 z_1 & 6\mathcal{P}_1 z_1^2 - 4z_1^3 - 2\mathcal{P}_1^2(2+z_1) & 8\mathcal{P}_1^2 \end{pmatrix}, \\
\mathcal{A}_2 &= m_t^2 \mathcal{P}_3 (\mathcal{P}_1 - z_1) z_1 \,, \\
\mathcal{P}_1 &= y_1 + z_1 \,, \; \mathcal{P}_2 = 2(y_1 + z_1) + y_1^2 \,, \; \mathcal{P}_3 = y_1^2 + z_1^2 \,.
\end{aligned} \tag{3.66}$$

As for the color-correlated Born, the closure relation Eq. (3.63) is implemented in `POWHEG BOX` allowing the user to check the consistency of his implementation.

3.4.3 Implementation of the virtual corrections in `POWHEG BOX`

The calculations of the virtual corrections presented in Section 3.2.2 for the top-pair production and in Section 3.3.2 for the single-top lead to amplitudes squared which are slightly different from the one required for the `POWHEG BOX` implementation and we now give some details regarding the form in which the virtual corrections must be provided.

The user must provide a numerical routine `setvirtual` in `virtual.f` which, given a set of external momenta, and a flavour configuration, returns the corresponding finite part of the virtual amplitude, $\mathcal{V}_{\text{fin.}}$. The contribution $\mathcal{V}_{\text{fin.}}$, calculated in dimensional regularization must be in the form

$$\mathcal{V} = \mathcal{N} \frac{\alpha_S}{2\pi} \left[\frac{1}{\varepsilon^2} a\mathcal{B} + \frac{1}{\varepsilon} \sum_{i,j} c_{ij} \mathcal{B}_{ij} + \mathcal{V}_{\text{fin.}} \right] . \tag{3.67}$$

In the above equation a and c_{ij} are coefficients that do not depend upon ε while the Born and colour-correlated Born $\mathcal{B}$ and $\mathcal{B}_{ij}$ contain powers of ε. The normalization factor $\mathcal{N}$ is defined by

$$\mathcal{N} = \frac{(4\pi)^\varepsilon}{\Gamma(1-\varepsilon)} \left(\frac{\mu_R^2}{Q^2} \right)^\varepsilon , \tag{3.68}$$

where Q is the Ellis-Sexton scale [237]. The expressions for a and c_{ij} can be found in [238] and are closely related to the dipoles presented in Section 3.2.2. This step is in principle straightforward but one must take special care to take the various normalizations into account. For this reason, we show the details of the terms that must be subtracted in our case to bring the virtual corrections into the form of Eq. (3.67).

We begin by writing our virtual amplitude (interfered with the Born) resulting from the evaluation of the Feynman diagrams and expanded in powers of $1/\varepsilon$ in the following form

$$\mathcal{V}^{\text{our}} = \mathcal{N} \frac{\alpha_{EW} \alpha_S}{2\pi} \left[\mathcal{V}_0 + \frac{\mathcal{V}_{-1}}{\varepsilon} + \frac{\mathcal{V}_{-2}}{\varepsilon^2} \right] . \tag{3.69}$$

In the same way we expand the Born[15], $\mathcal{B}$ and colour-correlated Born, $\mathcal{B}_{ij}$ in powers

[15] The Born is calculated in d-dimension as explained in Section 3.1 and therefore does depend on $d = 2\varepsilon + 4$.

of ε

$$\begin{aligned}\mathcal{B} &= \alpha_{EW}\left[\mathcal{B}_0+\varepsilon\mathcal{B}_1+\varepsilon^2\mathcal{B}_2\right],\\ \mathcal{B}_{ij} &= \alpha_{EW}\left[\mathcal{B}^0_{ij}+\varepsilon\mathcal{B}^1_{ij}+\varepsilon^2\mathcal{B}^2_{ij}\right].\end{aligned} \tag{3.70}$$

For convenience we remind the expressions for the dipoles presented in Eq. (3.46)

$$\begin{aligned}\mathbf{I}_{\text{init.}} &= \tilde{\mathcal{N}}\frac{\alpha_S}{2\pi}2\left(\frac{\hat{s}}{m_t^2}\right)^{-\varepsilon}\left[\frac{C_F}{\varepsilon^2}+\frac{\gamma_q}{\varepsilon}\right],\\ \mathbf{I}_{\text{final}} &= \tilde{\mathcal{N}}\frac{\alpha_S}{2\pi}\frac{C_F}{\varepsilon}2\left[1+\left(\frac{\hat{s}-2m_t^2}{m_t^2}\right)^{-\varepsilon}\frac{1+x^2}{1-x^2}\ln x\right],\\ \mathbf{I} &= \mathbf{I}_{\text{init.}}+\mathbf{I}_{\text{final}},\end{aligned} \tag{3.71}$$

in which we have introduced $\tilde{\mathcal{N}}=\dfrac{(4\pi)^\varepsilon}{\Gamma(1-\varepsilon)}\left(\dfrac{\mu_R^2}{m_t^2}\right)^\varepsilon$ and where we omitted the finite terms since they are irrelevant for the following discussion.

Since the dipoles are constructed to reproduce the singular behaviour of the virtual we have the relation

$$\mathbf{I}\mathcal{B}+\mathcal{V}^{\text{our}}=\text{finite}, \tag{3.72}$$

from which we can identify the terms order by order in $1/\varepsilon$. For the second order poles, it comes immediately

$$\mathcal{V}_{-2}=-2C_F\mathcal{B}_0\equiv C_{-2}\mathcal{B}_0.$$

For the first order pole one has to be careful and take into account the expansion of the factors

$$\begin{aligned}\tilde{\mathcal{N}} &= \mathcal{N}\left(\frac{Q^2}{m_t^2}\right)^\varepsilon=\mathcal{N}\left(1+\varepsilon\log\frac{Q^2}{m_t^2}+\frac{1}{2}\varepsilon^2\log^2\frac{Q^2}{m_t^2}\right)+\mathcal{O}(\varepsilon^3),\\ \left(\frac{\hat{s}}{m_t^2}\right)^{-\varepsilon} &= 1-\varepsilon\log\frac{\hat{s}}{m_t^2}+\frac{1}{2}\varepsilon^2\log^2\frac{\hat{s}}{m_t^2}+\mathcal{O}(\varepsilon^3),\end{aligned} \tag{3.73}$$

as well as the expansion of the Born. Taking this into account we obtain the relation

$$\mathcal{V}_{-1}=-C_F\left(2\left[\frac{1+x^2}{1-x^2}\ln x\right]+5-2\log\frac{\hat{s}}{m_t^2}+2\log\frac{Q^2}{m_t^2}\right)\mathcal{B}_0-2C_F\mathcal{B}_1\equiv C_{-2}\mathcal{B}_1+C_{-1}\mathcal{B}_0. \tag{3.74}$$

We can now focus on determining the pieces that need to be subtracted from our result to obtain $\mathcal{V}_{\text{fin}}$. Comparing Eqs. (3.67, 3.69) and identifying equal powers of $1/\varepsilon$ we obtain

$$\alpha_{EW}\mathcal{V}_{-2}=a\mathcal{B}_0\Rightarrow a=\alpha_{EW}C_{-2}, \tag{3.75}$$

which means that the two definitions of the second order poles are identical. Now, it is clear from Eq. (3.67) that the expected first order pole in POWHEG BOX notation is $\sum_{i,j}c_{ij}\mathcal{B}_0$ which is linked to our result through the relation

$$\begin{aligned}\alpha_{EW}\mathcal{V}_{-1}=a\mathcal{B}_1+\sum_{i,j}c_{ij}B^0_{ij}\Rightarrow\sum_{i,j}c_{ij}B^0_{ij} &= \alpha_{EW}\mathcal{V}_{-1}-\alpha_{EW}C_{-2}\mathcal{B}_1,\\ &= \alpha_{EW}C_{-1}\mathcal{B}_0,\end{aligned} \tag{3.76}$$

which can be simplified further since from Eq. (3.56) we have $\mathcal{B}_{ij} \sim \mathcal{B}$ and by redefining c_{ij} we can write

$$\sum_{ij} c_{ij} = \alpha_{EW} C_{-1} \,. \tag{3.77}$$

Finally, following the same reasoning we obtain the finite part $\mathcal{V}_{\text{fin.}}$

$$\begin{aligned} \alpha_{EW}\mathcal{V}_{-2} = aB_2 + \sum_{ij} c_{ij}\mathcal{B}^1_{ij} + \mathcal{V}_{\text{fin.}} \Rightarrow \mathcal{V}_{\text{fin.}} \quad &= \quad \alpha_{EW}\mathcal{V}_{-2} - \alpha_{EW} C_{-2}\mathcal{B}_2 \\ &\quad -\alpha_{EW} C_{-1}\mathcal{B}_1 \,, \end{aligned} \tag{3.78}$$

with C_{-1}, C_{-2} given by Eq. (3.74) and take into account the difference in normalization.

3.4.4 Regularization of the QED divergence

We now turn to the discussion of the treatment of the QED divergence in POWHEG BOX, and how we perform it despite the fact that it is not a feature of the framework.

The POWHEG BOX has been written to deal with the QCD corrections to general processes. Therefore, if the photon exchanged leading to the collinear singularity in the third and fourth diagrams of Fig. 3.5 was a gluon[16] then POWHEG BOX would be able to handle the corresponding QCD singularity.

On the other hand, since POWHEG BOX v2, spontaneous emissions of real photons can be included in POWHEG BOX, that is to say the collinear remnants corresponding to photon emissions are implemented in the framework as demonstrated in [239,240][17]. Consequently, it is clear that the missing piece in POWHEG BOX is that of distinguishing the internal photon from the gluon which is simply in contradiction with the very idea of the framework because the relevant algorithms rely only on the external particles.

One question arises at this point: how is it that POWHEG BOX does not wrongly classify the third and fourth diagrams as QCD divergent ? Looking at the details of the implementation, it is clear that the reason for that lies in the way the singular regions are identified: (i) each possibly singular region is identified, (ii) for each region found, POWHEG BOX constructs the underlying Born process, (iii) finally, if this Born process is valid, i.e. it is among the list of Born flavour structures input by th user, the region is kept, otherwise, it is discarded. Hence, it appears that the reason for POWHEG BOX not to include a fake QCD divergence is that we excluded the gluon induced top-pair production from our calculation[18].

Our strategy to have the QED divergences treated in the POWHEG BOX is the following:

(i) Implement our process in POWHEG BOX v2, to benefit from the machinery to treat spontaneous emissions of photons, including the implementation of collinear remnants.

[16] This case is excluded of our calculation since this contribution would lead to order $\mathcal{O}(\alpha_S^2)$

[17] These terms are implemented in `sigcollremn.f`.

[18] Adding this process to the list of Born flavour structures, it can be checked explicitly that there is a new singular region identified by POWHEG BOX.

(ii) Since the corresponding process to diagrams (c) and (d) in Fig. 3.5, in which a gluon instead of a photon is internally exchanged, is excluded from our calculation, we can safely replace in the algorithm constructing the corresponding underlying Born a gluon by a photon.

This procedure has been successfully applied to the electroweak top-pair production as will be shown in the validation section, see Section 2.4.11. Point (ii) in the above list, makes sure that diagrams (c) and (d) are linked to the photon induced top-pair production Born diagram, Fig. 3.6 and subsequently treated properly by the `POWHEG BOX` v2. Finally, one has to be careful and switch on the QED flag for real photon emissions to true, `flg_with_em` as well as `pdf_nparton = 22`[19] to indicate `POWHEG BOX` that photon PDFs will be used.

3.4.5 Final remarks

After downloading the latest `POWHEG BOX v2` from the svn repository at `svn://powhegbox.mib.infn.it/trunk/POWHEG-BOX`, the above implementation has been added to the list of the `POWHEG BOX` processes under the name `PBZp`. However, since we modified the main code of the `POWHEG BOX` in order to treat the QED divergences, we cannot directly make public our implementation in the present status without the authorization of the authors and, at the time of writing, the code is therefore not publicly available.

To allow for maximum flexibility, we have implemented the various channels and their interferences separately, such that the user can investigate to his convenience the production via any of the gauge bosons, γ, Z, Z' or any pair of two as well as the complete process. This is easily done, by setting the variable `channel` to `1 (photon), 2 (Z), 3 (Z'), 4 (photon/Z), 5 (photon/Z'), 6 (Z/Z')` or `7 (photon/Z/Z')` corresponding to the desired process in the input parameter file `powheg.input`. Also in the same file, the user has the freedom to set the vector and axial couplings of the Z'-boson to up and down type quarks, `azpu,bzpu,azpd,bzpd`.

The implementation also provides various choices of scheme for the renormalization and factorization scales through the value of the `scale` switch: (i) 0, the scales are running according to $\mu_R = \mu_F = \sqrt{p_T^2 + m_t^2}$, (ii) 1, the running scales satisfy $\mu_R = \mu_F = \sqrt{\hat{s}}$, (iii) 2, the scales are fixed to the user chosen value of `muR` and `muF`.

Finally, a series a switches control the number of generated events, `numevts`, the level of approximation `Born`, as well as general properties of `POWHEG BOX` common to all the implementations and described in the user manual [241].

Note also that the photon induced top-pair production is taken into consideration only when necessary, i.e. if the real diagrams leading to the QED divergence are included in the run. In the next section we present our first results of the top-pair production obtained with the implementation described above.

[19] These two switches are in `init_couplings.f`.

3.5 Numerical results

This section is devoted to our numerical results. We review the validation of the implementation before discussing some typical distributions of the top-pair production in presence of a new heavy neutral resonance.

3.5.1 Validation

Validating NLO computations is an involved task that requires a very good knowledge of the inner working of various tools. In addition, it is also the most time consuming and important step of the calculation.

In our case, there are two sets of tests that can be carried out:

(i) internal consistency checks related to the `POWHEG BOX` implementation and the validity of the IR regularization of real amplitudes,

(ii) comparisons with existing SM calculations of top-pair production, i.e. neglecting the Z'-channel.

Note that one could also think about comparing our results with the ones of Melnikov et al. [196] that appeared before the completion of this work. However, even though they consider the top-pair production by a heavy Z'-boson, and their subsequent decay, the set of NLO corrections they consider is slightly different from ours and it is not straightforward to compare our predictions[20]. In addition, they provide a fixed order calculation while we match ours with a shower Monte Carlo program. We now briefly review points (i) and (ii).

Soft and collinear limits

The `POWHEG BOX` framework provides some very useful information on the internal consistency of the implementation. Indeed, the routine `checklims` allows the user to validate the limiting behaviour of the real squared amplitudes against their soft and collinear approximations. Hence, for each singular region identified by `POWHEG BOX` algorithms the real squared amplitude and its soft and collinear approximations built from the colour- and spin-correlated Born amplitudes are compared and their ratio in the soft and collinear regions must be one. This allows one to make sure that: (i) all the expected singularities have been identified, (ii) for each one of them the colour- and spin-correlated Born amplitudes are consistent with the squared real amplitude. Note that the double soft and collinear regions are also tested. The results of these checks are output in the file `pwhg_checklimits` and exhibit the expected behaviour for our implementation.

In addition, as mentioned in Section 3.4.1 and 3.4.2, the consistency of the colour- and spin-correlated Born amplitudes is internally validated in `POWHEG BOX` via the implementations of Eqs. (3.55, 3.63).

During the integration of the real contributions, `POWHEG BOX` produces a set of histograms representing the Monte Carlo sampling of all the kinematical variables, three for the Born integration and three for the real amplitude squared. The three variables

[20] For instance they do not include diagrams including photon exchange but consider some corrections of order $\mathcal{O}(\alpha_S^2 \alpha_{EM})$.

spanning the integration of the real amplitude are denoted ξ, y and θ, which we do not need to define further to demonstrate our point. Soft, as well as collinear limits, are located at $\xi \to 0$, and $y \to 1$ with ξ fixed (or $y \to 1$, $\xi \to 0$ for collinear-soft singularities) respectively. Hence the QED divergence appears in these histograms as an over-sampled region (vertical lines) around $y = 1$. In Fig. 3.10 we show two examples of such histograms for the y variable, in the case where we do not regularize the QED divergence (left) and in the case where we do (right). This confirms that the treatment presented in Section 3.4.4 is effective in regularizing the QED collinear singularities.

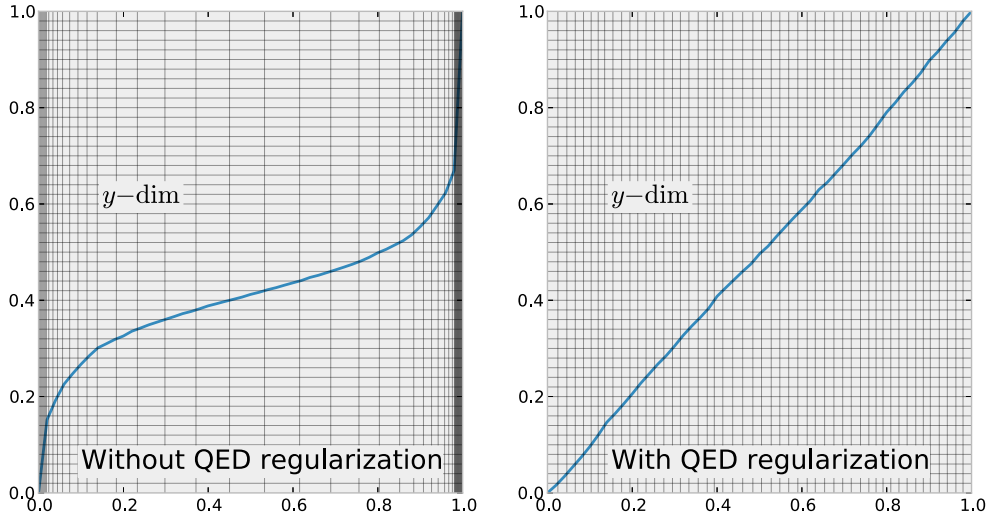

Figure 3.10: Monte Carlo sampling of the real integration variable y, without the regularization of the QED divergence (left) and after regularization (right).

Matrix elements and total cross sections

In order to validate our implementation we have compared numerically at the matrix element level[21] all the expressions for the Born, real and virtual amplitudes in the SM against MadGraph5_aMC@NLO [242] as well as against GoSam [243] which provides a numerical expansion of the virtual corrections in $1/\varepsilon$. We have found a perfect agreement below the per mille level, for all the channels (including interferences) and all the amplitudes across a detailed sampling of the entire kinematical parameter space[22]. We have also verified the dependence of the matrix elements on the renormalization scale.

Once the matrix elements have been validated, they can be safely convoluted with PDFs to yield total cross sections. In Fig. 3.11, we show the comparison of the LO total cross sections in the SM for the Z- and $\gamma - g$-channels as predicted by MadGraph5_aMC@NLO and `PBZp`. These results have been obtained using the MRST2004qed PDF set [244],

[21] This is a highly non-trivial task since it involves extracting the matrix elements from the intricate structure of the various tools and compile them in a consistent way in an independent library that can then be called externally. This then allows us to avoid any dependence on the physical parameters.

[22] We generated order of 10^4 evenly distributed phase space points for which we did the comparison.

$\alpha_{EW} = 1/137$, $m_t = 175$ GeV, $\sin\theta_W = 0.23112$ and for various values of the hadronic center of mass energy, $\sqrt{s}_{\text{had.}}$. The numerical errors are similar for all the channels. Note that the agreement across all the channels is of order 1% including the γ-channel (not shown).

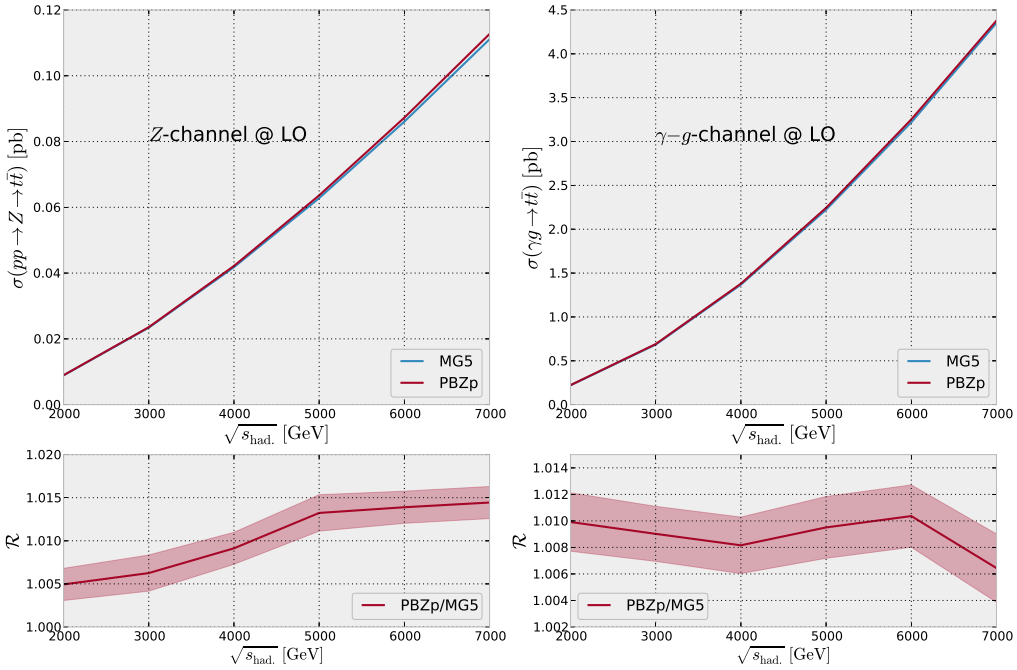

Figure 3.11: Born total cross sections as predicted by PBZp and MadGraph5_aMC@NLO as a function of the center-of-mass energy $\sqrt{s_{\text{had.}}}$. The Z- and $\gamma - g$-channels are shown on the left and right panels respectively.

Finally, we show in Fig. 3.12 the PBZp NLO predictions for the γ- and Z-channels compared against MadGraph5_aMC@NLO. Note that only the $q\bar{q}$ real corrections have been included in this comparison since it is not possible to obtain the qg and $\bar{q}g$ channels in MadGraph5_aMC@NLO because of the QED divergence. The physical parameters have been fixed to the values quoted above and we have used fixed renormalization and factorization scales, $\mu_F = \mu_R = 175$ GeV. Again, the agreement is within a few percents.

3.5.2 Impact of the NLO corrections

The rest of this section is devoted to PBZp results. In Tab. 3.1 we present our SM predictions for the sum of all the channels as well as the contribution of each channel separately for the LHC running at 13 and 14 TeV. Note that the $Z - \gamma$ channel is the sum of Z- and γ channels including their interference. Also, the $q\bar{q} + qg$-channel contains contributions from quark gluon initial states as well as from anti-quark gluon ones. Its contribution from the γ and $Z - \gamma$ channels is much larger due to the photon initiated contribution whose value is listed in Tab. 3.2 with the other Born contributions. For the NLO predictions, we also indicate the uncertainties due to the scale variation by a factor

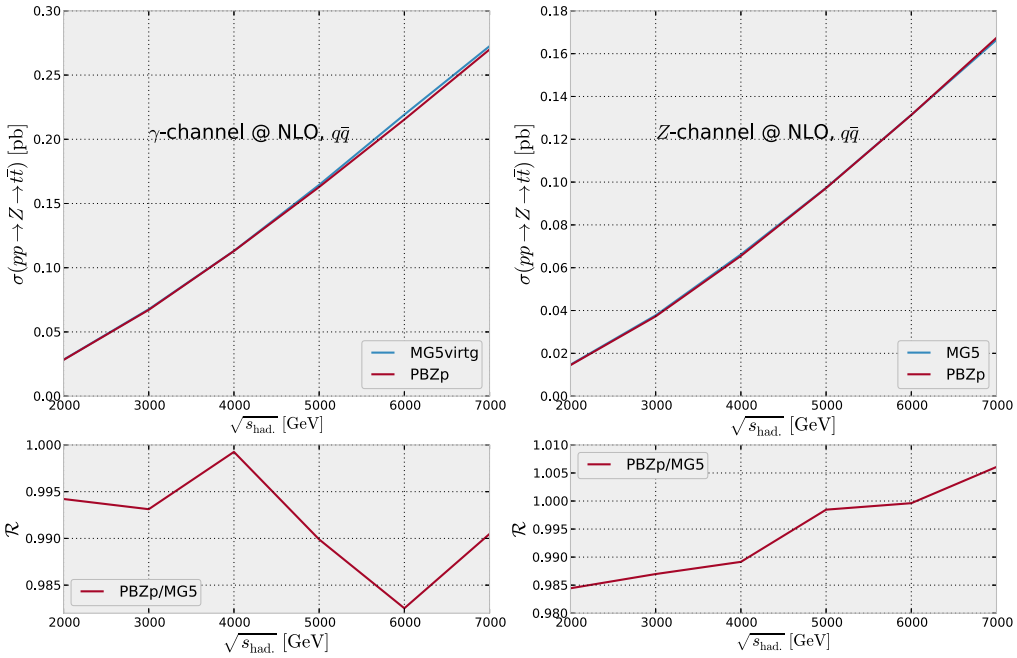

Figure 3.12: PBZp NLO predictions for the Z- and γ-channels compared with MadGraph5_aMC@NLO for several values of the center-of-mass energy $\sqrt{s_{\text{had.}}}$. Note that the qg and $\bar{q}g$ real corrections are not included, see text.

of two up and down around the top-quark mass, i.e. muF = muR $\in \{87.5, 350\}$. Note that we show these uncertainties only for the channels with the full set of corrections, i.e. the $q\bar{q} + qg$-channels. The QCD corrections to the electroweak top-pair production are large due to the fact that the qg channel opens up at NLO.

Table 3.1: PBZp predictions at NLO per channel and for the sum in pb. We show predictions for the LHC running at 13 and 14 TeV.

channel	13 TeV		14 TeV	
sub-channel	$q\bar{q}$	$q\bar{q} + qg$	$q\bar{q}$	$q\bar{q} + qg$
γ	0.25	$4.95^{+0.970}_{-0.400}$	0.28	$5.73^{+1.121}_{-0.465}$
Z	0.15	$2.15^{+0.400}_{-0.317}$	0.17	$2.56^{+0.461}_{-0.368}$
$Z - \gamma$	0.49	$7.24^{+1.387}_{-0.732}$	0.54	$8.45^{+1.604}_{-0.849}$

Table 3.2: PBZp predictions at LO per channel in pb. We show predictions for the LHC running at 13 and 14 TeV.

channel	13 TeV	14 TeV
γ	0.18	0.20
Z	0.11	0.13
$Z-\gamma$	0.35	0.39
$\gamma-g$	3.98	4.57

3.5.3 Z' production at the LHC

In this last section we present results including the effects of a SSM Z' gauge boson with a mass of 3.6 TeV, still allowed by the latest exclusion limits, see Chapter 1. We also show the dependence of the total cross section on the mass of the new resonance for the LHC13 and LHC14 as well as the invariant mass spectrum of the $t\bar{t}$ pair and discuss the impact of the matching to a parton shower (PS) program, Pythia 8 [189,245]. A cut on the invariant mass of the $t\bar{t}$ system of $3/4M_{Z'}$ is imposed on all the cross sections presented in this section in order to suppress the contributions coming from the Z-boson.

Total cross section of the electroweak top-pair production in the SSM

In Tab. 3.4, we show the contributions of the various channels to the total cross section. For the sum of all the channels, i.e. the column and row labeled $q\bar{q}+qg$, $Z'-Z-\gamma$ respectively, we include the combined uncertainties due to scale variation and numerical integration[23] where as before the former have been obtained by varying muR = muF $\in \{87.5, 350\}$. Tab. 3.3 contains the corresponding Born total cross section. Concentrating on the Born cross sections, we see that while the impact of the Z-boson contributions are negligible (due to the invariant mass cut) the inclusion of the photon can lead to a relative increase of about 40 %. Similar conclusion holds for the relative size of the NLO corrections for which we find that the cross section including the photon channel ($Z'-\gamma$) is roughly 50% larger than the one with only the Z'-boson channel.

Exclusion limits on new heavy neutral resonances are derived by the experimental collaboration in the plane $M_{Z'}$, $\sigma \times$ BR for a given channel, see e.g. [45,60]. Indeed, in this plane the intersection of the theoretical prediction with the observed limit gives the lower mass limit on the Z'-boson. It is therefore interesting to study the dependence of the total cross section on the mass of the new particle. Such an analysis is shown in Fig. 3.13 for a SSM Z' with mass $M_{Z'} \in [3000, 6000]$ GeV and for the LHC running at 13 and 14 TeV. The bands on this figure represent the scale variation and numerical uncertainties combined. In the same figure, we also show the ratio of the NLO predictions over the LO ones. Note that the $\mathcal{K}$-factor varies between 1.3 and 1.5 over the range of masses probed. Finally, note that we impose the same cut on the invariant mass of the $t\bar{t}$ system as previously.

[23] Hence, the error is defined by $\delta_{\pm} = \pm\sqrt{(\delta_{\mu}^{\pm})^2 + (\delta_{\text{num.}}^{\pm})^2}$ with $\delta_{\mu}^{\pm}$ the positive (negative) contribution due to scale variation and $\delta_{\text{num.}}^{\pm}$ the corresponding errors due to the numerical integration.

Table 3.3: Top-pair total Born cross section in fb for a SSM Z'-boson of 3.6 TeV. The error due to numerical integration is of the order 10^{-3} fb. We impose a cut on the invariant mass of the $t\bar{t}$ system, $M_{t\bar{t}} \geq 3/4 M_{Z'}$.

channel	13 TeV	14 TeV
Z'	1.17	1.77
$Z' - Z$	1.17	1.78
$Z' - \gamma$	1.67	2.50
$Z' - Z - \gamma$	1.68	2.52

Table 3.4: Top-pair total cross section in fb for a SSM Z'-boson of 3.6 TeV. Contributions from the various channels are detailed and the impact of scale variation as well as the numerical errors combined as explained in the text are shown. Note that we impose a cut on the invariant mass of the $t\bar{t}$ system, $M_{t\bar{t}} \geq 3/4 M_{Z'}$.

channel	13 TeV		14 TeV	
sub-channel	$q\bar{q}$	$q\bar{q} + qg$	$q\bar{q}$	$q\bar{q} + qg$
Z'	1.48	1.49	2.22	2.22
$Z' - \gamma$	1.50	2.23	2.24	3.30
$Z' - Z$	1.49	1.56	2.22	2.34
$Z' - Z - \gamma$	1.51	$2.32^{+.13}_{-.08}$	2.26	$3.44^{+.18}_{-.11}$

Invariant mass spectrum of the $t\bar{t}$ system

The invariant mass of the top-pair produced via a heavy resonance, is peaked around the mass of the resonance. This can be reconstructed by the experiments from the decays of the two tops, e.g. with one of the two tops decaying into a b-jet and a lepton plus missing energy and the other one fully hadronically. In Fig. 3.14, we show the invariant mass spectrum[24] of the $t\bar{t}$ pair in presence of a SSM Z'-boson of 3.6 TeV for the LHC13. In the upper-left corner we show the LO and NLO prediction without showering while in the upper-right corner we show the impact of the PS on the NLO invariant mass spectrum. The bottom plot contains the LO+PS as well as NLO+PS predictions with its associated $\mathcal{K}$-factor. The two $\mathcal{K}$-factors, NLO/LO and NLO+PS/NLO, are also shown on the same figure. The showering is done with Pythia 8 [189, 245] and even though the top quarks are decayed we obtain the invariant mass of the $t\bar{t}$ pair directly from the Monte Carlo intermediate information, i.e. the top- (and anti-top) quark momenta just before they decay. For all the runs we use a sampling of 300000 events and normalize the histograms to

[24] The invariant mass is simply defined by $(p_1 + p_2)^2$ where $p_{1,2}$ are the 4-momenta of the top-quark and anti top-quark, respectively.

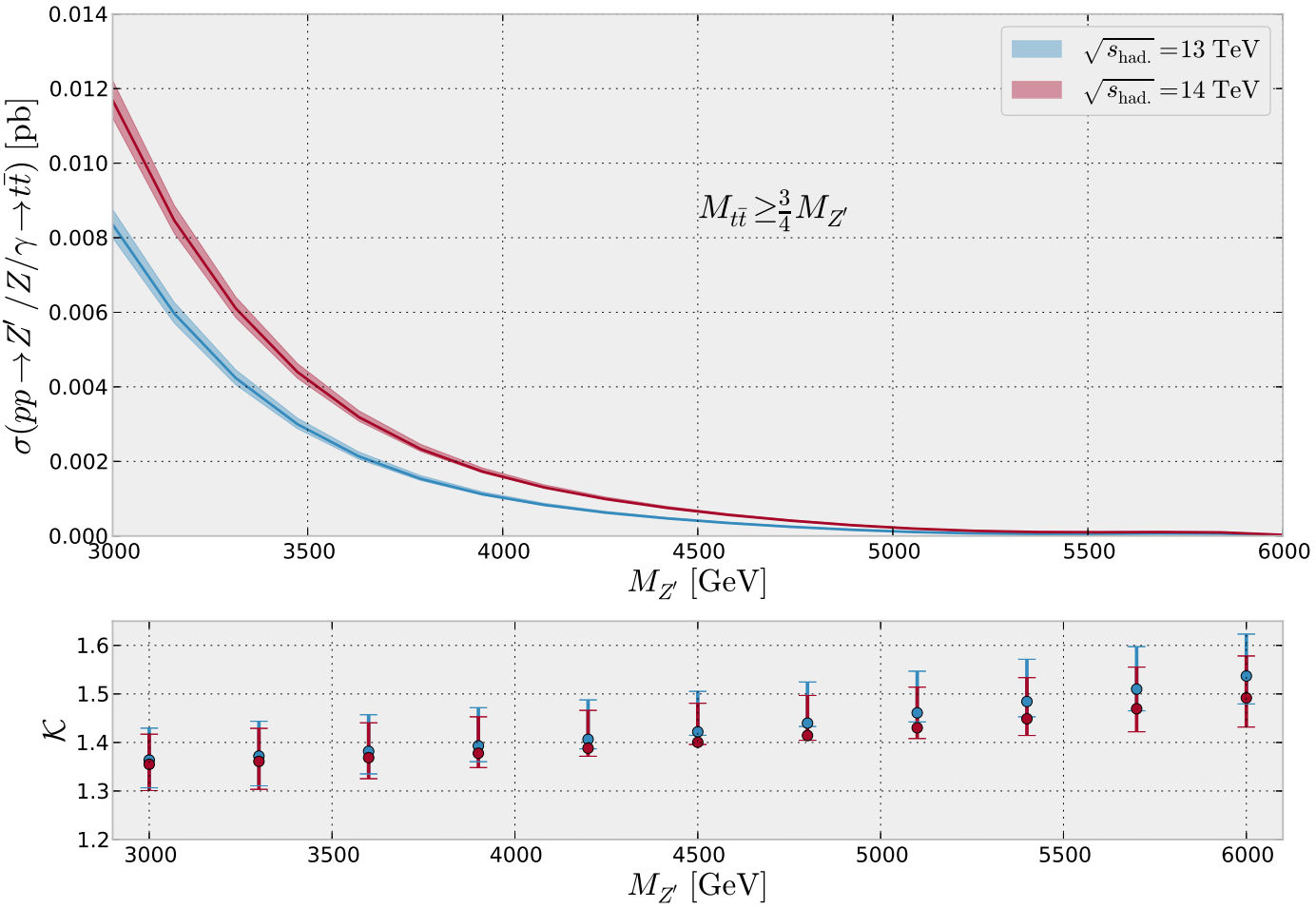

Figure 3.13: NLO cross section in dependence of the mass of the new resonance for the LHC13 and LHC14. The bands represent the scale variation and numerical error. We also show the $\mathcal{K}$-factor for the same range of masses, i.e. $[3000, 6000]$ GeV.

the total cross sections. From the upper left plot, we clearly see the impact of having the first hard radiation generated by POWHEG (`PBZp`) in the higher tail in the low invariant mass region. Indeed, for instance, if a gluon is emitted from one of the two top-quark in the final state, the invariant mass of the top pair is reduced accordingly by the momentum carried away by the gluon. In the same spirit, we understand that the effect of the parton shower is to populate the low invariant mass region as can be confirmed by studying the upper right plot. Finally, we see that the PS increases the $\mathcal{K}$-factor in the region below the Z' peak to reach 6 at its maximum. Note that the peak at 2750 is an artefact of the cut off on the invariant mass[25] (at 2700 GeV).

[25]The bins below 2700 GeV are filled up only by the PS.

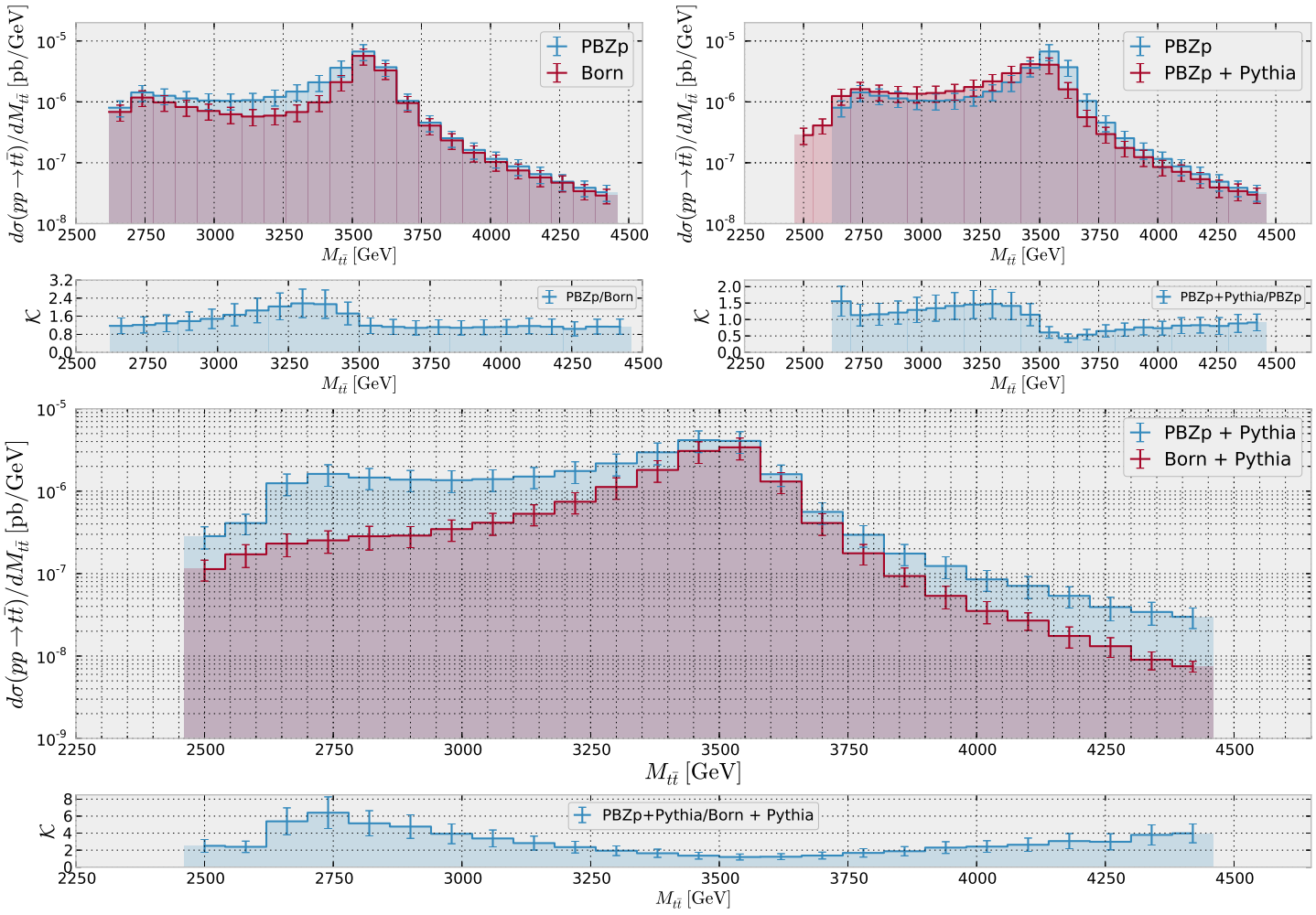

Figure 3.14: Invariant mass spectrum of the $t\bar{t}$ pair in presence of a SSM Z'-boson of 3.6 TeV at the LHC13. We show predictions for the LO, NLO, LO+PS and NLO+PS as well as for the corresponding ratios, $\mathcal{K} = \{\text{PBZp/Born}, \text{PBZp} + \text{PS/PBZp}, \text{PBZP} + \text{PS/Born} + \text{PS}\}$.

After the discovery of the Higgs boson by ATLAS and CMS, the main challenge of the LHC remains to explore the TeV region in search for new phenomena. If new physics is found, precise theoretical predictions will be required to discriminate between various new physics scenarios and extract the fundamental underlying parameters. Making precise predictions at hadronic colliders requires to use Monte Carlo event generators to model the intense hadronic activity surrounding the hard process.

In this chapter, we presented NLO QCD corrections to the electroweak top-pair and single-top production in presence of new resonances as predicted by the $\mathcal{G}_{221}$ models. While the later process is not yet finalized, the former has been integrated to a general Monte Carlo event generator allowing for a consistent matching of NLO matrix elements and parton shower algorithms, the `POWHEG BOX`.

After having reviewed the various techniques employed, we presented details of the calculation for both processes. Finally, we reviewed the main elements needed for the `POWHEG BOX` implementation of the corrections to the top-pair production and presented our first numerical results including the total cross section for electroweak top-pair production per channel for a Z'-boson of 3.6 TeV as well as the mass dependence of the same cross section for $M_{Z'} \in [3000, 6000]$ GeV and the invariant mass cut $M_{t\bar{t}} > 3/4 M_{Z'}$. It turns out that the contribution of the γ channel to the NLO corrections can lead to a relative increase of 50%, and must be taken into account contrary to what has been done in previous studies [196]. Finally, we presented the invariant mass spectrum of the $t\bar{t}$ pair in presence of a SSM Z'-boson of 3.6 TeV for the upcoming LHC run at 13 TeV. The results at the partonic level were compared to the ones matched to parton shower. We found that the $\mathcal{K}$-factors in all these cases are sizeable: within $[1.3 - 1.5]$ for the total cross sections and even larger in some bins of the invariant mass of the top-quark pair.

CHAPTER 4
W' AND Z' AT THE PIERRE AUGER OBSERVATORY

New charged and neutral resonances are predicted in many well-motivated extensions of the Standard Model (SM) such as theories of grand unification (GUTs) or models with extra spatial dimensions [68]. These extensions generally do not predict the precise energy scale at which the new heavy states should manifest themselves. However, for various theoretical reasons (e.g. the hierarchy problem) new physics is expected to appear at the TeV scale and is searched for at the Large Hadron Collider (LHC) which will soon operate at a center-of-mass energy of $\sqrt{s} = 13$ TeV. At the same time, important restrictions on new physics scenarios are imposed by low-energy precision observables. On the other hand, highly energetic interactions of cosmic rays in the atmosphere involve processes at higher center-of-mass energies than those reached by the LHC. Motivated by this fact, we study the prospects to observe new spin-1 resonances in collisions of ultra-high energy neutrinos (UHEν) with nuclei in the atmosphere as analyzed by the Pierre Auger Collaboration or a future neutrino telescope. For example, for neutrinos with an energy of about 10^{19} eV, the center-of-mass energy of the neutrino-nucleon interactions is about $\sqrt{s} \simeq 140$ TeV, considerably extending the energy range accessible at the LHC. So far, no UHEν events have been observed by the Pierre Auger Observatory which has led to improved limits on the diffuse flux of UHEν in the energy range $E_\nu \geq 10^{18}$ eV [246, 247].

The potential of the Pierre Auger Observatory for testing new physics scenarios like extra dimensions or the formation of micro-black holes has been studied in [248] and [249, 250]. In this section we revisit the predictions for cross sections in the SM, and we explore the impact of new charged (W') and neutral (Z') gauge bosons on these quantities. We address the following questions: (i) Assuming the LHC does observe new charged or neutral spin-1 resonances, how would this affect the predicted neutrino cross sections? (ii) Assuming the LHC does not discover any new spin-1 resonances, what are the prospects to observe heavy W'- and Z'-bosons with masses larger than 5 TeV using ultra-high energy cosmic neutrino events?

For definiteness, we consider W' and Z' bosons due to an extended $\mathcal{G}_{221} \equiv \mathrm{SU}(2)_1 \times \mathrm{SU}(2)_2 \times \mathrm{U}(1)_X$ gauge group. In this framework, constraints on the parameter space from low-energy precision observables have been derived in [63], see Chapter 1 and the collider phenomenology has been studied in [64, 74, 251, 252]. Several well-known models emerge naturally from different ways of breaking the $\mathcal{G}_{221}$ symmetry down to the SM gauge group [63], in particular Left-Right (LR) [71–73], Un-Unified (UU) [83, 84], Non-Universal (NU) [85, 86], Lepto-Phobic (LP), Hadro-Phobic (HP) and Fermio-Phobic (FP) [87, 88]

models as presented in Chapter 1. In addition, we present results for the Sequential Standard Model (SSM) [8], where the W'- and Z'-bosons are just heavy copies of the W- and Z-bosons in the SM. This is motivated by the fact that the SSM often serves as a benchmark model in the literature [15, 18, 24, 29].

This Chapter is organized as follows. In Section 4.1 we briefly present the Pierre Auger Observatory and specificities about UHEν that allow the Pierre Auger Collaboration to detect them. Section 4.2 is dedicated to the calculation of the interaction cross sections of UHEν with nuclei of the atmosphere while the last section contains our numerical results.

4.1 Ultra-high energy neutrinos at the Pierre Auger Observatory

Ultra-high energy neutrinos propagating through the atmosphere interact with an energy in the center-of-mass of about $\sqrt{S} \simeq 100$ TeV, probing SM interactions in a kinematical region not accessible by current collider experiments. New spin-1 resonances as the one presented in the previous section could be produced in these processes modifying the SM cross sections. In this section we study the impact of such resonances on the interaction of UHEν in the atmosphere at the Pierre Auger Observatory. We start by presenting the Auger Observatory and details about the detection of UHEν induced showers. Then, we review the calculation of the relevant cross sections and the modifications due to new heavy gauge bosons. Finally, we discuss our numerical results and conclude.

4.1.1 The Pierre Auger Observatory

Cosmic rays (CR) are charged particles that rain down on us from space. While cosmic rays of low and moderate energies, below 10^9 GeV, are well understood, the origin and composition of the highest energetic particles observed still remain a mystery. It is to study the CR in this regime, above 10^8 GeV, that the Auger Project, was first proposed in 1992 by Jim Cronin and Alan Watson. Twelve years later, the observatory was collecting its first data and after four more years the construction was completed [253].

Highly energetic particles arriving down on earth interact with the nuclei of the atmosphere and produce extensive electromagnetic as well as hadronic showers of particles that keep extending until they reach the ground. These particles can be detected via the Cherenkov light they emit when travelling through water. Hence the first detector of the observatory is a Cherenkov ground array telescope composed of 1600 water tanks distributed over 3000 square kilometers in the vast plain of Pampa Amarilla near the town of Malargue in Argentina. Each one of these tanks contains 12 tonnes of water viewed by 9" photomultipliers that detect photons and charged particles. The large size of the detector is justified by the expected event rate at these extreme energies, 1 particle/km^2 per year [254].

The other effect exploited at the Auger Observatory to obtain information on the cosmic rays is the fluorescent light emitted by nitrogen molecules after being excited by charged particles traversing the atmosphere. The wavelength of this emission is between 300 and 400 nm and is detected by the Auger's optic detectors. The Auger Observatory has 27 fluorescent light detectors grouped in four sites overlooking the ground array telescope. Fluorescent light detectors are very good to estimate the total energy of the shower while it is very difficult to access this information with the ground array telescope.

On the other hand the duty cycle of the fluorescent light detector is only 10% rendering these two methods complementary[1] [255]. The fact that we observed cosmic rays of energies $10^9 - 10^{10}$ GeV points toward the existence of associated flux of ultra-high energy neutrinos (UHEν).

4.1.2 Cosmogenic flux

In the early sixties the bigbang theory was not yet an established theory but astrophysicist, A. G. Doroshkevich and I. Novikov, postulated the existence of a detectable cosmic microwave background (CMB) radiation in 1964 [256]. The same year, A. Penzias and R. Wilson working on a 6 meter horn antenna originally built to detect radio waves bounced off Echo balloon satellites discovered the predicted radiation [257]. It was soon realized that ultra-high energy cosmic rays propagating through the universe would interact with such a radiation. Almost simultaneously Greisen in the US [258] and Zatsepin & Kuzmin [259] in the USSR calculated the mean path of extragalactic nucleons interacting with the CMB and showed that it is shorter than the typical distance between two galaxies capable of producing particles of such energy. The extragalactic component of the cosmic ray spectrum should then be drastically reduced for energies above $5{\times}10^{10}$ GeV, which is nowadays known as the GZK cutoff.

The idea of a "guaranteed" extragalactic cosmogenic neutrino flux is a consequence of the GZK effect and was first formulated by Berezinsky and Zatsepin in 1969 [260]. Indeed, the proton interact with the photons from the CMB via the following two processes:

$$p + \gamma_{CMB} \rightarrow \Delta^+ \rightarrow \pi^+ + n \tag{4.1}$$
$$p + \gamma_{CMB} \rightarrow \Delta^+ \rightarrow \pi^0 + p\,, \tag{4.2}$$

followed by the subsequent decays of pions [90]:

$$\pi^+ \rightarrow \mu^+ + \nu_\mu \quad (99.98\%) \tag{4.3}$$
$$\pi^0 \rightarrow \gamma + \gamma \quad (98.82\%) \tag{4.4}$$
$$\pi^0 \rightarrow e^+ + e^- + \gamma \quad (1.17\%)\,. \tag{4.5}$$

Despite the fact that the production of Δ^+ and its decay to π^0 is the main channel at the origin of the GZK cutoff, Eq. (4.2), it is not relevant for further discussions on the cosmogenic neutrino flux [261]. Adding the beta decay of neutron we see that for each proton interacting with a photon, a muon, an anti-electronic as well as a muonic neutrino are produced. Looking at the kinematical production threshold we can estimate the minimal energy the proton must carry so that the process in Eq.(4.1) happens:

$$E_{th} = \frac{((M_n + M_\pi)^2 - M_p^2)}{4E_\gamma}\,. \tag{4.6}$$

Inserting the values for the different parameters one obtains $E_{th} = 3.05 \times 10^{11}$ GeV which is close to the value of the GZK cutoff quoted above. A more precise estimate would require to take into account the statistical spread of photon energies in the CMB, which effectively lowers the threshold.

[1] The fluorescent light detectors are efficient only at night and under specific atmospheric conditions.

The data from the Auger Observatory rejects the hypothesis that the cosmic-ray spectrum continues with a constant slope above 4×10^{11} GeV, at the level of 6 sigmas [254], clearly indicating a decrease in the flux of particles with such an energy. Together with the indications that cosmic-ray above 5.7×10^{11} GeV are from extragalactic origins [262] this is a strong indication in favor of the GZK cutoff and therefore the existence of a cosmogenic neutrino flux.

Accurate predictions of this neutrino flux relies on multiple assumptions including the composition of cosmic-rays, the cosmological evolution of the sources and the maximum acceleration energy. In 2010, Kotera et al. [263] have carried out a complete numerical Monte Carlo study of neutrino fluxes produced by the interaction of propagating cosmic-rays of ultra high energy over cosmological distances. In Fig. 4.1 we show the obtained flux of neutrinos in dependence of several parameters. Without going into the details of the different lines it is interesting to note that between optimistic fluxes, soon to be probed by experiments, and the most pessimistic ones there is a large spread of almost three orders of magnitude, at an energy of 10^9 eV. At this energy a reasonable flux would be of the order of 7×10^9 GeVcm^{-2}s^{-1}sr^{-1}, still one order of magnitude below the current sensitivity of the Pierre Auger Observatory. These neutrino events are actively searched for by the Auger Observatory and we now briefly review the specificities of neutrino induced showers with respect to "regular" cosmic-ray induced ones.

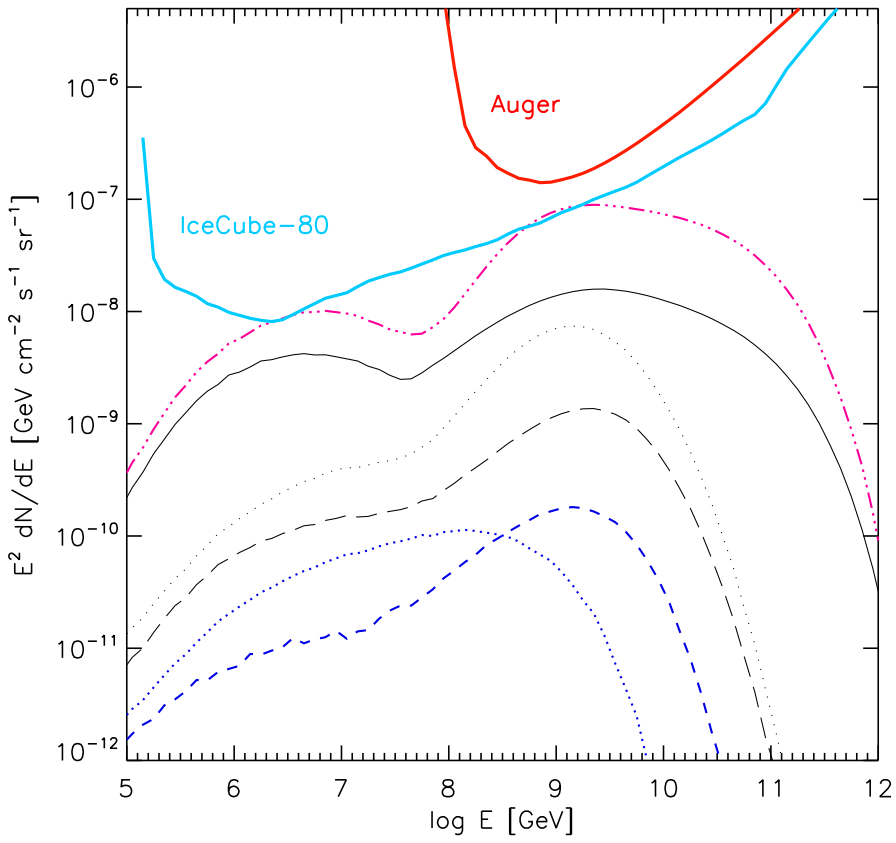

Figure 4.1: From [263], cosmogenic neutrino fluxes for all flavors, for different parameters compared to various instrument sensitivities. The spread of the predictions due to the dependence on the parameters of the simulation covers almost three orders of magnitude.

4.1.3 Distinguishing neutrino induced showers

The main challenge in detecting neutrino induced showers lies in separating them from those initiated by regular cosmic-rays. Already in the 70's it was suggested that this could be achieved at large zenith angle because the atmosphere slant depth provides a large target for the neutrinos [264]. The idea is that the tiny cross sections of neutrinos allow them to interact deep in the atmosphere, while protons and heavier nuclei will interact much higher up on their way to earth. Hence, the strategy is to look for inclined showers interacting deep in the atmosphere.

The surface detector of the Pierre Auger Observatory can detect inclined showers induced by neutrinos of energy larger than 10^{17} eV [265]. There are two different categories of neutrino events that can be detected:

(i) **Downward-going** neutrinos: the charged current (CC) and neutral current (NC) interaction of neutrinos[2] scattering off nuclei in the atmosphere produce extensive air showers that can be detected at ground [266].

(ii) **Earth-skimming** tau neutrinos: in this channel, the decay products of a tau lepton, originating from an upward-going tau neutrino travelling through the earth crust and interacting, produce a shower close to the ground that can be detected [267, 268].

In both cases the neutrino induced showers can be identified and separated from the background for zenith angle around $65° - 75°$ [247]. In addition, there are fundamental properties of the shower that can be used to distinguish neutrino induced showers. Among these, the time distribution of the shower particles is very useful. Indeed, vertical showers induced by nuclei will have a large electromagnetic component typical of "young" shower front while inclined ones, angle larger than 75°, will be mainly composed of muons because of the large depth of air, "old" shower front. On the other hand, for the same zenith angle neutrinos will produce showers with young fronts and large electromagnetic component. Finally, young showers produce signals spread over hundreds of nano-seconds in a fraction of the stations triggered by the shower while old showers will have a narrow signal spreading over tens of nano-seconds in almost all the stations involved. Based on these differences, the selection of neutrino events can be easily accomplished [255]. In the following we will only consider "downward-going" neutrinos as they represent an independent channel on their own and dealing with earth-skimming events would require extensive simulation not well suited for a first estimate of the impact of new physics.

4.2 Interactions of UHE in the atmosphere in presence of new heavy resonances

Working in the framework of $\mathcal{G}_{221}$ models, we are now interested in the issue of estimating the interaction cross section of UHEν with nuclei of the atmosphere, when additional Z' and W' gauge bosons can mediate their interaction in the atmosphere. In the SM, the following neutrino interactions can take place [269, 270]:

(i) Charged current deep-inelastic scattering (CC DIS): $\nu_\ell + N \to \ell^- + X$, $\bar{\nu}_\ell + N \to \ell^+ + X$. Here, ν_ℓ stands for the three neutrino flavors ν_e, ν_μ, ν_τ.

[2] All three flavours contribute to this channel.

(ii) Neutral current deep-inelastic scattering (NC DIS): $\nu_\ell + N \to \nu_\ell + X$, $\bar{\nu}_\ell + N \to \bar{\nu}_\ell + X$.

(iii) The Glashow resonance (GR) [271–273]: $\bar{\nu}_e + e^- \to \bar{\nu}_\ell + \ell^-$, $\bar{\nu}_e + e^- \to q + \bar{q}'$, where $q = u, d, s, c, b$. Obviously, charged current resonant s-channel scattering occurs only for incoming anti-electron neutrinos. The process $\bar{\nu}_e + e^- \to \bar{\nu}_e + e^-$ also has a non-resonant neutral current t-channel contribution.

(iv) Non-resonant neutrino-electron scattering:

  (a) $\nu_e + e^- \to \nu_e + e^-$, which has contributions from W and Z exchange diagrams.

  (b) Charged current $\nu_\mu e^-$ and $\nu_\tau e^-$ scattering in the atmosphere: $\nu_\ell + e^- \to \ell^- + \nu_e$ ($\ell = \mu, \tau$). Note that the corresponding process with incoming anti-neutrinos is not possible.

  (c) Neutral current scattering of ν_μ, $\bar{\nu}_\mu$, ν_τ, $\bar{\nu}_\tau$ and $\bar{\nu}_e$: $\nu_\ell + e^- \to \nu_\ell + e^-$, $\bar{\nu}_\ell + e^- \to \bar{\nu}_\ell + e^-$.

In the following, we mainly focus on the dominant cross sections of neutrino–nucleon DIS and neglect the contributions from non-resonant neutrino–electron scattering which are smaller by several orders of magnitude. The W' and Z' resonances contribute to the νN DIS, where the main contribution comes from the interference with the SM amplitudes. We also consider the Glashow resonance, which has attracted a lot of interest in the literature as a way to detect extra-galactic neutrinos and as a discriminator of the neutrino production mechanism and of the relative abundance of the pp and $p\gamma$ sources [274–279]. While the GR is entirely negligible[3] at energies $E_\nu \geq 10^8$ GeV there is a new, potentially interesting, resonance due to the W'-boson which we call GR$'$ in the following. Before presenting our results we start be reviewing the calculation of the DIS as well as GR cross sections in the SM and the extensions considered here.

4.2.1 Deep Inelastic Scattering

Charged-current deep inelastic scattering of neutrinos off nucleons can be schematically represented as:

$$\overset{(-)}{\nu}_\ell(k) + N(p) \to \ell^\mp(k') + X(p')\,,$$

where ℓ is a charged lepton and N is a nucleon. As $M_n \approx M_p$ we will denote M_p either the neutron or the proton mass in the following. The differential cross section for DIS mediated by interfering gauge bosons B and B' can be written as

$$\frac{d^2\sigma}{dxdy} = \sum_{B,B'} \frac{d^2\sigma^{BB'}}{dxdy}\,, \tag{4.7}$$

where the Bjorken variable x and the inelasticity y are defined as

$$x \equiv \frac{-q^2}{2p\cdot q} = \frac{Q^2}{2M_p\nu}\,,\ \nu \equiv \frac{p\cdot q}{M_p} = E_L - E_{L'}\,,\ y \equiv \frac{p\cdot q}{p\cdot k} = \frac{\nu}{E_\nu} = \frac{E_L - E_{L'}}{E_L}\,, \tag{4.8}$$

[3]Note that the threshold of the Pierre Auger Observatory is $E_\nu = 10^8$ GeV which is above the GR peak of the SM.

in which $E_L(E_{L'})$ is the energy of the incoming (outgoing) neutrino (lepton) respectively. Furthermore, $B, B' \in \{W, W'\}$ in the case of CC DIS and $B, B' \in \{\gamma, Z, Z'\}$ in the case of NC DIS. In the following we assume a general interaction term of a fermion with a vector boson of the form

$$\mathcal{L}^B_{int} = \overline{\psi_f}\gamma_\mu[g^B_R(1+\gamma_5) + g^B_L(1-\gamma_5)]\psi_f B^\mu \,, \tag{4.9}$$

where ψ_f denotes a generic fermion field. The couplings g^B_R and g^B_L of the gauge boson B to the right- and left-chiral components of the quark and lepton fields are given by

$$g^B_R = g(B)\; C^B_{q(\ell),R} \quad , \quad g^B_L = g(B)\; C^B_{q(\ell),L} \,, \tag{4.10}$$

where $g(B) = \dfrac{g_W}{2\sqrt{2}}$ for charged-current interactions ($B = W, W'$) and $g(B) = \dfrac{g_W}{2c_{\theta_W}}$ for neutral-current interactions ($B = Z, Z'$). We also define a short hand notation that will be used later on and in which the relevant couplings at work are grouped together:

$$g^{BB'}_{\pm f} = C^B_{f,L}C^{B'}_{f,L} \pm C^B_{f,R}C^{B'}_{f,R} \,, \tag{4.11}$$

where $B, B' \in \{W, W'\}$ for CC DIS and $B, B' \in \{Z, Z'\}$ in the NC case. Furthermore, f denotes either quarks ($f = q$) or leptons ($f = \ell$).

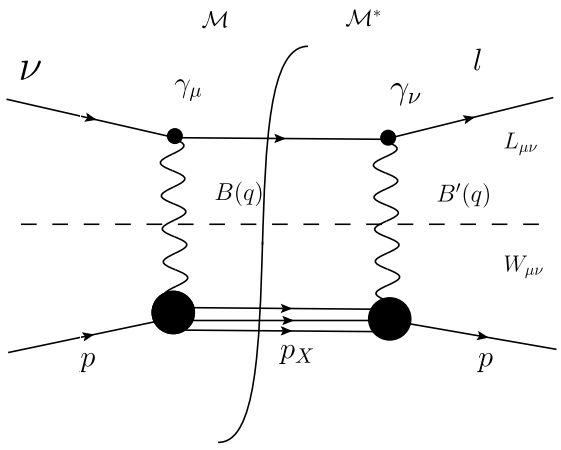

Figure 4.2: Representation of the matrix element squared for the DIS of neutrinos off a proton.

We are now set up to write down the sum-averaged matrix element[4] corresponding to $d^2\sigma^{BB'}/dxdy$ as the contraction of a leptonic tensor $L_{\mu\nu}$ and an hadronic tensor $W_{\mu\nu}$:

$$\overline{\sum} \mid \mathcal{M} \mid^2 = G_B G_{B'} 4\pi Q^2 L_{\mu\nu} W^{\mu\nu} \,, \tag{4.12}$$

with

$$L_{\mu\nu} = \frac{1}{Q^2}\overline{\sum} \left\langle \nu_l \left| j^\dagger_\nu \right| l \right\rangle \left\langle l \left| j_\mu \right| \nu_l \right\rangle \,, \tag{4.13}$$

$$W^{\mu\nu} = \frac{1}{4\pi}\overline{\sum_X}(2\pi)^4\delta^4(p+q-p_X) \left\langle p \left| J^\mu \right| p_X \right\rangle \left\langle p_X \left| J^{\nu\dagger} \right| p \right\rangle \,. \tag{4.14}$$

[4]We calculate the DIS off a proton from which the interaction with a nuclei will be inferred.

The leptonic tensor represents the upper fermionic line of the diagram shown in Fig. 4.2 while the hadronic tensor parametrizes the lower part of the same diagram. The term $G_B = g(B)^2/(Q^2 + M_B^2)$ contains the product of the gauge boson propagator and its gauge coupling. The leptonic tensor can be fully calculated in perturbation theory, while the hadronic tensor contains non perturbative physics and therefore cannot be calculated perturbatively. Using the same convention as in [280] the leptonic tensor reads

$$L_{\mu\nu} = \frac{8}{Q^2}\left\{g_{+l}^{BB'}[k_\mu k'_\nu + k_\nu k'_\mu - g_{\mu\nu}(k\cdot k')] - g_{-l}^{BB'}[i\epsilon_{\mu\nu\rho\sigma}k^\rho k'^\sigma]\right\}. \tag{4.15}$$

The hadronic tensor is written in terms of fundamental Lorentz tensors

$$W^{\mu\nu} = -g^{\mu\nu}W_1 + \frac{p^\mu p^\nu}{M_p^2}W_2 - i\frac{\epsilon^{\mu\nu\alpha\beta}p_\alpha q_\beta}{2M_p^2}W_3 + \frac{q^\mu q^\nu}{M_p^2}W_4 + \frac{p^\mu q^\nu + p^\nu q^\mu}{2M_p^2}W_5 + \frac{p^\mu q^\nu - p^\nu q^\mu}{2M_p^2}W_6\,, \tag{4.16}$$

where the $W_i = W_i(Q^2,\nu)$ are the *invariant hadron structure function* and $\epsilon^{\mu\nu\alpha\beta}$ the Levi-Civita tensor. Contracting $L_{\mu\nu}$ and $W_{\mu\nu}$ we finally obtain :

$$L\cdot W = \frac{16E_\nu E_l}{Q^2}\left\{g_{+l}^{BB'}\left[2\sin^2\frac{\theta}{2}W_1 + (1-\sin^2\frac{\theta}{2})W_2\right] + g_{-l}^{BB'}\left[\frac{E_\nu + E_l}{M_p}\sin^2\frac{\theta}{2}W_3\right]\right\}, \tag{4.17}$$

in which terms of the order $\mathcal{O}(\frac{m_l^2}{s})$ have been neglected[5] resulting in the dropping of the terms proportional to $\{W_4, W_5, W_6\}$. In addition we have introduced the angle θ between the momenta k and k'.

Adding the flux factor, the phase space of the outgoing lepton and expressing the result in terms of the kinematical variables x and y, one obtains the differential cross section[6] for neutrinos (+ sign) and anti-neutrinos (− sign) scattering of a proton [281]

$$\frac{d^2\sigma^{BB'}(\nu,\bar\nu p)}{dxdy} = \frac{2M_pE_\nu G_B G_{B'}}{\pi}\left\{g_{+l}^{BB'}\left[xF_1y^2 + F_2\left[(1-y) - \left(\frac{M_pxy}{2E_\nu}\right)\right]\right] \pm g_{-l}^{BB'}\left[xF_3y\left(1-\tfrac{y}{2}\right)\right]\right\}, \tag{4.18}$$

in which we have introduced the CC or NC *scaling structure functions* $F_i(x,Q^2)$ defined by

$$F_1 = W_1\,,\ F_2 = \frac{\nu}{M_p}W_2\,,\ F_3 = \frac{\nu}{M_p}W_3\,. \tag{4.19}$$

Note that from Eq. (4.8) we have $Q^2 = sxy$ so that the structure functions $F_i(x,Q^2)$ depend only x and y as the differential cross section. The structure functions are generally given as convolutions of parton distribution functions with Wilson coefficients. We now review the expressions for the structure functions in terms of the parton density functions (PDF).

[5] Note that at the energies considered here, $E_\nu \simeq 10^8$ GeV, these terms are extremely small.

[6] θ and Q^2 variables are mapped onto x and y using the relations Eq. (4.8).

Structure Functions @LO

Expressing the structure functions in terms of the PDF of the various quarks can be done by exploiting the parton model framework [282]. Here we review the derivation of the structure functions directly from the *factorization theorem* which enables for a rigorous treatment of the heavy quarks. We will calculate the contribution of a quark $Q_1(m_1 = 0)$ to the CC structure functions $F_1^{\nu,CC}, F_2^{\nu,CC}, F_3^{\nu,CC}$ in presence of W-,W'-bosons keeping the effects of the top-quark mass m_t. In the following we drop the superscript ν, CC.

The factorization theorem asserts that the hadronic tensor of Eq. (4.14) takes the form [283]:

$$W_{BN}^{\mu\nu} = f_N^a \otimes \hat{w}_{Ba}^{\mu\nu} = \int \frac{d\xi}{\xi} f_N^a(\xi,\mu)\hat{w}_{Ba}^{\mu\nu}(q, k_a, \ldots, \alpha_s)(\mu)\,, \tag{4.20}$$

to the leading power of exchanged momentum, q^2. We denote f_N^a the parton distribution function of parton a in the nucleon N and $\hat{w}_{Ba}^{\mu\nu}$ the hard scattering tensor parametrizing the parton interaction[7]. The variable ξ is the momentum fraction carried by the parton with respect to the hadron and μ the renormalization and factorization scale taken identical. The factorization theorems allows us to relate the hadronic tensor to the partonic dynamics of the process. In order to obtain the structure functions we proceed as follows:

(i) derive the projectors on the various structure functions, $P_i^{\mu\nu}$, such that $P_{i\mu\nu} \cdot W_{BN}^{\mu\nu} = W_i$,

(ii) calculate the partonic tensor $\hat{w}_{Ba}^{\mu\nu}$,

(iii) apply the projector to Eq. (4.20) to obtain the structure functions.

Projectors We first calculate P_3 and P_6 because they can easily be disentangled. Contracting Eq. (4.16) with $\frac{p_\mu q_\nu - q_\mu p_\nu}{2p\cdot q}, ip^\rho q^\sigma \frac{\epsilon_{\mu\nu\rho\sigma}}{q^2}$ one obtains:

$$\frac{\alpha_1}{2p\cdot q} W_6\,, \frac{-\alpha_1}{q^2} W_3\,, \tag{4.21}$$

where we have defined $\alpha_1 = q^2 - \frac{(p\cdot q)^2}{M_p^2}$, and from which the corresponding projectors can be read off immediately. Next, we contract Eq. (4.16) with $g_{\mu\nu}, \frac{p_\mu p_\nu}{M_p^2}, \frac{q_\mu q_\nu}{q^2}, \frac{p_\mu q_\nu + p_\nu q_\mu}{2p\cdot q}$ and obtain a set of four equations which in the basis $\{W_1, W_2, W_4, W_5\}$ reads:

$$\tilde{P} = \begin{pmatrix} -4 & 1 & \frac{q^2}{M_p^2} & \frac{p\cdot q}{M_p^2} \\ -1 & 1 & \frac{(p\cdot q)^2}{M_p^4} & \frac{p\cdot q}{M_p^2} \\ -1 & \frac{(p\cdot q)^2}{M_p^2 q^2} & \frac{q^2}{M_p^2} & \frac{p\cdot q}{M_p^2} \\ -1 & 1 & \frac{q^2}{M_p^2} & \frac{p\cdot q}{2M_p^2} + \frac{q^2}{2p\cdot q} \end{pmatrix}. \tag{4.22}$$

[7] When dealing with NLO effects, long distance contributions must be subtracted off from $\hat{w}_{Ba}^{\mu\nu}$ [284].

Inverting $\tilde{P}$ one obtains the expressions for the projectors. We give here only the result for P_1, P_2, P_3 since they are the relevant ones for deriving the corresponding structure functions.

$$P_1 = \frac{-1}{2} g_{\mu\nu} + \frac{1}{2\alpha_1}\left(\frac{q^2}{M_p^2} p_\mu p_\nu + q_\mu q_\nu\right) + \left(1 - \frac{q^2}{\alpha_1}\right)\frac{p_\mu q_\nu + p_\nu q_\mu}{2p\cdot q}\,, \tag{4.23}$$

$$P_2 = \frac{-q^2}{2\alpha_1} g_{\mu\nu} + \frac{3}{2\alpha_1^2 M_p^2}\left(q^4 p_\mu p_\nu + \frac{\left(2(p\cdot q)^2 + M_p^2 q^2\right)}{3} q_\mu q_\nu - (p\cdot q) q^2 \left(p_\mu q_\nu + p_\nu q_\mu\right)\right)\,, \tag{4.24}$$

$$P_3 = \frac{-i}{\alpha_1} p_\rho q_\sigma \epsilon^{\mu\nu\rho\sigma}\,. \tag{4.25}$$

Partonic tensor $\hat{w}^{\mu\nu}_{Ba}$ We neglect all the masses but the top-quark mass and use the same current parametrization as for the leptonic tensor Eq. (4.9) and we will refer to the couplings of the gauge boson B to a parton a by g_{Ra}, g_{La}. The partonic tensor for the heavy quark production, $B^* Q_1(m_1 = 0) \to Q_2(m_2)$, is given by

$$\hat{w}^{\mu\nu}_{Ba} = \frac{1}{(4\pi)}\overline{\sum} < p_i, \sigma_i | j_\mu | p', \sigma' >< p', \sigma' | {j_\nu}^* | p_i, \sigma_i > (2\pi)\delta({p'}^2 - m_2^2)\,, \tag{4.26}$$

where the delta function coming from the phase space element reads

$$\delta({p'}^2 - m_2^2) = \delta\left((p_i + q)^2 - m_2^2\right) = \delta\left(2\xi(p\cdot q) - (m_2^2 + Q^2)\right) = \frac{1}{2p\cdot q}\delta\left(\xi - \chi\right)\,,$$

in which $\chi = \dfrac{Q^2 + m_2^2}{2p\cdot q} = x\left(1 + \dfrac{m_2^2}{Q^2}\right)$ and the sum leads to

$$\begin{aligned}
\hat{w}^{\mu\nu}_{Ba} &= \frac{\delta\left(\xi - \chi\right)}{2p\cdot q}\frac{1}{4}\mathrm{Tr}\left[\not{p}_i \Gamma^\mu (\not{p}' + m_2)\Gamma^{\nu *}\right] \\
&= \frac{1}{2p\cdot q}\delta\left(\xi - \chi\right)\Big(\\
&\quad 2 g^B_{Ra} g^{B'}_{Ra}\left\{-g^{\mu\nu}(p_i\cdot p') + p_i^\mu p'^\nu + p_i^\nu p'^\mu + i\epsilon^{\mu\nu\rho\sigma} p_{i\rho} p'_\sigma\right\} \\
&+ \quad 2 g^B_{La} g^{B'}_{La}\left\{-g^{\mu\nu}(p_i\cdot p') + p_i^\mu p'^\nu + p_i^\nu p'^\mu - i\epsilon^{\mu\nu\rho\sigma} p_{i\rho} {p'}_\sigma\right\}\Big)\,.
\end{aligned} \tag{4.27}$$

Note that the average over the polarization of the parton a gives a factor $\frac{1}{2}$.

Structure functions Using the projectors Eq. (4.25) one can obtain the following expressions for the contribution of a single quark $Q_1(m_1 = 0)$ to the various the structure functions

$$\begin{aligned}
F_1 &= \int \frac{d\xi}{\xi}\frac{\delta(\xi - \chi)}{2(p\cdot q)}(2p\cdot q)\xi(g^B_{La} g^{B'}_{La} + g^B_{Ra} g^{B'}_{Ra}) Q(\xi) = (g^B_{La} g^{B'}_{La} + g^B_{Ra} g^{B'}_{Ra}) Q(\chi)\,, \\
F_2 &= \int \frac{d\xi}{\xi}\frac{\delta(\xi - \chi)}{2(p\cdot q)} 4M_p^2 (g^B_{La} g^{B'}_{La} + g^B_{Ra} g^{B'}_{Ra})\xi^2 \frac{\nu}{M_p} Q(\xi) = 2\chi(g^B_{La} g^{B'}_{La} + g^B_{Ra} g^{B'}_{Ra}) Q(\chi)\,, \\
F_3 &= \int \frac{d\xi}{\xi}\frac{\delta(\xi - \chi)}{2(p\cdot q)} 4M_p^2 \xi (g^B_{La} g^{B'}_{La} - g^B_{Ra} g^{B'}_{Ra})\frac{\nu}{M_p} Q(\xi) = 2(g^B_{La} g^{B'}_{La} - g^B_{Ra} g^{B'}_{Ra}) Q(\chi)\,.
\end{aligned} \tag{4.28}$$

For quarks different from the bottom quark, χ reduces to the Bjorken x variable and F_1, F_2 satisfy the Callan-Gross relation $F_2 = 2xF_1$. This set of equations show how to express the structure functions in terms of the parton density function, $Q(\chi)$, as well as how the top-quark mass modifies this relation. Note that these results are in agreement with results in the literature [285]. The structure functions for the NC and anti-neutrinos are obtained following the same procedure and are not reported here.

4.2.2 Glashow Resonance

The Glashow resonance is the resonant s-channel scattering of anti-electron neutrinos off electrons of the atmosphere

$$\bar{\nu}_e + e^- \to \bar{\nu}_\ell + \ell^-, \ \bar{\nu}_e + e^- \to q + \bar{q}', \tag{4.29}$$

which in the SM peaks around $s \simeq M_W^2 \Rightarrow E_\nu \simeq M_W^2/2m_e \simeq 6.3 \times 10^6$ GeV, which is below the energy threshold of the Pierre Auger Observatory. However, for heavier resonances, the same process, denoted GR$'$, will lead to a resonant cross section for energies much higher and possibly in the region of interest for the Pierre Auger Observatory. Therefore, we review the cross section for this process in presence of a hypothetic heavier resonance W' including the interferences with the SM W-boson.

The differential cross section is obtained from straightforward application of the Feynman rules and can be written as (p_1, p_2 designate incoming momenta while p_a and p_b refer to the outgoing ones)

$$\begin{aligned} d\sigma^{BB'} = d\Omega \ \times \ & \mathcal{D}\frac{g_B^2 g_{B'}^2}{32\pi^2 s} \times \\ & \Big[(p_a \cdot p_2)(p_b \cdot p_1)(g_{+l}^{BB'} g_{+f}^{BB'} + g_{-l}^{BB'} g_{-f}^{BB'}) \\ & + (p_a \cdot p_1)(p_b \cdot p_2)(g_{+l}^{BB'} g_{+f}^{BB'} - g_{-l}^{BB'} g_{-f}^{BB'})\Big] , \end{aligned} \tag{4.30}$$

where $d\Omega$ is the solid angle of the final state fermion f which can be either a quark or a lepton, and

$$\mathcal{D} = \frac{(s - M_B^2)(s - M_{B'}^2) + M_B M_{B'} \Gamma_B \Gamma_{B'}}{[(s - M_B^2)^2 + M_B^2 \Gamma_B^2]\,[(s - M_{B'}^2)^2 + M_{B'}^2 \Gamma_{B'}^2]} . \tag{4.31}$$

Here, $B, B' \in \{W, W'\}$ and Γ_B is the total decay width of a B-boson, which we approximate by the sum of its partial decay widths into two fermions[8]

$$\Gamma_B = \sum_{\{f_i, f_j\}} \Gamma_{B \to f_i \bar{f}_j} = \frac{g_B^2 M_B g_{+f}^{BB}(f_i, \bar{f}_j)}{6\pi} . \tag{4.32}$$

Integrating over the solid angle $d\Omega$ and summing over the gauge bosons B, B' one obtains the total GR cross section

$$\sigma(s) = \sum_{B,B'} \frac{s}{12\pi} g_B^2 g_{B'}^2 g_{+l}^{BB'} g_{+f}^{BB'} \mathcal{D} . \tag{4.33}$$

[8]We estimated using Pythia that the W' decay into a pair of gauge bosons is at the level of 1-2%. Note that there are regions of parameter space where the decay of the new gauge boson into additional scalars may be significant. However, even in that case this would not affect our conclusions.

Collecting the expressions of the cross sections for the various processes of interest we are now in position to discuss numerical results for the cross sections of UHEν in the atmosphere.

4.3 Results and discussion

In this section we present our numerical results for the DIS and GR(GR$'$) cross sections in the SM, SSM as well as in several realization of the $\mathcal{G}_{221}$ class. We study the impact of the new resonances for various masses and explore a special kind of signature: "the pure muon" events. Background and uncertainties are also discussed.

4.3.1 PDF choice

For the CC and NC DIS, we consider an isoscalar target and neglect nuclear effects so that the structure functions are given by the average of the proton and the neutron structure functions, $F_i = (F_i^n + F_i^p)/2$. As is well-known, the UHEν cross sections in DIS are sensitive to the PDFs at very small momentum fractions x down to $x \simeq 10^{-12}$ which results in large uncertainties as shown in Sarkar et al. [281]. On the other hand, the UHE neutrino cross sections are quite insensitive to the lower bound for the Q^2 integration for which we take $Q^2_{\rm min} = 1$ GeV^2. In our calculations we use the next-to-leading order (NLO) ZEUS2002_TR proton PDFs and QCDNUM 16.12 [286] for the scale evolution of the PDFs. Furthermore, for simplicity, we neglect the contributions from the NLO Wilson coefficients which are known to be small. Note that the uncertainties due to the extrapolation of the PDFs into the small-x region and the scale uncertainties are much larger.

4.3.2 Cross Sections

Our total cross sections for CC and NC DIS are displayed in Fig. 4.3 as a function of the incoming neutrino energy E_ν. We have verified that our cross section for CC DIS (red line) agrees with the results by Cooper-Sarkar et al. [281] within a few percent in the entire energy range shown. It exceeds the CC cross section of Gandhi et al. [270] by about 25% at the highest energies $E_\nu = 10^{12}$ GeV. Conversely, our result for the NC cross section (green line) is 15% - 20% below the one in [270].

In addition to the SM results, we present predictions for the total cross sections in the SSM (red and green crosses) assuming $M_{W'} = M_{Z'} = 4$ TeV. The DIS cross sections in the SM and the SSM differ at the 1% level and the corresponding curves lie on top of each other. Similar observations hold for the other $\mathcal{G}_{221}$ models introduced above. This can be seen in Fig. 4.4, where the ratio of the DIS cross sections in the new physics scenario and in the SM is presented. The areas have been obtained by fixing, depending on the model, either $M_{W'} = 4(6)$ TeV or $M_{Z'} = 4(6)$ TeV and by scanning over the allowed range of values for t_ϕ in each model, see Chapter 1. We find that the new physics contributions modify the SM results by at most 1%, which is much smaller than the theoretical uncertainty of the DIS cross sections. Similar results have been obtained for masses of the heavy resonance of 5 TeV. Note that even though it might look peculiar that the cross sections seems larger for $M_{B'} = 6$ TeV than for 3 TeV, this is an artifact of

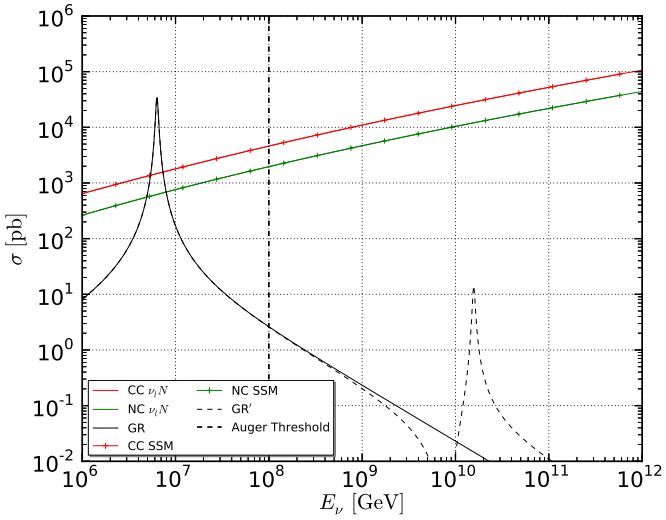

Figure 4.3: Total cross sections for CC $\nu_\mu N$ DIS (red line), NC $\nu_\mu N$ DIS (green line) and the Glashow resonance (solid black line) in dependence of the incoming neutrino energy. The vertical line at $E_\nu = 10^8$ GeV indicates the lower energy threshold of the Auger Observatory. The red and green crosses show the CC DIS and NC DIS cross sections, respectively, in the SSM with $M_{W'} = M_{Z'} = 4$ TeV. The resonant $\bar{\nu}_e e^-$ scattering including the contribution from the W' resonance is represented by the dashed, black line.

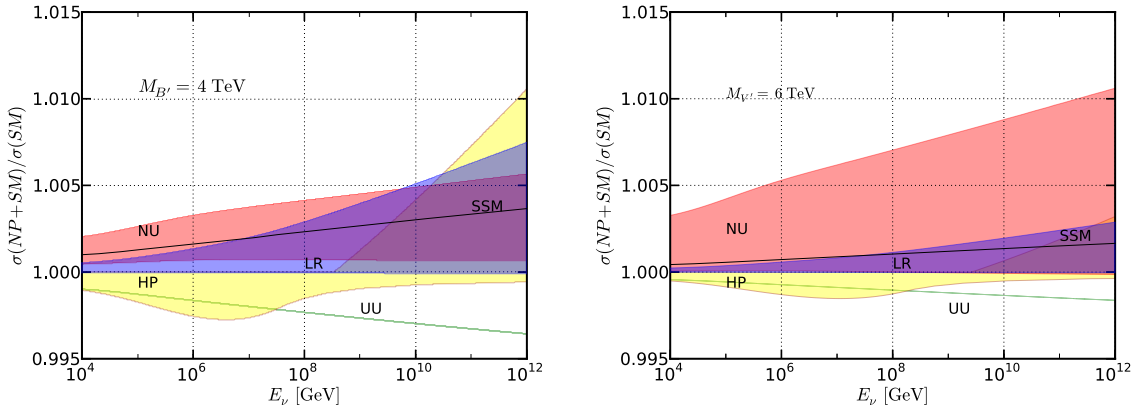

Figure 4.4: The CC+NC $\nu_\mu N$ DIS cross sections in different $\mathcal{G}_{221}$ models scaled to the cross section in the SM. The areas have been obtained by fixing either $M_{W'} = 4(6)$ TeV or $M_{Z'} = 4(6)$ TeV and scanning over the allowed parameter range of the model. For details see Chapter 1 or [74]. For comparison we also show the ratio obtained with the SSM using $M_{W'} = M_{Z'} = 4(6)$ TeV.

the weaker constraints available for 6 TeV and hence of the larger range of allowed values over which we scan. Also interesting is the behaviour of the cross section in the UU model. Indeed, the DIS cross section is roughly proportional to the couplings of the W'-boson to leptons times the couplings to partons, which in this model are proportional to $-t_\phi$, $1/t_\phi$ respectively, see Chapter 1, therefore resulting in this line shape negative ratio. We note that the ratio of the total cross sections could be enhanced by a few more percents by

imposing a suitable minimal x_{min}-cut on the x-integration at the price of reducing the cross sections. Indeed, the dominant contribution to the cross section comes from a region with ultra-small x-values (see Fig. 3 in [287]) and this region is shifted to larger x due to the heavy resonance mass so that a cut on x can considerably reduce the SM DIS cross section while affecting less the result in the SSM. For a similar reason, any suppression of the nuclear PDFs in the small x region due to saturation effects would also lead to an enhanced signal to background ratio. However, an increase of the SM DIS cross section by 1 or 2% is clearly not measurable with the Auger Observatory or any foreseeable UHEν experiment.

In Fig. 4.3, we also show numerical results for the production of hadrons in resonant $\bar{\nu}_e e^-$ scattering in the SM (solid, black line) and in the SSM (dashed, black line). More specifically, we include the contributions with first and second generation quarks in the final state. As can be seen, the GR cross section is more than one order of magnitude larger than the total CC neutrino DIS cross section at the resonance energy $E_\nu = 6.3 \cdot 10^6$ GeV. However, it decreases sharply away from the resonance, and the GR cross section is smaller than the CC DIS cross section by several orders of magnitude for energies greater than the Auger Observatory threshold, i.e. $E_\nu > 10^8$ GeV. On the other hand, the contribution from the W' resonance interferes destructively with the SM amplitude at energies below 10^{10} GeV but leads to a clear enhancement of the cross section in a bin around the W'-resonance energy $E_\nu^{res} = M_{W'}^2/(2m_e) \simeq 1.56 \cdot 10^{10}$ GeV. Still it remains more than two orders of magnitude smaller than the DIS cross sections as can be inferred from Tab. 4.1 where we list the values of the different cross sections at the peak of the resonance with mass $M_{W'} = 4$ TeV. For this reason, the effect of the GR$'$ resonance is irrelevant for events with hadronic showers.

4.3.3 "Pure muon" events

One way to enhance the relative importance of the new physics signal is to consider pure 'muon events' discussed in Ref. [279] as a rather background free signal of the GR (in the SM). The corresponding cross section for the resonant production of an electron or a muon is a factor 1/6 smaller than the one shown in Fig. 4.3 (see rows 3, 4, and 5 in Tab. 4.1). As can be seen, at the resonance, the GR$'$ cross section in the SSM (row 5, column 4) is about 600 times larger than the one from the SM GR (row 5, column 3). However, it is necessary to take into account the non-resonant production of pure muon events which, contrary to the SM case, is more important than the resonant mechanism. The corresponding cross section in the SM, due to the process $\nu_\mu e^- \to \mu^- \nu_e$, can be inferred from Fig. 8 in [270]. It depends only very mildly on the neutrino energy for $E_\nu > 10^8$ GeV and we provide its value at the energy of the W'-resonance in row 7 of Tab. 4.1. For completeness, we also list the cross section for the elastic neutrino scattering (ES) in row 6.

We have not calculated the non-resonant elastic neutrino–electron scattering cross sections including additional W' and Z' bosons but it is reasonable to assume that such contributions will modify the SM result at the low percent level in the SSM and the $\mathcal{G}_{221}$ models when scanning over the allowed parameter range, similar to the DIS case in Fig. 4.4. Therefore, we estimate that the contribution from the GR$'$ resonance enhances the cross section for muon production in the SM by about 7% at the resonance peak.

Table 4.1: Cross sections at $E_\nu = 1.56 \cdot 10^{10}$ GeV in the SM and the SSM assuming $M_{W'} = M_{Z'} = 4$ TeV. The numbers in the 6th and 7th rows have been taken from figure 8 in [270]. The elastic neutrino scattering off electrons into an electron (row 6) receives contributions from the following processes: $\nu_e e^- \to \nu_e e^-, \bar{\nu}_e e^- \to \bar{\nu}_e e^-, \nu_\mu e^- \to \nu_\mu e^-$, and $\bar{\nu}_\mu e^- \to \bar{\nu}_\mu e^-$. The non-resonant production of a muon (row 7) is due to the process $\nu_\mu e^- \to \mu^- \nu_e$.

	Process	σ [pb] (SM)	σ [pb] (SSM)
1.) CC DIS	$\nu_\mu N \to \mu^- + X$	$2.84 \cdot 10^4$	$2.84 \cdot 10^4$
2.) NC DIS	$\nu_\mu N \to \nu_\mu + X$	$1.20 \cdot 10^4$	$1.20 \cdot 10^4$
3.) GR$^{(\prime)}$ to had.	$\bar{\nu}_e e^- \to hadrons$	$6.6 \cdot 10^{-2}$	41.16
4.) GR$^{(\prime)}$ to e^-	$\bar{\nu}_e e^- \to \bar{\nu}_e e^-$	$1.1 \cdot 10^{-2}$	6.86
5.) GR$^{(\prime)}$ to μ^-	$\bar{\nu}_e e^- \to \bar{\nu}_\mu \mu^-$	$1.1 \cdot 10^{-2}$	6.86
6.) ES into e^-	$\nu_e e^- \to \nu_e e^-, \ldots$	154.50	—
7.) ES into μ^-	$\nu_\mu e^- \to \mu^- \nu_e$	102.17	—

Needless to say, that this enhancement gets reduced when calculating event numbers in appropriate energy bins. In addition, we have estimated the background to the pure muon events due to CC DIS events where the hadronic shower energy is below the detection threshold which turns out to be much smaller than the signal so that it can be neglected. The flux of UHEν will not be known with a better precision than the uncertainty of the DIS cross sections at very small x. Therefore, it seems impossible for general reasons that the very precisely known leptonic cross sections can be used to discover new spin-1 W' and Z' resonances. In addition to these general considerations, the Auger Observatory has not yet detected UHEν events. A detector with a much larger acceptance would be required to measure the much smaller UHE neutrino–electron cross sections.

Cosmic-rays of ultra-high energy as measured by the Pierre Auger Observatory are fascinating astrophysical objects. The tremendous energy they carry rank their sources among the most powerful objects in our Universe and studying cosmic-ray properties gives us insight about the most violent processes ever considered and the physics at work in these extreme environments. As we have seen, the GZK cutoff may have already been observed in which case it is likely that neutrinos of extreme energy, $E_\nu > 10^8$ GeV, are being produced by primary cosmic-rays while travelling through the universe. Because neutrinos interact so weakly with matter and propagate without being deflected, detecting events of such energies would be very exciting and promising.

With such an energy, UHEν may allow us to probe new physics scenarios in kinematical regions out of reach for the LHC. In this spirit, we have computed UHEν cross sections in the SSM and $\mathcal{G}_{221}$ models including additional charged and neutral spin-1 resonances. We find that the effects of such resonances are too small to be observed with the Auger Observatory or any foreseeable upgrade of it. Conversely, should such resonances be observed at the LHC or a future hadron collider they will have no measurable impact on

the UHEν events. Any deviation from the SM seen in UHE cosmic neutrino events would require another explanation.

SUMMARY AND OUTLOOK

With the upcoming run of the LHC planned for early 2015, particle physics is more than ever an exciting field of research. The first run of the LHC shed some light on the nature of the electroweak symmetry breaking by unravelling the existence of a scalar spin-0 particle, the Higgs boson. Even though one might have hoped for even more to be discovered during this first stage, it is probably much too early to be over pessimistic. New physics might still be lying right in the soon to be accessible range at the LHC. Since theoretical principles pointing at new physics around the TeV scale are being challenged, it is also the right time to question them.

Among the various scenarios of new physics that will be extensively probed at the LHC next year, we focused in this manuscript on new heavy resonances of spin-1 generically called W'- and Z'-bosons. These resonances are predicted in theories based on an enlarged gauge group like the $\mathcal{G}_{221}$ models in which the SM electroweak gauge group is supplemented by an additional SU(2) group factor. Such extensions are particularly well motivated when they emerge as the low energy limit of theories based on much larger simple gauge groups like SO(10) or E_6. The $\mathcal{G}_{221}$ models based on the $\mathrm{SU}(2)_1 \times \mathrm{SU}(2)_2 \times \mathrm{U}(1)_X$ gauge group have been reviewed in the first chapter of this manuscript. We presented the various realizations of this class, the Left-right, Lepto-phobic, Fermio-phobic, Hadro-phobic, Non-universal and Un-unified models which differ from each other in the particle content and pattern of symmetry breaking. The expressions for the masses and couplings of the new resonances to SM fermions have also been presented and currently available bounds on the parameter space have been reviewed.

Since the measurement of the Higgs mass at $m_H \simeq 125$ GeV, we know that the SM electroweak vacuum can be stable up to a very high scale – at least 10^{10} GeV – without having its internal consistency challenged. Theories beyond the SM usually generate contributions to the effective potential that can modify it drastically and potentially make it unstable at a much lower scale than in the SM. Consequently, requiring the internal consistency of a given model up to a certain scale can lead to stringent constraints on its parameter space. So far, these studies have been limited to simple extensions because the required renormalization group equations for sophisticated models are not known and a calculation by hand is challenging[9]. In Chapter 2, we presented a new tool called PyR@TE, that aims at generating the RGEs for an arbitrary gauge field theory. In PyR@TE, once the gauge group and particle content have been specified, the two-loop RGEs are derived for all the dimensionful as well as dimensionless parameters of the model. After having presented the renormalization group equations for a general gauge

[9]Since the parameters need to be run over a large range of scale values, these RGEs must be known at the two-loop level if one wants to draw any reliable conclusion.

field theory, we reviewed the specificities of PyR@TE and explained in great details its use. To conclude, we used the code to present the complete set of two-loop RGEs for the $\mathcal{G}_{221}$ models concentrating on realizations following the breaking pattern one. We analysed the differences between the various models and showed that the effects of the two-loop contributions can be sizeable.

Chapter 3 was dedicated to a different phenomenological aspect of the $\mathcal{G}_{221}$ models, specifically precision calculations of processes involving top-quarks at the LHC. Indeed, we presented our calculation of the NLO QCD corrections to the electroweak top-pair production and its implementation in a Monte Carlo event generator that allows for a consistent matching of NLO matrix elements and parton shower, the `POWHEG BOX`. To do so, we had to extend the `POWHEG BOX` so that it identifies and properly treats the QED divergences present in the real corrections. After extensive validation, we showed our first numerical results and found that the electroweak top-pair production mediated by a photon can be comparable to the other channel. Various kinematical distributions for a Sequential Standard Model Z'-boson have been obtained by interfacing our `POWHEG BOX` implementation with Pythia 8 for subsequent showering. We explored the impact of the NLO corrections as implemented according to the `POWHEG` method along with the effect of the parton shower. Finally, in the same chapter, we presented our ongoing calculation of the NLO QCD corrections to the single-top production.

The last chapter of this manuscript, Chapter 4, was devoted to the phenomenological study of the impact of new heavy resonances on the interaction of ultra-high energy neutrinos in the atmosphere and the subsequent shower that can be detected by the Pierre Auger Observatory. We focused on $\mathcal{G}_{221}$ models and scanned the allowed parameter space, calculating for each configuration the deep inelastic scattering of neutrinos off nuclei in the atmosphere as well as the Glashow resonance. We found that the modifications to the total cross sections due to new physics are too small to be detected by the Auger Observatory or any upgrade of it. Therefore, if such resonances are found at the LHC or a future collider, there would be no measurable impact on ultra-high energy neutrino events. Any deviation in ultra-high energy neutrino events from the SM would require another explanation.

In the near future, the work presented in this manuscript will be extended in several directions. First, as already discussed there are many ways to extend PyR@TE: (i) include kinetic mixing, (ii) implement the running of the *vevs*, (iii) extend the existing implementation by including higher-order corrections. In addition, PyR@TE is not bounded to the $\mathcal{G}_{221}$ models of course and can be used to perform various phenomenological studies. A publication on the electroweak top-pair production is being finalized and the single-top calculation will be finalized in the coming months with a publication expected in fall. Also, we now have the know-how for such calculations and we can foresee future work in this direction. In addition to all these plans, we will be awaiting with great excitement the new run of the LHC and look for the potential first cracks in the SM.

Appendix A
LIST OF AVAILABLE IRREDUCIBLE REPRESENTATIONS IN PyR@TE

We list below all the gauge groups with their respective irreps available in PyR@TE.

Table A.1: List of all the irreps available in PyR@TE. Note that the True argument for SU(2) represents the conjugate representation.

Gauge Group	Irreps: dimension	Gauge Group	Irreps: dimension
SU(2)	(0,) : 1 (1,) : 2 (1,True) : 2 (2,) : 3 (2,True) : 3 (3,) : 4 (3,True) : 4	SU(4)	(0,0,0) : 1 (0,0,1) : 4 (0,0,2) : 10 (0,1,0) : 6 (1,0,0) : 4 (1,0,1) : 15 (2,0,0) : 10
SU(3)	(0,0) : 1 (0,1) : 3 (0,2) : 6 (0,3) : 10 (1,0) : 3 (1,1) : 8 (2,0) : 6 (3,0) : 10	SU(5)	(0,0,0,0) : 1 (0,0,0,1) : 5 (0,0,0,2) : 15 (0,0,1,0) : 10 (0,1,0,0) : 10 (1,0,0,0) : 5 (1,0,0,1) : 24 (2,0,0,0) : 15
SU(6)	(0,0,0,0,0) : 1 (0,0,0,0,1) : 6 (0,0,0,0,2) : 21 (0,0,0,1,0) : 15 (0,0,1,0,0) : 20 (0,1,0,0,0) : 15 (1,0,0,0,0) : 6 (1,0,0,0,1) : 35 (2,0,0,0,0) : 21	$U(1)_Y$	

Appendix B
DEFINITION OF THE TENSOR AND SCALAR INTEGRALS

Our definition for the tensor, vector and scalar integrals are reviewed below, we follow the definitions of [154].

B.1 Scalar integrals

The tadpole integral is defined by

$$A_0(m) = \frac{\mu^{4-d}}{i\pi^2}\int \frac{d^dk}{(2\pi)^{d-4}}\frac{1}{k^2-m^2+i\varepsilon}\,. \tag{B.1}$$

Performing the Wick rotation to Euclidian space and the integration yields[1]

$$A_0(m) = -\left(\frac{4\pi\mu^2}{m^2}\right)^{\varepsilon}\Gamma(-1+\varepsilon)m^2\,, \tag{B.2}$$

which can be expanded in Laurent series in the following way

$$A_0(m) = m^2\left(\Delta - \log\frac{m^2}{\mu^2}+1\right)\,. \tag{B.3}$$

In the same spirit we define the two point function $B_0(p^2;m_1,m_2)$ by

$$B_0(p^2;m_1,m_2) = \frac{(2\pi\mu)^{4-d}}{i\pi^2}\int\frac{d^dk}{(k^2-m_1^2)((k+p^2)-m_2^2)}\,, \tag{B.4}$$

in which we have suppressed the $i\varepsilon$ term. B_0 can be integrated directly by performing a Wick rotation and inserting Feynman parameters to yield

$$B_0(p^2;m_{1,2}) = \Delta + 2 - \log\frac{m_1m_2}{\mu^2} + \frac{m_1^2-m_2^2}{p^2}\log\frac{m_2}{m_1} - \frac{m_1m_2}{p^2}\left(\frac{1}{r}-r\right)\log r\,, \tag{B.5}$$

where r is and $1/r$ are the solutions of the quadratic equation

$$r^2 + \frac{p^2-m_1^2-m_2^2}{m_1m_2}r + 1 = 0\,. \tag{B.6}$$

[1] Note that we denote ε the dimension parameter $\varepsilon = d-4$.

B.2 Tensor integrals

We can now move to the tensor integrals and we consider in turn B_μ and $B_{\mu\nu}$.

$$B_\mu(p^2;m_1,m_2) = \frac{(2\pi\mu)^{4-d}}{i\pi^2}\int\frac{d^dk k_\mu}{(k^2-m_1^2)((k+p^2)-m_2^2)}\,, \tag{B.7}$$

$$B_{\mu\nu}\left(p^2;m_1,m_2\right) = \frac{(2\pi\mu)^{4-d}}{i\pi^2}\int\frac{d^dk k_\mu k_\nu}{(k^2-m_1^2)((k+p^2)-m_2^2)}\,. \tag{B.8}$$

These integrals are Lorentz-covariant and can therefore be decomposed onto Lorentz-covariant structures in the following way

$$B_\mu = p_\mu B_1\,, \tag{B.9}$$

$$B_{\mu\nu} = g_{\mu\nu}B_{00} + p_\mu p_\nu B_{11}\,, \tag{B.10}$$

in which we have introduced the invariant scalar coefficient functions B_1, B_{00} and B_{11}. To solve this system one has to first invert it

$$B_1 = \frac{1}{2p^2}p^\mu B_\mu\,, \tag{B.11}$$

$$B_{00} = \frac{1}{d-1}\left(g_{\mu\nu}-\frac{p_\mu p_\nu}{p^2}\right)B^{\mu\nu}\,, \tag{B.12}$$

$$B_{11} = \frac{1}{d-1}\frac{1}{p^2}\left(-g_{\mu\nu}+d\frac{p_\mu p_\nu}{p^2}\right)B^{\mu\nu}\,, \tag{B.13}$$

and express it in terms of the scalar integrals

$$B_1 = \frac{1}{p^2}\left(A_0(m_1)-A_0(m_2)-(p^2+m_1^2-m_2^2)B_0(p^2;m_1,m_2)\right)\,, \tag{B.14}$$

$$B_{00} = \frac{1}{2(d-1)}\left(A_0(m_2)+2m_1^2B_0(p^2;m_1,m_2)+(p^2+m_1^2-m_2^2)B_1(p^2;m_1,m_2)\right)\,, \tag{B.15}$$

$$B_{11} = \frac{1}{2(d-1)p^2}\left((d-2)A_0(m_2)-2m_1^2B_0(p^2;m_1,m_2)-d(p^2+m_1^2-m_2^2)B_1(p^2;m_1,m_2)\right)\,. \tag{B.16}$$

Finally, one obtains the expression for the tensor integrals B_μ and $B_{\mu\nu}$

$$B_\mu = \frac{p_\mu}{2p^2}\left(A_0(m_1)-A_0(m_2)-(p^2+m_1^2-m_2^2)B_0(p^2;m_1,m_2)\right)\,, \tag{B.17}$$

$$\begin{aligned}B_{\mu\nu} = \frac{1}{2}\Bigg[&\frac{1}{d-1}\left(g_{\mu\nu}-\frac{p_\mu p_\nu}{p^2}\right)\left(A_0(m_2)+2m_1^2B_0(p^2;m_1,m_2)+(p^2+m_1^2-m_2^2)B_1(p^2;m_1,m_2)\right)\\ &+\frac{p_\mu p_\nu}{p^2}\left(A_0(m_2)-(p^2+m_1^2-m_2^2)B_1(p^2;m_1,m_2)\right)\Bigg]\,.\end{aligned} \tag{B.18}$$

Appendix C
RENORMALIZATION GROUP EQUATIONS FOR THE $\mathcal{G}_{221}$ MODEL

Here we give the full results of the RGEs for the $\mathcal{G}_{221}$ models at two-loop. We start by the quartic couplings and scalar mass terms before completing the gauge couplings RGEs.

C.1 Quartic and scalar mass terms RGEs

We present the model independent parts Δ for the doublet and triplet realizations and then present the dependent parts for each one of the couplings, $\tilde{\beta}_{\lambda_i}$. The complete RGEs for a given coupling λ_i is then given by Eq. (2.213), which re-write here for convenience

$$\beta^{(2)}_{\lambda_i}(M) = \tilde{\beta}^{(2)}_{\lambda_i}(M) + \Delta^{D(T)}_{\lambda_i}\,. \tag{C.1}$$

Note that in the following we will drop the superscript (2).

$$\begin{aligned}\Delta^{D}_{\lambda_\phi} &= -192\lambda^2_{H\phi,1}\lambda_{H\phi,2} - 160\lambda^2_{H\phi,1}\lambda_\phi + 96\lambda^2_{H\phi,1}g_1^2 + 96\lambda^2_{H\phi,1}g_2^2 - 16\lambda^3_{H\phi,2} - 40\lambda^2_{H\phi,2}\lambda_\phi \\ &\quad + 24\lambda^2_{H\phi,2}g_1^2 + 24\lambda^2_{H\phi,2}g_2^2 + 15\lambda_{H\phi,2}g_2^4 - 312\lambda^3_\phi + 36\lambda^2_\phi g_X^2 + 108\lambda^2_\phi g_2^2 + \frac{39}{4}\lambda_\phi g_X^2 g_2^2\end{aligned} \tag{C.2}$$

$$\begin{aligned}\Delta^{D}_{\mu_{H,2}} &= -160\lambda^2_{H,1}\mu_{H,2} - 576\lambda_{H,1}\lambda_{H,2}\mu_{H,1} - 80\lambda_{H,1}\lambda_{H,4}\mu_{H,2} + 48\lambda_{H,1}g_1^2\mu_{H,2} + 48\lambda_{H,1}g_2^2\mu_{H,2} \\ &\quad - 240\lambda^2_{H,2}\mu_{H,2} - 1152\lambda_{H,2}\lambda_{H,3}\mu_{H,1} - 576\lambda_{H,2}\lambda_{H,4}\mu_{H,1} + 288\lambda_{H,2}g_1^2\mu_{H,1} + 288\lambda_{H,2}g_2^2\mu_{H,1} \\ &\quad - 960\lambda^2_{H,3}\mu_{H,2} - 100\lambda^2_{H,4}\mu_{H,2} + 120\lambda_{H,4}g_1^2\mu_{H,2} + 120\lambda_{H,4}g_2^2\mu_{H,2} - 8\lambda^2_{H\phi,1}\mu_{H,2} \\ &\quad - 32\lambda^2_{H\phi,1}\mu_\phi - 32\lambda_{H\phi,1}\lambda_{H\phi,2}\mu_{H,1} - 2\lambda^2_{H\phi,2}\mu_{H,2} - 8\lambda^2_{H\phi,2}\mu_\phi + 8\lambda_{H\phi,2}g_X^2\mu_\phi \\ &\quad + 24\lambda_{H\phi,2}g_2^2\mu_\phi - \frac{3}{16}g_1^4\mu_{H,2} + \frac{45}{8}g_1^2g_2^2\mu_{H,2} + \frac{15}{2}g_2^4\mu_\phi\end{aligned} \tag{C.3}$$

$$\begin{aligned}\Delta^{D}_{\mu_{H,1}} &= -144\lambda_{H,1}\lambda_{H,2}\mu_{H,2} - 384\lambda_{H,1}\lambda_{H,3}\mu_{H,1} - 144\lambda_{H,1}\lambda_{H,4}\mu_{H,1} + 96\lambda_{H,1}g_1^2\mu_{H,1} \\ &\quad + 96\lambda_{H,1}g_2^2\mu_{H,1} - 240\lambda^2_{H,2}\mu_{H,1} - 288\lambda_{H,2}\lambda_{H,3}\mu_{H,2} - 144\lambda_{H,2}\lambda_{H,4}\mu_{H,2} + 72\lambda_{H,2}g_1^2\mu_{H,2} \\ &\quad + 72\lambda_{H,2}g_2^2\mu_{H,2} + 192\lambda^2_{H,3}\mu_{H,1} - 384\lambda_{H,3}\lambda_{H,4}\mu_{H,1} + 288\lambda_{H,3}g_1^2\mu_{H,1} + 288\lambda_{H,3}g_2^2\mu_{H,1} \\ &\quad - 36\lambda^2_{H,4}\mu_{H,1} + 24\lambda_{H,4}g_1^2\mu_{H,1} + 24\lambda_{H,4}g_2^2\mu_{H,1} - 8\lambda^2_{H\phi,1}\mu_{H,1} - 8\lambda_{H\phi,1}\lambda_{H\phi,2}\mu_{H,2} \\ &\quad - 16\lambda_{H\phi,1}\lambda_{H\phi,2}\mu_\phi + 8\lambda_{H\phi,1}g_X^2\mu_\phi + 24\lambda_{H\phi,1}g_2^2\mu_\phi - 2\lambda^2_{H\phi,2}\mu_{H,1} - \frac{243}{16}g_1^4\mu_{H,1} + \frac{45}{8}g_1^2g_2^2\mu_{H,1}\end{aligned} \tag{C.4}$$

$$\Delta^D_{\mu_\phi} = -64\lambda^2_{H\phi,1}\mu_{H,2} - 16\lambda^2_{H\phi,1}\mu_\phi - 128\lambda_{H\phi,1}\lambda_{H\phi,2}\mu_{H,1} + 192\lambda_{H\phi,1}g_1^2\mu_{H,1} + 192\lambda_{H\phi,1}g_2^2\mu_{H,1}$$
$$- 16\lambda^2_{H\phi,2}\mu_{H,2} - 4\lambda^2_{H\phi,2}\mu_\phi + 48\lambda_{H\phi,2}g_1^2\mu_{H,2} + 48\lambda_{H\phi,2}g_2^2\mu_{H,2} - 60\lambda^2_\phi\mu_\phi + 24\lambda_\phi g_X^2\mu_\phi$$
$$+ 72\lambda_\phi g_2^2\mu_\phi + \frac{15}{8}g_X^2g_2^2\mu_\phi + 15g_2^4\mu_{H,2} \tag{C.5}$$

$$\Delta^D_{\lambda_{H,2}} = -1088\lambda^2_{H,1}\lambda_{H,2} - 3840\lambda_{H,1}\lambda_{H,2}\lambda_{H,3} - 1888\lambda_{H,1}\lambda_{H,2}\lambda_{H,4} + 216\lambda_{H,1}\lambda_{H,2}g_1^2$$
$$+ 216\lambda_{H,1}\lambda_{H,2}g_2^2 - 48\lambda_{H,1}\lambda_{H\phi,1}\lambda_{H\phi,2} - 1248\lambda^3_{H,2} - 4992\lambda_{H,2}\lambda^2_{H,3} - 3456\lambda_{H,2}\lambda_{H,3}\lambda_{H,4}$$
$$+ 432\lambda_{H,2}\lambda_{H,3}g_1^2 + 432\lambda_{H,2}\lambda_{H,3}g_2^2 - 1064\lambda_{H,2}\lambda^2_{H,4} + 216\lambda_{H,2}\lambda_{H,4}g_1^2 + 216\lambda_{H,2}\lambda_{H,4}g_2^2$$
$$- 80\lambda_{H,2}\lambda^2_{H\phi,1} - 20\lambda_{H,2}\lambda^2_{H\phi,2} - \frac{51}{8}\lambda_{H,2}g_1^4 + \frac{117}{4}\lambda_{H,2}g_1^2g_2^2 - 96\lambda_{H,3}\lambda_{H\phi,1}\lambda_{H\phi,2}$$
$$- 48\lambda_{H,4}\lambda_{H\phi,1}\lambda_{H\phi,2} - 32\lambda^3_{H\phi,1} - 24\lambda_{H\phi,1}\lambda^2_{H\phi,2} + 8\lambda_{H\phi,1}\lambda_{H\phi,2}g_X^2 + 24\lambda_{H\phi,1}\lambda_{H\phi,2}g_2^2 + \frac{15}{2}\lambda_{H\phi,1}g_2^4 \tag{C.6}$$

$$\Delta^D_{\lambda_{H,3}} = -512\lambda^2_{H,1}\lambda_{H,3} - 480\lambda_{H,1}\lambda^2_{H,2} - 1312\lambda_{H,1}\lambda_{H,3}\lambda_{H,4} + 288\lambda_{H,1}\lambda_{H,3}g_1^2 + 288\lambda_{H,1}\lambda_{H,3}g_2^2$$
$$- 16\lambda_{H,1}\lambda^2_{H\phi,1} - 1248\lambda^2_{H,2}\lambda_{H,3} - 432\lambda^2_{H,2}\lambda_{H,4} + 54\lambda^2_{H,2}g_1^2 + 54\lambda^2_{H,2}g_2^2 - 24\lambda_{H,2}\lambda_{H\phi,1}\lambda_{H\phi,2}$$
$$+ 384\lambda^3_{H,3} - 488\lambda_{H,3}\lambda^2_{H,4} + 72\lambda_{H,3}\lambda_{H,4}g_1^2 + 72\lambda_{H,3}\lambda_{H,4}g_2^2 + 16\lambda_{H,3}\lambda^2_{H\phi,1} - 20\lambda_{H,3}\lambda^2_{H\phi,2}$$
$$- \frac{231}{8}\lambda_{H,3}g_1^4 + \frac{57}{4}\lambda_{H,3}g_1^2g_2^2 - 16\lambda_{H,4}\lambda^2_{H\phi,1} - 16\lambda^2_{H\phi,1}\lambda_{H\phi,2} + 4\lambda^2_{H\phi,1}g_X^2 + 12\lambda^2_{H\phi,1}g_2^2 \tag{C.7}$$

$$\Delta^D_{\lambda_{H,1}} = -192\lambda^3_{H,1} - 1024\lambda^2_{H,1}\lambda_{H,3} - 896\lambda^2_{H,1}\lambda_{H,4} + 96\lambda^2_{H,1}g_1^2 + 96\lambda^2_{H,1}g_2^2 - 3040\lambda_{H,1}\lambda^2_{H,2}$$
$$- 4480\lambda_{H,1}\lambda^2_{H,3} - 2624\lambda_{H,1}\lambda_{H,3}\lambda_{H,4} + 576\lambda_{H,1}\lambda_{H,3}g_1^2 + 576\lambda_{H,1}\lambda_{H,3}g_2^2 - 664\lambda_{H,1}\lambda^2_{H,4}$$
$$+ 120\lambda_{H,1}\lambda_{H,4}g_1^2 + 120\lambda_{H,1}\lambda_{H,4}g_2^2 - 48\lambda_{H,1}\lambda^2_{H\phi,1} - 20\lambda_{H,1}\lambda^2_{H\phi,2} - \frac{171}{8}\lambda_{H,1}g_1^4$$
$$+ \frac{149}{4}\lambda_{H,1}g_1^2g_2^2 - 6208\lambda^2_{H,2}\lambda_{H,3} - 2832\lambda^2_{H,2}\lambda_{H,4} + 324\lambda^2_{H,2}g_1^2 + 324\lambda^2_{H,2}g_2^2 - 144\lambda_{H,2}\lambda_{H\phi,1}\lambda_{H\phi,2}$$
$$+ 768\lambda^3_{H,3} - 4800\lambda^2_{H,3}\lambda_{H,4} + 864\lambda^2_{H,3}g_1^2 + 864\lambda^2_{H,3}g_2^2 - 976\lambda_{H,3}\lambda^2_{H,4} + 144\lambda_{H,3}\lambda_{H,4}g_1^2$$
$$+ 144\lambda_{H,3}\lambda_{H,4}g_2^2 - 96\lambda_{H,3}\lambda^2_{H\phi,1} - 40\lambda_{H,3}\lambda^2_{H\phi,2} - \frac{231}{4}\lambda_{H,3}g_1^4 + \frac{57}{2}\lambda_{H,3}g_1^2g_2^2$$
$$- 228\lambda^3_{H,4} + 78\lambda^2_{H,4}g_1^2 + 78\lambda^2_{H,4}g_2^2 - 72\lambda_{H,4}\lambda^2_{H\phi,1} - 10\lambda_{H,4}\lambda^2_{H\phi,2} + \frac{69}{16}\lambda_{H,4}g_1^4$$
$$+ \frac{165}{8}\lambda_{H,4}g_1^2g_2^2 - 80\lambda^2_{H\phi,1}\lambda_{H\phi,2} + 16\lambda^2_{H\phi,1}g_X^2 + 48\lambda^2_{H\phi,1}g_2^2 - 4\lambda^3_{H\phi,2} + 2\lambda^2_{H\phi,2}g_X^2$$
$$+ 6\lambda^2_{H\phi,2}g_2^2 + \frac{15}{4}\lambda_{H\phi,2}g_2^4 + \frac{291}{32}g_1^6 - \frac{415}{32}g_1^4g_2^2 \tag{C.8}$$

$$
\begin{aligned}
\Delta^D_{\lambda_{H\phi,2}} &= -160\lambda^2_{H,1}\lambda_{H\phi,2} - 576\lambda_{H,1}\lambda_{H,2}\lambda_{H\phi,1} - 80\lambda_{H,1}\lambda_{H,4}\lambda_{H\phi,2} - 320\lambda_{H,1}\lambda^2_{H\phi,1} \\
&- 48\lambda_{H,1}\lambda^2_{H\phi,2} + 48\lambda_{H,1}\lambda_{H\phi,2}g_1^2 + 48\lambda_{H,1}\lambda_{H\phi,2}g_2^2 + 15\lambda_{H,1}g_2^4 - 240\lambda^2_{H,2}\lambda_{H\phi,2} \\
&- 1152\lambda_{H,2}\lambda_{H,3}\lambda_{H\phi,1} - 576\lambda_{H,2}\lambda_{H,4}\lambda_{H\phi,1} - 576\lambda_{H,2}\lambda_{H\phi,1}\lambda_{H\phi,2} + 288\lambda_{H,2}\lambda_{H\phi,1}g_1^2 \\
&+ 288\lambda_{H,2}\lambda_{H\phi,1}g_2^2 - 960\lambda^2_{H,3}\lambda_{H\phi,2} - 768\lambda_{H,3}\lambda^2_{H\phi,1} - 100\lambda^2_{H,4}\lambda_{H\phi,2} - 224\lambda_{H,4}\lambda^2_{H\phi,1} \\
&- 120\lambda_{H,4}\lambda^2_{H\phi,2} + 120\lambda_{H,4}\lambda_{H\phi,2}g_1^2 + 120\lambda_{H,4}\lambda_{H\phi,2}g_2^2 + \frac{75}{2}\lambda_{H,4}g_2^4 - 152\lambda^2_{H\phi,1}\lambda_{H\phi,2} \\
&- 288\lambda^2_{H\phi,1}\lambda_\phi + 4\lambda^2_{H\phi,1}g_X^2 + 12\lambda^2_{H\phi,1}g_1^2 + 24\lambda^2_{H\phi,1}g_2^2 - 14\lambda^3_{H\phi,2} - 72\lambda^2_{H\phi,2}\lambda_\phi \\
&+ \lambda^2_{H\phi,2}g_X^2 + 3\lambda^2_{H\phi,2}g_1^2 + 6\lambda^2_{H\phi,2}g_2^2 - 60\lambda_{H\phi,2}\lambda^2_\phi + 24\lambda_{H\phi,2}\lambda_\phi g_X^2 \\
&+ 72\lambda_{H\phi,2}\lambda_\phi g_2^2 + \frac{15}{8}\lambda_{H\phi,2}g_X^2g_2^2 - \frac{3}{16}\lambda_{H\phi,2}g_1^4 + \frac{45}{8}\lambda_{H\phi,2}g_1^2g_2^2 \qquad \text{(C.9)} \\
&+ \frac{45}{2}\lambda_\phi g_2^4 - \frac{45}{16}g_X^2g_2^4 - \frac{135}{16}g_1^2g_2^4 \qquad \text{(C.10)} \\
\Delta^D_{\lambda_{H,4}} &= -384\lambda^3_{H,1} - 704\lambda^2_{H,1}\lambda_{H,4} + 48\lambda^2_{H,1}g_1^2 + 48\lambda^2_{H,1}g_2^2 - 1792\lambda_{H,1}\lambda^2_{H,2} - 5632\lambda_{H,1}\lambda^2_{H,3} \\
&- 352\lambda_{H,1}\lambda^2_{H,4} + 96\lambda_{H,1}\lambda_{H,4}g_1^2 + 96\lambda_{H,1}\lambda_{H,4}g_2^2 - 64\lambda_{H,1}\lambda^2_{H\phi,1} + 15\lambda_{H,1}g_1^4 + 14\lambda_{H,1}g_1^2g_2^2 \\
&+ 15\lambda_{H,1}g_2^4 - 3328\lambda^2_{H,2}\lambda_{H,3} - 2208\lambda^2_{H,2}\lambda_{H,4} + 216\lambda^2_{H,2}g_1^2 + 216\lambda^2_{H,2}g_2^2 - 96\lambda_{H,2}\lambda_{H\phi,1}\lambda_{H\phi,2} \\
&- 3456\lambda^2_{H,3}\lambda_{H,4} - 128\lambda_{H,3}\lambda^2_{H\phi,1} - 456\lambda^3_{H,4} + 156\lambda^2_{H,4}g_1^2 + 156\lambda^2_{H,4}g_2^2 - 16\lambda_{H,4}\lambda^2_{H\phi,1} \\
&- 20\lambda_{H,4}\lambda^2_{H\phi,2} + \frac{69}{8}\lambda_{H,4}g_1^4 + \frac{69}{4}\lambda_{H,4}g_1^2g_2^2 - 32\lambda^2_{H\phi,1}\lambda_{H\phi,2} - 8\lambda^3_{H\phi,2} + 4\lambda^2_{H\phi,2}g_X^2 \\
&+ 12\lambda^2_{H\phi,2}g_2^2 + \frac{15}{2}\lambda_{H\phi,2}g_2^4 + \frac{291}{16}g_1^6 - \frac{191}{16}g_1^4g_2^2 \qquad \text{(C.11)} \\
\Delta^D_{\lambda_{H\phi,1}} &= -144\lambda_{H,1}\lambda_{H,2}\lambda_{H\phi,2} - 384\lambda_{H,1}\lambda_{H,3}\lambda_{H\phi,1} - 144\lambda_{H,1}\lambda_{H,4}\lambda_{H\phi,1} \\
&- 160\lambda_{H,1}\lambda_{H\phi,1}\lambda_{H\phi,2} + 96\lambda_{H,1}\lambda_{H\phi,1}g_1^2 + 96\lambda_{H,1}\lambda_{H\phi,1}g_2^2 - 240\lambda^2_{H,2}\lambda_{H\phi,1} - 288\lambda_{H,2}\lambda_{H,3} \\
&\lambda_{H\phi,2} - 144\lambda_{H,2}\lambda_{H,4}\lambda_{H\phi,2} - 288\lambda_{H,2}\lambda^2_{H\phi,1} - 72\lambda_{H,2}\lambda^2_{H\phi,2} + 72\lambda_{H,2}\lambda_{H\phi,2}g_1^2 \\
&+ 72\lambda_{H,2}\lambda_{H\phi,2}g_2^2 + \frac{45}{2}\lambda_{H,2}g_2^4 + 192\lambda^2_{H,3}\lambda_{H\phi,1} - 384\lambda_{H,3}\lambda_{H,4}\lambda_{H\phi,1} - 384\lambda_{H,3}\lambda_{H\phi,1}\lambda_{H\phi,2} \\
&+ 288\lambda_{H,3}\lambda_{H\phi,1}g_1^2 + 288\lambda_{H,3}\lambda_{H\phi,1}g_2^2 - 36\lambda^2_{H,4}\lambda_{H\phi,1} - 112\lambda_{H,4}\lambda_{H\phi,1}\lambda_{H\phi,2} \\
&+ 24\lambda_{H,4}\lambda_{H\phi,1}g_1^2 + 24\lambda_{H,4}\lambda_{H\phi,1}g_2^2 - 56\lambda^3_{H\phi,1} - 38\lambda_{H\phi,1}\lambda^2_{H\phi,2} - 144\lambda_{H\phi,1}\lambda_{H\phi,2}\lambda_\phi \\
&+ 2\lambda_{H\phi,1}\lambda_{H\phi,2}g_X^2 + 6\lambda_{H\phi,1}\lambda_{H\phi,2}g_1^2 + 12\lambda_{H\phi,1}\lambda_{H\phi,2}g_2^2 - 60\lambda_{H\phi,1}\lambda^2_\phi \\
&+ 24\lambda_{H\phi,1}\lambda_\phi g_X^2 + 72\lambda_{H\phi,1}\lambda_\phi g_2^2 + \frac{15}{8}\lambda_{H\phi,1}g_X^2g_2^2 - \frac{243}{16}\lambda_{H\phi,1}g_1^4 + \frac{45}{8}\lambda_{H\phi,1}g_1^2g_2^2 \\
& \qquad \text{(C.12)}
\end{aligned}
$$

$$
\begin{aligned}
\Delta^T_{\lambda_\phi} &= -32\lambda^2_{H\phi,1}\lambda_\phi + 96\lambda^2_{H\phi,1}g_1^2 + 96\lambda^2_{H\phi,1}g_2^2 - 8\lambda^2_{H\phi,2}\lambda_\phi \\
&\quad + 24\lambda^2_{H\phi,2}g_1^2 + 24\lambda^2_{H\phi,2}g_2^2 - 96\lambda^3_\phi + 40\lambda^2_\phi g_X^2 + 152\lambda^2_\phi g_2^2 \\
&\quad + 24\lambda_\phi g_X^2 g_2^2 - 15 g_X^2 g_2^4 \\
\Delta^T_{\lambda_{H,1}} &= -192\lambda^3_{H,1} - 896\lambda^2_{H,1}\lambda_{H,4} + 96\lambda^2_{H,1}g_1^2 + 96\lambda^2_{H,1}g_2^2 - 4480\lambda_{H,1} \\
&\quad \lambda^2_{H,3} - 664\lambda_{H,1}\lambda^2_{H,4} + 120\lambda_{H,1}\lambda_{H,4}g_1^2 + 120\lambda_{H,1}\lambda_{H,4}g_2^2 - 30\lambda_{H,1}\lambda^2_{H\phi,2} \\
&\quad - \frac{171}{8}\lambda_{H,1}g_1^4 + \frac{149}{4}\lambda_{H,1}g_1^2 g_2^2 - 4800\lambda^2_{H,3}\lambda_{H,4} + 864\lambda^2_{H,3}g_1^2 + 864\lambda^2_{H,3}g_2^2 \\
&\quad - 228\lambda^3_{H,4} + 78\lambda^2_{H,4}g_1^2 + 78\lambda^2_{H,4}g_2^2 - 15\lambda_{H,4}\lambda^2_{H\phi,2} + \frac{69}{16}\lambda_{H,4}g_1^4 + \frac{165}{8}\lambda_{H,4}g_1^2 g_2^2 \\
&\quad + 3\lambda^2_{H\phi,2}g_X^2 + 12\lambda^2_{H\phi,2}g_2^2 + \frac{291}{32}g_1^6 - \frac{415}{32}g_1^4 g_2^2 \qquad \text{(C.13)} \\
\Delta^T_{\lambda_{H,2}} &= -1088\lambda^2_{H,1}\lambda_{H,2} - 3840\lambda_{H,1}\lambda_{H,2}\lambda_{H,3} - 1888\lambda_{H,1}\lambda_{H,2}\lambda_{H,4} \\
&\quad + 216\lambda_{H,1}\lambda_{H,2}g_1^2 + 216\lambda_{H,1}\lambda_{H,2}g_2^2 - 72\lambda_{H,1}\lambda_{H\phi,1}\lambda_{H\phi,2} - 1248\lambda^3_{H,2} - 4992\lambda_{H,2}\lambda^2_{H,3} \\
&\quad - 3456\lambda_{H,2}\lambda_{H,3}\lambda_{H,4} + 432\lambda_{H,2}\lambda_{H,3}g_1^2 + 432\lambda_{H,2}\lambda_{H,3}g_2^2 - 1064\lambda_{H,2}\lambda^2_{H,4} \\
&\quad + 216\lambda_{H,2}\lambda_{H,4}g_1^2 + 216\lambda_{H,2}\lambda_{H,4}g_2^2 - 120\lambda_{H,2}\lambda^2_{H\phi,1} - 30\lambda_{H,2}\lambda^2_{H\phi,2} - \frac{51}{8}\lambda_{H,2}g_1^4 \\
&\quad + \frac{117}{4}\lambda_{H,2}g_1^2 g_2^2 - 144\lambda_{H,3}\lambda_{H\phi,1}\lambda_{H\phi,2} - 72\lambda_{H,4}\lambda_{H\phi,1}\lambda_{H\phi,2} + 12\lambda_{H\phi,1}\lambda_{H\phi,2}g_X^2 \\
&\quad + 48\lambda_{H\phi,1}\lambda_{H\phi,2}g_2^2 \qquad \text{(C.14)} \\
\Delta^T_{\lambda_{H,3}} &= -512\lambda^2_{H,1}\lambda_{H,3} - 480\lambda_{H,1}\lambda^2_{H,2} - 1312\lambda_{H,1}\lambda_{H,3}\lambda_{H,4} \\
&\quad + 288\lambda_{H,1}\lambda_{H,3}g_1^2 + 288\lambda_{H,1}\lambda_{H,3}g_2^2 - 24\lambda_{H,1}\lambda^2_{H\phi,1} - 1248\lambda^2_{H,2}\lambda_{H,3} - 432\lambda^2_{H,2}\lambda_{H,4} \\
&\quad + 54\lambda^2_{H,2}g_1^2 + 54\lambda^2_{H,2}g_2^2 - 36\lambda_{H,2}\lambda_{H\phi,1}\lambda_{H\phi,2} + 384\lambda^3_{H,3} - 488\lambda_{H,3}\lambda^2_{H,4} \\
&\quad + 72\lambda_{H,3}\lambda_{H,4}g_1^2 + 72\lambda_{H,3}\lambda_{H,4}g_2^2 + 24\lambda_{H,3}\lambda^2_{H\phi,1} - 30\lambda_{H,3}\lambda^2_{H\phi,2} - \frac{231}{8}\lambda_{H,3}g_1^4 \\
&\quad + \frac{57}{4}\lambda_{H,3}g_1^2 g_2^2 - 24\lambda_{H,4}\lambda^2_{H\phi,1} + 6\lambda^2_{H\phi,1}g_X^2 + 24\lambda^2_{H\phi,1}g_2^2 \qquad \text{(C.15)} \\
\Delta^T_{\lambda_{H,4}} &= -384\lambda^3_{H,1} - 704\lambda^2_{H,1}\lambda_{H,4} + 48\lambda^2_{H,1}g_1^2 + 48\lambda^2_{H,1}g_2^2 \\
&\quad - 1792\lambda_{H,1}\lambda^2_{H,2} - 5632\lambda_{H,1}\lambda^2_{H,3} - 352\lambda_{H,1}\lambda^2_{H,4} + 96\lambda_{H,1}\lambda_{H,4}g_1^2 + 96\lambda_{H,1}\lambda_{H,4}g_2^2 \\
&\quad - 96\lambda_{H,1}\lambda^2_{H\phi,1} + 15\lambda_{H,1}g_1^4 + 14\lambda_{H,1}g_1^2 g_2^2 + 15\lambda_{H,1}g_2^4 - 3328\lambda^2_{H,2}\lambda_{H,3} \\
&\quad - 2208\lambda^2_{H,2}\lambda_{H,4} + 216\lambda^2_{H,2}g_1^2 + 216\lambda^2_{H,2}g_2^2 - 144\lambda_{H,2}\lambda_{H\phi,1}\lambda_{H\phi,2} - 3456\lambda^2_{H,3}\lambda_{H,4} \\
&\quad - 192\lambda_{H,3}\lambda^2_{H\phi,1} - 456\lambda^3_{H,4} + 156\lambda^2_{H,4}g_1^2 + 156\lambda^2_{H,4}g_2^2 - 24\lambda_{H,4}\lambda^2_{H\phi,1} \\
&\quad - 30\lambda_{H,4}\lambda^2_{H\phi,2} + \frac{69}{8}\lambda_{H,4}g_1^4 + \frac{69}{4}\lambda_{H,4}g_1^2 g_2^2 + 6\lambda^2_{H\phi,2}g_X^2 + 24\lambda^2_{H\phi,2}g_2^2 \\
&\quad + \frac{291}{16}g_1^6 - \frac{191}{16}g_1^4 g_2^2 \qquad \text{(C.16)}
\end{aligned}
$$

$$
\begin{aligned}
\Delta^T_{\lambda_{H\phi,1}} &= -144\lambda_{H,1}\lambda_{H,2}\lambda_{H\phi,2} - 384\lambda_{H,1}\lambda_{H,3}\lambda_{H\phi,1} - 144\lambda_{H,1}\lambda_{H,4}\lambda_{H\phi,1} \\
&+ 96\lambda_{H,1}\lambda_{H\phi,1}g_1^2 + 96\lambda_{H,1}\lambda_{H\phi,1}g_2^2 - 240\lambda_{H,2}^2\lambda_{H\phi,1} - 288\lambda_{H,2}\lambda_{H,3}\lambda_{H\phi,2} \\
&- 144\lambda_{H,2}\lambda_{H,4}\lambda_{H\phi,2} + 72\lambda_{H,2}\lambda_{H\phi,2}g_1^2 + 72\lambda_{H,2}\lambda_{H\phi,2}g_2^2 + 192\lambda_{H,3}^2\lambda_{H\phi,1} \\
&- 384\lambda_{H,3}\lambda_{H,4}\lambda_{H\phi,1} + 288\lambda_{H,3}\lambda_{H\phi,1}g_1^2 + 288\lambda_{H,3}\lambda_{H\phi,1}g_2^2 - 36\lambda_{H,4}^2\lambda_{H\phi,1} \\
&+ 24\lambda_{H,4}\lambda_{H\phi,1}g_1^2 + 24\lambda_{H,4}\lambda_{H\phi,1}g_2^2 - 60\lambda_{H\phi,1}^3 - 43\lambda_{H\phi,1}\lambda_{H\phi,2}^2 - 32\lambda_{H\phi,1}\lambda_\phi^2 \\
&+ 32\lambda_{H\phi,1}\lambda_\phi g_X^2 + 124\lambda_{H\phi,1}\lambda_\phi g_2^2 + 12\lambda_{H\phi,1}g_X^2 g_2^2 \\
&- \frac{243}{16}\lambda_{H\phi,1}g_1^4 + \frac{45}{8}\lambda_{H\phi,1}g_1^2 g_2^2 \qquad \text{(C.17)} \\
\Delta^T_{\lambda_{H\phi,2}} &= -160\lambda_{H,1}^2\lambda_{H\phi,2} - 576\lambda_{H,1}\lambda_{H,2}\lambda_{H\phi,1} - 80\lambda_{H,1}\lambda_{H,4}\lambda_{H\phi,2} \\
&+ 48\lambda_{H,1}\lambda_{H\phi,2}g_1^2 + 48\lambda_{H,1}\lambda_{H\phi,2}g_2^2 - 240\lambda_{H,2}^2\lambda_{H\phi,2} - 1152\lambda_{H,2}\lambda_{H,3}\lambda_{H\phi,1} \\
&- 576\lambda_{H,2}\lambda_{H,4}\lambda_{H\phi,1} + 288\lambda_{H,2}\lambda_{H\phi,1}g_1^2 + 288\lambda_{H,2}\lambda_{H\phi,1}g_2^2 - 960\lambda_{H,3}^2\lambda_{H\phi,2} \\
&- 100\lambda_{H,4}^2\lambda_{H\phi,2} + 120\lambda_{H,4}\lambda_{H\phi,2}g_1^2 + 120\lambda_{H,4}\lambda_{H\phi,2}g_2^2 - 172\lambda_{H\phi,1}^2\lambda_{H\phi,2} \\
&- 15\lambda_{H\phi,2}^3 - 32\lambda_{H\phi,2}\lambda_\phi^2 + 32\lambda_{H\phi,2}\lambda_\phi g_X^2 + 124\lambda_{H\phi,2}\lambda_\phi g_2^2 + 12\lambda_{H\phi,2}g_X^2 g_2^2 \qquad \text{(C.18)} \\
&- \frac{3}{16}\lambda_{H\phi,2}g_1^4 + \frac{45}{8}\lambda_{H\phi,2}g_1^2 g_2^2 \\
\Delta^T_{\mu_\phi} &= -16\lambda_{H\phi,1}^2\mu_\phi + 192\lambda_{H\phi,1}g_1^2\mu_{H,1} + 192\lambda_{H\phi,1}g_2^2\mu_{H,1} - 4\lambda_{H\phi,2}^2\mu_\phi \\
&+ 48\lambda_{H\phi,2}g_1^2\mu_{H,2} + 48\lambda_{H\phi,2}g_2^2\mu_{H,2} - 32\lambda_\phi^2\mu_\phi + 32\lambda_\phi g_X^2\mu_\phi + 124\lambda_\phi g_2^2\mu_\phi \\
&+ 12g_X^2 g_2^2\mu_\phi \qquad \text{(C.19)} \\
\Delta^T_{\mu_{H,1}} &= -144\lambda_{H,1}\lambda_{H,2}\mu_{H,2} - 384\lambda_{H,1}\lambda_{H,3}\mu_{H,1} - 144\lambda_{H,1}\lambda_{H,4}\mu_{H,1} + 96\lambda_{H,1}g_1^2\mu_{H,1} \\
&+ 96\lambda_{H,1}g_2^2\mu_{H,1} - 240\lambda_{H,2}^2\mu_{H,1} - 288\lambda_{H,2}\lambda_{H,3}\mu_{H,2} - 144\lambda_{H,2}\lambda_{H,4}\mu_{H,2} + 72\lambda_{H,2}g_1^2\mu_{H,2} \\
&+ 72\lambda_{H,2}g_2^2\mu_{H,2} + 192\lambda_{H,3}^2\mu_{H,1} - 384\lambda_{H,3}\lambda_{H,4}\mu_{H,1} + 288\lambda_{H,3}g_1^2\mu_{H,1} + 288\lambda_{H,3}g_2^2\mu_{H,1} \\
&- 36\lambda_{H,4}^2\mu_{H,1} + 24\lambda_{H,4}g_1^2\mu_{H,1} + 24\lambda_{H,4}g_2^2\mu_{H,1} - 12\lambda_{H\phi,1}^2\mu_{H,1} - 12\lambda_{H\phi,1}\lambda_{H\phi,2}\mu_{H,2} \\
&+ 12\lambda_{H\phi,1}g_X^2\mu_\phi + 48\lambda_{H\phi,1}g_2^2\mu_\phi - 3\lambda_{H\phi,2}^2\mu_{H,1} \\
&- \frac{243}{16}g_1^4\mu_{H,1} + \frac{45}{8}g_1^2 g_2^2\mu_{H,1} \qquad \text{(C.20)} \\
\Delta^T_{\mu_{H,2}} &= -160\lambda_{H,1}^2\mu_{H,2} - 576\lambda_{H,1}\lambda_{H,2}\mu_{H,1} - 80\lambda_{H,1}\lambda_{H,4}\mu_{H,2} + 48\lambda_{H,1}g_1^2\mu_{H,2} \\
&+ 48\lambda_{H,1}g_2^2\mu_{H,2} - 240\lambda_{H,2}^2\mu_{H,2} - 1152\lambda_{H,2}\lambda_{H,3}\mu_{H,1} - 576\lambda_{H,2}\lambda_{H,4}\mu_{H,1} + 288\lambda_{H,2}g_1^2\mu_{H,1} \\
&+ 288\lambda_{H,2}g_2^2\mu_{H,1} - 960\lambda_{H,3}^2\mu_{H,2} - 100\lambda_{H,4}^2\mu_{H,2} + 120\lambda_{H,4}g_1^2\mu_{H,2} + 120\lambda_{H,4}g_2^2\mu_{H,2} \\
&- 12\lambda_{H\phi,1}^2\mu_{H,2} - 48\lambda_{H\phi,1}\lambda_{H\phi,2}\mu_{H,1} - 3\lambda_{H\phi,2}^2\mu_{H,2} + 12\lambda_{H\phi,2}g_X^2\mu_\phi \\
&+ 48\lambda_{H\phi,2}g_2^2\mu_\phi - \frac{3}{16}g_1^4\mu_{H,2} + \frac{45}{8}g_1^2 g_2^2\mu_{H,2} \qquad \text{(C.21)} \\
& \qquad \text{(C.22)}
\end{aligned}
$$

LR-D:

$$\tilde{\beta}_{\mu_{H,2}} = \frac{19}{16} g_2^4 \mu_{H,2} \tag{C.23}$$

$$\tilde{\beta}_{\mu_{H,1}} = -\frac{221}{16} g_2^4 \mu_{H,1} \tag{C.24}$$

$$\tilde{\beta}_{\lambda_\phi} = \frac{389}{24} \lambda_\phi g_X^4 - \frac{29}{8} \lambda_\phi g_2^4 - \frac{187}{48} g_X^6 - \frac{367}{48} g_X^4 g_2^2 - \frac{317}{48} g_X^2 g_2^4 + \frac{277}{16} g_2^6 \tag{C.25}$$

$$\tilde{\beta}_{\mu_\phi} = \frac{317}{48} g_X^4 \mu_\phi - \frac{101}{16} g_2^4 \mu_\phi \tag{C.26}$$

$$\tilde{\beta}_{\lambda_{H,2}} = -\frac{29}{8} \lambda_{H,2} g_2^4 \tag{C.27}$$

$$\tilde{\beta}_{\lambda_{H,3}} = -\frac{209}{8} \lambda_{H,3} g_2^4 \tag{C.28}$$

$$\tilde{\beta}_{\lambda_{H,1}} = -\frac{149}{8} \lambda_{H,1} g_2^4 - \frac{209}{4} \lambda_{H,3} g_2^4 + \frac{91}{16} \lambda_{H,4} g_2^4 - \frac{1315}{96} g_1^2 g_2^4 + \frac{277}{32} g_2^6 \tag{C.29}$$

$$\tilde{\beta}_{\lambda_{H\phi,2}} = \frac{317}{48} \lambda_{H\phi,2} g_X^4 - \frac{29}{8} \lambda_{H\phi,2} g_2^4 + \frac{277}{8} g_2^6 \tag{C.30}$$

$$\tilde{\beta}_{\lambda_{H,4}} = \frac{91}{8} \lambda_{H,4} g_2^4 - \frac{587}{48} g_1^2 g_2^4 + \frac{277}{16} g_2^6 \tag{C.31}$$

$$\tilde{\beta}_{\lambda_{H\phi,1}} = \frac{317}{48} \lambda_{H\phi,1} g_X^4 - \frac{149}{8} \lambda_{H\phi,1} g_2^4 \tag{C.32}$$

LP-D:

$$\tilde{\beta}_{\mu_{H,2}} = -\frac{41}{16} g_2^4 \mu_{H,2} \tag{C.33}$$

$$\tilde{\beta}_{\mu_{H,1}} = -\frac{281}{16} g_2^4 \mu_{H,1} \tag{C.34}$$

$$\tilde{\beta}_{\lambda_\phi} = \frac{449}{24} \lambda_\phi g_X^4 - \frac{89}{8} \lambda_\phi g_2^4 - \frac{235}{48} g_X^6 - \frac{415}{48} g_X^4 g_2^2 - \frac{269}{48} g_X^2 g_2^4 + \frac{325}{16} g_2^6 \tag{C.35}$$

$$\tilde{\beta}_{\mu_\phi} = \frac{377}{48} g_X^4 \mu_\phi - \frac{161}{16} g_2^4 \mu_\phi \tag{C.36}$$

$$\tilde{\beta}_{\lambda_{H,2}} = -\frac{89}{8} \lambda_{H,2} g_2^4 \tag{C.37}$$

$$\tilde{\beta}_{\lambda_{H,3}} = -\frac{269}{8} \lambda_{H,3} g_2^4 \tag{C.38}$$

$$\tilde{\beta}_{\lambda_{H,1}} = -\frac{209}{8} \lambda_{H,1} g_2^4 - \frac{269}{4} \lambda_{H,3} g_2^4 + \frac{31}{16} \lambda_{H,4} g_2^4 - \frac{1075}{96} g_1^2 g_2^4 + \frac{325}{32} g_2^6 \tag{C.39}$$

$$\tilde{\beta}_{\lambda_{H\phi,2}} = \frac{377}{48} \lambda_{H\phi,2} g_X^4 - \frac{89}{8} \lambda_{H\phi,2} g_2^4 + \frac{325}{8} g_2^6 \tag{C.40}$$

$$\tilde{\beta}_{\lambda_{H,4}} = \frac{31}{8} \lambda_{H,4} g_2^4 - \frac{539}{48} g_1^2 g_2^4 + \frac{325}{16} g_2^6 \tag{C.41}$$

$$\tilde{\beta}_{\lambda_{H\phi,1}} = \frac{377}{48} \lambda_{Hphi1} g_X^4 - \frac{209}{8} \lambda_{H\phi,1} g_2^4 \tag{C.42}$$

HP-D:

$$\tilde{\beta}_{\mu_{H,2}} = -\frac{161}{16} g_2^4 \mu_{H,2} \tag{C.43}$$

$$\tilde{\beta}_{\mu_{H,1}} = -\frac{401}{16} g_2^4 \mu_{H,1} \tag{C.44}$$

$$\tilde{\beta}_{\lambda_\phi} = \frac{569}{24} \lambda_\phi g_X^4 - \frac{209}{8} \lambda_\phi g_2^4 - \frac{331}{48} g_X^6 - \frac{511}{48} g_X^4 g_2^2 - \frac{173}{48} g_X^2 g_2^4 + \frac{421}{16} g_2^6 \tag{C.45}$$

$$\tilde{\beta}_{\mu_\phi} = \frac{497}{48} g_X^4 \mu_\phi - \frac{281}{16} g_2^4 \mu_\phi \tag{C.46}$$

$$\tilde{\beta}_{\lambda_{H,2}} = -\frac{209}{8} \lambda_{H,2} g_2^4 \tag{C.47}$$

$$\tilde{\beta}_{\lambda_{H,3}} = -\frac{389}{8} \lambda_{H,3} g_2^4 \tag{C.48}$$

$$\tilde{\beta}_{\lambda_{H,1}} = -\frac{329}{8} \lambda_{H,1} g_2^4 - \frac{389}{4} \lambda_{H,3} g_2^4 - \frac{89}{16} \lambda_{H,4} g_2^4 - \frac{595}{96} g_1^2 g_2^4 + \frac{421}{32} g_2^6 \tag{C.49}$$

$$\tilde{\beta}_{\lambda_{H\phi,2}} = \frac{497}{48} \lambda_{H\phi,2} g_X^4 - \frac{209}{8} \lambda_{H\phi,2} g_2^4 + \frac{421}{8} g_2^6 \tag{C.50}$$

$$\tilde{\beta}_{\lambda_{H,4}} = -\frac{89}{8} \lambda_{H,4} g_2^4 - \frac{443}{48} g_1^2 g_2^4 + \frac{421}{16} g_2^6 \tag{C.51}$$

$$\tilde{\beta}_{\lambda_{H\phi,1}} = \frac{497}{48} \lambda_{H\phi,1} g_X^4 - \frac{329}{8} \lambda_{H\phi,1} g_2^4 \tag{C.52}$$

FP-D:

$$\tilde{\beta}_{\mu_{H,2}} = -\frac{221}{16} g_2^4 \mu_{H,2} \tag{C.53}$$

$$\tilde{\beta}_{\mu_{H,1}} = -\frac{461}{16} g_2^4 \mu_{H,1} \tag{C.54}$$

$$\tilde{\beta}_{\lambda_\phi} = \frac{629}{24} \lambda_\phi g_X^4 - \frac{269}{8} \lambda_\phi g_2^4 - \frac{379}{48} g_X^6 - \frac{559}{48} g_X^4 g_2^2 - \frac{125}{48} g_X^2 g_2^4 + \frac{469}{16} g_2^6 \tag{C.55}$$

$$\tilde{\beta}_{\mu_\phi} = \frac{557}{48} g_X^4 \mu_\phi - \frac{341}{16} g_2^4 \mu_\phi \tag{C.56}$$

$$\tilde{\beta}_{\lambda_{H,2}} = -\frac{269}{8} \lambda_{H,2} g_2^4 \tag{C.57}$$

$$\tilde{\beta}_{\lambda_{H,3}} = -\frac{449}{8} \lambda_{H,3} g_2^4 \tag{C.58}$$

$$\tilde{\beta}_{\lambda_{H,1}} = -\frac{389}{8} \lambda_{H,1} g_2^4 - \frac{449}{4} \lambda_{H,3} g_2^4 - \frac{149}{16} \lambda_{H,4} g_2^4 - \frac{355}{96} g_1^2 g_2^4 + \frac{469}{32} g_2^6 \tag{C.59}$$

$$\tilde{\beta}_{\lambda_{H\phi,2}} = \frac{557}{48} \lambda_{H\phi,2} g_X^4 - \frac{269}{8} \lambda_{H\phi,2} g_2^4 + \frac{469}{8} g_2^6 \tag{C.60}$$

$$\tilde{\beta}_{\lambda_{H,4}} = -\frac{149}{8} \lambda_{H,4} g_2^4 - \frac{395}{48} g_1^2 g_2^4 + \frac{469}{16} g_2^6 \tag{C.61}$$

$$\tilde{\beta}_{\lambda_{H\phi,1}} = \frac{557}{48} \lambda_{H\phi,1} g_X^4 - \frac{389}{8} \lambda_{H\phi,1} g_2^4 \tag{C.62}$$

LR-T:

$$\tilde{\beta}_{\lambda_\phi} = \frac{164}{3}\lambda_\phi g_X^4 - \frac{68}{3}\lambda_\phi g_2^4 - \frac{157}{6}g_2^6 \tag{C.63}$$

$$\begin{aligned}\tilde{\beta}_{\lambda_{H,1}} = &-1024\lambda_{H,1}^2\lambda_{H,3} - 3040\lambda_{H,1}\lambda_{H,2}^2 - 2624\lambda_{H,1}\lambda_{H,3}\lambda_{H,4} + 576\lambda_{H,1}\lambda_{H,3}g_1^2 \\ &+ 576\lambda_{H,1}\lambda_{H,3}g_2^2 - 72\lambda_{H,1}\lambda_{H\phi,1}^2 - \frac{83}{8}\lambda_{H,1}g_2^4 - 6208\lambda_{H,2}^2\lambda_{H,3} - 2832\lambda_{H,2}^2 \\ &\lambda_{H,4} + 324\lambda_{H,2}^2 g_1^2 + 324\lambda_{H,2}^2 g_2^2 - 216\lambda_{H,2}\lambda_{H\phi,1}\lambda_{H\phi,2} + 768\lambda_{H,3}^3 - 976\lambda_{H,3}\lambda_{H,4}^2 \\ &+ 144\lambda_{H,3}\lambda_{H,4}g_1^2 + 144\lambda_{H,3}\lambda_{H,4}g_2^2 - 144\lambda_{H,3}\lambda_{H\phi,1}^2 - 60\lambda_{H,3}\lambda_{H\phi,2}^2 - \frac{231}{4}\lambda_{H,3}g_1^4 \\ &+ \frac{57}{2}\lambda_{H,3}g_1^2 g_2^2 - \frac{143}{4}\lambda_{H,3}g_2^4 - 108\lambda_{H,4}\lambda_{H\phi,1}^2 + \frac{157}{16}\lambda_{H,4}g_2^4 + 24\lambda_{H\phi,1}^2 g_X^2 \\ &+ 96\lambda_{H\phi,1}^2 g_2^2 - \frac{1525}{96}g_1^2 g_2^4 + \frac{235}{32}g_2^6\end{aligned} \tag{C.64}$$

$$\tilde{\beta}_{\lambda_{H,2}} = \frac{37}{8}\lambda_{H,2}g_2^4 \tag{C.65}$$

$$\tilde{\beta}_{\lambda_{H,3}} = -\frac{143}{8}\lambda_{H,3}g_2^4 \tag{C.66}$$

$$\tilde{\beta}_{\lambda_{H,4}} = \frac{157}{8}\lambda_{H,4}g_2^4 - \frac{629}{48}g_1^2 g_2^4 + \frac{235}{16}g_2^6 \tag{C.67}$$

$$\tilde{\beta}_{\lambda_{H\phi,1}} = \frac{82}{3}\lambda_{H\phi,1}g_X^4 - \frac{1297}{48}\lambda_{H\phi,1}g_2^4 \tag{C.68}$$

$$\tilde{\beta}_{\lambda_{H\phi,2}} = \frac{82}{3}\lambda_{H\phi,2}g_X^4 - \frac{577}{48}\lambda_{H\phi,2}g_2^4 \tag{C.69}$$

$$\tilde{\beta}_{\mu_\phi} = \frac{82}{3}g_X^4\mu_\phi - \frac{55}{3}g_2^4\mu_\phi \tag{C.70}$$

$$\tilde{\beta}_{\mu_{H,1}} = -\frac{155}{16}g_2^4\mu_{H,1} \tag{C.71}$$

$$\tilde{\beta}_{\mu_{H,2}} = \frac{85}{16}g_2^4\mu_{H,2} \tag{C.72}$$

LP-T:

$$\tilde{\beta}_{\lambda_\phi} = \frac{194}{3}\lambda_\phi g_X^4 - \frac{128}{3}\lambda_\phi g_2^4 - \frac{133}{6}g_2^6 \tag{C.73}$$

$$\begin{aligned}\tilde{\beta}_{\lambda_{H,1}} = &-1024\lambda_{H,1}^2\lambda_{H,3} - 3040\lambda_{H,1}\lambda_{H,2}^2 - 2624\lambda_{H,1}\lambda_{H,3}\lambda_{H,4} \\ &+ 576\lambda_{H,1}\lambda_{H,3}g_1^2 + 576\lambda_{H,1}\lambda_{H,3}g_2^2 - 72\lambda_{H,1}\lambda_{H\phi,1}^2 - \frac{143}{8}\lambda_{H,1}g_2^4 - 6208\lambda_{H,2}^2\lambda_{H,3} \\ &- 2832\lambda_{H,2}^2\lambda_{H,4} + 324\lambda_{H,2}^2 g_1^2 + 324\lambda_{H,2}^2 g_2^2 - 216\lambda_{H,2}\lambda_{H\phi,1}\lambda_{H\phi,2} + 768\lambda_{H,3}^3 \\ &- 976\lambda_{H,3}\lambda_{H,4}^2 + 144\lambda_{H,3}\lambda_{H,4}g_1^2 + 144\lambda_{H,3}\lambda_{H,4}g_2^2 - 144\lambda_{H,3}\lambda_{H\phi,1}^2 - 60\lambda_{H,3}\lambda_{H\phi,2}^2 \\ &- \frac{231}{4}\lambda_{H,3}g_1^4 + \frac{57}{2}\lambda_{H,3}g_1^2 g_2^2 - \frac{203}{4}\lambda_{H,3}g_2^4 - 108\lambda_{H,4}\lambda_{H\phi,1}^2 + \frac{97}{16}\lambda_{H,4}g_2^4 \\ &+ 24\lambda_{H\phi,1}^2 g_X^2 + 96\lambda_{H\phi,1}^2 g_2^2 - \frac{1285}{96}g_1^2 g_2^4 + \frac{283}{32}g_2^6\end{aligned} \tag{C.74}$$

$$\tilde{\beta}_{\lambda_{H,2}} = -\frac{23}{8}\lambda_{H,2}g_2^4 \tag{C.75}$$

$$\tilde{\beta}_{\lambda_{H,3}} = -\frac{203}{8}\lambda_{H,3}g_2^4 \tag{C.76}$$

$$\tilde{\beta}_{\lambda_{H,4}} = \frac{97}{8}\lambda_{H,4}g_2^4 - \frac{581}{48}g_1^2 g_2^4 + \frac{283}{16}g_2^6 \tag{C.77}$$

$$\tilde{\beta}_{\lambda_{H\phi,1}} = \frac{97}{3}\lambda_{H\phi,1}g_X^4 - \frac{1957}{48}\lambda_{H\phi,1}g_2^4 \tag{C.78}$$

$$\tilde{\beta}_{\lambda_{H\phi,2}} = \frac{97}{3}\lambda_{H\phi,2}g_X^4 - \frac{1237}{48}\lambda_{H\phi,2}g_2^4 \tag{C.79}$$

$$\tilde{\beta}_{\mu_\phi} = \frac{97}{3}g_X^4\mu_\phi - \frac{85}{3}g_2^4\mu_\phi \tag{C.80}$$

$$\tilde{\beta}_{\mu_{H,1}} = -\frac{215}{16}g_2^4\mu_{H,1} \tag{C.81}$$

$$\tilde{\beta}_{\mu_{H,2}} = \frac{25}{16}g_2^4\mu_{H,2} \tag{C.82}$$

HP-T:

$$\tilde{\beta}_{\lambda_\phi} = \frac{254}{3}\lambda_\phi g_X^4 - \frac{248}{3}\lambda_\phi g_2^4 - \frac{85}{6}g_2^6 \tag{C.83}$$

$$\begin{aligned}\tilde{\beta}_{\lambda_{H,1}} = {} & 1024\lambda_{H,1}^2\lambda_{H,3} - 1120\lambda_{H,1}\lambda_{H,2}^2 + 2624\lambda_{H,1}\lambda_{H,3}\lambda_{H,4} - 576\lambda_{H,1}\lambda_{H,3}g_1^2 \\ & - 576\lambda_{H,1}\lambda_{H,3}g_2^2 + 24\lambda_{H,1}\lambda_{H\phi,1}^2 - \frac{263}{8}\lambda_{H,1}g_2^4 - 1216\lambda_{H,2}^2\lambda_{H,3} - 1104\lambda_{H,2}^2\lambda_{H,4} \\ & + 108\lambda_{H,2}^2g_1^2 + 108\lambda_{H,2}^2g_2^2 - 72\lambda_{H,2}\lambda_{H\phi,1}\lambda_{H\phi,2} - 768\lambda_{H,3}^3 + 976\lambda_{H,3}\lambda_{H,4}^2 \\ & - 144\lambda_{H,3}\lambda_{H,4}g_1^2 - 144\lambda_{H,3}\lambda_{H,4}g_2^2 - 240\lambda_{H,3}\lambda_{H\phi,1}^2 + 60\lambda_{H,3}\lambda_{H\phi,2}^2 + \frac{231}{4}\lambda_{H,3}g_1^4 \\ & - \frac{57}{2}\lambda_{H,3}g_1^2g_2^2 + \frac{323}{4}\lambda_{H,3}g_2^4 \\ & - 12\lambda_{H,4}\lambda_{H\phi,1}^2 - \frac{23}{16}\lambda_{H,4}g_2^4 - \frac{805}{96}g_1^2g_2^4 + \frac{379}{32}g_2^6\end{aligned} \tag{C.84}$$

$$\tilde{\beta}_{\lambda_{H,2}} = -\frac{143}{8}\lambda_{H,2}g_2^4 \tag{C.85}$$

$$\tilde{\beta}_{\lambda_{H,3}} = -\frac{323}{8}\lambda_{H,3}g_2^4 \tag{C.86}$$

$$\tilde{\beta}_{\lambda_{H,4}} = -\frac{23}{8}\lambda_{H,4}g_2^4 - \frac{485}{48}g_1^2g_2^4 + \frac{379}{16}g_2^6 \tag{C.87}$$

$$\tilde{\beta}_{\lambda_{H\phi,1}} = \frac{127}{3}\lambda_{H\phi,1}g_X^4 - \frac{3277}{48}\lambda_{H\phi,1}g_2^4 \tag{C.88}$$

$$\tilde{\beta}_{\lambda_{H\phi,2}} = \frac{127}{3}\lambda_{H\phi,2}g_X^4 - \frac{2557}{48}\lambda_{H\phi,2}g_2^4 \tag{C.89}$$

$$\tilde{\beta}_{\mu_\phi} = \frac{127}{3}g_X^4\mu_\phi - \frac{145}{3}g_2^4\mu_\phi \tag{C.90}$$

$$\tilde{\beta}_{\mu_{H,1}} = -\frac{335}{16}g_2^4\mu_{H,1} \tag{C.91}$$

$$\tilde{\beta}_{\mu_{H,2}} = -\frac{95}{16}g_2^4\mu_{H,2} \tag{C.92}$$

FP-T:

$$\tilde{\beta}_{\lambda_\phi} = \frac{284}{3}\lambda_\phi g_X^4 - \frac{308}{3}\lambda_\phi g_2^4 - \frac{61}{6}g_2^6 \tag{C.93}$$

$$\begin{aligned}\tilde{\beta}_{\lambda_{H,1}} &= -1024\lambda_{H,1}^2\lambda_{H,3} - 3040\lambda_{H,1}\lambda_{H,2}^2 - 2624\lambda_{H,1}\lambda_{H,3}\lambda_{H,4} + 576\lambda_{H,1}\lambda_{H,3}g_1^2 \\ &+ 576\lambda_{H,1}\lambda_{H,3}g_2^2 - 72\lambda_{H,1}\lambda_{H\phi,1}^2 - \frac{323}{8}\lambda_{H,1}g_2^4 - 6208\lambda_{H,2}^2\lambda_{H,3} - 2832\lambda_{H,2}^2\lambda_{H,4} \\ &+ 324\lambda_{H,2}^2g_1^2 + 324\lambda_{H,2}^2g_2^2 - 216\lambda_{H,2}\lambda_{H\phi,1}\lambda_{H\phi,2} + 768\lambda_{H,3}^3 - 976\lambda_{H,3}\lambda_{H,4}^2 \\ &+ 144\lambda_{H,3}\lambda_{H,4}g_1^2 + 144\lambda_{H,3}\lambda_{H,4}g_2^2 - 144\lambda_{H,3}\lambda_{H\phi,1}^2 - 60\lambda_{H,3}\lambda_{H\phi,2}^2 - \frac{231}{4}\lambda_{H,3}g_1^4 \\ &+ \frac{57}{2}\lambda_{H,3}g_1^2g_2^2 - \frac{383}{4}\lambda_{H,3}g_2^4 - 108\lambda_{H,4}\lambda_{H\phi,1}^2 - \frac{83}{16}\lambda_{H,4}g_2^4 + 24\lambda_{H\phi,1}^2g_X^2 \\ &+ 96\lambda_{H\phi,1}^2g_2^2 - \frac{565}{96}g_1^2g_2^4 + \frac{427}{32}g_2^6\end{aligned} \tag{C.94}$$

$$\tilde{\beta}_{\lambda_{H,2}} = -\frac{203}{8}\lambda_{H,2}g_2^4 \tag{C.95}$$

$$\tilde{\beta}_{\lambda_{H,3}} = -\frac{383}{8}\lambda_{H,3}g_2^4 \tag{C.96}$$

$$\tilde{\beta}_{\lambda_{H,4}} = -\frac{83}{8}\lambda_{H,4}g_2^4 - \frac{437}{48}g_1^2g_2^4 + \frac{427}{16}g_2^6 \tag{C.97}$$

$$\tilde{\beta}_{\lambda_{H\phi,1}} = \frac{142}{3}\lambda_{H\phi,1}g_X^4 - \frac{3937}{48}\lambda_{H\phi,1}g_2^4 \tag{C.98}$$

$$\tilde{\beta}_{\lambda_{H\phi,2}} = \frac{142}{3}\lambda_{H\phi,2}g_X^4 - \frac{3217}{48}\lambda_{H\phi,2}g_2^4 \tag{C.99}$$

$$\tilde{\beta}_{\mu_\phi} = \frac{142}{3}g_X^4\mu_\phi - \frac{175}{3}g_2^4\mu_\phi \tag{C.100}$$

$$\tilde{\beta}_{\mu_{H,1}} = -\frac{395}{16}g_2^4\mu_{H,1} \tag{C.101}$$

$$\tilde{\beta}_{\mu_{H,2}} = -\frac{155}{16}g_2^4\mu_{H,2} \tag{C.102}$$

C.2 Gauge couplings RGEs

We now give the two-loop quartic couplings RGEs which complete the set of RGEs for the $\mathcal{G}_{221}$ models.

LR-D:

$$\beta_{g_3} = \frac{1}{3}g_X^2 g_3^3 + \frac{9}{2}g_1^2 g_3^3 + \frac{9}{2}g_2^2 g_3^3 - 26 g_3^5 \tag{C.103}$$

$$\beta_{g_X} = \frac{37}{18}g_X^5 + 3g_X^3 g_1^2 + \frac{9}{2}g_X^3 g_2^2 + \frac{8}{3}g_X^3 g_3^2 \tag{C.104}$$

$$\beta_{g_2} = \frac{3}{2}g_X^2 g_2^3 + 3g_1^2 g_2^3 + \frac{61}{6}g_2^5 + 12 g_2^3 g_3^2 \tag{C.105}$$

$$\beta_{g_X} = g_X^2 g_1^3 + 8 g_1^5 + 3 g_1^3 g_2^2 + 12 g_1^3 g_3^2 \tag{C.106}$$

LP-D:

$$\beta_{g_3} = \frac{1}{3}g_X^2 g_3^3 + \frac{9}{2}g_1^2 g_3^3 + \frac{9}{2}g_2^2 g_3^3 - 26 g_3^5 \tag{C.107}$$

$$\beta_{g_X} = \frac{263}{36}g_X^5 + 3g_X^3 g_1^2 + \frac{9}{4}g_X^3 g_2^2 + \frac{8}{3}g_X^3 g_3^2 \tag{C.108}$$

$$\beta_{g_2} = \frac{3}{4}g_X^2 g_2^3 + 3g_1^2 g_2^3 - \frac{25}{12}g_2^5 + 12 g_2^3 g_3^2 \tag{C.109}$$

$$\beta_{g_X} = g_X^2 g_1^3 + 8 g_1^5 + 3 g_1^3 g_2^2 + 12 g_1^3 g_3^2 \tag{C.110}$$

HP-D:

$$\beta_{g_3} = \frac{11}{6}g_X^2 g_3^3 + \frac{9}{2}g_1^2 g_3^3 - 26 g_3^5 \tag{C.111}$$

$$\beta_{g_X} = \frac{209}{36}g_X^5 + 3g_X^3 g_1^2 + \frac{15}{4}g_X^3 g_2^2 + \frac{44}{3}g_X^3 g_3^2 \tag{C.112}$$

$$\beta_{g_2} = \frac{5}{4}g_X^2 g_2^3 + 3g_1^2 g_2^3 - \frac{319}{12}g_2^5 \tag{C.113}$$

$$\beta_{g_X} = g_X^2 g_1^3 + 8 g_1^5 + 3 g_1^3 g_2^2 + 12 g_1^3 g_3^2 \tag{C.114}$$

FP-D:

$$\beta_{g_3} = \frac{11}{6}g_X^2 g_3^3 + \frac{9}{2}g_1^2 g_3^3 - 26 g_3^5 \tag{C.115}$$

$$\beta_{g_X} = \frac{199}{18}g_X^5 + 3g_X^3 g_1^2 + \frac{3}{2}g_X^3 g_2^2 + \frac{44}{3}g_X^3 g_3^2 \tag{C.116}$$

$$\beta_{g_2} = \frac{1}{2}g_X^2 g_2^3 + 3g_1^2 g_2^3 - \frac{233}{6}g_2^5 \tag{C.117}$$

$$\beta_{g_X} = g_X^2 g_1^3 + 8 g_1^5 + 3 g_1^3 g_2^2 + 12 g_1^3 g_3^2 \tag{C.118}$$

LR-T:

$$\beta_{g_3} = \frac{1}{3}g_X^2 g_3^3 + \frac{9}{2}g_1^2 g_3^3 + \frac{9}{2}g_2^2 g_3^3 - 26 g_3^5 \tag{C.119}$$

$$\beta_{g_X} = \frac{122}{9}g_X^5 + 3g_X^3 g_1^2 + 27 g_X^3 g_2^2 + \frac{8}{3}g_X^3 g_3^2 \tag{C.120}$$

$$\beta_{g_2} = 9g_X^2 g_2^3 + 3g_1^2 g_2^3 + \frac{80}{3}g_2^5 + 12 g_2^3 g_3^2 \tag{C.121}$$

$$\beta_{g_X} = g_X^2 g_1^3 + 8g_1^5 + 3g_1^3 g_2^2 + 12 g_1^3 g_3^2 \tag{C.122}$$

LP-T:

$$\beta_{g_3} = \frac{1}{3}g_X^2 g_3^3 + \frac{9}{2}g_1^2 g_3^3 + \frac{9}{2}g_2^2 g_3^3 - 26 g_3^5 \tag{C.123}$$

$$\beta_{g_X} = \frac{677}{36}g_X^5 + 3g_X^3 g_1^2 + \frac{99}{4}g_X^3 g_2^2 + \frac{8}{3}g_X^3 g_3^2 \tag{C.124}$$

$$\beta_{g_2} = \frac{33}{4}g_X^2 g_2^3 + 3g_1^2 g_2^3 + \frac{173}{12}g_2^5 + 12 g_2^3 g_3^2 \tag{C.125}$$

$$\beta_{g_X} = g_X^2 g_1^3 + 8g_1^5 + 3g_1^3 g_2^2 + 12 g_1^3 g_3^2 \tag{C.126}$$

HP-T:

$$\beta_{g_3} = \frac{11}{6}g_X^2 g_3^3 + \frac{9}{2}g_1^2 g_3^3 - 26 g_3^5 \tag{C.127}$$

$$\beta_{g_X} = \frac{623}{36}g_X^5 + 3g_X^3 g_1^2 + \frac{105}{4}g_X^3 g_2^2 + \frac{44}{3}g_X^3 g_3^2 \tag{C.128}$$

$$\beta_{g_2} = \frac{35}{4}g_X^2 g_2^3 + 3g_1^2 g_2^3 - \frac{121}{12}g_2^5 \tag{C.129}$$

$$\beta_{g_X} = g_X^2 g_1^3 + 8g_1^5 + 3g_1^3 g_2^2 + 12 g_1^3 g_3^2 \tag{C.130}$$

FP-T:

$$\beta_{g_3} = \frac{11}{6}g_X^2 g_3^3 + \frac{9}{2}g_1^2 g_3^3 - 26 g_3^5 \tag{C.131}$$

$$\beta_{g_X} = \frac{203}{9}g_X^5 + 3g_X^3 g_1^2 + 24 g_X^3 g_2^2 + \frac{44}{3}g_X^3 g_3^2 \tag{C.132}$$

$$\beta_{g_2} = 8g_X^2 g_2^3 + 3g_1^2 g_2^3 - \frac{67}{3}g_2^5 \tag{C.133}$$

$$\beta_{g_X} = g_X^2 g_1^3 + 8g_1^5 + 3g_1^3 g_2^2 + 12 g_1^3 g_3^2 \tag{C.134}$$

Appendix D
SAMPLE MODEL FILES FOR PyR@TE

Listing D.1: models/G221BPI-LRD.model

```
# YAML 1.1
---
Author: Florian Lyonnet
Date: 21.04.2014
Name: G221BPILRD
#Here we have four gauge group factors
Groups: {'U1': U1, 'SU21': SU2, 'SU22': SU2, 'SU3c': SU3}

################################
#Fermions assumed weyl spinors
################################
Fermions: {
   QbarL: {Gen: 3, Qnb:{ U1: -1/6, SU21: -2, SU22: 1, SU3c: -3}},
   LbarL: {Gen: 3, Qnb:{ U1: 1/2, SU21: -2, SU22: 1, SU3c: 1}},
   LR: {Gen: 3, Qnb:{ U1: -1/2, SU21: 1, SU22: 2, SU3c: 1}},
   QR: {Gen: 3, Qnb:{ U1: 1/6, SU21: 1, SU22: 2, SU3c: 3}},
}

#############
#Real Scalars
#############

RealScalars: {
        #Only for the LR-T variant here we have to add the real triplet
        #phi: {U1: 1, SU21: 1, SU22: 3, SU3c: 1},
        #phic: {U1: -1, SU21: 1, SU22: 3, SU3c: 1},
}

#############################################################################
#Complex Scalars : have to be expressed in terms of Real Scalars see above
#############################################################################

CplxScalars: {
  H: {RealFields: [Pi,I*Sigma], Norm: 1/Sqrt(2), Qnb : {U1: 0, SU21: 2, SU22
      : -2, SU3c: 1}},
  H*: {RealFields: [Pi,-I*Sigma], Norm: 1/Sqrt(2), Qnb : {U1: 0, SU21: -2,
      SU22: 2, SU3c: 1}},
        #In the doublet case we need the complex scalar field and its
            conjugate form
  phi: {RealFields: [phi1,I*phi2], Norm: 1/Sqrt(2), Qnb: {U1: 1/2, SU21: 1,
      SU22: 2, SU3c: 1}},
  phi*: {RealFields: [phi1,-I*phi2], Norm: 1/Sqrt(2), Qnb: {U1: -1/2, SU21:
      1, SU22: -2, SU3c: 1}},
}

Potential: {

#######################################
# All particles must be defined above !
#######################################

QuarticTerms: {
 '\lambda_H1' : {Fields : [H,H,H*,H*], Norm : 1},
 '\lambda_H2' : {Fields : [[H*,H*,H*,H],[H,H,H,H*]], Norm : 1},
 '\lambda_H3' : {Fields : [[H,H,H,H],[H*,H*,H*,H*]], Norm : 1},
```

```
51   '\lambda_H4' : {Fields : [H,H*,H,H*], Norm : 1},
52   #For the LR-T model, replace phi* -> phic
53   '\lambda_Hphi1' : {Fields : [[phi*,phi,H,H],[phi*,phi,H*,H*]], Norm : 1},
54   '\lambda_Hphi2' : {Fields : [phi*,phi,H,H*], Norm : 1},
55   '\lambda_phi' : {Fields : [phi*,phi,phi*,phi], Norm : 1}
56   },
57  ScalarMasses: {
58   #For the LR-T model, replace phi* -> phic
59   '\mu_phi' : {Fields : [phi*,phi], Norm : 1},
60   '\mu_H1' : {Fields : [[H,H],[H*,H*]], Norm : 1},
61   '\mu_H2' : {Fields : [H,H*], Norm : 1}
62   }
63  }
```

Listing D.2: models/SM_BiD.model

```
1   # YAML 1.1
2   ---
3   Author: Florian Lyonnet
4   Date: 9.08.2013
5   Name: SMBiD
6   Groups: {'U1': U1, 'SU2L': SU2, 'SU2R': SU2}
7
8   ##############################
9   #Fermions assumed weyl spinors
10  ##############################
11  Fermions: {
12     QL: {Gen: 3, Qnb:{ U1: 1/6, SU2L: 2, SU2R: 1}},
13     QR: {Gen: 3, Qnb:{ U1: -1/6, SU2L: 1, SU2R: 2}},
14     LL: {Gen: 3, Qnb:{ U1: -1/2, SU2L: 2, SU2R: 1}},
15     LR: {Gen: 3, Qnb:{ U1: 1/2, SU2L: 1, SU2R: 2}},
16  }
17
18  #############
19  #Real Scalars
20  #############
21
22  RealScalars: {
23  }
24
25  ########################################################
26  #Complex Scalars : give names for the real components
27  ########################################################
28
29  CplxScalars: {
30    H: {RealFields: [Pi,I*Sigma], Norm: 1/Sqrt(2), Qnb : {U1: 0, SU2L: 2, SU2R
          : 2}},
31    H*: {RealFields: [Pi,-I*Sigma], Norm: 1/Sqrt(2), Qnb : {U1: 0, SU2L: -2,
          SU2R: -2}}
32  }
33
34  Potential: {
35
36  ######################################
37  # All particles must be defined above !
38  ######################################
39
40  Yukawas:{
41   'Y_{q}': {Fields: [H,QL,QR], Norm: 1},
42   'Y_{l}': {Fields: [H,LL,LR], Norm: 1}
43   },
44  QuarticTerms: {
45  '\lambda_{1}' : {Fields : [H,H*,H,H*], Norm : 1/2}
46   },
47  ScalarMasses: {
48  '\mu_{1}' : {Fields : [H*,H], Norm : 1}
49   }
50  }
```

Listing D.3: models/SMCplexDoubletScalar.model

```
# YAML 1.1
# #This is the A.4 Model of 1203.5106
---
Author: Florian Lyonnet
Date: 26.07.2013
Name: SMCplexDoubletScalar
Groups: {'U1': U1, 'SU2L': SU2, 'SU3c': SU3}

##############################
#Fermions assumed weyl spinors
##############################
Fermions: {
   Qbar: {Gen: 3, Qnb:{ U1: -1/6, SU2L: -2, SU3c: -3}},
   Lbar: {Gen: 3, Qnb:{ U1: 1/2, SU2L: -2, SU3c: 1}},
   uR: {Gen: 3, Qnb:{ U1: 2/3, SU2L: 1, SU3c: [1,0]}},
   dR: {Gen: 3, Qnb:{ U1: -1/3, SU2L: 1, SU3c: 3}},
   eR: {Gen: 3, Qnb:{ U1: -1, SU2L: 1, SU3c: 1}},
}

#############
#Real Scalars
#############

RealScalars: {
}

########################################################
#Complex Scalars : give names for the real components
########################################################

CplxScalars: {
  H: {RealFields: [Pi,I*Sigma], Norm: 1/Sqrt(2), Qnb : {U1: 1/2, SU2L: 2, SU3c: 1}},
  H*: {RealFields: [Pi,-I*Sigma], Norm: 1/Sqrt(2), Qnb : {U1: -1/2, SU2L: -2, SU3c: 1}},
  D: {RealFields: [PiD,I*SigmaD], Norm: 1/Sqrt(2), Qnb : {U1: 1/2, SU2L: 2, SU3c: 1}},
  D*: {RealFields: [PiD,-I*SigmaD], Norm: 1/Sqrt(2), Qnb : {U1: -1/2, SU2L: -2, SU3c: 1}},
}

Potential: {

#######################################
# All particles must be defined above !
#######################################

Yukawas:{
  'Y_{u}': {Fields: [Qbar,uR,H*], Norm: 1},
  'Y_{d}': {Fields: [Qbar,dR,H], Norm: 1},
  'Y_{e}': {Fields: [Lbar,eR,H], Norm: 1}
 },
QuarticTerms: {
'\lambda_{1}' : {Fields : [H,H*,H,H*], Norm : 1/2},
'\lambda_{D}' : {Fields: [D,D*,D,D*], Norm : 1/2},
'\kappa_{D}' : {Fields: [D,D*,H,H*], Norm : 1/2},
'\Pkappa_{D}' : {Fields: [D,H*,H,D*], Norm : 1/2}
 },
ScalarMasses: {
'\mu_{H}' : {Fields : [H,H*], Norm : 1},
'\mu_{D}' : {Fields : [D,D*], Norm : 1}
 }
}
```

Listing D.4: models/SM.model

```
# YAML 1.1
---
Author: Florian Lyonnet
Date: 11.06.2013
Name: SM
Groups: {'U1': U1, 'SU2L': SU2, 'SU3c': SU3}

##############################
#Fermions assumed weyl spinors
##############################
Fermions: {
   Qbar: {Gen: 3, Qnb:{ U1: -1/6, SU2L: -2, SU3c: -3}},
   Lbar: {Gen: 3, Qnb:{ U1: 1/2, SU2L: -2, SU3c: 1}},
   uR: {Gen: 3, Qnb:{ U1: 2/3, SU2L: 1, SU3c: [1,0]}},
   dR: {Gen: 3, Qnb:{ U1: -1/3, SU2L: 1, SU3c: 3}},
   eR: {Gen: 3, Qnb:{ U1: -1, SU2L: 1, SU3c: 1}}
}

#############
#Real Scalars
#############

RealScalars: {
}

########################################################
#Complex Scalars : give names for the real components
########################################################

CplxScalars: {
  H: {RealFields: [Pi,I*Sigma], Norm: 1/Sqrt(2), Qnb : {U1: 1/2, SU2L: 2,
      SU3c: 1}},
  H*: {RealFields: [Pi,-I*Sigma], Norm: 1/Sqrt(2), Qnb : {U1: -1/2, SU2L:
      -2, SU3c: 1}}
}

Potential: {

#######################################
# All particles must be defined above !
#######################################

Yukawas:{
  'Y_{u}': {Fields: [Qbar,uR,H*], Norm: 1},
  'Y_{d}': {Fields: [Qbar,dR,H], Norm: 1},
  'Y_{e}': {Fields: [Lbar,eR,H], Norm: 1}
 },
QuarticTerms: {
'\Lambda_{1}' : {Fields : [H,H*,H,H*], Norm : 1/2}
 },
ScalarMasses: {
'\mu_{1}' : {Fields : [H*,H], Norm : 1}
 }
}
```

Listing D.5: models/ScalarSinglet.model

```
# YAML 1.1
---
Author: Florian Lyonnet
Date: 22.07.2013
Name: ScalarSinglet
Groups: {'U1': U1, 'SU2L': SU2, 'SU3c': SU3}

##############################
#Fermions assumed weyl spinors
##############################
Fermions: {
   Qbar: {Gen: 2, Qnb:{ U1: -1/6, SU2L: -2, SU3c: -3}},
   Lbar: {Gen: 2, Qnb:{ U1: 1/2, SU2L: -2, SU3c: 1}},
   uR: {Gen: 3, Qnb:{ U1: 2/3, SU2L: 1, SU3c: [1,0]}},
   dR: {Gen: 3, Qnb:{ U1: -1/3, SU2L: 1, SU3c: 3}},
   eR: {Gen: 3, Qnb:{ U1: -1, SU2L: 1, SU3c: 1}}
}

############
#Real Scalars
#############

RealScalars: {
  si : {U1: 0, SU2L: 1, SU3c: 1}
}

#########################################################
#Complex Scalars : give names for the real components
#########################################################

CplxScalars: {
  H: {RealFields: [Pi,I*Sigma], Norm: 1/Sqrt(2), Qnb : {U1: 1/2, SU2L: 2,
      SU3c: 1}},
  H*: {RealFields: [Pi,-I*Sigma], Norm: 1/Sqrt(2), Qnb : {U1: -1/2, SU2L:
      -2, SU3c: 1}}
}

Potential: {

#######################################
# All particles must be defined above !
#######################################
 Yukawas:{
  'Y_{u}': {Fields: [Qbar,uR,H*], Norm: 1},
  'Y_{d}': {Fields: [Qbar,dR,H], Norm: 1},
  'Y_{e}': {Fields: [Lbar,eR,H], Norm: 1}
 },

QuarticTerms: {
'\lambda_{1}' : {Fields : [H,H*,H,H*], Norm: 1/2},
 '\lambda_{s}' : {Fields : [si,si,si,si], Norm: 1/2},
 '\kappa_{s}' : {Fields : [H,H*,si,si], Norm: 1/2}
 },

ScalarMasses: {
 '\mu_{1}' : {Fields: [H,H*], Norm: 1},
 '\mu_{s}' : {Fields: [si,si], Norm: 1/2}
 }
}
```

Listing D.6: models/SMSingletDoublet.model

```
# YAML 1.1
---
Author: Florian Lyonnet
Date: 30.07.2013
Name: SMSingletDoublet
Groups: {'U1': U1, 'SU2L': SU2, 'SU3c': SU3}

##############################
#Fermions assumed weyl spinors
##############################
Fermions: {
   Qbar: {Gen: 3, Qnb:{ U1: -1/6, SU2L: -2, SU3c: -3}},
   Lbar: {Gen: 3, Qnb:{ U1: 1/2, SU2L: -2, SU3c: 1}},
   uR: {Gen: 3, Qnb:{ U1: 2/3, SU2L: 1, SU3c: [1,0]}},
   dR: {Gen: 3, Qnb:{ U1: -1/3, SU2L: 1, SU3c: 3}},
   eR: {Gen: 3, Qnb:{ U1: -1, SU2L: 1, SU3c: 1}},
   D: {Gen : 1, Qnb:{ U1:  -1/2, SU2L: 2, SU3c: 1}},
   Dc: {Gen: 1, Qnb:{ U1: 1/2, SU2L: 2,SU3c: 1}},
   S: {Gen: 1, Qnb:{ U1: 0, SU2L: 1, SU3c: 1}}
}

#############
#Real Scalars
#############

RealScalars: {
}

######################################################
#Complex Scalars : give names for the real components
######################################################

CplxScalars: {
  H: {RealFields: [Pi,I*Sigma], Norm: 1/Sqrt(2), Qnb : {U1: 1/2, SU2L: 2,
      SU3c: 1}},
  H*: {RealFields: [Pi,-I*Sigma], Norm: 1/Sqrt(2), Qnb : {U1: -1/2, SU2L:
      -2, SU3c: 1}}
}

Potential: {

#######################################
# All particles must be defined above !
#######################################

Yukawas:{
  'Y_{u}': {Fields: [Qbar,uR,H*], Norm: 1},
  'Y_{d}': {Fields: [Qbar,dR,H], Norm: 1},
  'Y_{e}': {Fields: [Lbar,eR,H], Norm: 1},
  'g_{d}': {Fields: [H,S,D], Norm: 1/Sqrt(2)},
  'g_{u}': {Fields: [H*,S,Dc], Norm: 1/Sqrt(2)}
 },
QuarticTerms: {
 '\lambda_1' : {Fields : [H,H*,H,H*], Norm : 1/2}
 },
ScalarMasses: {
 '\mu_1' : {Fields : [H*,H], Norm : 1},
 },
FermionMasses:{
 '\mD': {Fields: [D,Dc], Norm: 1},
 '\mS': {Fields: [S,S], Norm: 1/2}
}
}
```

Listing D.7: models/SMCplxTriplet.model

```
# YAML 1.1
---
Author: Florian Lyonnet
Date: 9.07.2013
Name: SMCplxTriplet
Groups: {'U1': U1, 'SU2L': SU2, 'SU3c': SU3}

##############################
#Fermions assumed weyl spinors
##############################
Fermions: {
   Qbar: {Gen: 3, Qnb:{ U1: -1/6, SU2L: -2, SU3c: -3}},
   L: {Gen: 3, Qnb:{ U1: -1/2, SU2L: 2, SU3c: 1}},
   uR: {Gen: 3, Qnb:{ U1: 2/3, SU2L: 1, SU3c: 3}},
   dR: {Gen: 3, Qnb:{ U1: -1/3, SU2L: 1, SU3c: 3}},
   eR: {Gen: 3, Qnb:{ U1: -1, SU2L: 1, SU3c: 1}},
   PsiL: {Gen: 1, Qnb: {U1: -1/2, SU2L: 2, SU3c: 1}},
   PsiRbar: {Gen: 1, Qnb: {U1: 1/2, SU2L: -2, SU3c: 1}}
}
#############
#Real Scalars
#############

RealScalars: {
}

#########################################################
#Complex Scalars : give names for the real components
#########################################################
CplxScalars: {
  H: {RealFields: [Pi,I*Sigma], Norm: 1/Sqrt(2), Qnb : {U1: 1/2, SU2L: 2,
      SU3c: 1}},
  H*: {RealFields: [Pi,-I*Sigma], Norm: 1/Sqrt(2), Qnb : {U1: -1/2, SU2L:
      -2, SU3c: 1}},
  T : {RealFields: [T1,I*T2], Norm: 1/Sqrt(2), Qnb: {U1: 1, SU2L : 3, SU3c:
      1}},
  T* : {RealFields: [T1,-I*T2], Norm: 1/Sqrt(2), Qnb: {U1: -1, SU2L : 3,
      SU3c: 1}}
}

Potential: {
#######################################
# All particles must be defined above !
#######################################
###############
#The doublet vector like and the yukawa corresponding to the triplet are not
     included yet
Yukawas:{
  'Y_{u}': {Fields: [H*,Qbar,uR], Norm: 1},
  'f_{L}': {Fields: [T,L,L], Norm: 1/Sqrt(2)},
        'f_{\psi}': {Fields: [T, PsiL,PsiL], Norm: 1/Sqrt(2)}
 },
QuarticTerms: {
'\lambda_{1}' : {Fields : [H,H*,H,H*], Norm : 1/2},
'\lambda_{T}' : {Fields: [T,T*,T,T*], Norm: 1/2},
'\kappa_{T}': {Fields: [T,T*,H,H*], Norm: 1}
 },
ScalarMasses: {
'\mu_{1}' : {Fields : [H,H*], Norm : 1},
 mT : {Fields: [T,T*], Norm: 1/2},
 },
TrilinearTerms: {
 fH : {Fields: [T*,H,H], Norm: 1/Sqrt(2)},
 },
FermionMasses : {
 mD : {Fields: [PsiL,PsiRbar], Norm: 1, latex: \m_D},
 }
}
```

Listing D.8: models/SMTripletDoublet.model

```
# YAML 1.1
---
Author: Florian Lyonnet
Date: 30.07.2013
Name: SMTripletDoublet
Groups: {'U1': U1, 'SU2L': SU2, 'SU3c': SU3}

##############################
#Fermions assumed weyl spinors
##############################
Fermions: {
   Qbar: {Gen: 3, Qnb:{ U1: -1/6, SU2L: -2, SU3c: -3}},
   Lbar: {Gen: 3, Qnb:{ U1: 1/2, SU2L: -2, SU3c: 1}},
   uR: {Gen: 3, Qnb:{ U1: 2/3, SU2L: 1, SU3c: [1,0]}},
   dR: {Gen: 3, Qnb:{ U1: -1/3, SU2L: 1, SU3c: 3}},
   eR: {Gen: 3, Qnb:{ U1: -1, SU2L: 1, SU3c: 1}},
   D: {Gen : 1, Qnb:{ U1:  -1/2, SU2L: 2, SU3c: 1}},
   Dc: {Gen: 1, Qnb:{ U1: 1/2, SU2L: 2,SU3c: 1}},
   T: {Gen: 1, Qnb: { U1: 0, SU2L: 3, SU3c: 1}}
}

#############
#Real Scalars
#############

RealScalars: {
}

#########################################################
#Complex Scalars : give names for the real components
#########################################################

CplxScalars: {
  H: {RealFields: [Pi,I*Sigma], Norm: 1/Sqrt(2), Qnb : {U1: 1/2, SU2L: 2,
      SU3c: 1}},
  H*: {RealFields: [Pi,-I*Sigma], Norm: 1/Sqrt(2), Qnb : {U1: -1/2, SU2L:
      -2, SU3c: 1}}
}

Potential: {

#######################################
# All particles must be defined above !
#######################################

Yukawas:{
  'Y_{u}': {Fields: [Qbar,uR,H*], Norm: 1},
  'Y_{d}': {Fields: [Qbar,dR,H], Norm: 1},
  'Y_{e}': {Fields: [Lbar,eR,H], Norm: 1},
  'g_{d}': {Fields: [T,D,H], Norm: -1},
  'g_{u}': {Fields: [T,Dc,H*] ,Norm: 1}
 },
QuarticTerms: {
 '\lambda_1' : {Fields : [H,H*,H,H*], Norm : 1/2},
 },
ScalarMasses: {
 '\mu_1' : {Fields : [H,H*], Norm : 1},
 },
FermionMasses: {
 'm_{T}' : {Fields: [T,T], Norm: 1/2},
 'm_{D}' : {Fields: [D,Dc], Norm: 1}
}
}
```

Appendix E
TOP-PAIR PRODUCTION: BORN EXPRESSION

For completeness, the complete expression for the Born amplitude squared of the electroweak top-pair production is summarized below. In addition to Eq. (3.38)

$$\begin{aligned}\mathcal{B}_q(B,B') = \frac{2\alpha_{EW}^2}{\hat{s}^2 D_B D_{B'} s_W^4}\Big\{&\hat{s}(\hat{t}-\hat{u})\left(A_B^q B_{B'}^q + A_{B'}^q B_B^q\right)\left(A_B^{\mathrm{t}} B_{B'}^{\mathrm{t}} + A_{B'}^{\mathrm{t}} B_B^{\mathrm{t}}\right) + \\ &\left(A_B^q A_{B'}^q + B_B^q B_{B'}^q\right)\left[\left(\hat{t}^2+\hat{u}^2+4\hat{s}m_{\mathrm{t}}^2-2m_{\mathrm{t}}^4\right)A_B^{\mathrm{t}}A_{B'}^{\mathrm{t}} + \left(\hat{t}^2+\hat{u}^2-2m_{\mathrm{t}}^4\right)B_B^{\mathrm{t}}B_{B'}^{\mathrm{t}}\right]\Big\} \\ &\Big\{\left[(\hat{s}-M_B^2)(\hat{s}-M_{B'}^2)+m_B m_{B'}\Gamma_B\Gamma_{B'}\right] + i\left[(\hat{s}-M_B^2)m_{B'}\Gamma_{B'} - (\hat{s}-M_{B'}^2)m_B\Gamma_B\right]\Big\}\,,\end{aligned} \tag{E.1}$$

we give the expressions for the various definitions

$$\begin{aligned}&D_\gamma = \frac{1}{\hat{s}^2}, && A_\gamma^q = s_W Q_q, \quad A_\gamma^{\mathrm{t}} = s_W Q_u, \quad B_\gamma^q = 0, \quad B_\gamma^{\mathrm{t}} = 0,\\ &D_Z = \frac{1}{(\hat{s}-M_Z^2)^2+m_Z^2\Gamma_Z^2}, && A_Z^q = \frac{a_Z^q}{4c_W}, \quad A_Z^{\mathrm{t}} = \frac{a_Z^u}{4c_W}, \quad B_Z^q = \frac{b_Z^q}{4c_W}, \quad B_Z^{\mathrm{t}} = \frac{b_Z^u}{4c_W},\\ &D_{Z'} = \frac{1}{(\hat{s}-M_{Z'}^2)^2+m_{Z'}^2\Gamma_{Z'}^2}, && A_{Z'}^q = \frac{a_{Z'}^q}{4c_W}, \quad A_{Z'}^{\mathrm{t}} = \frac{a_{Z'}^{\mathrm{t}}}{4c_W}, \quad B_{Z'}^q = \frac{b_{Z'}^q}{4c_W}, \quad B_{Z'}^{\mathrm{t}} = \frac{b_{Z'}^{\mathrm{t}}}{4c_W}.\end{aligned} \tag{E.2}$$

In the above equation, $B, B' \in \{\gamma, Z, Z'\}$, the subscript q denotes the flavor of the incoming massless parton and $\hat{s}$, $\hat{t}$, $\hat{u}$ are the usual partonic Mandelstam variables. Finally, the expression for the total Born matrix element is written in terms of general interference terms as

$$\mathcal{B} = \sum_q \left(\mathcal{B}_q(\gamma,\gamma) + \mathcal{B}_q(Z,Z) + \mathcal{B}_q(Z',Z') + \sum_{B\neq B'}\mathcal{B}_q(B,B')\right). \tag{E.3}$$

Bibliography

[1] G. Arnison et al. Experimental Observation of Isolated Large Transverse Energy Electrons with Associated Missing Energy at s**(1/2) = 540-GeV. *Phys.Lett.*, B122:103–116, 1983.

[2] G. Arnison et al. Experimental Observation of Lepton Pairs of Invariant Mass Around 95-GeV/c**2 at the CERN SPS Collider. *Phys.Lett.*, B126:398–410, 1983.

[3] M. Banner et al. Observation of Single Isolated Electrons of High Transverse Momentum in Events with Missing Transverse Energy at the CERN anti-p p Collider. *Phys.Lett.*, B122:476–485, 1983.

[4] P. Bagnaia et al. Evidence for Z0 to e+ e- at the CERN anti-p p Collider. *Phys.Lett.*, B129:130–140, 1983.

[5] Georges Aad et al. Observation of a new particle in the search for the Standard Model Higgs boson with the ATLAS detector at the LHC. *Phys.Lett.*, B716:1–29, 2012.

[6] Serguei Chatrchyan et al. Observation of a new boson at a mass of 125 GeV with the CMS experiment at the LHC. *Phys.Lett.*, B716:30–61, 2012.

[7] Giuseppe Degrassi, Stefano Di Vita, Joan Elias-Miro, Jose R. Espinosa, Gian F. Giudice, et al. Higgs mass and vacuum stability in the Standard Model at NNLO. *JHEP*, 1208:098, 2012.

[8] Guido Altarelli, B. Mele, and M. Ruiz-Altaba. Searching for New Heavy Vector Bosons in $p\bar{p}$ Colliders. *Z.Phys.*, C45:109, 1989.

[9] R. Martinez and F. Ochoa. Constraints on 3-3-1 models with electroweak Z pole observables and Z' search at LHC. 2014.

[10] J. de Blas, J.M. Lizana, and M. Perez-Victoria. Combining searches of Z' and W' bosons. *JHEP*, 1301:166, 2013.

[11] Christophe Grojean, Ennio Salvioni, and Riccardo Torre. A weakly constrained W' at the early LHC. *JHEP*, 1107:002, 2011.

[12] Ennio Salvioni, Alessandro Strumia, Giovanni Villadoro, and Fabio Zwirner. Non-universal minimal Z' models: present bounds and early LHC reach. *JHEP*, 1003:010, 2010.

[13] Ennio Salvioni, Giovanni Villadoro, and Fabio Zwirner. Minimal Z-prime models: Present bounds and early LHC reach. *JHEP*, 0911:068, 2009.

[14] ATLAS collaboration. Search for high-mass states with one lepton plus missing transverse momentum in *pp* collisions at $\sqrt{s} = 8$ TeV with the ATLAS detector. 2014.

[15] Georges Aad et al. ATLAS search for a heavy gauge boson decaying to a charged lepton and a neutrino in *pp* collisions at $\sqrt{s} = 7$ TeV. *Eur.Phys.J.*, C72:2241, 2012.

[16] Georges Aad et al. Search for a heavy gauge boson decaying to a charged lepton and a neutrino in 1 fb-1 of *pp* collisions at $\sqrt{s} = 7$ TeV using the ATLAS detector. *Phys.Lett.*, B705:28–46, 2011.

[17] Georges Aad et al. Search for high-mass states with one lepton plus missing transverse momentum in proton-proton collisions at $\sqrt{s} = 7$ TeV with the ATLAS detector. *Phys.Lett.*, B701:50–69, 2011.

[18] CMS-PAS-EXO-12-060. Search for leptonic decays of W' bosons in pp collisions at sqrt(s)=8 TeV. 2013.

[19] Serguei Chatrchyan et al. Search for new physics in final states with a lepton and missing transverse energy in pp collisions at the LHC. *Phys.Rev.*, D87(7):072005, 2013.

[20] Serguei Chatrchyan et al. Search for leptonic decays of W' bosons in *pp* collisions at $\sqrt{s} = 7$ TeV. *JHEP*, 1208:023, 2012.

[21] Serguei Chatrchyan et al. Search for a W' boson decaying to a muon and a neutrino in *pp* collisions at $\sqrt{s} = 7$ TeV. *Phys.Lett.*, B701:160–179, 2011.

[22] Vardan Khachatryan et al. Search for a heavy gauge boson W' in the final state with an electron and large missing transverse energy in *pp* collisions at $\sqrt{s} = 7$ TeV. *Phys.Lett.*, B698:21–39, 2011.

[23] Georges Aad et al. Search for high-mass dilepton resonances in pp collisions at $\sqrt{s}$ = 8 TeV with the ATLAS detector. 2014.

[24] ATLAS-CONF-2013-017. Search for high-mass dilepton resonances in 20 fb^{-1} of *pp* collisions at $\sqrt{s} = 8$ TeV with the ATLAS experiment. 2013.

[25] Search for high-mass dilepton resonances in 6.1/fb of pp collisions at sqrt(s)= 8 TeV with the ATLAS experiment. Technical Report ATLAS-CONF-2012-129, CERN, Geneva, Sep 2012.

[26] Georges Aad et al. Search for high-mass resonances decaying to dilepton final states in *pp* collisions at $\sqrt{s} = 7$ TeV with the ATLAS detector. *JHEP*, 1211:138, 2012.

[27] Georges Aad et al. Search for dilepton resonances in *pp* collisions at $\sqrt{s} = 7$ TeV with the ATLAS detector. *Phys.Rev.Lett.*, 107:272002, 2011.

[28] Georges Aad et al. Search for high mass dilepton resonances in *pp* collisions at $\sqrt{s} = 7$ TeV with the ATLAS experiment. *Phys.Lett.*, B700:163–180, 2011.

[29] CMS-PAS-EXO-12-061. Search for Resonances in the Dilepton Mass Distribution in pp Collisions at sqrt(s) = 8 TeV. 2013.

[30] Serguei Chatrchyan et al. Search for heavy narrow dilepton resonances in pp collisions at $\sqrt{s} = 7$ TeV and $\sqrt{s} = 8$ TeV. *Phys.Lett.*, B720:63–82, 2013.

[31] Serguei Chatrchyan et al. Search for narrow resonances in dilepton mass spectra in pp collisions at $\sqrt{s} = 7$ TeV. *Phys.Lett.*, B714:158–179, 2012.

[32] Serguei Chatrchyan et al. Search for Resonances in the Dilepton Mass Distribution in pp Collisions at $\sqrt{s} = 7$ TeV. *JHEP*, 1105:093, 2011.

[33] Georges Aad et al. ATLAS search for new phenomena in dijet mass and angular distributions using pp collisions at $\sqrt{s} = 7$ TeV. *JHEP*, 1301:029, 2013.

[34] Georges Aad et al. Search for heavy neutrinos and right-handed W bosons in events with two leptons and jets in pp collisions at $\sqrt{s} = 7$ TeV with the ATLAS detector. *Eur.Phys.J.*, C72:2056, 2012.

[35] Georges Aad et al. Search for resonant diboson production in the $WW/WZ \to \ell\nu jj$ decay channels with the ATLAS detector at $\sqrt{s} = 7$âĂĽâĂĽTeV. *Phys.Rev.*, D87(11):112006, 2013.

[36] Search for a WZ resonance in the fully leptonic channel using pp collisions at $\sqrt{s} = 8$ TeV with the ATLAS detector. Technical Report ATLAS-CONF-2014-015, CERN, Geneva, Mar 2014.

[37] Georges Aad et al. Search for resonant WZ production in the $WZ \to \ell\nu\ell'\ell'$ channel in $\sqrt{s} = 7$ TeV pp collisions with the ATLAS detector. *Phys.Rev.*, D85:112012, 2012.

[38] Search for resonant WZ âĘŠ 3âĎŞ Î¡ production in 1 âĹŽs = 8 TeV pp collisions with 13 fbâĹŠ1 at ATLAS. Technical Report ATLAS-CONF-2013-015, CERN, Geneva, Mar 2013.

[39] Georges Aad et al. Search for tb resonances in proton-proton collisions at $\sqrt{s} = 7$ TeV with the ATLAS detector. *Phys.Rev.Lett.*, 109:081801, 2012.

[40] Search for $W' \to t\bar{b}$ in proton-proton collisions at a centre-of-mass energy of $\sqrt{s} = 8$ TeV with the ATLAS detector. Technical Report ATLAS-CONF-2013-050, CERN, Geneva, May 2013.

[41] Georges Aad et al. A search for high-mass resonances decaying to $\tau^+\tau^-$ in pp collisions at $\sqrt{s} = 7$ TeV with the ATLAS detector. *Phys.Lett.*, B719:242–260, 2013.

[42] A search for high-mass ditau resonances decaying in the fully hadronic final state in pp collisions at $\sqrt{s} = 8$ TeV with the ATLAS detector. Technical Report ATLAS-CONF-2013-066, CERN, Geneva, Jul 2013.

[43] Georges Aad et al. Search for $t\bar{t}$ resonances in the lepton plus jets final state with ATLAS using 4.7 fb^{-1} of pp collisions at $\sqrt{s} = 7$ TeV. *Phys.Rev.*, D88(1):012004, 2013.

[44] A search for $t\bar{t}$ resonances in the lepton plus jets final state with ATLAS using 14 fb[1] of pp collisions at $\sqrt{s} = 8$ TeV. Technical Report ATLAS-CONF-2013-052, CERN, Geneva, May 2013. Not published in the proceedings.

[45] Georges Aad et al. A search for $t\bar{t}$ resonances with the ATLAS detector in 2.05 fb^{-1} of proton-proton collisions at $\sqrt{s} = 7$ TeV. *Eur.Phys.J.*, C72:2083, 2012.

[46] Georges Aad et al. Search for resonances decaying into top-quark pairs using fully hadronic decays in *pp* collisions with ATLAS at $\sqrt{s} = 7$ TeV. *JHEP*, 1301:116, 2013.

[47] Georges Aad et al. Search for new phenomena in events with three charged leptons at $/sqrts = 7$ TeV with the ATLAS detector. *Phys.Rev.*, D87(5):052002, 2013.

[48] Serguei Chatrchyan et al. Search for heavy neutrinos and W[R] bosons with right-handed couplings in a left-right symmetric model in pp collisions at sqrt(s) = 7 TeV. *Phys.Rev.Lett.*, 109:261802, 2012.

[49] Search for a heavy neutrino and right-handed W of the left-right symmetric model in pp collisions at 8 TeV. Technical Report CMS-PAS-EXO-12-017, CERN, Geneva, 2012.

[50] Serguei Chatrchyan et al. Search for high mass resonances decaying into τ^- lepton pairs in *pp* collisions at $\sqrt{s} = 7$ TeV. *Phys.Lett.*, B716:82–102, 2012.

[51] Serguei Chatrchyan et al. Search for Resonances in the Dijet Mass Spectrum from 7 TeV pp Collisions at CMS. *Phys.Lett.*, B704:123–142, 2011.

[52] Serguei Chatrchyan et al. Search for narrow resonances using the dijet mass spectrum in *pp* collisions at $\sqrt{s} = 8$âĂĽTeV. *Phys.Rev.*, D87(11):114015, 2013.

[53] Search for Narrow Resonances using the Dijet Mass Spectrum with 19.6fb-1 of pp Collisions at sqrts=8 TeV. Technical Report CMS-PAS-EXO-12-059, CERN, Geneva, 2013.

[54] Serguei Chatrchyan et al. Search for a W' or Techni-ρ Decaying into WZ in *pp* Collisions at $\sqrt{s} = 7$ TeV. *Phys.Rev.Lett.*, 109:141801, 2012.

[55] Serguei Chatrchyan et al. Search for exotic resonances decaying into WZ/ZZ in *pp* collisions at $\sqrt{s} = 7$ TeV. *JHEP*, 1302:036, 2013.

[56] Serguei Chatrchyan et al. Search for heavy resonances in the W/Z-tagged dijet mass spectrum in pp collisions at 7 TeV. *Phys.Lett.*, B723:280–301, 2013.

[57] Search for W'/technirho in WZ using leptonic final states. Technical Report CMS-PAS-EXO-12-025, CERN, Geneva, 2013.

[58] Serguei Chatrchyan et al. Search for narrow resonances and quantum black holes in inclusive and *b*-tagged dijet mass spectra from *pp* collisions at $\sqrt{s} = 7$ TeV. *JHEP*, 1301:013, 2013.

[59] Search for Heavy Resonances Decaying into bb and bg Final States in pp Collisions at sqrt(s) = 8 TeV. Technical Report CMS-PAS-EXO-12-023, CERN, Geneva, 2013.

[60] Serguei Chatrchyan et al. Search for anomalous $t\bar{t}$ production in the highly-boosted all-hadronic final state. *JHEP*, 1209:029, 2012.

[61] Serguei Chatrchyan et al. Search for a W ' boson decaying to a bottom quark and a top quark in pp collisions at $\sqrt{s} = 7$ TeV. *Phys.Lett.*, B718:1229–1251, 2013.

[62] Serguei Chatrchyan et al. Search for charge-asymmetric production of W ' bosons in top pair + jet events from pp collisions at $\sqrt{s} = 7$ TeV. *Phys.Lett.*, B717:351–370, 2012.

[63] Ken Hsieh, Kai Schmitz, Jiang-Hao Yu, and C.-P. Yuan. Global Analysis of General SU(2) x SU(2) x U(1) Models with Precision Data. *Phys.Rev.*, D82:035011, 2010.

[64] Qing-Hong Cao, Zhao Li, Jiang-Hao Yu, and C.P. Yuan. Discovery and Identification of W' and Z' in SU(2) x SU(2) x U(1) Models at the LHC. *Phys.Rev.*, D86:095010, 2012.

[65] F. del Aguila and A. Mendez. Low-energy Neutral Current Phenomenology and Grand Unified Theories. *Nucl.Phys.*, B189:212, 1981.

[66] Stephen M. Barr and A. Zee. Neutral Currents and Grand Unification. *Phys.Lett.*, B92:297, 1980.

[67] Aharon Davidson. B^{-}l as the Fourth Color, Quark - Lepton Correspondence, and Natural Masslessness of Neutrinos Within a Generalized Ws Model. *Phys.Rev.*, D20:776, 1979.

[68] Paul Langacker. The Physics of Heavy Z' Gauge Bosons. *Rev.Mod.Phys.*, 81:1199–1228, 2009. 50 pages, 2 figures, review for ARNPS.

[69] F. Del Aguila. The Physics of z-prime bosons. *Acta Phys.Polon.*, B25:1317–1336, 1994.

[70] Mirjam Cvetic and Stephen Godfrey. Discovery and identification of extra gauge bosons. 1995.

[71] R.N. Mohapatra and Jogesh C. Pati. A Natural Left-Right Symmetry. *Phys.Rev.*, D11:2558, 1975.

[72] Rabindra N. Mohapatra and Jogesh C. Pati. Left-Right Gauge Symmetry and an Isoconjugate Model of CP Violation. *Phys.Rev.*, D11:566–571, 1975.

[73] Rabindra N. Mohapatra and Goran Senjanovic. Neutrino Masses and Mixings in Gauge Models with Spontaneous Parity Violation. *Phys.Rev.*, D23:165, 1981.

[74] Tomas Jezo, Michael Klasen, and Ingo Schienbein. LHC phenomenology of general SU(2)xSU(2)xU(1) models. *Phys.Rev.*, D86:035005, 2012.

[75] Y.A. Coutinho, V. Salustino GuimarÃčes, and A.A. Nepomuceno. Bounds on ZâĂš from 3-3-1 model at the LHC energies. *Phys.Rev.*, D87(11):115014, 2013.

[76] E. Ramirez Barreto, Y.A. Coutinho, and J. Sa Borges. Searching for an Extra Neutral Gauge Boson from Muon Pair Production at LHC. *Phys.Lett.*, B689:36–41, 2010.

[77] Hoang Ngoc Long and Vo Thanh Van. Quark family discrimination and flavor changing neutral currents in the SU(3)(C) x SU(3)(L) x U(1) model with right-handed neutrinos. *J.Phys.*, G25:2319–2324, 1999.

[78] James T. Liu. Generation nonuniversality and flavor changing neutral currents in the 331 model. *Phys.Rev.*, D50:542–547, 1994.

[79] Stefano Profumo and Farinaldo S. Queiroz. Constraining the Z' Mass in 331 Models using Direct Dark Matter Detection. 2013.

[80] Alexandre Alves, Stefano Profumo, and Farinaldo S. Queiroz. The dark $Z^{'}$ portal: direct, indirect and collider searches. *JHEP*, 1404:063, 2014.

[81] Haipeng An, Xiangdong Ji, and Lian-Tao Wang. Light Dark Matter and Z' Dark Force at Colliders. *JHEP*, 1207:182, 2012.

[82] D. Cogollo, Alma X. Gonzalez-Morales, Farinaldo S. Queiroz, and Patricia R. Teles. Excluding the Light Dark Matter Window of a 331 Model Using LHC and Direct Dark Matter Detection Data. 2014.

[83] Howard Georgi, Elizabeth Ellen Jenkins, and Elizabeth H. Simmons. UNUNIFYING THE STANDARD MODEL. *Phys.Rev.Lett.*, 62:2789, 1989.

[84] Howard Georgi, Elizabeth Ellen Jenkins, and Elizabeth H. Simmons. THE UNUNIFIED STANDARD MODEL. *Nucl.Phys.*, B331:541, 1990.

[85] Ehab Malkawi, Timothy M.P. Tait, and C.P. Yuan. A Model of strong flavor dynamics for the top quark. *Phys.Lett.*, B385:304–310, 1996.

[86] Xiaoyuan Li and Ernest Ma. GAUGE MODEL OF GENERATION NONUNIVERSALITY. *Phys.Rev.Lett.*, 47:1788, 1981.

[87] Vernon D. Barger, Wai-Yee Keung, and Ernest Ma. A GAUGE MODEL WITH LIGHT W AND Z BOSONS. *Phys.Rev.*, D22:727, 1980.

[88] Vernon D. Barger, Wai-Yee Keung, and Ernest Ma. DOUBLING OF WEAK GAUGE BOSONS IN AN EXTENSION OF THE STANDARD MODEL. *Phys.Rev.Lett.*, 44:1169, 1980.

[89] Paul Langacker. The Standard Model and Beyond, Series in High Energy Physics, Cosmology, And Gravitation. 2009.

[90] K. Nakamura et al. Review of particle physics. *J.Phys.*, G37:075021, 2010.

[91] Tomas Jezo. Z' and W' gauge bosons in SU(2)xSU(2)xU(1) models: Collider phenomenology at LO and NLO QCD. 2013.

[92] Paul Langacker and S. Uma Sankar. Bounds on the Mass of W(R) and the W(L)-W(R) Mixing Angle xi in General SU(2)-L x SU(2)-R x U(1) Models. *Phys.Rev.*, D40:1569–1585, 1989.

[93] C. collaboration.

[94] Marc Sher. Electroweak Higgs Potentials and Vacuum Stability. *Phys.Rept.*, 179:273–418, 1989.

[95] Martin Holthausen, Kher Sham Lim, and Manfred Lindner. Planck scale Boundary Conditions and the Higgs Mass. *JHEP*, 1202:037, 2012.

[96] Hans Peter Nilles. Supersymmetry, supergravity and particle physics. *Phys. Rept.*, 110:1, 1984.

[97] Howard E. Haber and Gordon L. Kane. The Search for Supersymmetry: Probing Physics Beyond the Standard Model. *Phys.Rept.*, 117:75–263, 1985.

[98] Stephen P. Martin. A Supersymmetry primer. 1997.

[99] Ulrich Ellwanger and Cyril Hugonie. NMSPEC: A Fortran code for the sparticle and Higgs masses in the NMSSM with GUT scale boundary conditions. *Comput.Phys.Commun.*, 177:399–407, 2007.

[100] Werner Porod. SPheno, a program for calculating supersymmetric spectra, SUSY particle decays and SUSY particle production at e+ e- colliders. *Comput.Phys.Commun.*, 153:275–315, 2003.

[101] W. Porod and F. Staub. SPheno 3.1: Extensions including flavour, CP-phases and models beyond the MSSM. *Comput.Phys.Commun.*, 183:2458–2469, 2012.

[102] B.C. Allanach. SOFTSUSY: a program for calculating supersymmetric spectra. *Comput.Phys.Commun.*, 143:305–331, 2002.

[103] B.C. Allanach and M.A. Bernhardt. Including R-parity violation in the numerical computation of the spectrum of the minimal supersymmetric standard model: SOFTSUSY. *Comput.Phys.Commun.*, 181:232–245, 2010.

[104] Renato M. Fonseca. Calculating the renormalisation group equations of a SUSY model with Susyno. *Comput.Phys.Commun.*, 183:2298–2306, 2012.

[105] F. Staub. SARAH. 2008.

[106] Florian Staub. From Superpotential to Model Files for FeynArts and CalcHep/-CompHep. *Comput. Phys. Commun.*, 181:1077–1086, 2010.

[107] Florian Staub. Automatic Calculation of supersymmetric Renormalization Group Equations and Self Energies. *Comput.Phys.Commun.*, 182:808–833, 2011.

[108] Florian Staub. SARAH 3.2: Dirac Gauginos, UFO output, and more. *Computer Physics Communications*, 184:pp. 1792–1809, 2013.

[109] F. Lyonnet, I. Schienbein, F. Staub, and A. Wingerter. PyR@TE: Renormalization Group Equations for General Gauge Theories. *Comput.Phys.Commun.*, 185:1130–1152, 2014.

[110] Marie E. Machacek and Michael T. Vaughn. Two Loop Renormalization Group Equations in a General Quantum Field Theory. 1. Wave Function Renormalization. *Nucl.Phys.*, B222:83, 1983.

[111] Marie E. Machacek and Michael T. Vaughn. Two Loop Renormalization Group Equations in a General Quantum Field Theory. 2. Yukawa Couplings. *Nucl.Phys.*, B236:221, 1984.

[112] Marie E. Machacek and Michael T. Vaughn. Two Loop Renormalization Group Equations in a General Quantum Field Theory. 3. Scalar Quartic Couplings. *Nucl.Phys.*, B249:70, 1985.

[113] I. Jack and H. Osborn. Two Loop Background Field Calculations for Arbitrary Background Fields. *Nucl.Phys.*, B207:474, 1982.

[114] I. Jack and H. Osborn. General Two Loop Beta Functions for Gauge Theories With Arbitrary Scalar Fields. *J.Phys.*, A16:1101, 1983.

[115] I. Jack and H. Osborn. General Background Field Calculations With Fermion Fields. *Nucl.Phys.*, B249:472, 1985.

[116] Ming Xing Luo and Yong Xiao. Two-loop renormalization group equations in the standard model. *Phys. Rev. Lett.*, 90:011601, 2003.

[117] Akin Wingerter. Implications of the Stability and Triviality Bounds on the Standard Model with Three and Four Chiral Generations. *Phys.Rev.*, D84:095012, 2011.

[118] Florian Staub. SARAH 4: A tool for (not only SUSY) model builders. *Comput.Phys.Commun.*, 185:1773–1790, 2014.

[119] Clifford Cheung, Michele Papucci, and Kathryn M. Zurek. Higgs and Dark Matter Hints of an Oasis in the Desert. *JHEP*, 1207:105, 2012.

[120] G.F. Giudice and A. Romanino. Split supersymmetry. *Nucl.Phys.*, B699:65–89, 2004.

[121] H.F. Jones. Groups, representations and physics. *Dover Books on Mathematics Series.*, 1990.

[122] Renato Miguel Sousa da Fonseca. Renormalization in supersymmetric models. 2013.

[123] R. Cahn. Semi-simple lie algebras and their representations. 2006.

[124] R. Slansky. Group theory for unified model building. *Phys. Rept.*, 79:1–128, 1981.

[125] T. Muta. Foundations of quantum chromodynamics. 2010 (Third edition).

[126] D.I. Kazakov. Radiative corrections, divergences, regularization, renormalization and renormalization group and all that in examples in quantum field theory. 2008.

[127] Lewis H. Ryder. Quantum field theory. 1996 (second edition).

[128] Steven Weinberg. New approach to the renormalization group. *Phys.Rev.*, D8:3497–3509, 1973.

[129] Murray Gell-Mann and F.E. Low. Quantum electrodynamics at small distances. *Phys.Rev.*, 95:1300–1312, 1954.

[130] K. Symanzik. Small distance behavior in field theory and power counting. *Commun.Math.Phys.*, 18:227–246, 1970.

[131] David J. Gross and Frank Wilczek. Ultraviolet Behavior of Nonabelian Gauge Theories. *Phys.Rev.Lett.*, 30:1343–1346, 1973.

[132] H. David Politzer. Reliable Perturbative Results for Strong Interactions? *Phys.Rev.Lett.*, 30:1346–1349, 1973.

[133] G. 't Hooft and M. Veltman. Proceedings of the Colloquium on Renormalization of Yang-Mills Fields, Marseille, June 19-23, 1972. 1972.

[134] William E. Caswell. Asymptotic Behavior of Nonabelian Gauge Theories to Two Loop Order. *Phys.Rev.Lett.*, 33:244, 1974.

[135] D.R.T. Jones. Two Loop Diagrams in Yang-Mills Theory. *Nucl.Phys.*, B75:531, 1974.

[136] E. Egorian and O.V. Tarasov. Two Loop Renormalization of the QCD in an Arbitrary Gauge. *Teor.Mat.Fiz.*, 41:26–32, 1979.

[137] O.V. Tarasov, A.A. Vladimirov, and A. Yu. Zharkov. The Gell-Mann-Low Function of QCD in the Three Loop Approximation. *Phys.Lett.*, B93:429–432, 1980.

[138] S.A. Larin and J.A.M. Vermaseren. The Three loop QCD Beta function and anomalous dimensions. *Phys.Lett.*, B303:334–336, 1993.

[139] T. van Ritbergen, J.A.M. Vermaseren, and S.A. Larin. The Four loop beta function in quantum chromodynamics. *Phys.Lett.*, B400:379–384, 1997.

[140] M. Czakon. The Four-loop QCD beta-function and anomalous dimensions. *Nucl.Phys.*, B710:485–498, 2005.

[141] E. Brezin, J.C. Le Guillou, and Jean Zinn-Justin. Addendum to wilson's theory of critical phenomena and callan-symanzik equations in 4-epsilon dimensions. *Phys.Rev.*, D9:1121–1124, 1974.

[142] D.I. Kazakov, O.V. Tarasov, and A.A. Vladimirov. Calculation of Critical Exponents by Quantum Field Theory Methods. *Sov.Phys.JETP*, 50:521, 1979.

[143] T.P. Cheng, E. Eichten, and Ling-Fong Li. Higgs Phenomena in Asymptotically Free Gauge Theories. *Phys.Rev.*, D9:2259, 1974.

[144] K. Fujikawa, B.W. Lee, and A.I. Sanda. Generalized Renormalizable Gauge Formulation of Spontaneously Broken Gauge Theories. *Phys.Rev.*, D6:2923–2943, 1972.

[145] E.S. Abers and B.W. Lee. Gauge Theories. *Phys.Rept.*, 9:1–141, 1973.

[146] Gerard 't Hooft. An algorithm for the poles at dimension four in the dimensional regularization procedure. *Nucl.Phys.*, B62:444–460, 1973.

[147] H. Kluberg-Stern and J.B. Zuber. Renormalization of Nonabelian Gauge Theories in a Background Field Gauge. 1. Green Functions. *Phys.Rev.*, D12:482–488, 1975.

[148] S. Sarkar and H. Strubbe. Anomalous Dimensions in Background Field Gauges. *Nucl.Phys.*, B90:45, 1975.

[149] I. Ya. Arefeva, L.D. Faddeev, and A.A. Slavnov. Generating Functional for the s Matrix in Gauge Theories. *Theor.Math.Phys.*, 21:1165, 1975.

[150] R.E. Kallosh. The Renormalization in Nonabelian Gauge Theories. *Nucl.Phys.*, B78:293, 1974.

[151] J. Honerkamp. Chiral multiloops. *Nucl.Phys.*, B36:130–140, 1972.

[152] Bryce S. DeWitt. Quantum Theory of Gravity. 2. The Manifestly Covariant Theory. *Phys.Rev.*, 162:1195–1239, 1967.

[153] Marcus T. Grisaru, P. van Nieuwenhuizen, and C.C. Wu. Background Field Method Versus Normal Field Theory in Explicit Examples: One Loop Divergences in S Matrix and Green's Functions for Yang-Mills and Gravitational Fields. *Phys.Rev.*, D12:3203, 1975.

[154] Hans Joos Manfred Bohm, Angsar Denner. Gauge theories of the strong and electroweak interaction. 2001.

[155] Ian Jack. Two Loop Background Field Calculations for Gauge Theories With Scalar Fields. *J.Phys.*, A16:1083, 1983.

[156] L.F. Abbott. The Background Field Method Beyond One Loop. *Nucl.Phys.*, B185:189, 1981.

[157] A.A. Slavnov. Ward Identities in Gauge Theories. *Theor.Math.Phys.*, 10:99–107, 1972.

[158] J.C. Taylor. Ward Identities and Charge Renormalization of the Yang-Mills Field. *Nucl.Phys.*, B33:436–444, 1971.

[159] Ming-xing Luo, Hua-wen Wang, and Yong Xiao. Two loop renormalization group equations in general gauge field theories. *Phys.Rev.*, D67:065019, 2003.

[160] Stephen P. Martin and Michael T. Vaughn. Two loop renormalization group equations for soft supersymmetry breaking couplings. *Phys. Rev.*, D50:2282, 1994.

[161] I. Jack and D.R.T. Jones. Soft supersymmetry breaking and finiteness. *Phys.Lett.*, B333:372–379, 1994.

[162] Youichi Yamada. Two loop renormalization group equations for soft SUSY breaking scalar interactions: Supergraph method. *Phys.Rev.*, D50:3537–3545, 1994.

[163] Bob Holdom. Two U(1)'s and Epsilon Charge Shifts. *Phys. Lett.*, B166:196, 1986.

[164] Renato M. Fonseca, Michal Malinsky, and Florian Staub. Renormalization group equations and matching in a general quantum field theory with kinetic mixing. 2013.

[165] Florian Lyonnet, Ingo Schienbein, Florian Staub, and Akın Wingerter. The PyR@TE web page, 2013. http://pyrate.hepforge.org.

[166] Guido van Rossum and Jelke de Boer. Interactively testing remote servers using the python programming language. *CWI Quarterly*, 4:283–303, 1991.

[167] Paul F. Dubois, Konrad Hinsen, and James Hugunin. Numerical python. *Computers in Physics*, 10(3), May/June 1996.

[168] Eric Jones, Travis Oliphant, Pearu Peterson, et al. SciPy: Open source scientific tools for Python. http://www.scipy.org.

[169] SymPy Development Team. Sympy: Python library for symbolic mathematics. http://www.sympy.org.

[170] Fernando Pérez and Brian E. Granger. IPython: a System for Interactive Scientific Computing. *Comput. Sci. Eng.*, 9(3):21–29, May 2007.

[171] Kirill Simonov. Pyyaml. http://pyyaml.org/wiki/PyYAML.

[172] Clark Evans. YAML Ain't Markup Language. http://www.yaml.org, 2001.

[173] G.C. Branco, P.M. Ferreira, L. Lavoura, M.N. Rebelo, Marc Sher, et al. Theory and phenomenology of two-Higgs-doublet models. *Phys.Rept.*, 516:1–102, 2012.

[174] Lorenzo Basso, Stefano Moretti, and Giovanni Marco Pruna. A Renormalisation Group Equation Study of the Scalar Sector of the Minimal B-L Extension of the Standard Model. *Phys.Rev.*, D82:055018, 2010.

[175] Chiara Arina, Jinn-Ouk Gong, and Narendra Sahu. Unifying darko-lepto-genesis with scalar triplet inflation. *Nucl.Phys.*, B865:430–460, 2012.

[176] Yu. F. Pirogov and O. V. Zenin. Two-loop renormalization group restrictions on the standard model and the fourth chiral family. *Eur. Phys. J.*, C10:629–638, 1999.

[177] Koji Ishiwata and Mark B. Wise. Higgs Properties and Fourth Generation Leptons. *Phys.Rev.*, D84:055025, 2011.

[178] Ming-xing Luo and Yong Xiao. Renormalization group equations in gauge theories with multiple U(1) groups. *Phys.Lett.*, B555:279–286, 2003.

[179] Marcus Sperling, Dominik Stöckinger, and Alexander Voigt. Renormalization of vacuum expectation values in spontaneously broken gauge theories. *JHEP*, 1307:132, 2013.

[180] Marcus Sperling, Dominik StÃűckinger, and Alexander Voigt. Renormalization of vacuum expectation values in spontaneously broken gauge theories: Two-loop results. *JHEP*, 1401:068, 2014.

[181] Thomas Hermann, Luminita Mihaila, and Matthias Steinhauser. Three-loop anomalous dimensions for squarks in supersymmetric QCD. *Phys.Lett.*, B703:51–59, 2011.

[182] Luminita N. Mihaila, Jens Salomon, and Matthias Steinhauser. Renormalization constants and beta functions for the gauge couplings of the Standard Model to three-loop order. *Phys.Rev.*, D86:096008, 2012.

[183] K.G. Chetyrkin and M.F. Zoller. Three-loop beta-functions for top-Yukawa and the Higgs self-interaction in the Standard Model. *JHEP*, 1206:033, 2012.

[184] A.V. Bednyakov, A.F. Pikelner, and V.N. Velizhanin. Yukawa coupling beta-functions in the Standard Model at three loops. *Phys.Lett.*, B722:336–340, 2013.

[185] A.V. Bednyakov, A.F. Pikelner, and V.N. Velizhanin. Three-loop Higgs self-coupling beta-function in the Standard Model with complex Yukawa matrices. *Nucl.Phys.*, B879:256–267, 2014.

[186] F. Abe et al. Observation of top quark production in $\bar{p}p$ collisions. *Phys.Rev.Lett.*, 74:2626–2631, 1995.

[187] S. Abachi et al. Observation of the top quark. *Phys.Rev.Lett.*, 74:2632–2637, 1995.

[188] First combination of Tevatron and LHC measurements of the top-quark mass. 2014.

[189] Torbjorn Sjostrand, Stephen Mrenna, and Peter Z. Skands. PYTHIA 6.4 Physics and Manual. *JHEP*, 0605:026, 2006.

[190] G. Corcella, I.G. Knowles, G. Marchesini, S. Moretti, K. Odagiri, et al. HERWIG 6.5 release note. 2002.

[191] Stefano Frixione and Bryan R. Webber. Matching NLO QCD computations and parton shower simulations. *JHEP*, 0206:029, 2002.

[192] Stefano Frixione, Paolo Nason, and Bryan R. Webber. Matching NLO QCD and parton showers in heavy flavor production. *JHEP*, 0308:007, 2003.

[193] Stefano Frixione and Bryan R Webber. The MC@NLO 2.0 event generator. 2003.

[194] Paolo Nason. A New method for combining NLO QCD with shower Monte Carlo algorithms. *JHEP*, 0411:040, 2004.

[195] Simone Alioli, Paolo Nason, Carlo Oleari, and Emanuele Re. A general framework for implementing NLO calculations in shower Monte Carlo programs: the POWHEG BOX. *JHEP*, 1006:043, 2010.

[196] Fabrizio Caola, Kirill Melnikov, and Markus Schulze. A complete next-to-leading order QCD description of resonant Z' production and decay into $t\bar{t}$ final states. *Phys.Rev.*, D87(3):034015, 2013.

[197] Gerard 't Hooft and M.J.G. Veltman. Regularization and Renormalization of Gauge Fields. *Nucl.Phys.*, B44:189–213, 1972.

[198] S.A. Larin. The Renormalization of the axial anomaly in dimensional regularization. *Phys.Lett.*, B303:113–118, 1993.

[199] F.V. Tkachov. A Theorem on Analytical Calculability of Four Loop Renormalization Group Functions. *Phys.Lett.*, B100:65–68, 1981.

[200] K.G. Chetyrkin and F.V. Tkachov. Integration by Parts: The Algorithm to Calculate beta Functions in 4 Loops. *Nucl.Phys.*, B192:159–204, 1981.

[201] A. von Manteuffel and C. Studerus. Reduze 2 - Distributed Feynman Integral Reduction. 2012.

[202] S. Laporta. High precision calculation of multiloop Feynman integrals by difference equations. *Int.J.Mod.Phys.*, A15:5087–5159, 2000.

[203] Charalampos Anastasiou and Achilleas Lazopoulos. Automatic integral reduction for higher order perturbative calculations. *JHEP*, 0407:046, 2004.

[204] C. Studerus. Reduze - Feynman integral reduction in C++. *Computer Physics Communications*, 181:1293–1300, July 2010.

[205] A.V. Kotikov. Differential equations method: New technique for massive Feynman diagrams calculation. *Phys.Lett.*, B254:158–164, 1991.

[206] Vladimir A. Smirnov. Analytical result for dimensionally regularized massless on shell double box. *Phys.Lett.*, B460:397–404, 1999.

[207] J.B. Tausk. Nonplanar massless two loop Feynman diagrams with four on-shell legs. *Phys.Lett.*, B469:225–234, 1999.

[208] C. Anastasiou, E.W. Nigel Glover, and C. Oleari. Scalar one loop integrals using the negative dimension approach. *Nucl.Phys.*, B572:307–360, 2000.

[209] Roberto Bonciani. A simple one-loop example: The vacuum polarization in qed. *Lecture given at the Ecole doctoral de Physique de Grenoble*, June 22, 2009.

[210] T. Gehrmann and E. Remiddi. Differential equations for two loop four point functions. *Nucl.Phys.*, B580:485–518, 2000.

[211] W. Zimmermann. One particle singularities of green functions in quantum field theory. *Il Nuovo Cimento Series 10*, 13(3):503–521, 1959.

[212] K. Symanzik. Many-particle structure of greenâĂŹs functions. pages 121–170, 1995.

[213] Thomas Gerhmann. Quantum field theory i. 2010.

[214] Kirill Melnikov and Timo van Ritbergen. The Three loop on-shell renormalization of QCD and QED. *Nucl.Phys.*, B591:515–546, 2000.

[215] T.D. Lee and M. Nauenberg. Degenerate Systems and Mass Singularities. *Phys.Rev.*, 133:B1549–B1562, 1964.

[216] T. Kinoshita. Mass singularities of Feynman amplitudes. *J.Math.Phys.*, 3:650–677, 1962.

[217] S. Catani and M.H. Seymour. The Dipole formalism for the calculation of QCD jet cross-sections at next-to-leading order. *Phys.Lett.*, B378:287–301, 1996.

[218] Stefano Catani, Stefan Dittmaier, Michael H. Seymour, and Zoltan Trocsanyi. The Dipole formalism for next-to-leading order QCD calculations with massive partons. *Nucl.Phys.*, B627:189–265, 2002.

[219] Wolfgang Hollik and Monika Kollar. NLO QED contributions to top-pair production at hadron collider. *Phys.Rev.*, D77:014008, 2008.

[220] S. Frixione, Z. Kunszt, and A. Signer. Three jet cross-sections to next-to-leading order. *Nucl.Phys.*, B467:399–442, 1996.

[221] P. Nason, S. Dawson, and R. Keith Ellis. The Total Cross-Section for the Production of Heavy Quarks in Hadronic Collisions. *Nucl.Phys.*, B303:607, 1988.

[222] P. Nason, S. Dawson, and R. Keith Ellis. The One Particle Inclusive Differential Cross-Section for Heavy Quark Production in Hadronic Collisions. *Nucl.Phys.*, B327:49–92, 1989.

[223] W. Beenakker, H. Kuijf, W.L. van Neerven, and J. Smith. QCD Corrections to Heavy Quark Production in p anti-p Collisions. *Phys.Rev.*, D40:54–82, 1989.

[224] W. Beenakker, W.L. van Neerven, R. Meng, G.A. Schuler, and J. Smith. QCD corrections to heavy quark production in hadron hadron collisions. *Nucl.Phys.*, B351:507–560, 1991.

[225] W. Beenakker, Ansgar Denner, W. Hollik, R. Mertig, T. Sack, et al. Electroweak one loop contributions to top pair production in hadron colliders. *Nucl.Phys.*, B411:343–380, 1994.

[226] Johann H. Kuhn, A. Scharf, and P. Uwer. Electroweak corrections to top-quark pair production in quark-antiquark annihilation. *Eur.Phys.J.*, C45:139–150, 2006.

[227] S. Moretti, M.R. Nolten, and D.A. Ross. Weak corrections to gluon-induced top-antitop hadro-production. *Phys.Lett.*, B639:513–519, 2006.

[228] Werner Bernreuther, Michael Fuecker, and Zong-Guo Si. Weak interaction corrections to hadronic top quark pair production. *Phys.Rev.*, D74:113005, 2006.

[229] M.J.G. Veltman. Diagrammatica: The Path to Feynman rules. *Cambridge Lect.Notes Phys.*, 4:1–284, 1994.

[230] Gerard 't Hooft and M.J.G. Veltman. Scalar One Loop Integrals. *Nucl.Phys.*, B153:365–401, 1979.

[231] U. Aglietti and R. Bonciani. Master integrals with one massive propagator for the two loop electroweak form-factor. *Nucl.Phys.*, B668:3–76, 2003.

[232] Stefano Frixione, Paolo Nason, and Carlo Oleari. Matching NLO QCD computations with Parton Shower simulations: the POWHEG method. *JHEP*, 0711:070, 2007.

[233] Stefano Frixione, Eric Laenen, Patrick Motylinski, and Bryan R. Webber. Single-top production in MC@NLO. *JHEP*, 0603:092, 2006.

[234] Simone Alioli, Paolo Nason, Carlo Oleari, and Emanuele Re. NLO single-top production matched with shower in POWHEG: s- and t-channel contributions. *JHEP*, 0909:111, 2009.

[235] Emanuele Re. Single-top Wt-channel production matched with parton showers using the POWHEG method. *Eur.Phys.J.*, C71:1547, 2011.

[236] Simone Alioli, Paolo Nason, Carlo Oleari, and Emanuele Re. NLO Higgs boson production via gluon fusion matched with shower in POWHEG. *JHEP*, 0904:002, 2009.

[237] R. Keith Ellis and J.C. Sexton. QCD Radiative Corrections to Parton Parton Scattering. *Nucl.Phys.*, B269:445, 1986.

[238] Rikkert Frederix, Stefano Frixione, Fabio Maltoni, and Tim Stelzer. Automation of next-to-leading order computations in QCD: The FKS subtraction. *JHEP*, 0910:003, 2009.

[239] Luca Barze, Guido Montagna, Paolo Nason, Oreste Nicrosini, and Fulvio Piccinini. Implementation of electroweak corrections in the POWHEG BOX: single W production. *JHEP*, 1204:037, 2012.

[240] Luca Barze, Guido Montagna, Paolo Nason, Oreste Nicrosini, Fulvio Piccinini, et al. Neutral current Drell-Yan with combined QCD and electroweak corrections in the POWHEG BOX. *Eur.Phys.J.*, C73:2474, 2013.

[241] Carlo Oleari Emanuele Re Simone Alioli, Paolo Nason. The powheg box user manual: common features. *http://mon.iihe.ac.be/ alkaloge/Files/manual-BOX.pdf*.

[242] J. Alwall, R. Frederix, S. Frixione, V. Hirschi, F. Maltoni, et al. The automated computation of tree-level and next-to-leading order differential cross sections, and their matching to parton shower simulations. 2014.

[243] Gavin Cullen, Nicolas Greiner, Gudrun Heinrich, Gionata Luisoni, Pierpaolo Mastrolia, et al. Automated One-Loop Calculations with GoSam. *Eur.Phys.J.*, C72:1889, 2012.

[244] A.D. Martin, R.G. Roberts, W.J. Stirling, and R.S. Thorne. Parton distributions incorporating QED contributions. *Eur.Phys.J.*, C39:155–161, 2005.

[245] Torbjorn Sjostrand, Stephen Mrenna, and Peter Z. Skands. A Brief Introduction to PYTHIA 8.1. *Comput.Phys.Commun.*, 178:852–867, 2008.

[246] Pedro Abreu et al. Ultrahigh Energy Neutrinos at the Pierre Auger Observatory. *Adv.High Energy Phys.*, 2013:708680, 2013.

[247] P. Abreu et al. Search for point-like sources of ultra-high energy neutrinos at the Pierre Auger Observatory and improved limit on the diffuse flux of tau neutrinos. *Astrophys.J.*, 755:L4, 2012.

[248] Kristina Giesel, J.H. Jureit, and E. Reya. Cosmic UHE neutrino signatures. *Astropart.Phys.*, 20:335–360, 2003.

[249] Luis Anchordoqui, Tao Han, Dan Hooper, and Subir Sarkar. Exotic neutrino interactions at the Pierre Auger Observatory. *Astropart.Phys.*, 25:14–32, 2006.

[250] Luis A. Anchordoqui, Jonathan L. Feng, Haim Goldberg, and Alfred D. Shapere. Black holes from cosmic rays: Probes of extra dimensions and new limits on TeV scale gravity. *Phys.Rev.*, D65:124027, 2002.

[251] Tomohiro Abe, Ning Chen, and Hong-Jian He. LHC Higgs Signatures from Extended Electroweak Gauge Symmetry. *JHEP*, 1301:082, 2013.

[252] A Jinaru, C Alexa, I Caprini, and A Tudorache. $W' \to hH^{\pm}$ decay in $G(221)$ models. 2013.

[253] http://www.auger.org.

[254] J. Abraham et al. Observation of the suppression of the flux of cosmic rays above 4×10^{19}eV. *Phys.Rev.Lett.*, 101:061101, 2008.

[255] Pedro Abreu et al. Ultrahigh Energy Neutrinos at the Pierre Auger Observatory. *Adv.High Energy Phys.*, 2013:708680, 2013.

[256] I. Novikov A. Doroshkevich. Mean density of radiation in the metagalaxy and certain problems in relativistic cosmology. *Soviet Physics-Doklady*, 11, 1964.

[257] Arno A. Penzias and Robert Woodrow Wilson. A Measurement of excess antenna temperature at 4080-Mc/s. *Astrophys.J.*, 142:419–421, 1965.

[258] Kenneth Greisen. End to the cosmic ray spectrum? *Phys.Rev.Lett.*, 16:748–750, 1966.

[259] G.T. Zatsepin and V.A. Kuzmin. Upper limit of the spectrum of cosmic rays. *JETP Lett.*, 4:78–80, 1966.

[260] V.S. Berezinsky and G.T. Zatsepin. Cosmic rays at ultrahigh-energies (neutrino?). *Phys.Lett.*, B28:423–424, 1969.

[261] E. Daw. Lecture 5: Ultra high energy cosmic rays and the gzk cutoff.

[262] J. Abraham et al. Correlation of the highest-energy cosmic rays with the positions of nearby active galactic nuclei. *Astropart.Phys.*, 29:188–204, 2008.

[263] K. Kotera, D. Allard, and A.V. Olinto. Cosmogenic Neutrinos: parameter space and detectabilty from PeV to ZeV. *JCAP*, 1010:013, 2010.

[264] V.S. Berezinsky and A. Yu. Smirnov. Cosmic neutrinos of ultra-high energies and detection possibility. *Astrophys.Space Sci.*, 32:461–482, 1975.

[265] J. Abraham et al. Properties and performance of the prototype instrument for the Pierre Auger Observatory. *Nucl.Instrum.Meth.*, A523:50–95, 2004.

[266] K.S. Capelle, J.W. Cronin, G. Parente, and E. Zas. On the detection of ultrahigh-energy neutrinos with the Auger Observatory. *Astropart.Phys.*, 8:321–328, 1998.

[267] Xavier Bertou, Pierre Billoir, O. Deligny, C. Lachaud, and A. Letessier-Selvon. Tau neutrinos in the Auger Observatory: A New window to UHECR sources. *Astropart.Phys.*, 17:183–193, 2002.

[268] Daniele Fargion. Discovering Ultra High Energy Neutrinos by Horizontal and Upward tau Air-Showers: Evidences in Terrestrial Gamma Flashes? *Astrophys.J.*, 570:909–925, 2002.

[269] Raj Gandhi, Chris Quigg, Mary Hall Reno, and Ina Sarcevic. Ultrahigh-energy neutrino interactions. *Astropart.Phys.*, 5:81–110, 1996.

[270] Raj Gandhi, Chris Quigg, Mary Hall Reno, and Ina Sarcevic. Neutrino interactions at ultrahigh-energies. *Phys.Rev.*, D58:093009, 1998.

[271] Sheldon L. Glashow. Resonant Scattering of Antineutrinos. *Phys.Rev.*, 118:316–317, 1960.

[272] V.S. Berezinsky and A.Z. Gazizov. Cosmic Neutrinos and Possibility to Search for W Bosons Having 30-GeV-100-GeV Masses in Underwater Experiments. *JETP Lett.*, 25:254–256, 1977.

[273] V.S. Berezinsky and A.Z. Gazizov. Neutrino - electron scattering at energies above the W boson production threshold. *Sov.J.Nucl.Phys.*, 33:120–125, 1981.

[274] Luis A. Anchordoqui, Haim Goldberg, Francis Halzen, and Thomas J. Weiler. Neutrinos as a diagnostic of high energy astrophysical processes. *Phys.Lett.*, B621:18–21, 2005.

[275] Pijushpani Bhattacharjee and Nayantara Gupta. Probing neutrino mixing angles with ultrahigh energy neutrino telescopes. *Phys.Rev.Lett.*, 2005.

[276] S. Hummer, M. Maltoni, W. Winter, and C. Yaguna. Energy dependent neutrino flavor ratios from cosmic accelerators on the Hillas plot. *Astropart.Phys.*, 34:205–224, 2010.

[277] Poonam Mehta and Walter Winter. Interplay of energy dependent astrophysical neutrino flavor ratios and new physics effects. *JCAP*, 1103:041, 2011.

[278] Zhi-zhong Xing and Shun Zhou. The Glashow resonance as a discriminator of UHE cosmic neutrinos originating from p-gamma and p-p collisions. *Phys.Rev.*, D84:033006, 2011.

[279] Atri Bhattacharya, Raj Gandhi, Werner Rodejohann, and Atsushi Watanabe. The Glashow resonance at IceCube: signatures, event rates and pp vs. $p\gamma$ interactions. *JCAP*, 1110:017, 2011.

[280] A. J. G. Hey I. J. R. Aitchison. Gauge theories in particle physics volume ii.

[281] Amanda Cooper-Sarkar, Philipp Mertsch, and Subir Sarkar. The high energy neutrino cross-section in the Standard Model and its uncertainty. *JHEP*, 1108:042, 2011.

[282] Richard P. Feynman. Very high-energy collisions of hadrons. *Phys.Rev.Lett.*, 23:1415–1417, 1969.

[283] John C. Collins, Davison E. Soper, and George F. Sterman. Heavy Particle Production in High-Energy Hadron Collisions. *Nucl.Phys.*, B263:37, 1986.

[284] M.A.G. Aivazis, John C. Collins, Fredrick I. Olness, and Wu-Ki Tung. Leptoproduction of heavy quarks. 2. A Unified QCD formulation of charged and neutral current processes from fixed target to collider energies. *Phys.Rev.*, D50:3102–3118, 1994.

[285] S. Kretzer and I. Schienbein. Heavy quark initiated contributions to deep inelastic structure functions. *Phys. Rev.*, D58:094035, 1998.

[286] M. Botje. QCDNUM: Fast QCD Evolution and Convolution. *Comput.Phys.Commun.*, 182:490–532, 2011.

[287] M. Gluck, S. Kretzer, and E. Reya. Dynamical QCD predictions for ultrahigh-energy neutrino cross-sections. *Astropart.Phys.*, 11:327–334, 1999.